Doctoral thesis

THE ROLE OF MEIS TRANSCRIPTION FACTORS IN THE EPICARDIUM

Mª Ester de la Cruz Crespillo

Universidad Autónoma de Madrid
Facultad de Ciencias
Departamento Biología Molecular

Madrid, 2021

DEPARTAMENTO DE BIOLOGÍA MOLECULAR

Universidad Autónoma de Madrid

FACULTAD DE CIENCIAS

The role of Meis transcription factors in the epicardium

Doctoral thesis

Mª Ester de la Cruz Crespillo

Graduada en Biotecnología

Director: Miguel Torres Sánchez

Centro Nacional de Investigaciones Cardiovasculares

Julio, 2021

I hereby certify that Mª Ester de la Cruz Crespillo has carried out the experimental work leading to her PhD thesis entitled "The role of Meis transcription factors in the epicardium" under my supervision at the Centro Nacional de Investigaciones Cardiovasculares (CNIC) in Madrid.

I also declare that the work presented is novel and of great importance in the field, and of sufficient quality to merit to be presented in order to obtain a PhD degree by the Universidad Autónoma de Madrid.

Madrid, 16-Abril-2021

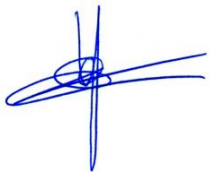

Miguel Torres Sánchez

This work was performed in Miguel Torres' laboratory in the Cell and Developmental Biology Area at the Centro Nacional de Investigaciones Cardiovasculares Carlos III (CNIC) in Madrid.

The CNIC is supported by the Ministerio de Ciencia, Innovación y Universidades (MCNU) and the Pro CNIC Foundation.

This study was funded by grants RD12/0019/0005 and RD16/0011/0019 (TerCel, RETICS); S2010-BMD-2315 (Comunidad de Madrid); BFU2012-31086 (MINECO); BFU2015-71519 (MEIC); PGC2018-096486-B-I00 (MICINN) and ref. 17CVD04 (Leducq Foundation Transatlantic Networks).

Mª Ester de la Cruz Crespillo was recipient of a "Formación del Profesorado Universitario" (FPU) fellowship from the Spanish Ministry (FPU15/02955) and EMBO Short Term fellowship (STF_8357).

"I do not know what I may appear to the world, but to myself I seem to have been only like a boy playing on the seashore, and diverting myself in now and then finding a smoother pebble or a prettier shell than ordinary, whilst the great ocean of truth lay all undiscovered before me."

~ Isaac Newton

Table of contents

Index of Figures

Index of Tables

Abbreviations

AMC Arterial mesothelial cells

AVC Atrioventricular canal

CC Cardiac crescent

CHD Congenital heart defect

cNCCs Cardiac neural crest cells

CM Cardiomyocyte

CVDs Cardiovascular diseases

DEGs Differentially expressed genes

DORV Double outlet right ventricle

E Embryonic day

ECM Extracellular matrix

ECs Endothelial cells

EMT Epithelial-to-mesenchymal transition

EMCN Endomucin

EndoMT Endothelial-to-mesenchymal transition

EPDCs Epicardium-derived cells

FHF First Heart Field

HT Heart Tube

LA Left atrium

LECs Lymphatic endothelial cells

LEPDCs Lymphatic-associated epicardium-derived cells

LV Left ventricle

LYVE1 Lymphatic vessel endothelial hyaluronan receptor 1

MEIS Myeloid ecotropic viral integration site

MI Myocardial infarction

OA Overriding aorta

OFT Outflow tract

PE Proepicardium

PROX1 Prospero homeobox protein 1

PTA Persistent truncus arteriosus

RA Retinoic acid

RV Right ventricle

SV Sinus venosus

Tbx18 T-box 18

Tcf21 Transcription factor 21

TF Transcription Factor

SHF Second Heart Field

SMCs Smooth muscle cells

VSD Ventricular septal defect

Wt1 Wilms tumor 1

SUMMARY

A single layer of cells could be perceived as insignificant in comparison to a whole organ. However, extensive evidence has shown that the epicardium, the outermost layer of the heart, is essential for cardiac development and regeneration. Epicardium-derived cells (EPDCs) and epicardial signalling are crucial for coronary vasculature development and myocardial growth. In this thesis, we show that MEIS homeodomain transcription factors are expressed and play a function in the epicardium during cardiac development. *Meis1* and *Meis2* epicardial-specific conditional mutant mice show 50% lethality associated to misalignment of the great vessels and die after birth, while the survivors do not show cardiac malformations. Epicardial epithelial-to-mesenchymal transition of epicardial cells is relatively unaffected in *Meis* mutants, but EPDCs specification is altered, resulting in an excess of myofibroblast differentiation in detriment of smooth muscle cell (SMC) and other fibroblast populations. The excess myofibroblasts observed in *Meis* mutants accumulate in the subepicardium. Retinoic acid signalling is a major signalling pathway in the epicardium and is strongly impaired in the mutants, which could account for the altered specification of EPDCs. Decreased SMC coverage leads to a delayed maturation of the blood coronary vasculature, which also shows patterning alterations.

Further characterization of *Meis1* and *Meis2* epicardial-specific conditional mutants has revealed the failure of prenatal lymphatic vessel development. This reveals a previously unknown non-autonomous function of the epicardium in promoting cardiac lymphangiogenesis. We characterize a population of subepicardial, fibroblast-like lymphatic-associated EPDCs (LEPCs) that completely enseaths lymphatic vessels as they grow towards the apex of the ventricles. LEPDC and Lymphatic Endothelial Cell (LECs) association is disrupted in *Meis* mutants, which suggests that LEPDC-LEC crosstalk is important for cardiac lymphangiogenesis. Transcriptomic analysis of Meis-mutant epicardium/subepicardium showed a downregulation of *Vegfc* and *Vegfd* lymphoangiocrine signals. Epicardial-specific *Vegfc* mutants present less developed and immature coronary lymphatic vessels, whereas analysis of the lymphatic vasculature of *Vegfd knockout* hearts shows that VEGFD is important for the development of ventral coronary lymphatics. These results show that direct cellular interactions and paracrine signalling from the epicardium/EPDCs orchestrate cardiac lymphatic development and that this process is regulated by MEIS transcription factors.

RESUMEN

Una sola capa de células podría percibirse como algo insignificante en comparación con un órgano completo. Sin embargo, son numerosos los estudios que han demostrado que el epicardio, la capa más externa del corazón, es esencial para el desarrollo y la regeneración del corazón. Las células derivadas del epicardio (EPDCs) y la señalización del epicardio, son cruciales para el desarrollo de la vasculatura coronaria y el crecimiento del miocardio. En esta tesis doctoral, mostramos que los factores de transcripción homeodominio MEIS se expresan y desempeñan una función en el epicardio durante el desarrollo cardíaco. Los ratones con una deleción condicional de *Meis1* y *Meis2* en el epicardio, presentan una letalidad del 50% asociada a la incorrecta alineación de la aorta y arteria pulmonar y mueren poco después de nacer. Los supervivientes no muestran malformaciones cardíacas. La transición epitelio-mesénquima de las células del epicardio, no se ve muy afectada en los mutantes de *Meis*, pero la especificación de las células derivadas del epicardio sí está alterada, consistente en un exceso de especificación de miofibroblastos en detrimento de las células del músculo liso (SMC) y otras poblaciones de fibroblastos. El exceso de miofibroblastos se acumulan en el subepicardio de los mutantes. La señalización del ácido retinoico, muy importante en la función del epicardio, está reducida en los mutantes, lo que podría explicar la especificación alterada de las EPDCs. La disminución del recubrimiento de las coronarias con SMC provoca un retraso en la maduración de la vasculatura coronaria sanguínea, que también presenta una alteración del patrón de sus ramificaciones.

Los mutantes condicionales de *Meis1* y *Meis2* en el epicardio, no desarrollan vasculatura linfática coronaria prenatal. Estos resultados han revelado un papel no autónomo del epicardio, anteriormente desconocido, promoviendo la linfangiogénesis cardíaca. Hemos caracterizado una población de EPDCs asociadas a linfáticos (LEPDC), similares a fibroblastos, que se localizan en el subepicardio y que rodean completamente los vasos linfáticos a medida que crecen hacia el ápex de los ventrículos. La asociación de LEPDCs y células endoteliales linfáticas (LECs) se interrumpe en mutantes de *Meis*, lo que sugiere que la comunicación LEPDC-LEC es importante para la linfangiogénesis cardíaca. El análisis del transcriptoma del epicardio/subepicardio de los mutantes de *Meis*, mostró una disminución de la expresión de las moléculas paracrinas *Vegfc* y *Vegfd*. Los mutantes condicionales de *Vegfc* en el epicardio presentan vasos linfáticos coronarios menos desarrollados e inmaduros, mientras que el análisis de los mutantes *Vegfd* muestra que VEGFD es importante para el desarrollo de los vasos linfáticos coronarios ventrales. Estos resultados demuestran que las interacciones celulares directas y la señalización paracrina del epicardio/EPDC controlan el desarrollo linfático cardíaco y que este proceso está regulado por factores de transcripción MEIS.

INTRODUCTION

"To know that we know what we know,
and to know that we do not know what
we do not know, that is true knowledge."
~ Nicolaus Copernicus

Why are the heart and the cardiovascular system important?

Cardiovascular diseases (CVDs) are the first cause of death globally. According to the World Health Organization, each year around 17.9 million people die from CVDs in the world.

The heart is the main organ of the cardiovascular system and, actually, it is the first functional organ to be formed during embryonic development. Its function as a pump of blood that supplies the entire body with oxygen and nutrients starts to be vital soon, once diffusion is not enough.

This muscular pump contracts rhythmically during systole and relaxes during diastole. Its four-chambered structure and its valves allow the unidirectional blood flow. The deoxygenated blood from the systemic circulation comes from the body and enters the heart through the superior and inferior cava veins and reaches the right atrium. The tricuspid valve controls the passage to the right ventricle where the blood will be pumped out to the lungs through the pulmonary valve and the pulmonary artery. The gas exchange takes place and the blood becomes oxygenated again. It returns to the heart, to the left atrium and then to its adjacent chamber, the left ventricle through the mitral valve. The blood leaves the ventricle through the aortic valve an aorta and irrigates the whole body (Figure 1B).

In the same sense, it is essential that the heart itself is irrigated by its own vasculature, the coronary vasculature. As the oxygenated blood is propelled out from the heart through the aorta, the blood is also sent through the coronary arteries. The deoxygenated blood is removed by the coronary veins (Figure 1A).

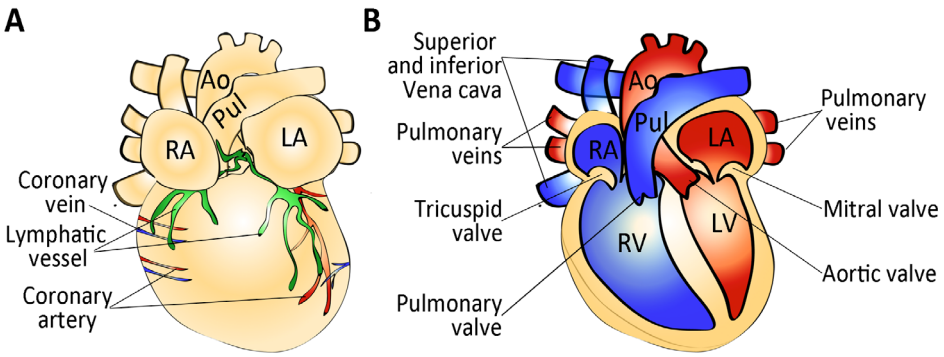

Figure 1. Anatomy of the adult mammalian heart. A) Schematic representation of ventral view of adult mammalian heart. B) Inside view of the heart. Deoxygenated blood is depicted in blue and oxygenated blood in red. Ao: aorta; LA: left atrium; LV: left ventricle; Pul: Pulmonary artery; RA: right atrium; RV: right ventricle.

Cardiac development is a complex process that requires a tight regulation. An alteration in this process can lead to congenital heart defects (CHD). Unfortunately, this occurs too often. If every type of cardiac malformation is included, 75 of every 1000 live babies present a CHD (Hoffman and Kaplan, 2002). Moreover, 10% of stillbirths also present some kind of CHD (Fahed et al., 2013). This is why it is so important to understand how the heart forms, so in the future CHD and CVDs could be prevented or treated trying to recapitulate the native developmental process.

Heart Development

Human embryonic development spans for 9 months. 3 weeks after conception the heart starts to beat and it is completely formed by eight weeks but it will continue growing and maturing even after birth. The mouse is the genetic laboratory model closer to humans and mouse cardiac morphogenesis has been shown to be comparable to human in many aspects (Krishnan et al., 2014), so we have chosen the mouse model to study heart development.

Mouse prenatal development concludes at embryonic day 19 (E19). At this time, the four-chambered heart is composed of three layers: the innermost layer, the endocardium; the myocardium and the epicardium (the outermost layer). But how is this well-organized four chambered heart formed?

In the mouse, the first cardiac progenitors appear at E6.5 in the primitive streak. This mesoderm is specified into cardiogenic mesoderm simultaneously to the expression of the transcription factor (TF) *Mesp1* (Mesoderm posterior 1), a key factor in cardiac specification. During gastrulation cardiac progenitors migrate to colonize two initial bilateral regions that at E7.5 fuse in the midline forming the cardiac crescent (CC) underlying the head folds (Figure 2) (Buckingham et al., 2005). At this time, Mesp1 upregulates essential cardiac transcription factors such as *Gata4* or *Nkx2.5* (Bondue et al., 2008). At the CC stage, the heart is formed by two layers, the endocardium and the myocardium. This CC continues growing and forms the heart tube (HT) that initially is dorsally open and bound to the dorsal pericardial walls in all its length. After dorsal closure, it remains attached to the dorsal pericardial walls only at its arterial and venous poles (Rana et al., 2013). The CC and early HT are mainly formed by the contribution of a first pool of progenitor cells known as First Heart Field (FHF). They will give rise to most of the left ventricle (LV) and part of the atria (Buckingham et al., 2005; Zaffran et al., 2004).

However, as the heart elongates, the contribution of another source of progenitor cells is needed: The Second Heart Field (SHF). These cells remain undifferentiated until they are added afterwards at the arterial and venous poles of the heart (Kelly, 2012). Their incorporation enables also the closure of the initially open HT, with addition of SHF cells to its dorsal wall (Ivanovitch et al., 2017). SHF recruitment enables the formation of the outflow tract (OFT) right ventricle (RV), ventricular septum, the atria and atrial septum (Kelly, 2012; Zaffran et al., 2004). Among the important regulators of SHF specification and incorporation we can find *Islet1* (Cai et al., 2003), *Fgf10* (Kelly et al., 2001) and *Tbx1* (Chen et al., 2009).

In parallel to HT elongation, the heart undergoes a rightward looping at E8.5 that establishes the basic type of topological left-right asymmetry of the ventricular chambers. It brings the inflow and OFT closer and into an approximation of their final location with the atria displaced cranially when compared to the ventricles (Männer, 2009). The looping and myocardial expansion lead to the formation of the initial cardiac chambers that, by E10.5, are already formed (Buckingham et al., 2005). However, both ventricles and both atria are still connected without a separation between left-right chambers.

As cardiac growth and morphogenesis continue, cardiac valve development becomes essential

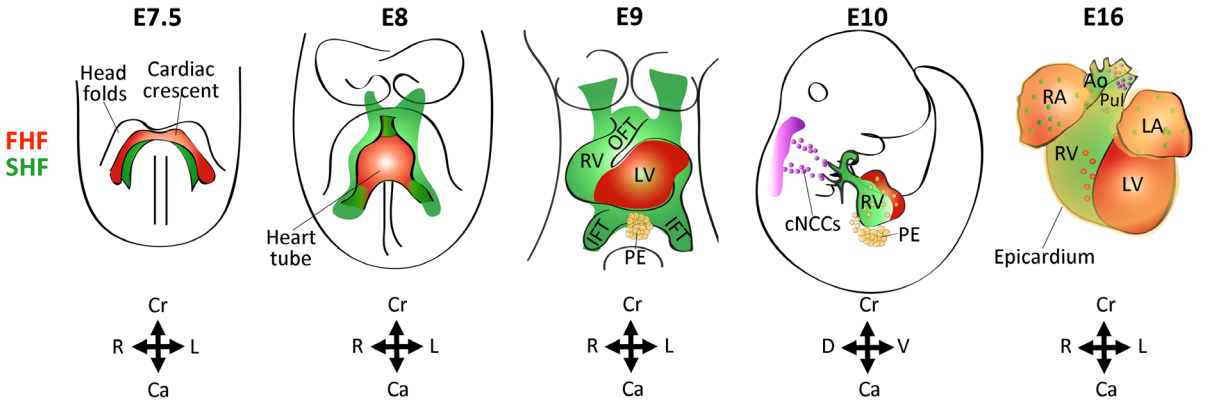

Figure 2. Cardiac development and cardiac progenitors. At E7.5 the cardiac crescent is formed under the head folds with First Heart Field (FHF, red) and Second Heart Field (SHF, green) progenitors. At E8, cardiac progenitors are forming the heart tube that suffers a rightward looping that brings closer the Inflow tract (IFT) and Outflow tract (OFT) regions (E8-E9.5). At E10.5, left and right atria (LA and RA respectively), left and right ventricles (LV and RV respectively) have been specified and extracardiac progenitors have been incorporated into the heart. Cardiac neural crest cells (cNCCs) contribute to the OFT and semilunar valve formation. The proepicardium (PE) protrudes cells that migrate to the heart (E9-E10.5), attach to its surface and form the epicardium: the outermost layer of the heart. By E14.5 the four chambers, aorta (Ao) and pulmonary artery (Pul) are already discernible and the heart continues growing and maturing. The last drawing represents the contribution of the different progenitors to the final heart (E16). Ca: caudal; Cr: cranial; D: dorsal; L: left; R: right; V: ventral. (Modified from from Stéphane D. Vincent and Margaret E. Buckingham, 2010).

to establish unidirectional blood flow. By E9.5 in the atrioventricular canal (AVC), and by E10.5 in the OFT, cardiac cushions are formed. They are endocardial protrusions filled with cardiac jelly. Some of the endocardial cells surrounding the cushion undergo an endocardial-to-mesenchymal transition and populate the underlying valve primordia (Macgrogan et al., 2018). Notch signalling, BMP2 and BMP4 are some of the components essential in this process (Armstrong and Bischoff, 2004; Timmerman et al., 2004). These primitive protrusions are transformed into mature thin leaflets through a process of valve elongation and maturation (Macgrogan et al., 2018). The result is the formation of two semilunar (aortic and pulmonary) and two atrioventricular (mitral and tricuspid) valves in the OFT and AVC respectively. Cardiac valve development is also essential for proper ventricular and atrial septation (Lin et al., 2012; Macgrogan et al., 2018). However, the contribution of cardiac neural crest cells and epicardium is also essential for cardiac valve formation and it will be addressed later in this introduction.

As a result of these developmental processes, by E14.5 the heart is divided in its final four chambers with functional cardiac valves that control the unidirectional blood flow. However, it will continue growing and maturing even postnatally.

Cellular composition of the developing heart. Where do the cells come from?

While the morphogenetic changes in cardiac development are crucial for proper formation of a functional heart, the differentiation of progenitor cells into a variety of cell types specialised in different functions is also essential.

Cardiomyocytes are the contracting cells of the heart. They occupy most of its volume but, due to their large size, in the adult heart they only represent around 30-40% of its cells (Pinto et al., 2016). The rest are non-myocyte cell populations that are essential for normal heart homeostasis, providing the extracellular matrix (ECM), intercellular communication and vascular supply. Of these, around 60% are endothelial cells and can be found forming the endocardium or lining coronary vessels. Around 5-10% are hematopoietic-derived cells and 20% fibroblasts (Pinto et al., 2016). There are also mural cells (pericytes and vascular smooth muscle cells (SMCs)) that stabilize vessels.

Different groups of progenitor cells contribute to cardiac development and the different cell types involved are:

1) Cardiogenic mesoderm

2) Cardiac neural crest cells (cNCCs)

3) Epicardium

1) Cardiogenic mesoderm

As mentioned before, the cardiogenic mesoderm includes the contribution of FHF and SHF progenitors. The FHF gives rise mainly to cardiomyocytes and endocardium of the LV and atria while SHF progenitors contribute cardiomyocytes to the RV, atria and OFT. While the FHF precursors are unipotent, they can only give rise to either endocardium or myocardium (Wei and Mikawa, 2000), the SHF precursors are multipotent and can generate cardiomyocytes, endothelium and smooth muscle (Bu et al., 2009; Kattman et al., 2006; Moretti et al., 2006; Saga et al., 2000). The SMCs derived from the SHF populate the base of the great arteries and the sub-pulmonary and sub-aortic regions (Wu et al., 2006).

Moreover, FHF and SHF also give rise to the cardiac conduction system (Miquerol et al., 2013). Recently, the contribution of the SHF lineage to the ventral cardiac lymphatic vasculature has also been reported (Lioux et al., 2020; Maruyama et al., 2019).

2) Cardiac Neural Crest Cells (cNCCs)

The neural crest is a multipotent stem cell population that originates from the border between the developing neural plate and surface ectoderm. It contributes different cell types to various organs during embryonic development.

In particular, cNCCs delaminate from the rhombomeres 6 to 8 at the hindbrain towards the pharyngeal arches, where some of them differentiate into SMCs (Bergwerff et al., 1998). A subset of cNCCs continue their migration and reach the OFT at E10.5 (Kirby et al., 1983). They contribute to the formation of the aorticopulmonary septum and the OFT endocardial cushions (Kirby and Hutson, 2010). At E10.5, once the cardiac cushions that will give rise to the semilunar valves are formed, cNCCs migrate into the distal region of the OFT and interact with endocardium-derived mesenchymal cells

to pattern the arterial valves. At the same time, the condensation of cNCCs and formation of the aorticopulmonary septum allow the division of the OFT into aorta and pulmonary artery by E12.5 (Waldo et al., 1998). Some preotic cNCCs (mainly from rhombomere 4) migrate into the heart and differentiate into coronary artery SMCs. They colonise preferentially their proximal portion and their septal branches (Arima et al., 2012). In addition, cNCCs progenitors also give rise to the autonomous nervous system of the heart (Végh et al., 2016).

Alterations in the specification, delamination, migration or incorporation of cNCCs result in severe cardiac malformations. In fact, in the absence of neural crest, alterations such as persistent truncus arteriosus (PTA), transposition of the great vessels, double outlet right ventricle (DORV) and ventricular septal defect (VSD) have been described (Porras and Brown, 2008). Their ablation also results in a reduction in OFT myocardium (arterial pole defects), which also exemplifies the importance of SHF and cNCCs interaction for proper heart development (Waldo et al., 2005).

Different molecular pathways have been shown to play a relevant role in the different steps of cNCC journey until their incorporation and condensation into the heart. This includes members of myocardin, GATA, Notch, BMP, T-box pathways and semaphorins (High and Epstein, 2007). For example, Wnt1 is important for neural crest cell induction and Wnt1-Cre labels all premigratory neural crest cells (Hari et al., 2012). TGFβ2 (Transforming growth factor β II) is important for cNCC-mediated vascular remodelling (Wurdak et al., 2005). Signals from the OFT are also crucial. For example, in the absence of the semaphorin 3C (Sema3C), which is expressed in the OFT myocardium, the cNCCs cannot incorporate into the OFT and this results in PTA and interruption of the aortic arch (Feiner et al., 2001).

3) Epicardium

For the purpose of the present study, the epicardium, its origin, cellular and paracrine contributions will be addressed in more detail.

The epicardium is the outermost mesothelial layer of all vertebrate hearts. It was first described in the chick in 1909 by Kurkiewicz and then its presence on the surface of the heart was confirmed by Manasek (1968, 1969), using electron microscopy.

This mesothelial layer covers the entire surface of the ventricles, the atria and the OFT and appears as a continuous lining. However, differences between the atrial and ventricular epicardium regarding the thickness of the layer, its morphology and differentiation potential have been described in humans (Risebro et al., 2015). Although epicardium on the ventricles and the Arterial mesothelial cell (AMC) layer of the great arteries seem a continuous sheet, they are in fact independent and distinct in their origin (Gittenberger-de-Groot et al., 2000; Lioux et al., 2020; Peralta et al., 2013; Pérez-Pomares et al., 2003).

Because of its relevance, the origin, formation, function and role of the epicardium (both in development and cardiac regeneration) has been widely studied and has been reviewed recently (Cao and Poss, 2018; Cao et al., 2020; Quijada et al., 2020; Simões and Riley, 2018). Here we will try to

summarize what is known and what we consider important in order to put the present thesis into context.

3.1) Origin and formation

Although some CD45+ hematopoietic cells contribute to the epicardium (Balmer et al., 2014), most of this mesothelial layer derives from the proepicardium (PE). The PE is a transient protrusion of cells that appears at E8.5 in the mouse, dorsal and caudal to the heart tube, between the sinus venosus and the liver (Männer, 1993; Schulte et al., 2007). It is known that the PE already expresses markers that will be essential for epicardial identity like Transcription factor 21 (*Tcf21*), Wilms tumor 1 (*Wt1*) and T-box 18 (*Tbx18*). However, further knowledge is required in order to understand how the formation of this transient structure is induced (Schulte et al., 2007). Signals from the liver and the myocardium might be implicated in its induction. Studies in chick suggest that a balance of BMP and FGF levels might be implicated and regulate the differentiation towards PE or myocardium of the inflow (Cao et al., 2020). Moreover, just recently, Andrés-Delgado et al. (2019) elegantly showed in the zebrafish that PE formation might be the consequence of the movement of cells of the dorsal pericardium towards the midline. This movement, under the influence of actin dynamics and BMP signalling, causes local cell crowding that results in apical extrusion and the formation of the PE.

The mechanism by which the epicardial cells delaminate from the PE and reach the heart differs among species. In the mouse, between E9-E10.5 PE cells reach the myocardium following four different trajectories: 1) Some PE clusters form “cysts” and float across the pericardial cavity and attach to the myocardium. 2) Villous protrusions are formed in the PE and reach the dorsal surface of the heart (as occurs for example in the chick). 3) Some cells migrate along the surface of the inflow tract and reach the myocardium. 4) Through direct contact of the PE with the myocardium (Li et al., 2017; Rodgers et al., 2008). Once the cells attach to the myocardial surface, they collapse and proliferate giving rise to epicardial islands that expand and form the epicardium (Komiyama et al., 1987). α4-integrin and VCAM1 are adhesion molecules expressed during this process in the PE cells and myocardium respectively. In their absence, the epicardial cells cannot attach or migrate properly and this results in a disrupted epicardium (Kwee et al., 1995; Sengbusch et al., 2002; Yang et al., 1995).

As mentioned before, the epicardium of the ventricles and atria have a different origin than the AMC layer covering the OFT. While the first is mainly formed by PE-derived cells, the mesothelial layer of the OFT derives from the pericardium (Gittenberger-de-Groot et al., 2000; Lioux et al., 2020; Peralta et al., 2013; Pérez-Pomares et al., 2003).

None of the markers identified are solely expressed in the epicardium. Nevertheless, there are several well-established markers that have allowed us to better understand the function of the epicardium and track its progeny by lineage tracing. Among these, we can find: *Wt1*, *Tbx18*, *Scleraxis* (*Scx*), *Sema3d*, *Gata5* and *Tcf21*.

3.2) Epithelial-to-mesenchymal transition

Once the epicardium is formed, a subset of epicardial cells undergo a process of epithelial-to-mesenchymal transition (EMT) and invade the myocardium, giving rise to epicardium-derived cells (EPDCs). In this process, the epithelial cells lose their apical-basal polarity and cell-cell adhesions and acquire a migratory phenotype. However, it is not clear whether all epicardial cells have the ability to become mesenchymal or just a subset of them have "EMT capacity". In addition, it is not known whether cell-intrinsic properties or external cues participate in triggering EMT.

A series of different events have to occur and be tightly regulated spatiotemporally. Otherwise, EMT will not proceed normally and this has fatal consequences for cardiac and embryonic development that result in embryonic or perinatal lethality in many cases. It must be noted that, although we will try to classify the different steps according to the involvement of the most important players, some of these are important for more than one step during EMT. These are the events necessary for EMT (Figure 3):

- **Upregulation of transcriptional activators of EMT in epicardial cells:** TFs that regulate EMT repress epithelial adhesion genes such as claudins, E-cadherin and zonula-occludens and upregulate genes like N-cadherin, collagens and fibronectin for ECM production and migration (Lamouille et al.,

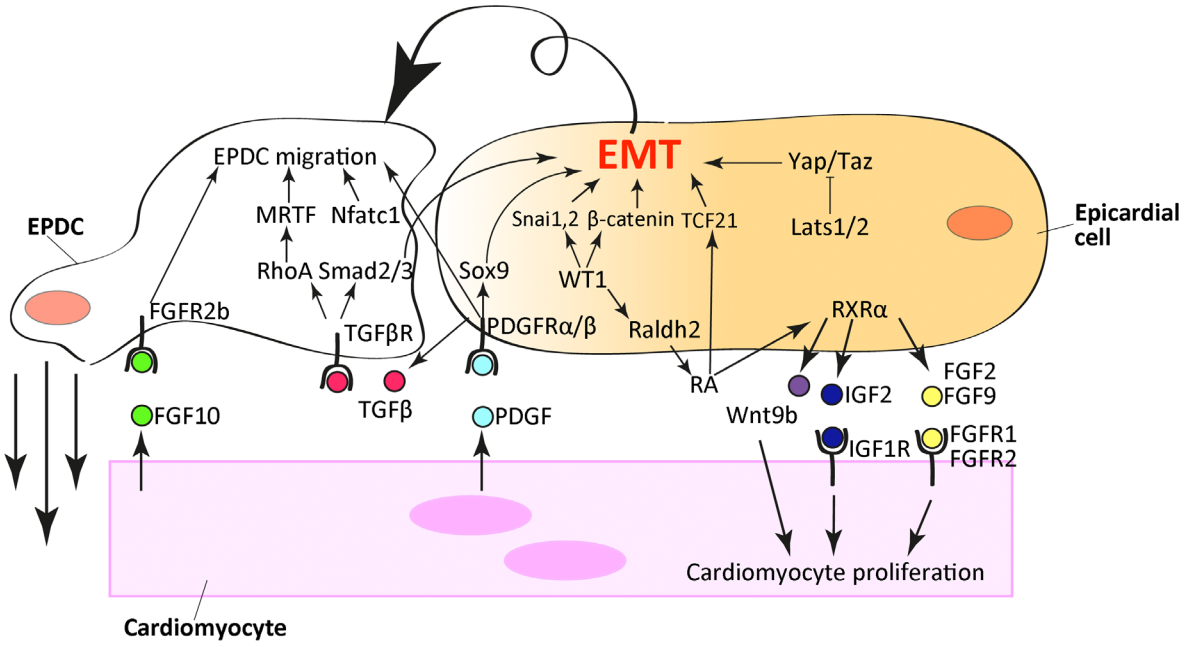

Figure 3. Epicardial epithelial-to-mesenchymal transition (EMT) and paracrine crosstalk during cardiac development. Schematic representation of the main factors regulating EMT, epicardium-derived cells (EPDCs) migration and some examples of the crosstalk between epicardial cells-cardiomyocytes. A subset of epicardial cells lose their apical-basal polarity, cell-cell adhesions and undergo a process of EMT giving rise to EPDCs. Four simultaneous processes promote EMT: Upregulation of EMT transcriptional activators as Wt1 and Tcf21; adequate orientation of cell division; growth factor-dependent regulation of EMT with TGFβ, PDGFs and FGFs factors; and induction of EPDC migration through MRTFs, NFATC1 and TGFβ. Crosstalk between cell types is also crucial for myocardial growth. (Modified from Quijada et al., 2020).

2014). Several genes have been described to be important regulators of EMT. For example, Wt1 and Tcf21 are two important inducers of this process.

Although the epicardium of *Tcf21* null embryos develops normally, it is detached from the myocardium and EMT is impaired (Acharya et al., 2012; Braitsch et al., 2012). *Wt1* null embryos die with severe cardiac defects, like thinner myocardium and subepicardium and abnormal coronaries. They also lack EPDCs in the myocardium, which correlates with defective EMT (von Gise et al., 2011a; Moore et al., 1999).

Several pathways have been described to act downstream of EMT transcriptional activators.

A) Wt1 stimulates Wnt/β-catenin signalling which suggests a role of **canonical Wnt pathway** promoting epicardial EMT (von Gise et al., 2011).

B) **Retinoic acid (RA)** regulates EMT too. The RA synthetizing enzyme Raldh2 is expressed in the epicardium (Moss et al., 1998) and under the regulation of *Wt1* (von Gise et al., 2011). RA function in the epicardium is triggered through binding to retinoid X receptors (RXRs). This results in the activation of FGF2 and *Wnt9b* epicardial expression, which induces EMT. Wnt9b is one of the canonical Wnt pathway ligands, which suggests that RA acts in conjunction with this pathway regulating EMT (Merki et al., 2005). At the same time, it was described that *Tcf21* is regulated by RA (Braitsch et al., 2012). RA has not only a function in EMT but also in EPDC differentiation (Azambuja et al., 2010).

C) **Hippo pathway**. Epicardial Yap/Taz (Hippo signalling mediators) deficient mice present defective EMT and coronary vasculature formation (Singh et al., 2016).

- **Adequate orientation of cell division**: It was described that a specific mitotic spindle orientation is important for EMT. Cell divisions perpendicular to the basement membrane occur in the epicardial cells that undergo EMT, generating one daughter cell that invades the subepicardium and the other remaining in the epicardium. When this regulation is lost, EMT is impaired, as it happens in β-catenin and Numb mutants, in which adherent junctions are disrupted (Wu et al., 2010).

- **Growth factor-dependent regulation of EMT**: Not only TFs but also several signals have been reported to regulate epicardial EMT. **TGFβ** ligands are important inducers of EMT. TGFβ1, TGFβ2 and TGFβ3 are all expressed in the epicardium (Molin et al., 2003). When one of their receptors, *Alk5*, is deleted in the epicardium, the hearts present defective EMT and consequently, coronary defects and myocardial hypoplasia (Sridurongrit et al., 2008). Moreover, supplementation of TGFβ ligands induces EMT and SMC differentiation in epicardial explants (Compton et al., 2006).

PDGF (Platelet derived growth factor) signalling has been reported to induce EMT, and EPDC migration and specification (Mellgren et al., 2008; Smith, C.L. et al., 2011). This signalling pathway is composed by two receptors (PDGFRα and PDGFRβ) and four ligands (PDGFA, PDGFB, PDGFC, PDGFD) that act as homo- or heterodimers in their active form (Fredriksson et al., 2004). For example, PDGFB-PDGFRβ axis has been shown to be important for SMC and pericyte differentiation and migration

(Hellström et al., 1999).

FGF signals also regulate EMT and EPDC migration. On the one hand, it was reported that RA induces FGF2 and FGF9 in the epicardial cells, which then signal to activate FGF signalling in the myocardium. FGF from the myocardium triggers Sonic hedgehog (Shh) signalling pathway in the epicardium, which promotes EMT and coronary development (Lavine et al., 2006). On the other hand, myocardial FGF10 promotes EMT and EPDC migration (Vega-Hernández et al., 2011). The role of FGF signalling in EMT exemplifies how complex is the cross talk between the epicardium and the myocardium in order to coordinate and promote EMT.

- **EPDC migration into the subepicardium and myocardium: Nfatc1** (Nuclear factor of activated T-cells) is expressed in the PE, epicardium and EPDCs. Combs et al. (2011) showed that epicardial RANKL/NFATC1 pathway is crucial for the invasion of EPDCs into the myocardium by promoting the degradation of the ECM. In addition to its role as EMT inducer, **TGFβ** also promotes EPDC migration (Craig et al., 2010).

MRTFs (myocardin-related transcription factors) were described as TFs that control the motility of EPDCs. MRTFs are translocated into the nucleus in response to both TGFβ signalling and cell contact disassembly, which triggers the cell motility program in EPDCs (Trembley et al., 2015).

Myocardial signals, such as **thymosin-β4**, are also essential to attract EPDCs (Smart et al., 2007).

3.3) The epicardium as a source of cells

After EMT, EPDCs populate the underlying subepicardium and myocardium to become part of the coronary vasculature or the fibrous skeleton of the heart. They also migrate and contribute to the formation of the *annulus fibrosus* and atrioventricular valves (Dettman et al., 1998; Gittenberger-de Groot et al., 1998; Männer, 1999). These diverse contributions are enabled because EPDCs have the potential to give rise to several cardiovascular cell types. They mainly contribute to fibroblasts, pericytes and SMCs, but also to a subset of endothelial cells (ECs). Whether they can give rise to CMs is something more controversial. Nevertheless, all of this will be addressed in more detail in this chapter.

What drives the epicardial diversification towards the different lineages derived from the EPDCs? Are external cues governing the specification of a common multipotent progenitor into the different cell types (Dettman et al., 1998)? Or is the epicardium heterogeneous and certain cells can give rise to certain lineages? (Mikawa and Fischman, 1992; Mikawa and Gourdie, 1996). This topic has generated some debate in the last few years. There is some evidence that suggests that at least some EPDC fates are already determined in the PE. Firstly, it was reported that there is not complete overlap of the different epicardial cell markers in the epicardium or PE. For example, *Sema3d* and *Scx* expression are only partially co-expressed with *Wt1* and *Tbx18* in the PE and are pre-specified into EC fate (Katz et al., 2012). Secondly, Acharya and colleagues (2012) suggested that there is a gradual loss of multipotency in the epicardium and that EPDC specification occurs around the time of EMT. In contrast, a recent report by Lupu et al. (2020) claims that all PE and epicardial cells express the different epicardial markers and

that EPDC fate is determined after EMT. They suggest that EPDC fate must be determined in response to extrinsic cues (Lupu et al., 2020)..

Lineage tracing experiments have allowed to follow EPDC fate and identify the cell types that derive from the epicardium (Figure 4):

3.3.1) Fibroblasts, pericytes and smooth muscle cells

Epicardial cells are a major source of cardiac fibroblasts and SMCs during heart development and a binary fate decision is thought to control if the epicardial cell gives rise to one of these cell types or the other. Several studies suggest that Tcf21 drives the transition towards fibroblasts (Acharya et al., 2012; Braitsch et al., 2012). *Tcf21* null hearts have few fibroblasts while SMC are still present. In fact, an accumulation of these cells can be observed in the subepicardium of these mutant hearts (Braitsch et al., 2012). This suggests an aberrant EPDC differentiation. Although the exact mechanism needs to be elucidated, RA is involved in this specification. RA promotes *Tcf21* expression and inhibits SMC differentiation. RA supplementation of chick hearts results in less SMCs, while RA deprivation causes an increase in their number (Braitsch et al., 2012). Moreover, epicardial Hippo pathway also promotes epicardial to fibroblast transition, promoting high epicardial RA levels (Xiao et al., 2018).

On the other hand, PDGF receptors (PDGFRα and PDGFRβ) are also involved in the fibroblast/SMC cell fate decision. Initially, both receptors are expressed in the epicardium but their expression becomes distinct later in development and they end up contributing to different cell types (Mellgren et al., 2008; Smith, C.L. et al., 2011). PDGFRα-expressing EPDCs give rise to fibroblasts and epicardial-specific deletion of PDGFRα results in a depletion of cardiac fibroblasts, while SMC are not affected (Smith, C.L. et al., 2011). On the other hand, PDGFRβ deletion affects SMC specification and migration (Mellgren et al., 2008).

The Notch pathway was described to be important for SMC differentiation (Grieskamp et al., 2011; Del Monte et al., 2011). The epicardial impairment or overexpression of this pathway results in defective or premature SMC differentiation respectively (Grieskamp et al., 2011).

One remaining question is the timing of EPDCs differentiation into SMCs. Signalling cues could promote their maturation once they reach the coronary arteries or they could become differentiated into SMCs just after EMT and continue migrating as such. A recent study using clonal analysis and lineage tracing has reported that SMCs in the mouse derive from epicardial-derived pericytes that differentiate into SMCs at arterial remodelling zones in response to Notch3-Jagged1 (in pericytes and ECs respectively) signalling (Volz et al., 2015). They also propose that PDGFRβ induces the epicardial to pericyte transition at the surface of the heart. Therefore, this would be in agreement with the first hypothesis, although the commitment to the pericyte/SMC fate would take place early.

In addition to their role as “intermediate-state” cells that give rise to SMCs, epicardial derived pericytes are required for the stability and growth of the coronary plexus (Armulik et al., 2011). Mutations that affect pericyte biology, as those reported in the epicardial-specific MRTFs mutant mice,

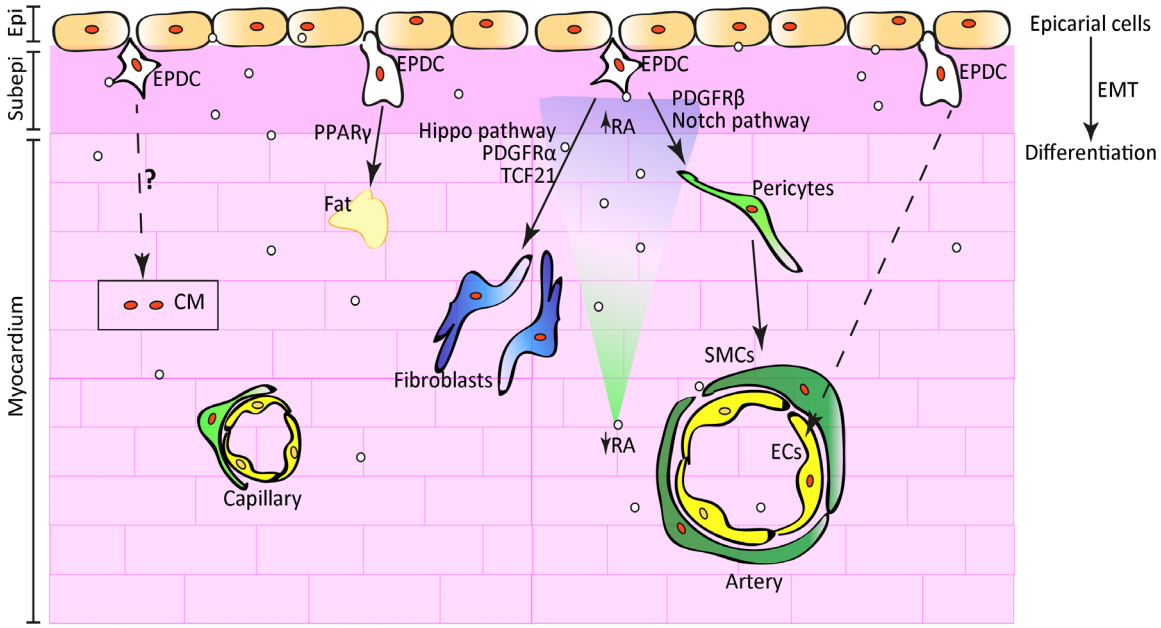

Figure 4. Cellular contribution of the epicardium during cardiac development. Some epicardial cells delaminate from the epicardium and undergo epithelial-to-mesenchymal transition (EMT). EPDCs (epicardium-derived cells, their nuclei depicted in red) differentiate into fibroblasts (blue cells), pericytes (light green cells), and smooth muscle cells (SMCs, dark green cells). In this process, TCF21, PDGFRα and Hippo pathway are important for fibroblasts specification while PDGFRβ and Notch pathway for pericytes and SMCs. High and low retinoic acid (RA) levels also regulate fibroblast (high levels, blue) and SMC (low levels, green) differentiation respectively. EPDCs also give rise to fat and to a small proportion of endothelial cells (ECs, yellow cells). Its contribution to cardiomyocytes (CM, pink cells) is controversial. EPDCs differentiation and paracrine molecules (white circles) that promote epicardium-CM, ECs-Epicardium crosstalk, are essential for myocardial growth and coronary vasculature development. Epi: epicardium; Subepi: subepicardium

result in severe cardiac defects, as subepicardial haemorrhages and reduced vascular integrity (Trembley et al., 2015).

3.3.2) Endothelial cells

The origin of ECs has been controversial. Early studies in avian models suggested that the epicardium could give rise to ECs and endocardial cells (Guadix et al., 2006; Mikawa and Fischman, 1992; Mikawa and Gourdie, 1996; Perez-Pomares et al., 2002a). The work of Katz et al. (2012) shed some light on this issue, suggesting that at least two subsets of PE cells can indeed give rise to coronary ECs and endocardium: the ones that express *Sema3d* and/or *Scx*. Singh and colleagues (2016) reported an involvement of Hippo pathway in the Sema3d+ PE subset giving rise to ECs. On the other hand, Lupu and colleagues (2020) proposed that these ECs do not derive from the PE but from cells in the adjacent septum transversum that also express *Sema3d* and *Scx*. Further research with *Sema3d* and *Scx* conditional mutants is needed in order to determine the origin of these ECs. Furthermore, in the lineage tracing experiments using $Wt1^{Cre}$, labelling of ECs could be due at least partially to *Wt1* expression in ECs (Rudat and Kispert, 2012).

It must be said that, in any case, the contribution of the epicardium to coronary ECs and endocardium is minor when compared to other sources, like sinus venosus and endocardium.

3.3.3) Adipose tissue

Lineage tracing using $Wt1^{Cre}$ and $Tbx18^{Cre}$ revealed a contribution of the epicardium to cardiac adipocytes (Chau et al., 2014; Liu et al., 2014; Yamaguchi et al., 2015). After EMT, adipocyte specification is controlled by the activation of the peroxisome proliferator activated receptor gamma (PPARγ) as reported by Yamaguchi et al. (2015).

3.3.4) CMs

Several reports have proposed that epicardial cells contribute to cardiomyocytes. Several studies reported the presence of *Wt1*-derived or *Tbx18*-derived CMs in the developing heart (Cai et al., 2008; Zhou et al., 2008). However, later it was demonstrated that both *Tbx18* is expressed in CMs and that $Wt1^{Cre}$ contribution to cardiomyocyte labelling was independent of its epicardial labelling activity (Christoffels et al., 2009; Rudat and Kispert, 2012; Villa del Campo et al., 2016) which made controversial the contribution of the epicardium to CMs. Katz and colleagues (2012) did show that *Sema3d* and *Scx* lineages could give rise to a small proportion of CMs. Although there might be species-related differences regarding to EPDCs contribution and this might be different in the mouse, experiments in either chick or zebrafish have failed to shown that cardiomyocytes can derived from the epicardium (Männer, 1999; Kikuchi et al., 2011). Therefore, nowadays, the consensus view is that this contribution, if any, is minor.

3.4) The epicardium as a paracrine signalling producer and receptor

Not only does the epicardium contribute with cells to cardiac development but also with signals. Non-cell autonomous communication between the epicardium and the myocardium and *vice versa* is essential for proper myocardial growth and coronary vasculature formation. Adequate endothelial-epicardial signalling is also crucial. In this chapter, we will focus on some of the paracrine molecules involved in this communication (Figure 3).

3.4.1) Epicardium-CM communication

The epicardium promotes myocardial growth by the secretion of different paracrine molecules.

In addition to activating EMT and EPDC differentiation, **RA** also has a role as mitogenic agent that functions in a non-cell autonomous way (Chen et al., 2002). Mutants in RA pathway present thinner myocardial walls and coronary vasculature defects (Chen et al., 1998; Merki et al., 2005).

Indeed several **FGF** members have been described as important signals in this epicardium-CM crosstalk. Lavine and colleagues (2005) showed that FGF9 is expressed in the epicardium and that through FGFR1 and FGFR2 (expressed in the CMs) promotes CM proliferation and vascular formation.

FGF16 might also be involved in this process, since knockout mice for this factor, although viable, also present decreased embryonic CM proliferation (Hotta et al., 2008). Other components of the family, like FGF10, are expressed in the myocardium itself and promote CM-epicardial communication. Vega-Hernández et al. (2011) reported that FGF10 signals to the epicardium binding FGFR1 and FGFR2. In response, the receptors promote EPDC migration into the myocardium and CM proliferation.

Furthermore, erythropoietin and its receptor are both expressed in the epicardium and they have been shown to be important for myocardial growth and coronary vasculature formation (Wu et al., 1999). In addition, it was proposed that RA induces hepatic erythropoietin that activates the secretion of epicardial IGF2, which promotes CMs proliferation (Brade et al., 2011; Li et al., 2011).

In addition to its role in SMC differentiation, epicardial **Notch** pathway has a function on the myocardium. Deletion or overexpression of *Notch1* in the epicardium provokes alterations in CM proliferation and in the thickness of the resulting myocardium (Del Monte et al., 2011).

3.4.2) Epicardium-EC communication

The epicardium is important for coronary vasculature development through secreted chemokines that regulate coronary vessel patterning.

CXCL12 is expressed in the epicardium and in mural EPDCs. The secretion of this chemokine is sensed by the receptor CXCR4 in ECs and this promotes capillary and coronary artery maturation (Cavallero et al., 2015).

Shh signalling also controls blood vessel growth inducing the expression of *Vegfa*, *Vegfb* and *Vegfc*, members of the Vascular endothelial growth factor (**VEGF**) family (Lavine et al., 2006). Moreover, *Vegfc* epicardial expression is important for proper development of the dorsal coronaries of the heart (Chen et al., 2014b).

3.5) The epicardium as an ECM secreting structure

The ECM is also essential for cardiac morphogenesis. It provides mechanical support for the cells that compose the growing heart and also allows the communication between them (reviewed in Lockhart et al., 2011). The developing heart contains: hyaluronan, proteoglycans, collagens, elastin, fibrillin, tenascin, fibronectins and laminins. Both the epicardium and fibroblasts have been shown to be important producers of ECM. ECM secreted by fibroblasts was described to modulate the proliferation, apoptosis, migration and differentiation of other cell types (Hortells et al., 2019).

3.6) The epicardium in response to injury and cardiac regeneration

Although the response to an injury like myocardial infarction (MI) in the adult mammalian heart is limited, other organisms like zebrafish retain their cardiac regeneration capacity throughout life (Gonzalez-Rosa et al., 2011; Poss et al., 2002). Surprisingly, mammals are born with a similar capacity to

regenerate their hearts, but they lose it after birth (Porrello et al., 2011; Soonpaa et al., 1996). In these contexts of response to injury and regeneration, the epicardium re-expresses fetal genes and increases its thickness (Braitsch et al., 2013; Gonzalez-Rosa et al., 2011; Lepilina et al., 2006; Porrello et al., 2011; Zhou et al., 2011). However, epicardial reaction after injury correlates with the regeneration potential. In the non-regenerative adult heart, the epicardium undergoes EMT but EPDCs do not infiltrate into the injured area but secrete paracrine molecules that promote angiogenesis (Zhou et al., 2011). The epicardial response in this case also modulates the inflammation regulating neutrophil and T-regulatory cells influx (Huang et al., 2012; Ramjee et al., 2017). Unlike in the adult mammalian heart, after a MI in zebrafish, EPDCs do migrate to the injured myocardium and differentiate into myofibroblasts and perivascular cells that support CM growth and promote angiogenesis (González-Rosa et al., 2012). In neonatal mice, after EMT, the resulting fibroblasts infiltrate into the subepicardium and the injured area (Mizutani et al., 2016). ECM production and paracrine signalling are also essential for cardiac regeneration. In zebrafish, the elimination of epicardial RA leads to defective CM proliferation and regeneration (Kikuchi et al., 2011). In addition, similar to their function during development, epicardial FGF, IGF, PDGF and VEGF signalling also stimulates CM proliferation and coronary vessel formation (Huang et al., 2013; Karra et al., 2018; Kim et al., 2010; Lepilina et al., 2006).

Coronary vasculature

In order to understand the spatiotemporal development of coronary blood vessels, it is important to mention that, in the mouse, the arteries and veins are located in two different locations. While arteries are deep in the myocardium, the veins are almost at the surface of the heart, in the subepicardium. This is different in humans, where both arteries and veins are found in the subepicardium (Sharma et al., 2017).

But, how are these coronary blood vessels formed? For coronary vasculature development, three processes are needed: vasculogenesis, angiogenesis and arteriogenesis. The first is the specification and differentiation of endothelial cells from mesodermal precursors and the formation of a primitive vascular network. Angiogenesis is the growth of blood vessels from the pre-existing vasculature by EC proliferation and migration, followed by remodelling and maturation of the vascular network. Arteriogenesis is the maturation of the coronary vasculature via the recruitment of SMCs and pericytes.

Vasculogenesis and angiogenesis

What is the origin of the endothelial precursor cells that contribute to vasculogenesis in the heart? We mentioned the **PE**-contribution, and that *Sema3d* and *Scx* lineages give rise to subsets of ECs in the developing coronaries (Katz et al., 2012). However, a majority of coronary ECs derive from the **sinus venosus** (SV) and the **endocardium**, and they seem to do so in a complementary fashion (Red-horse et al., 2010; Wu et al., 2012; Chen et al., 2014b). While SV-derived ECs give rise mainly to the dorsal and ventro-lateral coronaries, the endocardium contributes to coronaries in the septum

and mid-center of the ventral side of the heart (Chen et al., 2014b; Zhang et al., 2016). In the first study, Chen and colleagues used *Apj*^{Cre} (Apelin receptor), *Nfatc1*^{Cre} and *Sema3d*^{Cre} to trace the lineage of the SV, endocardium and PE derived ECs, respectively. However, the *Nfatc1* lineage also contributes to the SV, so *Npr3-CreER* (natriuretic peptide receptor 3) was later proposed as a better line to trace endocardium-derived ECs (Zhang et al., 2016). Furthermore, recently a fourth source of coronary ECs was proposed. Plein et al. (2018) described yolk sac-derived erythromyeloid progenitors that migrate into the heart and incorporate to the pre-existing vasculature.

The first coronary ECs in the mouse embryo sprout out from the SV at E11.5 and migrate to the atrioventricular groove, on the dorsal side of the heart, where they form a primitive vascular plexus (Lavine et al., 2006; Red-horse et al., 2010). This plexus expands towards the apex and laterally, towards the ventral side of the heart. These ECs populate first the subepicardium and later migrate to the compact myocardium (Chen et al., 2014b). Endocardium-derived ECs, on the contrary, appear first in the ventral interventricular groove region and are recruited through the formation of blood islands between E11 and E14 (Red-horse et al., 2010). These are endothelial spheres with erythrocytes on the inside that bud off from the endocardium. These endocardium-derived ECs populate predominantly the IVS and ventral aspect of the heart, where they meet and fuse with the SV-derived ECs that come from the dorsal side (Chen et al., 2014b; Zhang et al., 2016). PE-derived cells can be found either in the ventral or dorsal side of the heart, but almost none in the septum (Chen et al., 2014b).

While **VEGFA** signalling in the myocardium is important for endocardial-derived EC migration (Wu et al., 2012), **VEGFC** in the epicardium guides the migration of the subepicardial coronary plexus (Chen et al., 2014b). Furthermore, **angiopoietins** are endothelial growth factors expressed in the myocardium that direct coronary development (Ward et al., 2004a, b). **Notch** signalling is also essential for angiogenesis (reviewed in Potente and Carmeliet, 2017). **Hypoxia** might regulate cardiac angiogenesis too (Smart et al., 2009; Tomanek et al., 1999).

Arteriogenesis and artery remodelling

As a result of this complex angiogenic process, by E14.5 the dorsal, and by E15.5 the ventral sides of the heart are covered completely with an immature plexus that will undergo arteriovenous differentiation and an intense remodelling process to give rise to the future arteries, veins and capillaries (Red-horse et al., 2010) (Figure 5). Regarding arteriovenous differentiation, recent findings have shown that increased levels of VEGF and Notch signalling in pre-arterial capillary ECs lead to a reduction in metabolic and cell-cycle activity that promotes their incorporation into arteries (Luo et al., 2021). For the remodelling and maturation of the coronary plexus, the recruitment of SMCs and pericytes is also essential. In addition to the epicardium, other progenitor cells have been proposed to give rise to mural cells that support the growth of coronary vessels. Chen et al. (2016) showed that endocardial cells, through a process of EndoMT, give rise to PDGFRα+ PDGFRβ+ mesenchymal cells in the cushions of the cardiac valves. These mesenchymal cells migrate into the ventricular myocardium and differentiate into pericytes and SMC. As mentioned before, other sources of SMCs are the SHF and the preotic cNCCs (Arima et al., 2012). Wnt pathway mediates the migration and differentiation of the

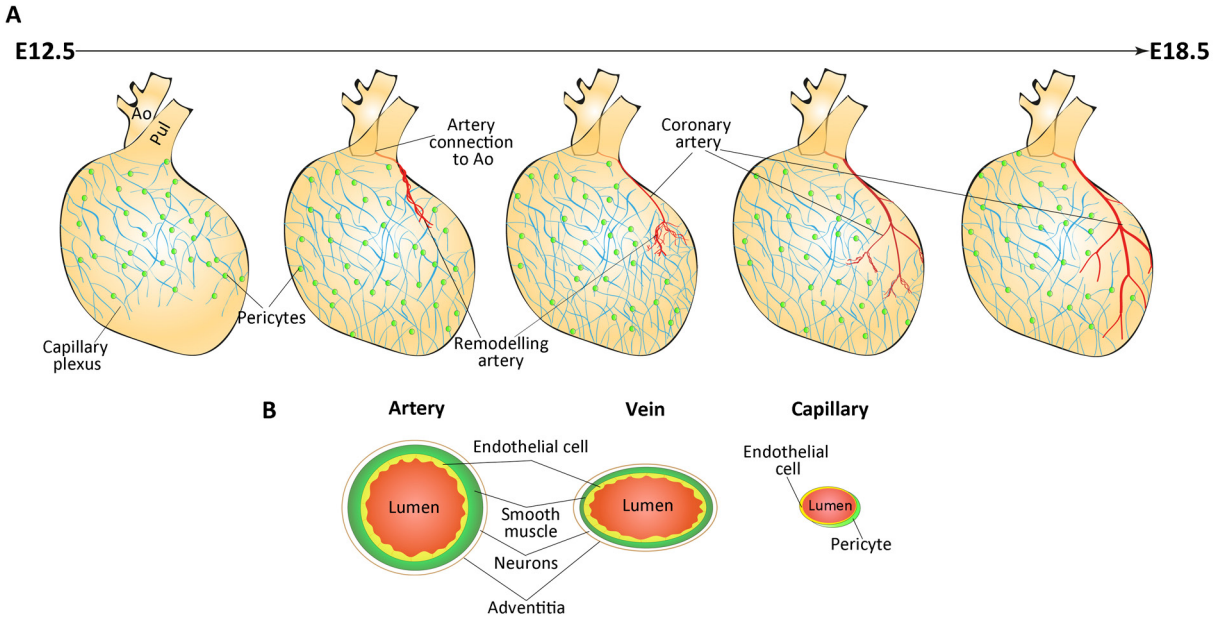

Figure 5. Coronary artery development, remodelling and maturation. (A) An immature capillary plexus with pericytes expands and colonises the subepicardium and myocardium. At E13.4-E14.5, the plexus attaches to the base of the aorta (Ao) and starts receiving blood flow. This process triggers arterial remodelling and maturation. (B) Schematic representation of the cellular components of coronary arteries, veins and capillaries (Modified from Sharma et al., 2017).

endocardium-derived SMCs while Endothelin1-Endothelin1 receptor interaction is necessary for cNCCs differentiation (Arima et al., 2012; Chen et al., 2016). As explained in more detail in the chapter about the epicardium, for epicardial-derived arteriogenesis, correct EMT, EPDC migration and pericyte differentiation at arterial remodelling zones are needed.

Another step essential for the remodelling of the coronary arteries is their connection to the systemic arterial blood flow at E13.5-E14.5 in the mouse (Figure 5A). The immature coronary vessels grow from the plexus towards the base of the aorta, where they connect to its lumen through the formation of two stems (Tian et al., 2013). These two vessels, in response to perfusion, express arterial markers such as Jagged1, and are remodelled into the left and right coronary arteries (Volz et al., 2015). Incorrect connection of the left coronary artery to the pulmonary artery can be lethal. In humans, this condition is known as ALCAPA (anomalous left coronary artery from the pulmonary artery) and requires surgery soon after birth (Wesselhoeft et al., 1968). The exact mechanism that drives stem formation in the aorta and not the pulmonary artery is not known. However, different studies suggest that VEGFC-VEGFR2/3, CXCL12-CXCR4, BMP and CMs at the base of the aorta regulate this process (Dyer et al., 2014; Chen et al., 2014a; Ivins et al., 2015). The three first, attract the vessels to the OFT, while some SHF-derived CM seem to localise where the future stems will be formed and maybe direct EC connection to the lumen of the aorta that forms sprouts (Chen et al., 2014a). Moreover, cNCC contribution to this region somehow controls this process too, since their ablation produces alterations in the formation of the orifices (Arima et al., 2012).

The resulting vasculature is composed of capillaries supported by pericytes, and arteries and veins with SMCs (Sharma et al., 2017) (Figure 5B). While SMC coverage in veins is sparser, in the arteries, in the regions under higher pressure, the media layer is composed by several layers of SMCs. Moreover, the adventitia layer is the outermost part of the arteries and is composed mainly by fibroblasts but also by dendritic cells, macrophages, nerves, pericytes and *vasa vasorum* ECs (Stenmark et al., 2013). We have mentioned and explained the PE-origin of the mayority of myocardial fibroblasts. However, lineage tracing experiments suggest that fibroblasts also have an endothelial origin, since some Tie2-derived cells express fibroblast markers. Probably, they derive from the endocardium after an EndoMT process, as the fibroblasts that compose cardiac valves (Ali et al., 2014; Moore-Morris et al., 2014).

After birth, the coronary vasculature needs to adapt to the increased myocardial thickness due to CM hypertrophy. In the first three weeks, capillary density and SMC-covered arteries increase three to fourfold and tenfold respectively (Luttun and Carmeliet, 2003).

Cardiac lymphatics

Lymphatics are important for the maintenance of fluid homeostasis, immune surveillance and fat absorption (Liu and Oliver, 2019). Indeed, defective lymphatics result in lymphedema, obesity, hypertension and cancer (Alitalo and Carmeliet, 2011; Vaahtomeri et al., 2017).

The Lymphatic endothelial cells (LECs) are characterized by the expression of Prospero homeobox protein 1 (**Prox1**), Lymphatic vessel endothelial hyaluronan receptor 1 (**LYVE1**), **podoplanin**, **VEGFR3**, **VEGFR2**, **CD31**, **CD144** and **Tie2** (Flaht-Zabost et al., 2014; Karunamuni et al., 2010).

How are lymphatic vessels formed?

Initially two hypotheses were proposed: Sabin's centrifugal model suggested a venous origin for lymphatic endothelium (Sabin, 1902). On the other hand, Huntington and McClure (1910) proposed the centripetal model in which mesenchymal-derived-cells were the source of lymphatic vessels. In both zebrafish (Yaniv et al., 2006) and mouse (Srinivasan et al., 2007) the most accepted model now is Sabin's, where lymphatic endothelial cells (LECs) bud from the cardinal vein and give rise to most of the lymphatic vasculature. But, when and how does this developmental process begin?

Stone and Stainier (2019) proposed that most LECs derive from somite-derived vascular precursors that transiently colonize embryonic veins. In the E9.5 mouse embryo, some ECs of the cardinal vein start to express Prox1, the master regulator of lymphatic specification and maintenance (Wigle and Oliver, 1999), *Sox18* and COUP-TFII expression is also important for Prox1 induction and lymphatic specification (François et al., 2008; Srinivasan et al., 2010). In response to VEGFC signalling, at E10.5 LECs start to bud off from the cardinal vein and coalesce forming primitive lymph sacs that give rise to most of the embryonic lymphatic vasculature via LEC sprouting and proliferation (van der Putte, 1975; Karkkainen et al., 2004; Hägerling et al., 2013).

Although most lymphatics have a somite/venous origin, alternative and complementary sources have been proposed in different organs. For example, in the skin, both venous and non-venous contribution have been reported (Martinez-Corral et al., 2015); mesenteric lymphatics derive from the veins but also from hemogenic ECs (Stanczuk et al., 2015). Cardiac lymphatics arise also from different sources, but this is something that will be addressed with more detail below.

An important question of early lymphatic specification is how LECs originate just from the dorsal side of the cardinal vein. In zebrafish, Wnt5b was proposed to be secreted by the underlying endoderm and control LEC induction (Nicenboim et al., 2015). In mice, RA has also been proposed to regulate this process. Asymmetric levels of RA in ventral-dorsal sides of the cardinal vein correlate to complementary expression of Raldh2 and Cyp26b1 (an enzyme responsible for RA degradation), respectively. When this equilibrium is modified, lymphatic sac formation is altered. This suggests that low levels of RA are needed in the cardinal vein for proper lymphatic specification (Bowles et al., 2014).

Paracrine molecules that guide lymphatic development are also really important. As mentioned before, **VEGFC** is essential for the migration of LECs. In fact, LECs are specified in the cardinal vein of *Vegfc* null mutants, but they never delaminate (Karkkainen et al., 2004), and *Vegfc* hetererozygous mutant mice develop lymphedema due to their lymphatic defects (Gordon et al., 2013). **VEGFD** is another VEGF family member involved in lymphangiogenesis. In zebrafish, VEGFD is essential for facial lymphangiogenesis (Bower et al., 2017) but *Vegfd* mutant mice survive and only mild defects in lung and dermal lymphatics have been reported (Baldwin et al., 2005; Paquet-Fifield et al., 2013). Nevertheless, in these studies cardiac lymphatics where not specifically characterized, so a role in this organ cannot be excluded. What is evident is that in different organs both VEGFC and VEGFD can cooperate to control lymphatic development and may compensate for each other (Astin et al., 2014; Bower et al., 2017; Haiko et al., 2008; Nurmi et al., 2015). In mice, VEGFC binds VEGFR2, and both ligands bind VEGFR3, which is expressed in LECs and blood ECs (Baldwin et al., 2001; Kukk et al., 1996). *Vegfr3* mutant mice die at E10.5 due to VEGFR3 function in blood vasculature development (Dumont et al., 1998). This function is independent of VEGFC and VEGFD, since double knockouts for these ligands do not have lymphatics but do develop blood vasculature (Haiko et al., 2008). In addition to its role in blood vasculature, VEGFR3 is necessary for LEC proliferation, sprouting and migration (Karkkainen et al., 2001), and heterozygous *Vegfr3* mutant mice develop severe lymphedema (Irrthum et al., 2000). VEGFR3 signaling is also crucial for the maintenance of the lymphatic vessels. When VEGFC and VEGFD are sequestered with a VEGFR3-trap, apoptosis is induced in lymphatics of many organs, including the heart, provoking their regression (Mäkinen et al., 2001).

VEGFC acts in a paracrine fashion so, what cell types are responsible for its secretion? Initially, mesenchymal cells near the cardinal vein are the ones that produce the ligand (Karkkainen et al., 2004; Kukk et al., 1996). Macrophages also produce VEGFC and VEGFD (Schoppmann et al., 2002) and defective macrophage-lymphatic association leads to decreased density of the dermal lymphatic network (Lee et al., 2014). SMCs and fibroblasts have also been proposed as sources of VEGFC. In the adult intestine, SMCs are the main source of VEGFC (Nurmi et al., 2015), while *in vitro* studies showed that fibroblasts expressed VEGFC and promoted lymphangiogenesis (Gibot et al., 2016). In the heart,

another source is the epicardium, although only its function regarding coronary blood vasculature development has been studied (Chen et al., 2014b).

Other paracrine molecules with described lymphangiocrine properties are FGF2, VEGF, angiopoietin 1 and 2, EGF and HGF. Some of them, like FGF2, angiopoietin 1 and HGF might induce lymphangiogenesis by inducing VEGFC and VEGFD signalling (reviewed in Vaahtomeri et al., 2017).

Can we extrapolate the extensive knowledge generated regarding embryonic lymphatic development to cardiac lymphangiogenesis? What do we know about cardiac lymphatics?

Cardiac lymphatics

In the heart, lymphatics appear at E12.5-E13.5 along the great arteries and SV, as if they were migrating towards the base of the heart (Flaht et al., 2012; Karunamuni et al., 2010) (Figure 6). At E14.5, the dorsal subepicardial region of the ventricles is colonised by lymphatics and about half day later, the ventral side. They continue migrating through the subepicardium towards the apex of the heart and laterally on both sides (Klotz et al., 2015). Two weeks after birth, development and maturation of cardiac lymphatics is completed (Klotz et al., 2015). As opposed to what happens in coronary blood vasculature development, mice are born just with a subepicardial lymphatic plexus and, only after birth, they develop lymphatics in the myocardium and subendocardium (Flaht-Zabost et al., 2014). In the adults, the main lymphatic branches run around the main coronary arteries and veins (Flaht-Zabost et al., 2014). Cardiac contraction and the smooth muscle coverage of the collector lymphatic vessels allow lymph flow return towards the venous system at the junction of the thoracic duct and subclavian vein (Brakenhielm and Alitalo, 2019).

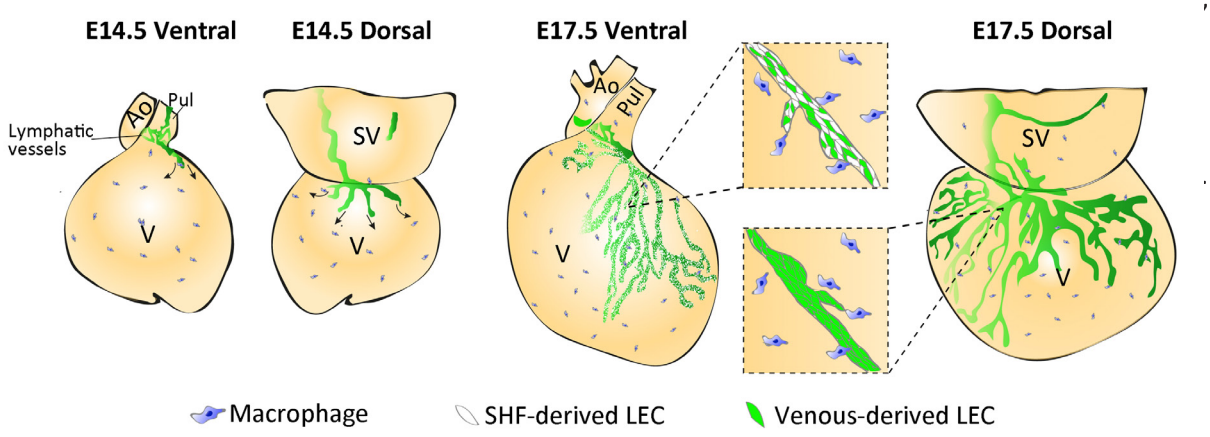

Figure 6. Cardiac lymphatic vasculature development of the murine heart. Schematic representation of two stages of cardiac lymphatic development. Lymphatic endothelial cells (LECs) appear on the heart at E12.5-E13.5 at the sinus venosus (SV) and great arteries area. Lymphatic vessels migrate towards the heart and reach its surface on the dorsal side of the ventricles at E14.5. Cardiac lymphatics continue growing through the subepicardium towards the apex of the heart and laterally on both sides (E17.5). Most LECs have a venous origin (depicted in green), but the Second Heart Field (SHF) gives rise to LECs (depicted in white) that contribute to the formation of the ventral lymphatic vasculature. Macrophages also promote cardiac lymphatics maturation and growth. Ao: aorta; Pul: pulmonary artery; SV: sinus venosus; V: ventricles.

As it occurs in the cardinal vein (Bowles et al., 2014), it seems that in the heart **RA** is important for LEC specification and maturation too. Low levels of RA in the AMC layer at the base of the pulmonary artery and high levels in the epicardium are needed for normal cardiac lymphatic patterning (Lioux et al., 2020). In addition, macrophages also contribute to cardiac lymphatic remodelling and maturation (Cahill et al., 2021). **VEGFC** and/or **VEGFD** are involved in cardiac lymphatic maintenance (Mäkinen et al., 2001), but whether they are also involved in their development has not been studied. Little is known either about the cell types or mechanisms that govern cardiac lymphatic development. We are in need of this knowledge, so we could control or promote their growth in pathological situations, for example, after an MI.

Rüdbeck first described cardiac lymphatics in the 17th century. However, not until recently they have been widely studied. Nowadays, they have been shown to be important in response to MI (Henri et al., 2016; Klotz et al., 2015; Liu et al., 2020; Vieira et al., 2018), congestive heart failure (Witte et al., 1969), atherosclerosis (Lim et al., 2013; Milasan et al., 2016, 2019), cardiac transplantation (Rinda Soong et al., 2010) and cardiac regeneration in zebrafish (Gancz et al., 2019; Harrison et al., 2019; Vivien et al., 2019), and mice (Liu et al., 2020). Furthermore, Liu et al. (2020) have recently shown that cardiac lymphatics promote cardiomyocyte proliferation and survival during cardiac development and adult life, through secreting paracrine molecules. Therefore, extensive evidence supports that cardiac lymphatics play an important role for cardiac development and repair.

Meis transcription factors

The ability of TFs to control gene expression is essential during development, orchestrating and regulating the different processes. We can find Myeloid ecotropic viral integration site (Meis) TFs, acting in this complex regulatory network. MEIS TFs are important regulators of embryonic development and cancer. In mammals, this family belongs to the TALE (Three amino acid loop extension) homeodomain-containing factors and is composed of three members: *Meis1*, *Meis2* and *Meis3* (Moskow et al., 1995; Nakamura et al., 1996; Oulad-Abdelghani et al., 1997). In order to understand their function, it is important to take into account that usually these TFs form dimers with Pbx proteins and, together, also form trimers with Hox and non-Hox factors (Chang et al., 1997; Jacobs et al., 1999; Mann and Affolter, 1998; Swift et al., 1998). This increases considerably the complexity of their regulatory capacity.

Meis1 is widely expressed in the embryo during development. It is present in the eyes and ears primordia, heart, lungs, gut, reproductive system, spinal cord and proximal domain of the forming limb (González-Lázaro et al., 2014; Hisa et al., 2004; Mercader et al., 1999; Williams et al., 2005). Similar to *Meis1*, *Meis2* expression is found in the heart, lungs, gut, reproductive system and limb bud. In addition, it is also expressed in the midbrain, forebrain and kidneys (Cecconi et al., 1997; Machon et al., 2015; Mercader et al., 1999; Oulad-Abdelghani et al., 1997; Williams et al., 2005). *Meis3* expression is mainly restricted to the hindbrain but later in development it is present in the heart, spleen and lung too (Nakamura et al., 1996).

A *Meis3*-deficient mouse model is not available, but studies in Xenopus and zebrafish suggest a role in neural anteroposterior patterning and neural crest cell invasion of the gut (Elkouby et al., 2010; Uribe and Bronner, 2015). *Meis1* null mice embryos do not survive beyond E14.5, as a consequence of defective hematopoiesis and severe hemorrhaging (Azcoitia et al., 2005; Hisa et al., 2004). *Meis1* deficiency causes eye malformations (Hisa et al., 2004), liver hypoplasia as well as brain, lung and kidney defects (Azcoitia et al., 2005; Hisa et al., 2004; Stankunas et al., 2008). Hisa et al. and Azcoitia et al. also reported vascular defects in these embryos, which could be due to a non-autonomous role of Meis1. Meis1 is essential for megakaryocyte and platelet development in the embryo and its mutation blocks the development of the lymphatic system, which needs platelets for the separation of the blood and lymphatic vasculatures (Carramolino et al. 2010). *Meis2*-deficient mice die at E14.5 too, showing smaller liver and hemorrhaging that could be the cause of embryonic lethality (Machon et al., 2015).

Despite *Meis1* and *Meis2* expression in the limb buds, none of the single knockouts show limb alterations and both need to be deleted to observe defects (Delgado et al., 2020). Redundancy between *Meis1* and *Meis2* has also been described during axial skeletal patterning (López-Delgado et al., 2021).

Moreover, both *Meis1* and *Meis2* mutant mice present severe cardiac abnormalities. *Meis1*-deficient hearts show ventricular septal defect and overriding aorta (OA), in which the aorta opens to both the right and left ventricle (Stankunas et al., 2008). *Meis2* null hearts have alterations in valves and show persistent truncus arteriosus (Machon et al., 2015). Although Machon and colleagues (2015) showed that *Meis2* defects could be due, at least in part, to the role of *Meis2* in cNCCs, we are in need of additional conditional mutants in order to dissect the exact function of these TFs in heart development. Muñoz-Martin et al (in preparation) have observed that CM-specific *Meis1* and *Meis2* deletion causes cardiac malformations as VSD, OA and atrial abnormalities, as well as alterations in the conduction system. However, these defects do not account for all the abnormalities described in *Meis1* and *Meis2* mutant hearts (Azcoitia et al., 2005; Hisa et al., 2004; Machon et al., 2015). Is it possible that these TFs are also playing a functional role in the other layers of the heart?

This is something that is worth looking at. It is essential to understand the role of these TFs, both for generating knowledge and for understanding their association with human diseases. In humans, Restless Legs Syndrome and cardiac conduction system defects have been associated with *Meis1* mutations (Butler et al., 2012; Pfeufer et al., 2010; Smith, J.G. et al., 2011; Spieler et al., 2014; Winkelmann et al., 2007); while *Meis2* mutations produce cleft palate, intellectual defects and septal defects in the heart (Crowley et al., 2010; Giliberti et al., 2020; Johansson et al., 2014; Louw et al., 2015).

OBJECTIVES

"Setting goals is the first step in turning the invisible into the visible."
~ Tony Robbins

Previous studies have shown the involvement of MEIS transcription factors in cardiogenesis, however, tissue-specific conditional mutants to dissect the involvement of these genes in the different layers of the heart are lacking. In this thesis, we addressed the function of *Meis1* and *Meis2* in the epicardium and its derivatives. With this purpose, we established the following main objectives:

1) Study the expression pattern of MEIS1 and MEIS2 in the epicardium during cardiac development

2) Generate epicardial specific *Meis1* and *Meis2* conditional mutant mice to study the effect of their deletion on cardiac development and adult homeostasis.

3) Characterize the epicardial-derived cell populations upon *Meis1* and *Meis2* epicardial deletion.

4) Study the coronary vasculature of epicardial specific *Meis1* and *Meis2* conditional mutant mice.

5) Study the development of cardiac lymphatic vasculature of epicardial specific *Meis1* and *Meis2* conditional mutant mice.

6) Identify molecular pathways and mechanisms involved in Meis function in the epicardium.

MATERIALS AND METHODS

"Insanity: doing the same thing over and over again and expecting different results."
~ Albert Einstein

ANIMAL PROCEDURES

Mouse lines

Animals were handled in accordance with CNIC Ethics Committee, Spanish laws and the EU Directive 2010/63/EU for the use of animals in research. All mouse experiments were approved by the CNIC and Universidad Autónoma de Madrid Committees for "Ética y Bienestar Animal" and the area of "Protección Animal" of the Community of Madrid with reference PROEX 220/15. For this study, mice were maintained on C57Bl/6 background. The mouse strains used for the different purposes and experiments were:

1) MEIS function in the epicardium

In order to study the role of *Meis1* and *Meis2* in the epicardium, *Meis1*^{flox} (Unnisa et al., 2012) and *Meis2*^{flox} (Delgado et al., 2020) mouse lines were combined with *Wt1*^{Cre} (Wessels et al., 2012) or *Tbx18*^{Cre} (Cai et al., 2008). With these strategies exon 8 of *Meis1* and exon 3 of *Meis2* are conditionally excised upon Cre expression (Figure 11A). This results in a non-functional protein for MEIS1 or no protein for MEIS2. To be able to track *Wt1Cre* lineage+ cells, these alleles were also combined with *Rosa26*^{tdtmt} (Madisen et al., 2010). This line contains a STOP cassette flanked by loxP sites, followed by Tomato fluorescent protein in *Rosa26* locus. Upon Cre recombination, STOP cassette is excised and the fluorescent protein is expressed in the recombined cells and in their descendants.

When *Meis1/2* were deleted with *Wt1*$^{Cre/wt}$ (The Cre was always maintained in heterozygosity, from now on, these animals will be referred to as *Wt1*^{Cre}), mice of different genotypes were crossed depending of the objective. The females carried *Meis1*$^{flox/flox}$*; Meis2*$^{flox/flox}$ allele combinations or *Meis1*$^{flox/flox}$*; Meis2*$^{flox/flox}$*; Rosa26*$^{tdtmt/tdtmt}$. These females were crossed with males that were *Wt1*^{Cre}*; Meis1*$^{flox/flox}$*; Meis2*$^{flox/wt}$ or *Wt1*^{Cre}*; Meis1*$^{flox/wt}$*; Meis2*$^{flox/flox}$. Additionally, to obtain controls in which *Wt1Cre* lineage+ cells could be tracked, *Rosa26*$^{tdtmt/tdtmt}$ females were crossed with *Wt1*^{Cre} males. Resulting from these crosses, the following genotypes were used as controls and double homozygous conditional mutants (dKOs):

	dKO	Control
Without tracking	Wt1^{Cre}; Meis1$^{flox/flox}$; Meis2$^{flox/flox}$	Meis1$^{flox/flox}$; Meis2$^{flox/flox}$
		Meis1$^{flox/wt}$; Meis2$^{flox/flox}$
		Meis1$^{flox/flox}$; Meis2$^{flox/wt}$
		(*)
Tracking Wt1+ lineage cells	Wt1^{Cre}; Meis1$^{flox/flox}$; Meis2$^{flox/flox}$; Rosa26$^{tdtmt/wt}$	
		Wt1^{Cre}; Rosa26$^{tdtmt/wt}$

(*) We also used as controls the embryos with these three Meis1 and Meis2 allele combinations carrying Rosa26^{tdtmt} to have controls from the same litter for *Wt1Cre; Meis1*$^{flox/flox}$*; Meis2*$^{flox/flox}$*; Rosa26*$^{tdtmt/wt}$ dKOs.

Table 1. Genotypes used as controls and dKOs for *Meis1*^{flox}, *Meis2*^{flox}, *Rosa26*^{tdtmt} and *Wt1*^{Cre} allele combinations, with or without tracking *Wt1Cre* lineage+ cells

When the other epicardial driver *Tbx18*^{Cre} was used to delete *Meis* TFs, the same allele combinations for controls and dKOs were used but, in this case, the females were the ones carrying the Cre.

2) RALDH2 function in the epicardium

To address the hypothesis that *Raldh2* downregulation in Meis dKOs was responsible, at least partially, for the EPDCs phenotype, an epicardial-specific *Raldh2* conditional mutant line was generated. For that purpose, *Raldh2*$^{flox/flox}$ (Vermot et al., 2003) females were crossed with *Wt1*^{Cre}*; Raldh2*$^{flox/flox}$ males. *Raldh2*$^{flox/flox}$ embryos were used as controls, and *Wt1*^{Cre}*; Raldh2*$^{flox/flox}$ embryos as mutants.

To study the possible genetic interaction between *Meis* and *Raldh2* in the epicardium, *Meis1*$^{flox/flox}$*; Meis2*$^{flox/flox}$ or *Meis1*$^{flox/flox}$*; Meis2*$^{flox/flox}$*; Rosa26*$^{tdtmt/tdtmt}$ females were crossed with *Wt1*^{Cre}*; Raldh2*$^{flox/flox}$ males. Additionally, *Rosa26*$^{tdtmt/tdtmt}$ females were crossed with *Wt1*^{Cre} males. The phenotype of *Wt1*^{Cre}*; Meis1*$^{flox/wt}$*; Meis2*$^{flox/wt}$*; Raldh2*$^{flox/wt}$ or *Wt1*^{Cre}*; Meis1*$^{flox/wt}$*; Meis2*$^{flox/wt}$*; Raldh2*$^{flox/wt}$*; Rosa26*$^{tdtmt/wt}$ embryos was compared with controls *Meis1*$^{flox/wt}$*; Meis2*$^{flox/wt}$*; Raldh2*$^{flox/wt}$ *or Wt1*$^{Cre;}$ *Rosa26*$^{tdtmt/wt}$.

3) VEGFC function in the epicardium

To study the role of VEGFC in the epicardium and cardiac lymphangiogenesis, *Vegfc*$^{flox/flox}$ mice were crossed with *Wt1*^{Cre}*; Vegfc*$^{flox/wt}$ mice. Mutant *Wt1*$^{Cre;}$ *Vegfc*$^{flox/flox}$ (Vegfc-KO) embryos were compared to controls (*Vegfc*$^{flox/flox}$ or *Vegfc*$^{flox/wt}$). We thank Wanshu Ma and Mark Kahn for *Vegfc*$^{flox/flox}$ mice.

To study the effect of increased VEGFC levels in *Wt1 lineage*, *Wt1*^{Cre} males were crossed with *Eef1a1*^{VegfcGOF} females (Pichol-Thievend et al., 2018). Briefly, in this mouse line, Vegfc cDNA was inserted into the first intron of *Eef1a1* locus. However, *Vegfc* overexpression is prevented by a floxed neomycin-triple poly(A) cassette preceding Vegfc cDNA (Figure 7). Only upon Cre recombination, the cassette is excised and *Vegfc* is overexpressed in a conditional manner.

Figure 7. Schematic representation of Eef1a1VegfcGOF mouse line. A genetic construct including VEGFC cDNA was inserted in *Eef1a1* intron 1. Only upon Cre recombination, the preceding STOP cassette (neomycin-triple poly(A) cassette) is eliminated, and Vegfc is overexpressed.

4) VEGFD function in cardiac lymphangiogenesis

In the mouse, *Vegfd* gene (ENSMUST00000033751.7) is codified in chromosome X (15,361,718-15,404,535). To study the possible role of this gene in cardiac lymphangiogenesis, a new *Vegfd* knockout line was generated using CRISPR-Cas9 technology. Four sgRNAs against *Vegfd* were designed using CRISPOR web tool (Concordet and Haeussler, 2018): two sgRNAS to target intron 2 (A and B), and two to target intron 4 (C and D). The four of them were used simultaneously (Figure 8A). Their sequences are provided below:

A) TAGGTTAAGTTCCCATATAG TGG

B) GCGTCATGAAAAGCATGTCA GGG

C) ATGCCTGTATAATGGGTAA AGG

D) GTGCAACACATGTCTTTCTG AGG

With this strategy, we aimed to delete around 3.4 kb of *Vegfd* gene including exons 3 to 4 and intron 3, which correspond to VEGFD aminoacids 106 to 218. Taking into account that VEGFD "VEGF homologous domain" (VHD) is codified by aminoacids 98 to 206, with this strategy most of this domain, which is essential for the binding of VEGFD to its receptor, VEGFR3, would be deleted (Achen et al., 1998; Baldwin et al., 2001a, b).

We provided sgRNAs to CNIC Transgenesis Unit and they generated the mouse line. Briefly, the superovulation of ten 3 to 5-weeks old C57BL/6JCrl females was induced with the injection of 5 IU of PMSG hormone and, 48 hours later, with 5 IU of hCG hormone. Females were crossed with males C57BL/6JCrl and, the next morning, they were checked for positive plug. The oviducts were extracted from those females and they were placed in M2 medium (Sigma M7167-100 mL). They were treated with 350 µg/mL of hyaluronidase (Sigma H3884-100mg) in M2 medium for 2 minutes at 37ºC to release the oocytes. This process was helped by the careful pipetting of a glass capillary. The fertilised zygotes were selected based on the presence of the second polar body and two pronuclei. They were incubated at 37ºC with 5% CO_2/5% O_2 in Evolve-KSOM medium (Zenith Biotech ZEKS-050) until the pronuclear microinjection was performed. For the pronuclear microinjection an inverted microscope ZEISS AxioObserver D-1 with Nomarski optics was used. A glass capillary (LG uPipets Holding, LifeGlobal MPHL-30) and an automatic electronic microinjector FemtoJet (Eppendorf) were used to hold the zygotes and microinject the mix respectively. Then, 1-2 pL of 100 µg Cas9 protein (IDT Alt-R® S.p. HiFi Cas9 Nuclease V3, 1081060) and 0.305 µM of each sgRNA (A to D) (IDT Alt-R® CRISPR-Cas9 sgRNA) were injected to each zygote. Once injected, the embryos were washed with Evolve-KSOM medium and incubated in this medium at 37ºC and 5% CO_2/5% O_2 for two hours. After this time, the lysed embryos were discarded and the rest were incubated in Evolve-KSOM medium at 37ºC and 5% CO_2/5% O_2 overnight. The next morning, the two-cell embryos were transferred to pseudopregnant CD-1 females. For that, the embryos were injected through the infundibulum of the oviduct using a sterile glass capillary.

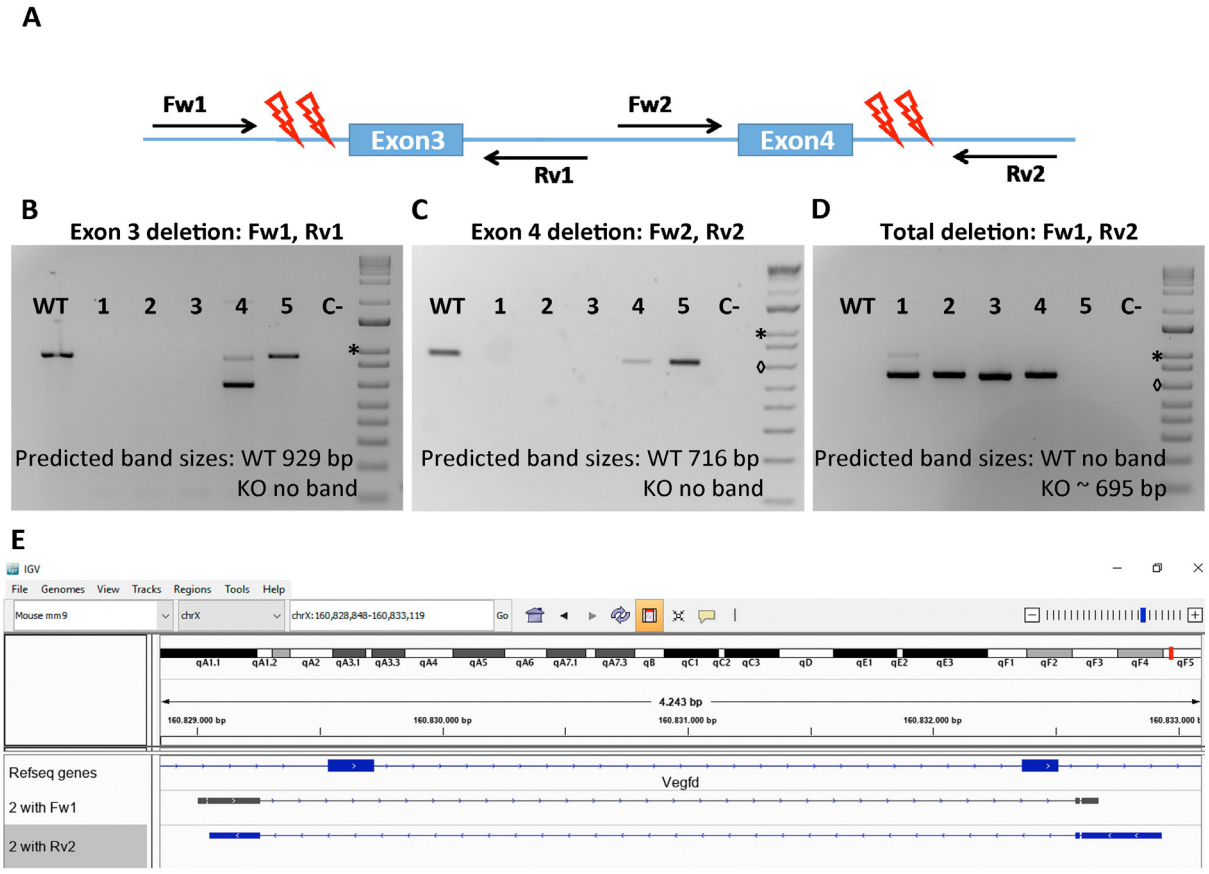

Figure 8. Generation and genotyping of *Vegfd* null mice. (A) Schematic representation of the strategy followed for the generation and genotyping of *Vegfd* null mice. Two sgRNAs were designed to target intron 2 and two to target intron 4 (red rays). The expected result was the deletion of 3.4 kb including exon 3, intron 3 and exon 4. The location and code for the genotyping primers are depicted with black arrows. (B-D) Genotypying of the first generation of *Vegfd* knockouts (1 to 5), wild type control (WT) and H2O negative control (C-). (B) PCR products for the detection of the deletion of Exon 3 using primers Fw1 and Rv1. (C) PCR products for the detection of the deletion of Exon 4 using primers Fw2 and Rv2. (D) PCR products for the detection of the total deletion of exon 3, intron 3 and exon 4. ◊: 650 bp band size; *: 1000 bp band size of 1 Kb Plus DNA Ladder (Invitrogen, 10787026). (E) Snapshot from IGV software showing the alignment of Vegfd with the sequence from animal number 2 resulting from Sanger DNA Sequencing. The PCR product from D was sequenced separately with primers Fw1 and Rv2.

Five microinjected animals were obtained at weaning. They, as well as their offspring, were genotyped with the following primers combinations:

- To detect the deletion of Exon 3 (Figure 8B):

Fw1: GTGCTATCCAGCTGTAGCCT; Rv1: CCCCTGAGCCTGTTTCTTTACT

- To detect the deletion of Exon 4 (Figure 8C):

Fw2: GGGCAAAAATGCAGATGGTGG; Rv2: GATCCTCAAGGTTTTGGGTCCT

- To detect the total deletion of both, exon 3 and exon 4 (Figure 8D):

Fw1: GTGCTATCCAGCTGTAGCCT; Rv2: GATCCTCAAGGTTTTGGGTCCT

The PCR program used for the different amplifications was the same:

1) 95 ºC – 3’
2) 95 ºC – 30’’
3) 59 ºC – 30’’
4) 72 ºC – 1’
5) Go to step 2, 30 cycles
6) 72 ºC – 7’
7) 12 ºC – ∞

The PCRs products from the agarose gel equivalent to Figure 8D were extracted with ZymocleanTM Gel DNA recovery kit (D4002) from animals 1 to 4 and validated their sequences using Secugen Sanger DNA sequencing service (https://www.secugen.es/en/sequencing/sanger/analysis-offered.php). We confirmed that the mutant sequences aligned with the flanking regions of exons 3 and 4 of *Vegfd* and had lost the predicted region (Figure 8E). Since animal number 5 was wild type, only animals 1 to 4 were kept and they were backcrossed with C57BL/6 wild type mice. The females were maintained in heterozygosity and the males in hemizygosity. These animals were crossed and the following embryos were used: $X^{wt}Y$ (Control), $X^{ko}X^{wt}$ (*Vegfd* heterozygous), $X^{ko}X^{ko}$ (*Vegfd* knockout), $X^{ko}Y$ (Vegfd knockout).

Embryo and embryonic organs harvest

Mice were crossed in the afternoon and the females were checked in the morning for vaginal plug. The morning in which the vaginal plug was detected, was considered as gestational day E0.5. At the stage of interest, females were sacrificed by carbon dioxide inhalation followed by cervical dislocation. To extract the embryos, the abdominal cavity of the female was opened and the uterus was transferred to PBS. In a petri dish with ice-cold PBS with a sprinkle of Heparin (ROVI 1000 IU/mL), the muscular layer, the decidual layer and amnion were removed with forceps so that the embryos were exposed. E10.5 or E11.5 embryos were fixed in paraformaldehyde (PFA) (Electron Microscopy Sciences 15710) 4% in PBS overnight at 4ºC and the yolk sac was used for genotyping. Older embryos were decapitated and placed in a 50 mM KCl (Sigma P9541) solution in PBS with heparin. Both, to stop beating in the phase of diastole and avoid blood clots. The heart was collected pulling it out from the opened thoracic cavity. In case other organs as mesenteric lymphatics were needed, they were also collected at this point using forceps. Mesenteric lymphatics were pulled apart from the intestine before fixation by carefully holding the intestine with one forceps and pulling the mesenteric tissue with the

other. The different organs and carcass were fixed in PFA 2% in PBS overnight at 4ºC. The tip of the tail of the embryos was used for genotyping.

The embryonic back skin, for the dermal lymphatics immunostaining, was dissected after fixation. Carefully, an incision in the dermis and underlying layers surrounding the region of interest was made, and the skin was peeled off. The attached fibres were removed with forceps.

Neonatal heart harvest

P1 and P7 neonatal mice were decapitated. Their thoracic cavity was opened and the heart was collected and put in ice-cold PBS. Lungs were removed and the heart was first transferred to 50 mM KCl solution and then fixed in PFA 2% in PBS overnight at 4ºC.

Adult heart and other organs harvest

Mice were euthanized by carbon dioxide inhalation followed by cervical dislocation. The thorax was opened as well as the abdominal cavity. Some cuts were made in the liver to facilitate the exit of blood once PBS with heparin was slowly injected in the left ventricle of the heart. After removing the blood, 50 mM KCl solution in PBS with heparin was injected through the LV and then the heart was collected. The spleen was dissected after exposing the stomach. After lungs, fat and other non-desired tissues were dissected out, the organs were fixed in PFA 4% in PBS overnight at 4ºC. The tip of the tail was used to genotype adult mice.

TISSUE PROCESSING

A1) Sucrose dehydration, gelatin embedding and cryo-sectioning

If we planned to perform cryo-sections of the hearts, they were washed with PBS after fixation and they were dehydrated in 15% sucrose (Sigma, 16104) in PBS at 4ºC overnight. The next morning, sucrose was removed and a 37ºC pre-heated solution of 7.5% gelatin (Sigma, G2500), 15% sucrose in PBS was added. Hearts were incubated in this solution for at least 4 hours, changing the solution and inverting occasionally. Then, in a P6 dish, the hearts were embedded and oriented in this solution and left to solidify. First, briefly at room temperature and then at 4ºC (usually overnight). Afterwards, gelatin blocks were snap-frozen in a -70ºC solution of isopentane (Sigma, 1060561000) for 1 minute. The frozen blocks were kept at -80ºC until they were used.

8 µm-thick cryo-sections were made using a Leica CM1950 automated Cryostat and they were stored at -20ºC.

A2) Immunofluorescence on gelatin sections

First, slides were left to thaw and warm at room temperature. Then, gelatin was removed from

the slides with two 10-minutes washes with 37ºC PBS and a quick wash with room temperature PBS. Next, we proceeded with the immunostaining protocol.

If a HRP-conjugated secondary antibody was going to be used, a peroxidase quenching step was performed. For this, the slides were incubated at room temperature in darkness for 1 hour in a 1% hydrogen peroxide (Sigma, H1009) solution in 40% methanol in PBS. Then, they were washed several times with PBS and put in a solution of 0.5% Triton X-100 (Sigma T9284) in PBS. This permeabilization step was performed at room temperature for 30 minutes. This solution was washed with PBS and the slides were placed in a humid chamber in darkness. To avoid unspecific binding of the antibodies, the universal TNB blocking reagent (Perkin Elmer, FP1012) was added to the slides and it was incubated for 1 hour at room temperature. The primary antibodies dilutions (See Table 2 for the primary antibodies and dilutions that were used) were prepared in the same TNB blocking solution and they were incubated in the humid chamber at 4ºC overnight. The secondary antibodies in TNB blocking reagent were

Target	Conjugated	Host species	Dilution	Reference
CD140α	APC	Rat	1:100	eBioscience™ 17-1401-81
CD140β	APC	Rat	1:100	eBioscience™ 17-1402-82
CD31	FITC	Rat	1:100	eBioscience™ 11-0311-82
CD31	-	Rat	1:100/1:200	BD Pharmingen™ 553370
CD90.2	FITC	Rat	1:100	eBioscience™ 11-0903-82
CX-40	-	Rabbit	1:200	Alpha Diagnostics CX40-A
EMCN	eFluor660	Rat	1:100/1:200	eBioscience™ 50-5851-82
LYVE1	-	Rabbit	1:100	ReliaTech 03-PA50S
LYVE1	Biotin	Rat	1:200	eBioscience™ 13-0443-82
LYVE1	-	Rabbit	1:200	AngioBio 11-034
MEIS (*)	-	Rabbit	1:800	Torres' Lab
NG2	-	Rabbit	1:200	Sigma AB5320
PERIOSTIN	-	Rabbit	1:200	Novusbio NBP1-30042
PROX1	-	Goat	1:200	R&D systems AF2727
RALDH2	-	Rabbit	1:200	abcam ab96060
SM22α	-	Rabbit	1:200	abcam ab14106
SMA	Cy3	Mouse	1:400	Sigma C6198
TH	-	Sheep	1:300	Sigma AB1542
VEGFC	-	Rabbit	1:100	Cusabio CSB-PA07545A0Rb
VEGFD	-	Rabbit	1:200	Cusabio CSB-PA07554A0Rb
VIMENTIN	-	Rabbit	1:200	abcam ab45939
WT1	-	Rabbit	1:100/1:200	abcam ab89901
ZO-1	-	Mouse	1:200	Life Technologies 33-9100

(*) Anti-Meis antibody was generated in rabbits with a synthetic peptide corresponding to the conserved C-terminal domain of Meis1 and Meis2 (GMNMGMDGQWHYM) (Mercader, 2005).

Table 2. List of the primary antibodies that were used.

incubated for 1 hour at room temperature in the humid chamber in darkness (Table 3). If a biotin-conjugated secondary antibody was used, an additional 1-hour incubation with streptavidin protein conjugated with fluorophore was performed (Table 3). If a HRP-conjugated secondary antibody was used, this protocol was followed by a peroxidase detection-based tyramide fluorescent amplification (Table 3). Slides were washed with 0.01% Tween-20 (Sigma P9416) in PBS several times between steps. Finally, slides were mounted with Dako fluorescence mounting medium (s3023) and coverslips.

In case DAPI was used, it was included in 1:1000 dilution with the secondary antibodies, with the streptavidins or in an additional 15-minute incubation step at room temperature before mounting.

Since for a time we did not have a Donkey anti-rat secondary antibody, when a primary antibody raised in goat and one raised in rat had to be combined, as PROX1 (Goat) and CD31 (rat), the procedure was slightly different. After washing the primary antibodies, after overnight incubation, the secondary antibody donkey anti-goat was incubated for one hour. Then, it was washed with 0.01% Tween-20 in PBS and an additional blocking step with 20% goat serum in PBS for one hour was performed. After washing, the rest of the secondary antibodies raised in goat were incubated in TNB and the immunofluorescence was finished as usual.

B1A) Dehydration, paraffin embedding and sectioning

PFA was washed from embryonic and adult hearts and they were transferred to 70% ethanol in distilled water at room temperature. The subsequent dehydration steps in increasing concentrations of ethanol, xylol and paraffin embedding were usually performed by CNIC Histopathology Unit. For this, they use a Thermo Excelsior SA processor. After paraffin blocks were left to solidify and cooled down at 4ºC, the hearts were cut in 5 µm-thick sections using a Leica RM2245 semi-automatic microtome. Sections were kept at 4ºC until they were used.

B2A) Hematoxylin & Eosin (H&E) staining

H&E staining was performed at the CNIC Histopathology Unit and it was carried out using the Leica Automated Slide Stainer ST5020.

B2B) Immunofluorescence on paraffin sections

If paraffin sections were not stained with H&E and were instead used for immunofluorescence, paraffin was removed and the tissue sections were rehydrated at room temperature in 5-minutes changes of 2x Xylol -> 2x Ethanol 100 % -> Ethanol 90 % -> Ethanol 70 % -> Ethanol 50 % -> water. Then, antigens were exposed using Citrate Buffer antigen retrieval method. For that, a solution of 10 mM Citric acid monohydrate (Sigma, 33114) with 0.05 % Tween 20 in distilled water was prepared. The required pH 6 was adjusted with sodium hydroxide tablets (Merck, 1064980500). The buffer was pre-heated in the microwave and, once it started to boil, the slides were immersed and boiled for 20 additional minutes. Next, the same protocol than for immunofluorescence on gelatin sections was followed.

Type	Species reactivity	Host species	Conjugate	Dilution	Reference
2^{ary}Antibody	Rabbit	Goat	405	1:500	Thermo Fisher A31556
2^{ary}Antibody	Rabbit	Goat	488	1:500	Life technologies™ A11034
2^{ary}Antibody	Rabbit	Donkey	488	1:500	Molecular Probes A21206
2^{ary}Antibody	Rabbit	Goat	633	1:500	Life technologies™ A21071
2^{ary}Antibody	Rabbit	Donkey	633	1:500	Sigma SAB4600132
2^{ary}Antibody	Rabbit	Donkey	Cy5	1:500	Jackson Immuno 711-495-152
2^{ary}Antibody	Rabbit	Goat	HRP	1:500	Dako P0448
2^{ary}Antibody	Mouse	Goat	633	1:500	Life technologies™ A21052
2^{ary}Antibody	Rat	Goat	488	1:500	Thermo Fisher A11006
2^{ary}Antibody	Rat	Donkey	488	1:500	Molecular Probes A21208
2^{ary}Antibody	Rat	Donkey	Cy5	1:500	Jackson Immuno 712-175-150
2^{ary}Antibody	Rat	Goat	HRP	1:500	Cell Signaling 7077S
2^{ary}Antibody	Rat	Goat	Biotin	1:500	abcam ab7096
2^{ary}Antibody	Goat	Donkey	488	1:500	Thermo Fisher A11055
2^{ary}Antibody	Goat	Donkey	647	1:500	Thermo Fisher A21447
2^{ary}Antibody	Goat	Donkey	HRP	1:500	Thermo Fisher A15999
2^{ary}Antibody	Goat	Donkey	Biotin	1:500	Jackson 705-065-003
2^{ary}Antibody	Sheep	Donkey	488	1:500	Life Technologies A-11015
Streptavidin	-	-	405	1:500	Thermo Fisher S-32351
Streptavidin	-	-	647	1:500	Thermo Fisher S21374
Tyramides	-	-	405	1:500	Biotium 92197
Tyramides	-	-	Cy3	1:100	Perkin Elmer NEL744001KT
Tyramides	-	-	Cy5	1:100	Perkin Elmer NEL745001KT

Table 3. List of the secondary antibodies, streptavidin and tyramides that were used

C) Whole mount immunofluorescence

For whole mount immunofluorescence the same protocol with mild variations was followed depending on the organ:

Heart immunofluorescence: After fixation and subsequent wash with PBS, all the following steps were performed at 4ºC in a rotating wheel. Up to four control and mutant hearts in total were put in the same 2ml Eppendorf to avoid inter-tube variance. A code with the atria was performed to recognise each heart after the protocol: The right atrium was cut from one heart, the left atrium from other, other had both atria cut and the last was left with both of them. 500 µL were added for each step. Except for the washes that were performed in a 50 ml Falcon tube. Protocol: Permeabilization for 2 days in 0.5% Triton X-100 in PBS was followed by 2-hour wash with PBS. TNB blocking was performed overday and it was replaced with the primary antibodies before the day was finished. They were incubated for 3 days and then the hearts were washed overday with 0.01% Tween 20 in PBS. Secondary antibodies were incubated overnight or for 2 days depending on the antigen and cardiac stage. Then, the hearts were thoroughly washed with 0.01% Tween 20 in PBS and a last wash was done with PBS to remove the detergent.

To improve image acquisition and to preserve fluorescence, hearts were mildy clarified with increasing glycerol (Merck 1.04094.1000) concentrations from 20% glycerol in PBS up to 80% glycerol. Samples were kept at 4ºC in darkness until acquisition.

For immunofluorescence of Figures 41 and 42, a slightly different protocol was followed. Instead of using TNB, a blocking solution of 3% BSA, 0.1% Triton and 5% donkey serum was used.

Mesenteric and skin whole mount immunofluorescence: Performed on a 48 or 96 well plate, each sample separately. The time of the different incubation steps was reduced. The tissues were permeabilised with 0.5% Triton X-100 in PBS and blocked with TNB for two hours each step. Primary and secondary antibodies were incubated overnight and overday at 4ºC and washed with 0.01% Tween 20 in PBS. Samples were mounted with Vectashield (Vector Laboratories) on a slide and flattened with a coverslip.

D) Whole mount immunohistochemistry

The same protocol than for whole mount immunofluorescence was followed with some variations. After permeabilization, a peroxidase quenching step was performed with 0.3% hydrogen peroxide in 100 % methanol for one day in darkness at room temperature. The hearts were blocked for one day. Primary and secondary antibodies incubations did not change but a biotin-conjugated antibody was always used. Signal was amplified with Vectastain ABC-HRP kit (Vector laboratories PK-6100) with avidin and biotinylated horseradish amplification, for 2 days at 4ºC. Signal was revealed with DAB (Vector Laboratories VC-SK-4100KI01).

E) Whole mount *in situ* hybridization

E11.5 embryos destined for whole mount *in situ* hybridization were dehydrated in increasing concentrations of methanol in 0.1% Tween-20 (PBT) in sterile PBS and stored at -20ºC in 100% methanol until they were used.

Four days were needed for this protocol

Day 1: Before starting with the *in situ* hybridization, embryos were rehydrated in 10-minutes changes in decreasing methanol concentrations and they were washed twice with PBT. At this point, the hearts were dissected from the body of the embryos but everything was kept as staining control. This was followed by a 1-hour bleaching step with 6% hydrogen peroxide in PBT, performed in darkness, at room temperature with gentle agitation. After this, embryos were washed with PBT, digested with 10 µg/ml Proteinase K (Sigma) in PBT for 5 minutes and washed again with PBT for 5 additional minutes. Then, the embryos and hearts were fixed for 20 minutes at room temperature with 0.2% glutaraldehyde in 4% PFA. The fixative was removed and it was washed with PBT for 30 minutes. In the meantime, prehybridization buffer (50% formamide, 4xSSC pH 4.5, 1% SDS, 50 µg/ml heparin, 10 µg/ml tRNA from baker's yeast (Sigma 1010949500), 1% w/v Blocking reagent (Sigma 11096176001)) was pre-heated at 65ºC. The hearts and embryos were incubated at 65 ºC with this buffer for at least 1 hour and a half with gentle agitation. After this time, *PlexinA2* or *Sema3C* riboprobes were diluted in this buffer and were heated at 80ºC for 2 minutes. The probes replaced the prehybridization buffer and were incubated overnight at 65ºC for the hybridization step.

PlexinA2 and *Sema3C* riboprobes were kindly provided by José Luis de la Pompa' laboratory.

Day 2: The next morning, the probes were retrieved and stored at -20ºC since the same dilution can be used several times. In their place, 65ºC pre-warmed 0.1% CHAPS (Sigma C5070-5G) in 2x SSC pH 5.5 buffer (300 mM NaCl, 30 mM C6H5Na3O7-2H2O) was added to the tubes. Three washes, of 30 minutes each, were done. Then three 30-minute additional washes with 65ºC 0.1% CHAPS in 0.2x SSC were performed. At this point, the samples were removed from the oven at 65ºC and were transferred to a horizontal shaker at room temperature where they were washed with TBST (5 mM Tris-HCl pH 7.5, 15 mM NaCl, 0.1% Triton X-100) for 30 minutes. Next, unspecific bindings were blocked with a 2-hour incubation step with 20% Goat serum and 1% blocking reagent in TBST. Anti-digoxigenin AP antibody (1:200, Roche 11093274910) was diluted in the blocking mixture and incubated overnight at 4ºC.

Day 3: Hearts and embryos were washed overday at room temperature with TBST. Several changes were done and, by the end of the day, they were transferred to the cold chamber where they were shaking overnight in TBST at 4ºC.

Day 4: Three washes with NTMT (125 mM Tris-HCl pH 9.5, 125 mM NaCl, 62.5 mM MgCl2, 0.5% Triton X-100), of 10 minutes each, preceded staining with BM Purple (Sigma 11442074001). Before adding it to the samples, BM Purple was centrifuged for 2 minutes at maximum speed to remove precipitates. BM Purple was left until good signal was achieved on the hearts. Finally, the hearts were

washed with TBST and re-fixed and stored with 4% PFA at 4ºC.

IMAGE ACQUISITION

H&E stained sections were scanned with Hamamatsu Nanozoomer 2.0 RS and NDP.Scan 2.5 software.

Whole-mount images of hearts and embryos were acquired with Nikon DXM1200F or Olympus DP71 cameras coupled to Leica MZFLIII scopes with a Plan Apo 1x objective.

Whole-mount and cardiac sections immunofluorescence were acquired with: Nikon A1R confocal microscope, Leica SP5 multiline inverted confocal microscope, Nikon W1 Spinning Disk inverted confocal microscope and Leica TCS SP8 inverted confocal microscope with Navigator module and equipped with white light laser. The standard parameters for most acquisitions were 400 Hz, 1024x1024 resolution and bidirectional mode activated when available. Maximum projections were acquired using TileScan and z-stack functions.

Images were analysed and quantifications were made using ImageJ (http://rsb.info.nih.gov/ij) and Imaris software.

SUBEPICARDIAL INDIAN INK INJECTIONS

To assess lymphatic functionality in basal conditions, subepicardial indian ink injections on adult hearts were performed. For that, mice were anesthetized with 6% isoflurane and 1.5% oxygen in a gas chamber. When they did not have reflexes upon pressure on the paw, they were intubated and connected to assisted ventilation with a constant 4% isoflurane and 1.5% oxygen flow. The thoracic cavity was exposed and kept opened with 2.5mm retractors (FST 18200-10). With forceps, the pericardium was removed to get better access to the heart. With a 30G needle and 1 mL syringe, Indian ink was injected in the subepicardium of the beating hearts several times per heart. Injections on the dorsal side of the heart were performed rotating gently anticlockwise the heart with forceps. Isoflurane concentration was increased and the animals were euthanised by extracting the hearts. Hearts were put in ice-cold PBS during image acquisition until they were fixed with 4% PFA in PBS.

CORONARY INDIAN INK AND GELATIN INJECTIONS

In order to visualise the coronary vasculature of adult hearts, Indian ink with gelatin injections were performed. For that, warm 2% gelatin in PBS was mixed with Indian ink in 1:1 proportion and, to

avoid gelatin solidification, the tube was kept in warm water until injection. Then, the animals were euthanised with carbon dioxide inhalation followed by cervical dislocation. The thoracic cavity and pericardium were opened and the right atrium slightly cut to avoid cardiac deformation by the increase of pressure. This was followed by the injection of PBS through the left ventricle with a 30G needle and 1 mL syringe to wash and remove blood from the coronaries and heart. 150 µL of gelatin and Indian ink mixture was then injected in the left ventricle. The heart was collected once the ink had been propelled to the coronaries helped by the remaining beating. It was transferred to ice-cold 50 mM KCl solution in PBS to stop beating and promote gelatin solidification to avoid its exit from the heart. As solidification control, the remaining gelatin and ink mixture was placed in the tube on ice and, once it had solidified, pictures of the hearts were acquired on ice-cold 50 mM KCl. Finally, the hearts were fixed with 4% PFA.

FLOW CITOMETRY

Hearts were extracted from the embryos as described before, with the difference that in this case the great arteries and atria were removed from the ventricles. Unless stated differently, all steps were performed on ice and with ice-cold solutions.

We followed the protocol described by Carmona et al. (2020) with mild variations. Briefly, after dissecting the hearts they were washed with sterile PBS to remove blood and 500 µL of 0.2 % Type II collagenase (Worthington LS004176) in FACS buffer (2% FBS, 1% HEPES in PBS) were added to each 1.5 ml tube (one ventricle per tube). Then, each ventricle was minced with scissors and they were digested for 25 minutes at 37 ºC using a shaking thermoblock. After this time, the tissue was disaggregated gently with the pipette until a homogenous solution was obtained. The tubes were centrifuged 5 minutes at x500 g at 4ºC and the supernatant was discarded. The cells were resuspended in 250 µL FACs buffer and they were passed through a 70 µm pre-wet cell strainer to remove non-digested tissue. An additional 250 µL of FACs buffer were used to wash the cell strainer. The cells were centrifuged for 5 additional minutes at x500 g at 4ºC, the supernatant was discarded and the cells were resuspended in 200 µL FACs buffer. From this: A) 80 µL of the cells were transferred to a new tube for fibroblasts staining with CD90-FITC and CD140α-APC antibodies. B) 80 µL were transferred to a different tube for endothelial cells staining with CD31-FITC and EMCN-eFLuor660 antibodies (See Table 2). C) The remaining 40 µL of the different tubes were used for the different controls. Primary antibodies in 1:100 dilution were incubated for at least 20 minutes on ice. Finally, the cells were washed with FACs buffer, centrifuged 5 minutes at x500 g at 4ºC and resuspended in 300 µL FACS buffer with DAPI 1:10000.

The following battery of controls was used: single-primary antibody staining, cells with endogenous tdtmt reporter, Rat IgG2a kappa Isotype Control-FITC (eBioscienceTM 11-4321-80), Rat IgG2a kappa Isotype Control-eFluor660 (eBioscienceTM 50-4321-82) and non-stained cells.

Sixty thousand events of each condition were quantified and analysed using an LSRFortessa 4L flow cytometer with 488, 640, 405 and 561 nm excitation lines. Acquisition parameters were established

with the help and advise of CNIC Flow Cytometry Unit. Data were analysed and represented using FlowJo_v1071 software.

RNAseq ANALYSIS

Epicardial dissection and RNA extraction

The epicardium/subepicardium was dissected as described previously (Lioux et al., 2020). The E16.5 hearts were quickly extracted from the pregnant females as described before. They were placed in ice-cold sterile PBS until their epicardium was dissected. Both atria and great arteries were cut and the ventricle was pinned down with a metallic thread on a 1% Agarose coated petri dish with ice-cold PBS (Figure 9). Taking advantage of the opening caused by the insertion of the metallic thread, the epicardium was delicately lifted and separated from the myocardium using fine forceps (Dumont #55 No11255-20). In this process, one forceps held the epicardium while the other was placed between the epicardium and myocardium. With careful movements, it was used to detach both layers. Once the epicardium was completely peeled off, it was placed between the tips of the forceps and, with an horizontal delicate movement, the non-attached myocardial cells were removed. The epicardium from each heart was quickly frozen in separate 1.5 ml Eppendorf tubes on dry ice.

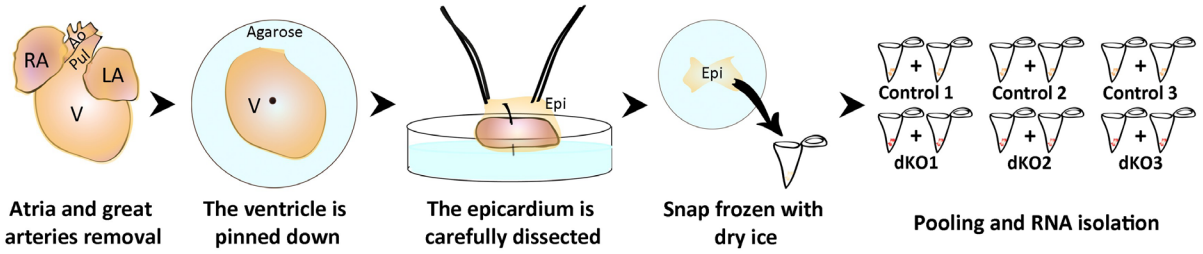

Figure 9. Epicardium dissection for RNAseq analysis. Schematic representation of the procedure. Ao: Aorta; Epi: Epicardium; LA: left atrium; Pul: pulmonary artery; RA: right atrium; V: ventricles.

For the RNA isolation, samples from at least three different litters were used. As low RNA amount from one single epicardial layer was expected, two dissected epicardia of the same genotype were pooled together. Therefore, our three biological replicates per genotype represent the RNA sequencing from six different hearts per genotype, pooled together in two hearts per biological replicate (Figure 9).

RNA was then purified from each pool using RNeasy Micro kit (Qiagen 74004).

RNA sequencing

CNIC Genomics Unit performed RNA sequencing. 40 ng of total RNA were used to generate barcoded RNA-seq libraries using the NEBNext Ultra RNA Library preparation kit (New England Biolabs). Briefly, poly A+ RNA was purified using poly-T oligo- attached magnetic beads followed by fragmentation

and then first and second cDNA strand synthesis. Next, cDNA 3' ends were adenylated and the adapters were ligated followed by PCR library amplification. Finally, the size of the libraries was checked using the Agilent 2100 Bioanalyzer DNA 1000 chip and their concentration was determined using the Qubit® fluorometer (Life Technologies). Libraries were sequenced on a HiSeq2500 (Illumina) to generate 60 bases single reads and processed with RTA v1.18.66.3. FastQ files for each sample were obtained using bcl2fastq v2.20.0.422 software (Illumina).

RNAseq analysis

The raw data analysis of RNA-seq data were generated by CNIC Bioinformatics unit. Read quality was assessed with FastQC (http://www.bioinformatics.babraham.ac.uk/projects/fastqc/). Illumina adaptor sequences were trimmed with Cutadapt 1.7.1 (Martin, 2012), which also discarded reads that were shorter than 30 bp. The resulting reads were mapped against the mouse transcriptome (GRCm38, release 91; aug2017 archive) and quantified using RSEM v1.2.20 (Ritchie et al., 2015). Data were then processed with a differential expression analysis pipeline that used Bioconductor package LIMMA (Ritchie et al., 2015) for normalization and differential expression testing. Genes with at least 1 count per million in at least 3 samples were considered for statistical analysis. We considered as differentially expressed those genes with Benjamin-Hochberg adjusted p-value < 0.05. Fold change and log (ratio) values were calculated to represent gene expression differences between conditions.

For pathways analysis, the Ingenuity Pathway Analysis software was used.

ECHOCARDIOGRAPHY

Transthoracic echocardiography was performed blinded by an expert operator using a high-frequency ultrasound system (Vevo 2100, Visualsonics, Canada) with a 40-MHz linear probe on a heating platform. Mice were lightly anesthetized with 0.5-2% isoflurane in oxygen, adjusting the isoflurane to maintain heart rate at 450±50 bpm. A base-apex electrocardiogram was continuously monitored. Images were analysed using Vevo 2100 Workstation software. Parasternal standard, 2D and MM, long and short axis views at the level of the papillary muscles (LAX and SAX view, respectively) were acquired.

STATISTICS

Parametrical T student test was performed to compare two groups of data. Two-way ANOVA was performed to compare three or more groups of data. Chi square test was used for comparisons between observed and expected frequencies. Data is indicated as mean ± SEM of the individual plotted values. All comparisons and graphs were made using GraphPad Prism 7.0 statistical analysis software. In all cases, adjusted values of $P<0.05$ were considered as statistically significant.

RESULTS

"You may never know what results come of your actions, but if you do nothing, there will be no results."
~ Mahatma Gandhi

Meis transcription factors are expressed in the developing epicardium

In order to better understand the role of MEIS TFs during cardiac development, we studied their expression pattern. Immunofluorescence (IF) performed on E12.5, E14.5, E16.5 and E18.5 mouse hearts using an antibody that recognizes both MEIS1 and 2, detects expression throughout development in this organ (Figure 10A-D'''). We used hearts from *Wt1*^{Cre}*; Rosa26*$^{tdtmt/wt}$ (*Rosa26*$^{tdtmt/wt}$ from now on referred to as *Rosa26*^{tdtmt}) embryos, in which we could follow the epicardial lineage by Tomato fluorescent protein expression. Aside from their expression in CMs (Muñoz-Martín et al., in preparation) and cardiac valves (Machon et al., 2015), we also found positive signal in the epicardium and in some EPDCs (arrowheads and arrows respectively in Figure 10) in all studied stages.

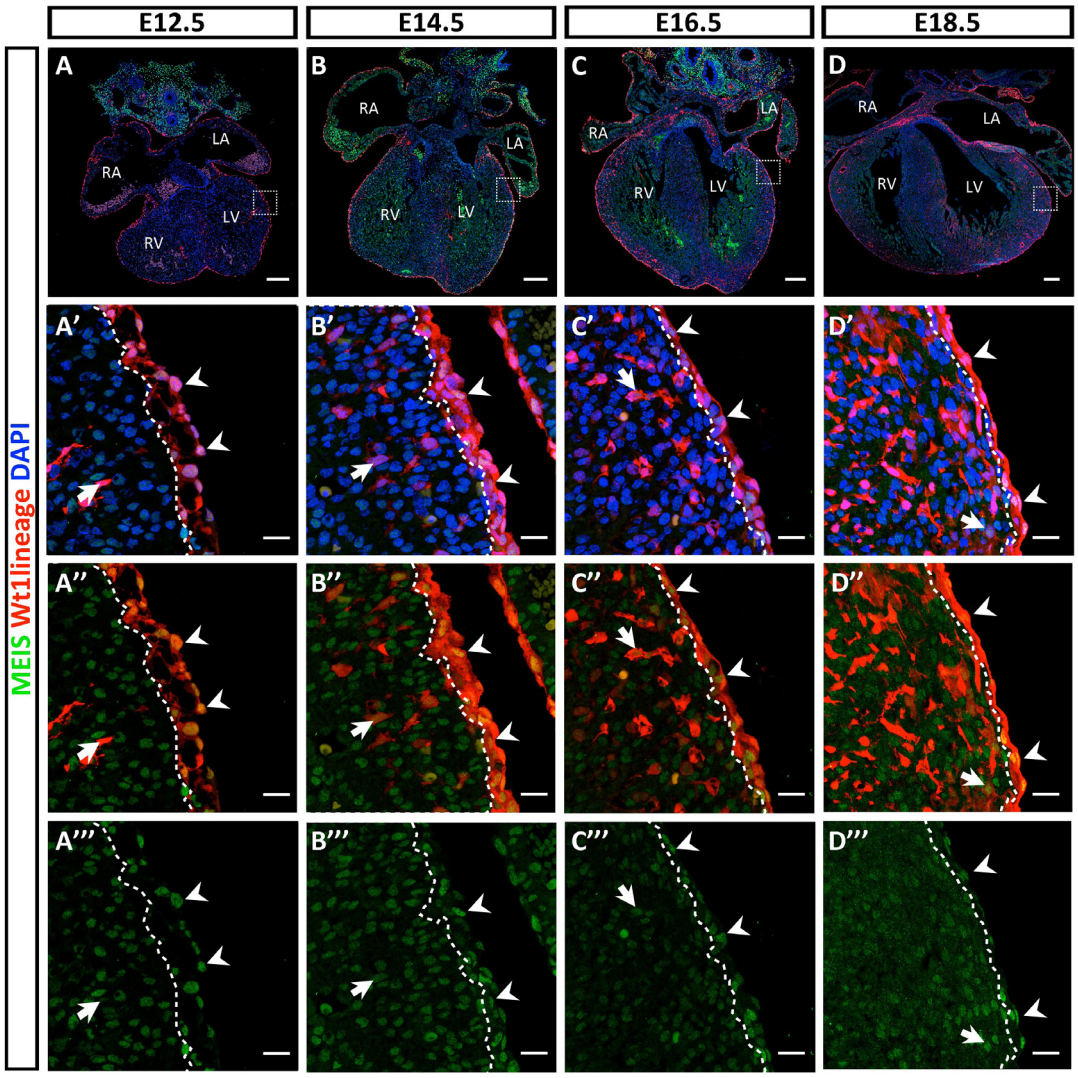

Figure 10. MEIS TFs are expressed in the epicardium and EPDCs throughout development. Immunofluorescence of cardiac sections of *Wt1*^{Cre}*; Rosa26*^{tdtmt} E12.5 (A-A'''), E14.5 (B-B'''), E16.5 (C-C''') and E18.5 (D-D''') hearts with an antibody that recognizes MEIS1 and MEIS2 TFs. Higher magnifications of the boxed regions in A, B, C and D show nuclear colocalization of Meis signal (Green) with some *Wt1Cre lineage+* cells (red) in all stages (A'-A''', B'-B''', D-D'''). Arrowheads and arrows show examples of epicardial cells and EPDCs expressing MEIS respectively (A'-D'''). LA: left atrium; LV: left ventricle; RA: right atrium; RV: right ventricle. Scale bars: 200 µm in A, B, C, D; 20 µm in A'-A''', B'-B''', C'-C''', D'-D'''.

Moreover, RNAseq analysis previously performed in the group (Lioux et al., 2020), showed expression of both *Meis1* and *Meis2* mRNAs in the epicardium. In addition, comparison of expression levels between the ventricular epicardium and the AMC layer of the base of the great arteries, showed higher *Meis1* and *Meis2* expression in the AMC. We confirmed this expression pattern by immunofluorescence (IF) (Figure 11B, B'').

All these results suggest that *Meis* genes may be playing a functional role in the epicardium, AMC and/or EPDCs during cardiac development.

Epicardial-specific conditional deletion of *Meis1* and *Meis2* produces no cardiac functional alterations on adult mice

In order to explore the possibility of Meis function in the epicardium, we generated a new mouse line with the epicardial-specific conditional deletion of *Meis1* and *Meis2* using the *Wt1Cre* driver (Figure 11A).

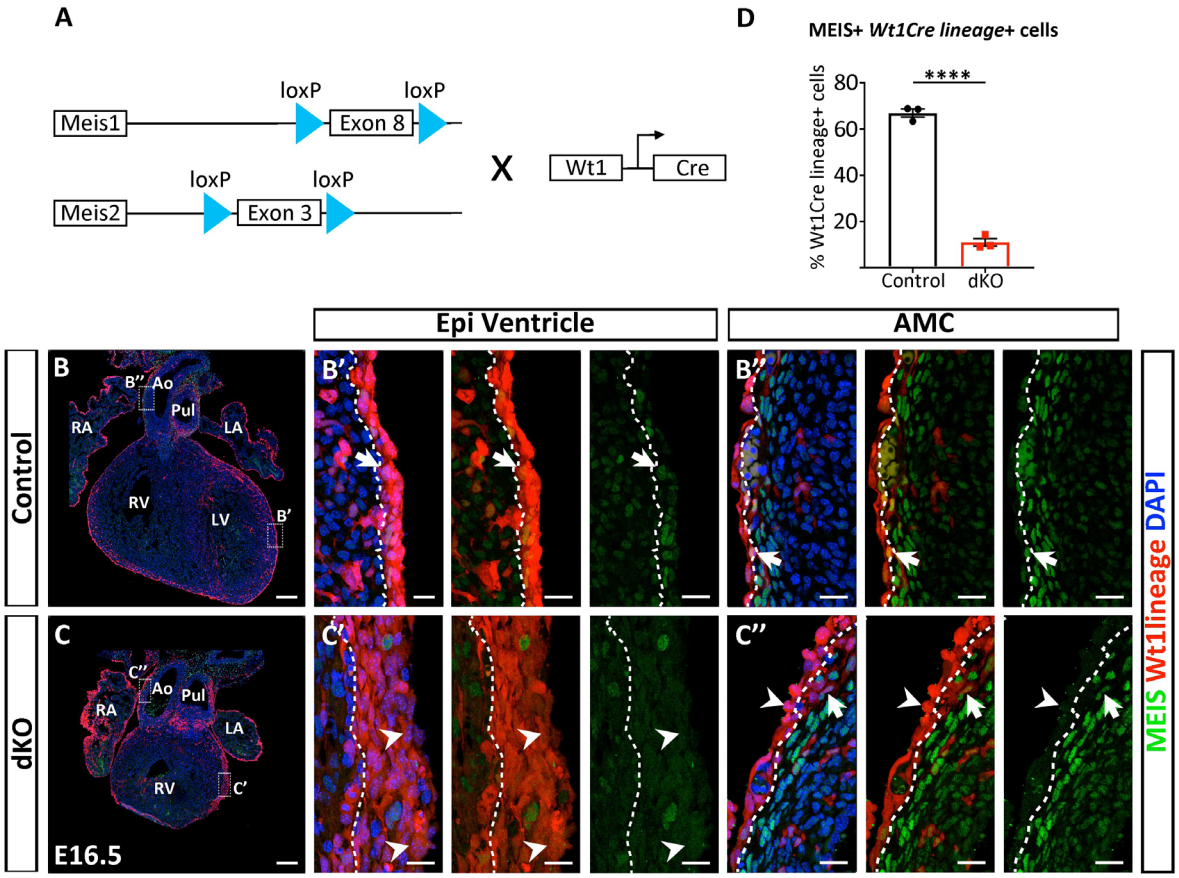

Figure 11. *Meis1* and *Meis2* epicardial-specific conditional mutant mice. (A) Schematic representation of the epicardial conditional deletion of *Meis1* and *Meis2* by the cleavage of their exons 8 and 3 respectively using *Wt1Cre* driver. (B-C'') MEIS IF of E16.5 $Wt1^{Cre}$; $Rosa26^{tdtmt}$ control (B-B'') and $Wt1^{Cre}$; $Meis1^{flox/flox;}$ $Meis2^{flox/flox}$; $Rosa26^{tdtmt}$ dKOs hearts (C-C''). Arrows and arrowheads point to *Wt1Cre lineage*+ MEIS+ and *Wt1Cre lineage*+ MEIS-negative cells respectively. (D) Proportion of MEIS+ *Wt1Cre lineage*+ cells in controls and dKOs in B-C''. (n = 3 hearts per genotype; at least two regions per section; three sections per heart). Unpaired t test. **** p value <0.0001. Error bars represent SEM. Ao: aorta; Epi: epicardium; LA: left atrium; LV: left ventricle; Pul: pulmonary artery; RA: right atrium; RV: right ventricle. Scale bar: 200 µm in B, C and 20 µm in B'-B'', C'-C''.

By IF, we confirmed an 84 % efficiency of the deletion in these mutants (Figure 11D). *Wt1^{Cre}; Meis1$^{flox/flox}$; Meis2$^{flox/flox}$; Rosa26^{tdtmt}* mutant E16.5 hearts, had lost most of MEIS expression in the epicardium (Figure 11C), EPDCs (Figure 11C') and AMC layer (Figure 11C''), in contrast with the controls expression (Figure Figure 11B-B''). However, some cells that had recombined the reporter *Rosa26tdtmt* still showed some residual Meis signal (arrow in Figure 11C''). While 67 % of *Wt1Cre lineage+* cells express MEIS in the controls, 11 % *Wt1Cre lineage+* cells express MEIS in the dKOs.

We wondered whether this deletion would have an effect on cardiac function. For this purpose, we studied the cardiac anatomy of control and mutant hearts by histology. We could not find any major morphological alterations in mutant hearts of 6-week old mice stained with H&E (Figure 12A-B'). Some *Wt1^{Cre}; Meis1$^{flox/flox}$; Meis2$^{flox/flox}$* (from now on referred as "dKO") had a rounder shape around the apex area (Figure 12B') but their overall anatomy was normal and the average size of the mutant hearts was similar to that of the controls (Figure 12C).

Although anatomically these hearts seemed normal, their cardiac function could be altered. We performed echocardiography to evaluate this possibility. However, dKOs LV ejection fraction (EF) did not differ from the controls (Figure 12D), suggesting that their function was normal. LV mass was also comparable to that of control animals (Figure 12E), suggesting that *Meis* deletion in the epicardium has no effect on adult cardiac homeostasis or function.

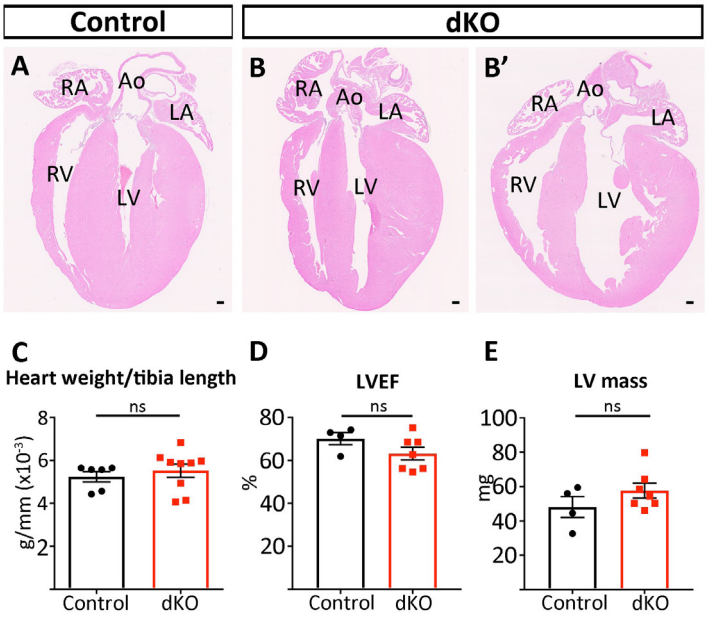

Figure 12. Epicardial *Meis* deletion produces no cardiac alterations on adult mice. (A-B') H&E staining of adult cardiac sections of controls (A) and dKOs (B-B'). Some dKOs present a rounder shape around the apex area (B'). (C) Heart size measured as the ratio of heart weight/ tibia length. (D-E) Echocardiography studies show no functional differences, as the Left Ventricular Ejection Fraction (LVEF) of dKOs does not differ from the control values. Measured in long axis (PSLAX) M-Mode. (E) Left ventricle (LV) mass estimated from echocardiography studies. Unpaired t test (n ≥ 4 animals per genotype). Ns: p value ≥ 0.05. Error bars represent SEM. Ao: aorta; LA: left atrium; LV: left ventricle; RA: right atrium; RV: right ventricle. Scale bar: 200 µm.

Meis deletion with *Wt1^{Cre}* produces other non-cardiac alterations

Although we were interested in *Wt1^{Cre}* because of its contribution to the epicardium and epicardial lineage, *Wt1* is expressed widely in the embryo. Its contribution to the mesothelium, kidney, gonads, spleen, nervous system, lung and liver has been reported (Aitken et al., 2016). We therefore could not discard the possibility that deleting *Meis* TFs using *Wt1^{Cre}* was affecting the development of other organs too.

We performed thorough necropsies of the 6-week old mutant and control mice and found that Meis dKOs mice indeed presented defects in their reproductive system and spleen with more frequency than the control mice (Figure 13C, F). Visual examination of the reproductive system revealed that 85% dKOs showed alterations. 2 out of 4 females had dysmorphic genital tracts and 2 had bigger ovaries. On the other hand, 2 out of 3 males presented hypogonadism and seminal vesicle agenesis. (Figure 13D-F). In fact, we have never been able to obtain offspring from dKOs. Therefore, MEIS function in the *Wt1+ lineage* seems to be required for gonadal development and fertility.

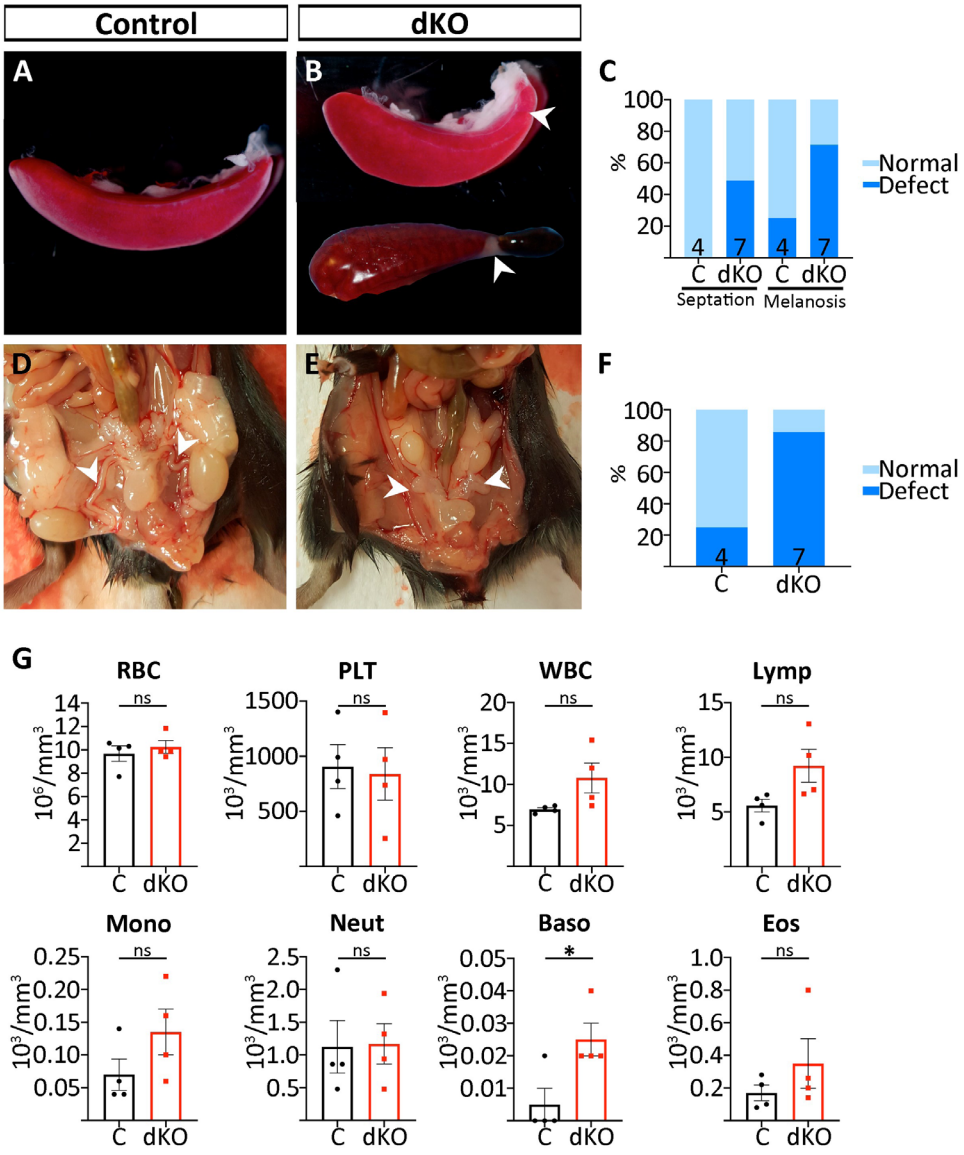

Figure 13. Meis dKOs present spleen defects and are sterile. (A-B) Whole mount pictures of Control (A) and dKOs (B) spleens identify an accessory spleen in the dKOs (arrowhead). (C) Quantification of the observed spleen alterations in controls and dKOs. (D-E) Whole mount pictures of control and dKO male reproductive system show an example of presumed sterile dKO with atrophied ducts (Arrowheads in E). (F) Quantification of proportion of animals with reproductive system alterations by visual examination. (G) Blood tests performed on controls and dKOs. (n ≥ 4 samples per genotype). Unpaired t test. ns: p value ≥ 0.05; * p value <0.05. Error bars represent SEM. RBC: red blood cells; PLT: platelets; WBC: white blood cells; Lymph: lymphocytes; Mono: monocytes; Neut: neutrophils; Baso: basophils; Eos: eosinophils.

While 1 out of 4 control mice had melanosis in the spleen, 5 out of 7 mutant animals presented this condition (Figure 13B, C). However, this is a non-pathological condition (Kristiansen, 1998). Moreover, 43% of dKOs also presented abnormal septation, presenting an accessory spleen (Figure 13B-C). This division was not found in any of the control mice (Figure 13A,C).

We also performed blood tests on these 6-week old mice to study whether their spleen alterations could have an impact in their hematopoietic populations. However, with exception of a small increase on basophils counts, no differences were found (Figure 13G).

In conclusion, while we found extra-cardiac defects associated to *Meis* deletion in the *Wt1Cre+* lineage, the alterations found do not seem to systemically affect physiology of the mutant mice.

MEIS TFs are required for proper alignment of the great vessels and ventricular septation

Although the characterization of dKO adult mice suggested no major alteration of cardiac or general physiology, analysis of the viability of mutant mice at weaning showed a strong reduction (~50%) (Figure 14E). In contrast, the viability of dKOs at P0 does not differ from the expected one (Figure 14E). However, some dKOs are not capable of living by their own and die immediately after birth and others do not survive beyond their first day of life, so that by P1 about 50% of them have died (Figure 14E).

We therefore wondered what could be causing the death of these animals and whether it could be due to the presence of cardiac malformations that are absent in the surviving adult dKOs. To study this, we focused on the morphology of hearts and performed H&E staining at E16.5, a stage in which all the main cardiac structures have been formed (Figure 14B-B'', D-D''). Surprisingly, we found severe defects in the dKOs (Figure 14C-D''). Epicardial *Meis* deletion results in rounder hearts (Figure 14C) that do not differ in their size when compared to the controls (Figure 14F). LV and RV compact myocardium thickness of dKOs is also similar to the controls (Figure 14G). However, 71% dKOs had some type of VSD (Figure 14D'', H) and 80% of these cases (57% of total dKOs) showed misalignment of the great vessels: 14% dKOs presented OA, a defect in which the Ao opens to the right and left ventricle through a septal defect; and 43% double-outlet right ventricle (DORV), a defect in which the two great arteries connect to the RV (Figure 14D', G). These results show that Meis TF activity in the *Wt1Cre+ lineage* is required for the proper alignment of the great vessels.

But, how is it possible that an alteration in the epicardium or AMC layer results in misalignment of the great vessels? Could these layers have a function in the OFT patterning? To our knowledge, there is no previous report of implication of the epicardium or mesothelium in the alignment of the great arteries. Because of the novelty of this implication, we decided to explore it further.

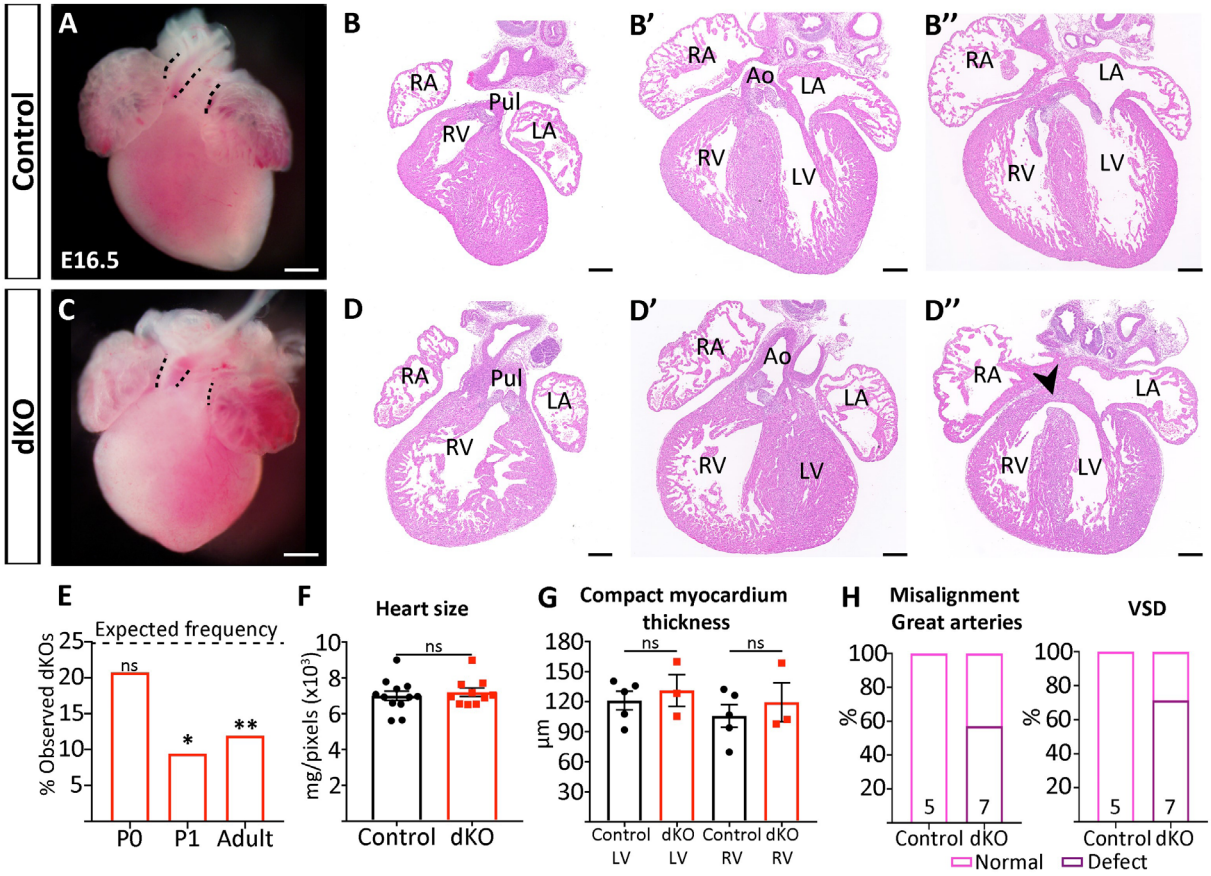

Figure 14. Cardiac morphological alterations produced by epicardial-specific deletion of *Meis1* and *Meis2* during development. (A, C) Whole mount images of control (A) and dKO (C) E16.5 hearts. (B-B'', D-D'') H&E staining of serial E16.5 cardiac sections of control (B-B'') and dKO hearts (D-D''). Arrowhead shows VSD of Meis dKO. (E) Observed and expected frequencies of dKOs at P0, P1 and adulthood. Chi-square statistical analysis reflects statistical significant differences. (F) Heart weight/body length ratio of E16.5 control and dKOs. (G) Compact myocardium thickness of the right and left ventricle of controls and dKOs. Only dKOs with no misalignment of the great arteries were quantified. (n ≥ 3 hearts per genotype; 4 sections per heart, and 3 measurements of RV and LV thickness per section), measured on H&E sections. (F-G) Unpaired t test. Ns: p value ≥ 0.05; * p value < 0.05; ** p value < 0.01. Error bars represent SEM (H) Quantification of the observed morphological alterations from H&E staining (n=5 for the controls and n=7 for the dKOs). 3 dKOs suffered DORV and 1 OA. 5 out of 7 presented some type of VSD. Ao: aorta; LA: left atrium; LV: left ventricle; Pul: pulmonary artery; RA: right atrium; RV: right ventricle; VSD: ventricular septal defect. Scale bar: 200 µm.

Meis deletion produces alterations in the AMC layer and OFT

In order to better understand the possible relationship between Meis, the AMC layer and OFT alignment, we dissected the OFT from E18.5 *Wt1^{Cre}; Rosa^{26tdtmt}* (control) and *Wt1^{Cre}; Meis1$^{flox/flox}$; Meis2$^{flox/flox}$; Rosa26^{tdtmt}* (dKOs) hearts and did a 3D reconstruction (of optical confocal sections) of *Wt1Cre lineage+* cells in both cases (Video 1 and 2 and Figure 15). With this approach, the AMCs and SMCs, ECs and fibroblasts that derive from the AMCs (Lioux et al., 2020) would be labelled.

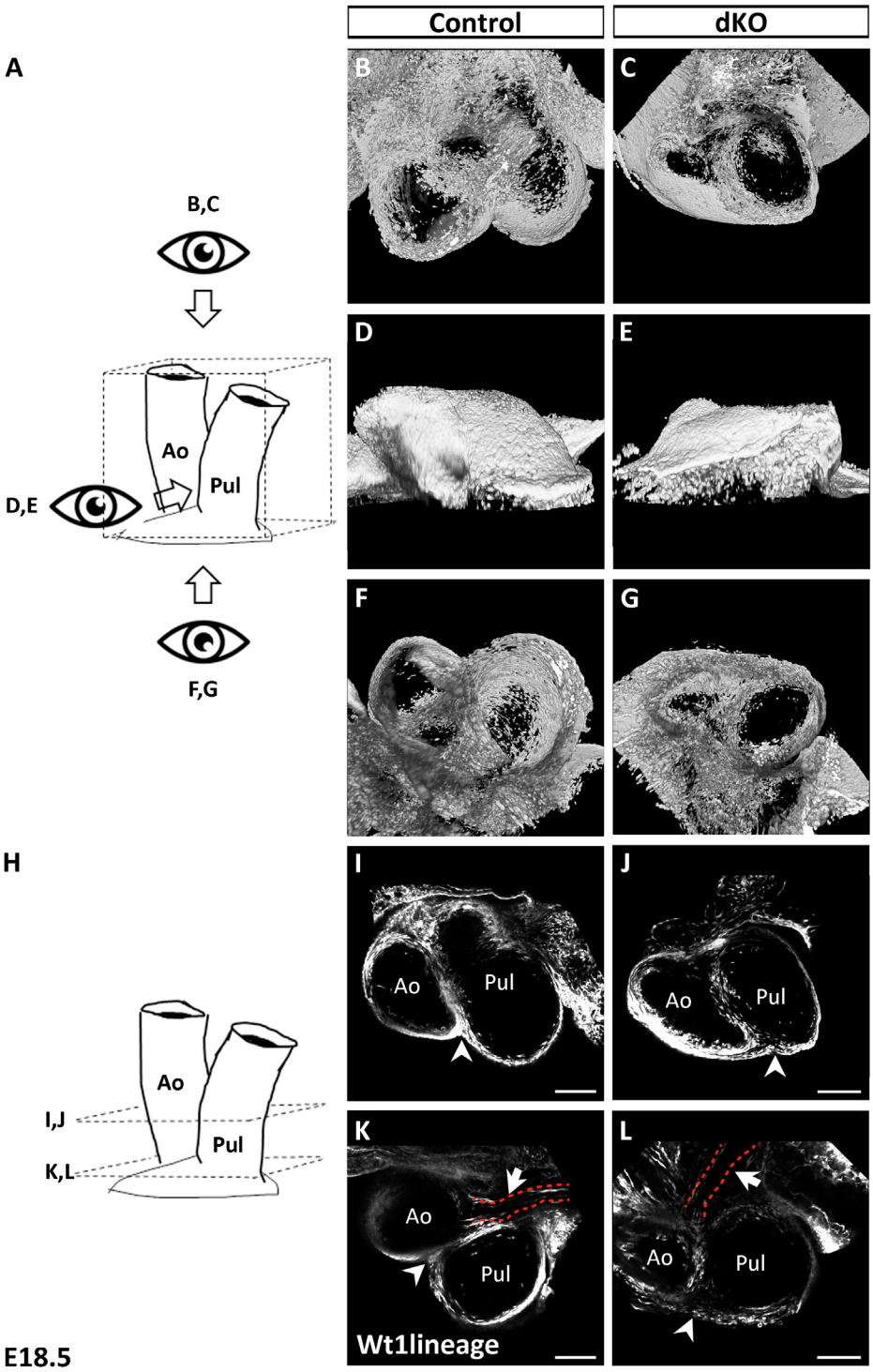

Figure 15. The AMC and its derivatives show an altered disposition in Meis dKOs OFT. (A) Schematic representation of the 3D reconstructed views shown in B-G of *Wt1Cre lineage+* cells in control (*Wt1*^{Cre}*; Rosa26*^{tdtmt}) and dKOs (*Wt1*^{Cre}*; Meis1*$^{flox/flox}$*; Meis2*$^{flox/flox}$*; Rosa26*^{tdtmt}) E18.5 OFT. Superior view (B-C), frontal ventral view (D,E) and inferior view (F,G). (H) Schematic representation of the represented single z (transverse optical section) in I-L. (I,L) Arrowheads in I, K show division between the AMC of Ao and Pul while in dKOs it is a continuous layer (arrowheads in J, L). (K, L) Arrow and red dash lines show the left coronary artery connection to the base of the Ao in control (K) and dKO (L). Ao: aorta; Pul: Pumonary artery. Scale bar: 200 µm

We found that in control specimens, the AMC and its derivatives form two layers that wrap separately the Ao and pulmonary arteries (view from the top (Figure 15B) and from the bottom (Figure 15F) of the 3D reconstruction and arrowheads in Figure 15I, K). In the dKO, however, it appears as a single layer that wraps the two vessels (Figure 15C, E, G and arrowheads in J, L). Moreover, in accordance with the DORV and OA defects from histological examination (Figure 14B', D', H), single optical sections in Figure 15K and L show different disposition of the Ao and pulmonary artery. Their trajectories appear parallel instead of crossed in the dKOs. Furthermore, their different sizes suggest asymmetrical septation of the OFT in the dKOs. These defects do not affect the connection of the coronary arteries at the base of the Ao, which appears normal (arrow and dash lines in Figure 15L).

Since cNCCs are important contributors to proper OFT alignment and septation (Waldo et al., 1998), and DORV and VSD are among the defects described for alterations in cNCCs (Porras and Brown, 2008), we decided to explore the possibility of cNCC involvement in the alterations of Meis dKOs. For that purpose, we performed whole mount *in situ* hybridization on E11.5 hearts with *PlexinA2* and *Sema3C* riboprobes. While *PlexinA2* is expressed in the migrating cNCCs, *Sema3C* is expressed and required in the myocardium of the OFT to attract the migrating cNCCs (Brown et al., 2001; Feiner et al., 2001). We did not find any differences when we compared control and dKOs for *PlexinA2* or *Sema3c* expression (Figure 16A-D). *PlexinA2 in situ* hybridization shows that cNCCs have reached the OFT (arrowheads in Figure 16A-B) and *Sema3C* is expressed in the OFT normally (Figure 16C-D). This suggests that cNCCs migration defects do not underlie the OFT phenotype in dKOs.

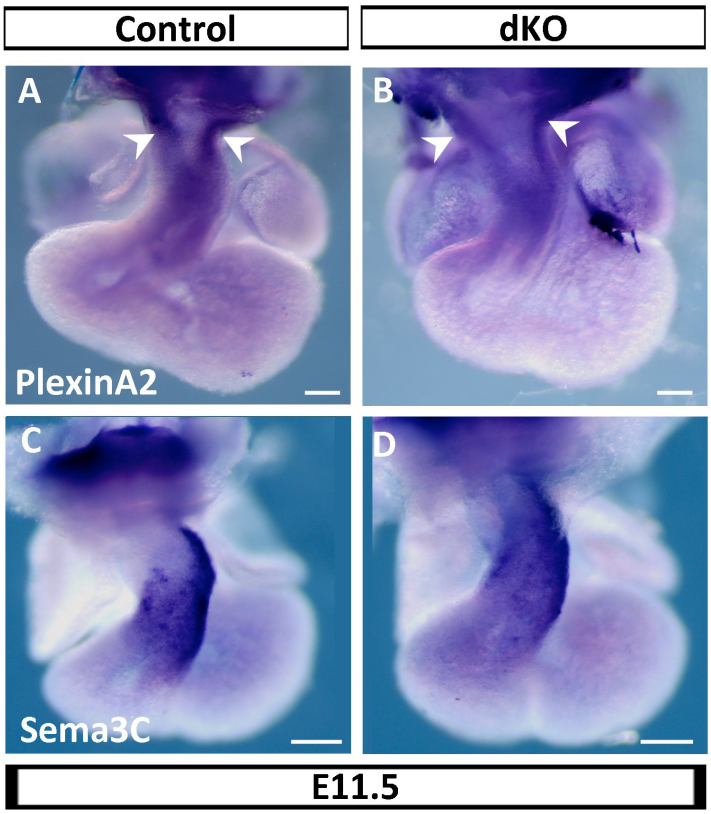

Figure 16. Cardiac neural crest cells migration into the heart is not affected in Meis dKOs. (A-B) In situ hybridization with *PlexinA2* riboprobe on E11.5 hearts labels migrating cNCCs (arrowheads) as they reach the OFT in control (A) and dKOs (B). (C-D) *Sema3C* in situ hybridization shows similar expression pattern in the control (C) and dKOs (D) E11.5 OFT. Scale bar: 20 µm

Meis function is required for proper epicardial patterning

Our results suggest that Meis TFs are required in the AMC for its proper structure and function and we wondered whether this could also be applied to the epicardium. For this purpose, we performed IF with Zonula occludens-1 (ZO-1) and WT1 antibodies, as epithelial and epicardial markers respectively (Figure 17A-D').

In the E16.5 control *Wt1^{Cre}; Rosa26^{tdtmt}* hearts, ZO-1 staining revealed a monolayer of epicardial cells (Figure 17A-A''). In the dKOs, however, we observed heterogeneity: in some regions, the epithelial arrangement seemed to be disrupted and an accumulation of *Wt1Cre lineage+* cells was observed (Figure 17B-B'). Other areas showed similar pattern to the controls (boxed region in Figure 17B''), while others had lost ZO-1 epicardial expression (arrowhead in Figure 17B'').

As expected, *Wt1Cre lineage+* cells in the controls showed high intensity WT1 expression in the epicardial monolayer (arrow in Figure 17C') and lower intensity in the EPDCs in the subepicardium and myocardium (arrowhead in Figure 17C'). In contrast, the epicardium in dKOs is formed by cells with variable intensity of WT1 expression (Figure 17D-D'). Moreover, EPDCs with lower WT1 protein levels in the dKOs tend to accumulate in the subepicardium (arrowhead in Figure 17D'). However, a small proportion of WT1+ EPDCs were also found migrating into the myocardium. This analysis suggested that *Wt1Cre lineage+* EPDCs may accumulate in the subepicardium instead of migrating into the myocardium.

To confirm this impression, we quantified the number of *Wt1Cre lineage+* cells in the epicardium/subepicardium and the myocardium in E15.5 cardiac sagittal sections (Figure 17E-H). A low proportion of CMs were found positive for tdtmt, however these were excluded from scoring, since previous work demonstrated that their labelling is due to recombination *in situ* and not because they are derived from the epicardium (Villa Del Campo et al., 2016). We did this exclusion based on their morphology and PROX1+ staining criteria (arrows in Figure 17E'-E'' and F'-F''). Epicardial *Meis* deletion results in a dual response: an increase in the abundance of epicardial/subepicardial cells (Figure 17G) and a tendency to reduction in the density of EPDCs in the myocardium (Figure 17H). A comparison of the proportion of *Wt1Cre lineage+* cells found in the epicardium versus the myocardium, showed that dKOs have a decreased proportion of the *Wt1Cre lineage+* cells in the myocardium (Figure 17I). However, the distribution of distances of *Wt1Cre lineage+* EPDCs to the epicardium is similar in controls and mutants, which suggests that mutant EPDCs migrate similarly to control EPDCs (Figure 17J).

To further validate these results, we stained E16.5 control and dKOs hearts with the mesenchymal marker VIMENTIN (Figure 18A-B'). The density of VIMENTIN+ cells in the epicardium and subepicardium in the dKOs (Figure 18B-B', C) did not differ statistically from that in the controls (Figure 18A-A', C). We did not find differences either in the proportion of epicardial/subepicardial VIMENTIN+ cells that derive from *Wt1+ lineage* (Figure 18D). In addition, we quantified the number of VIMENTIN+ EPDCs that had migrated into the compact myocardium (Figure 18E). The density of VIMENTIN+ EPDCs in the myocardium did not change between genotypes. However, we found a decrease in the proportion of

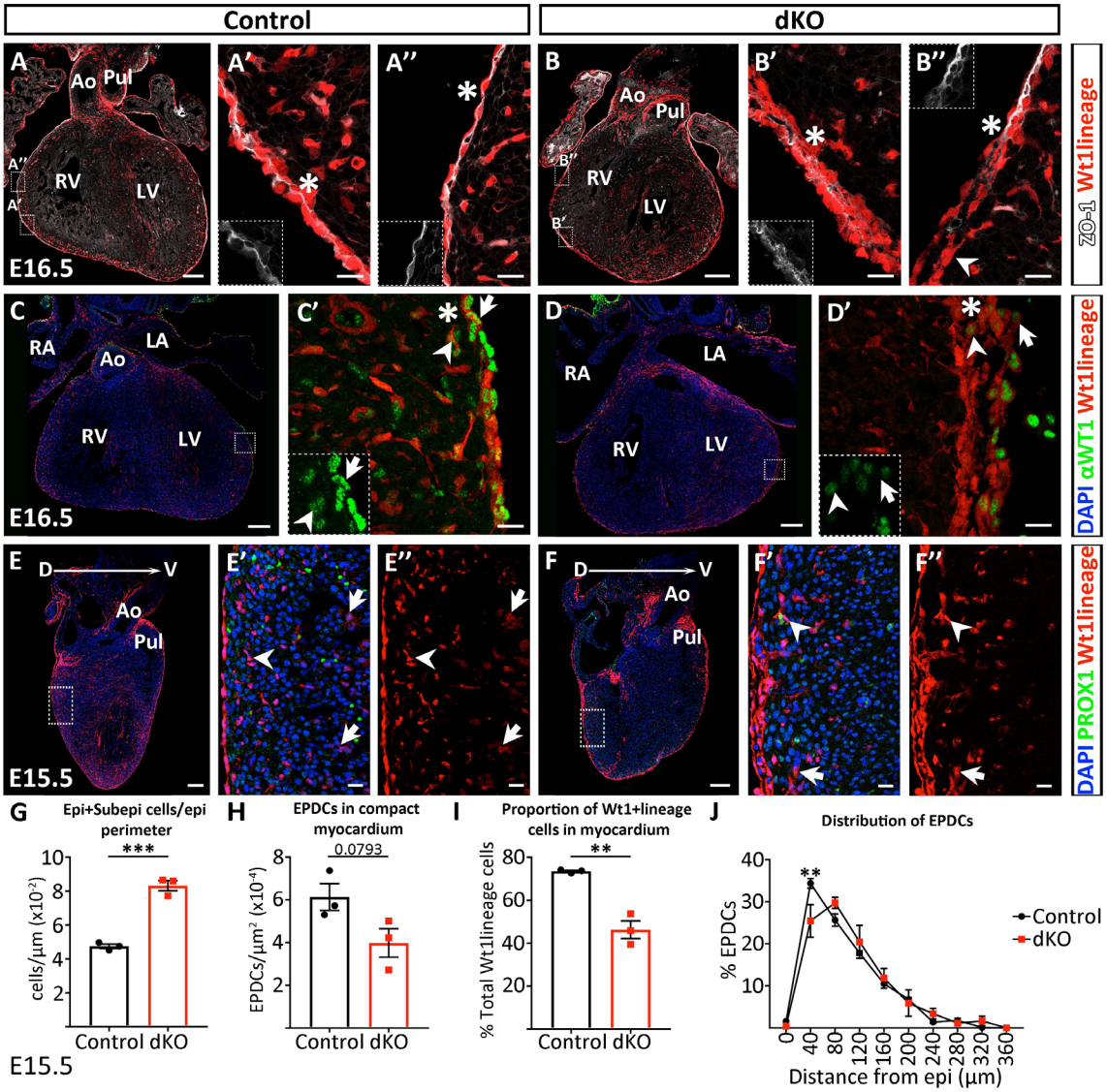

Figure 17. Epicardial *Meis* deletion produces alterations in the epicardium. (A-B'') ZO-1 immunostaining performed on E16.5 *Wt1^{Cre}; Rosa26^{tdtmt}* (Control) and *Wt1^{Cre}; Meis1$^{flox/flox}$; Meis2$^{flox/flox}$; Rosa26^{tdtmt}* (dKO) hearts. Arrowhead in B'' points to an epicardial region that lacks ZO-1 expression. (C-D') Immunofluorescence of the epicardial marker WT1 evidences differences in the expression and disposition of epicardial cells (arrows) and EPDCs (arrowheads) in E16.5 control (C-C') and mutant hearts (D-D'). C' and D' are higher magnifications of the boxed regions in C and D. Asterisks in A'-A'', B'-B'', C' and D' show the location of the boxed regions in each panel. (E-F'') E15.5 sagittal sections with *Wt1Cre lineage+* and PROX1 staining were used to quantify the number of *Wt1Cre lineage+* cells in the epicardium/subepicardium and EPDCs (arrowheads show examples) that were not cardiomyocytes (arrows). E'-E'' and F'-F'' show higher magnifications of the boxed regions in E and F respectively. (G) Quantification of *Wt1Cre lineage+* cells in the epicardium and subepicardium per epicardial perimeter. (H) Quantification of *Wt1Cre lineage+* EPDCs in the myocardium per compact myocardium area in control and dKOs. (I) Proportion of total *Wt1Cre lineage+* cells per heart found in the myocardium in controls and dKOs. (J) Distribution of *Wt1Cre lineage+* EPDCs depending on their distance from the epicardium. n=3 hearts per genotype. Three sections of each replicate were quantified and one ventral and one dorsal 340.9 x 340.9 µm2 fields were quantified per section. Unpaired t test. Ns: p value ≥ 0.05; ** p value <0.01; *** p value < 0.001. Error bars represent SEM. Ao: aorta; D: dorsal; LA: left atrium; LV: left ventricle; Pul: pulmonary artery; RA: right atrium; RV: right ventricle; V: ventral. Scale bar: 200 µm in A, B, C, D, E, F and 20 µm in A'-A'', B'-B'', C', D', E'-E'', F'-F''.

myocardial *Wt1Cre lineage+* VIMENTIN+ cells in the dKOs (Figure 18F). These results suggest that a decrease of VIMENTIN+ *Wt1Cre+ lineage* EPDCs in the dKOs may be compensated by other lineages, or that there is an excess of VIMENTIN+ *Wt1Cre*-negative cells in the mutant myocardium.

These data indicate that *Meis* genes are required for proper epicardial patterning and contribution to EPDCs but, are they important for the generation of all epicardial subpopulations? Or is their mutation just affecting a subset of the EPDCs? We decided to study SMCs and fibroblasts distribution and abundances to better understand the role of Meis TFs in the epicardium and EPDCs.

Decreased epicardial contribution to cardiac fibroblasts in Meis dKOs

We lack specific and robust cardiac fibroblasts markers, which makes their identification and quantification difficult (Ivey and Tallquist, 2016). For this study, we decided to use a combination of CD90 and CD140α antibodies (Figure 19). While CD90 labels mesenchymal and immature endothelial cells, CD140α labels cardiac fibroblasts and the epicardium (Carmona et al., 2020; Farbehi et al., 2019; Kang et al., 2008).

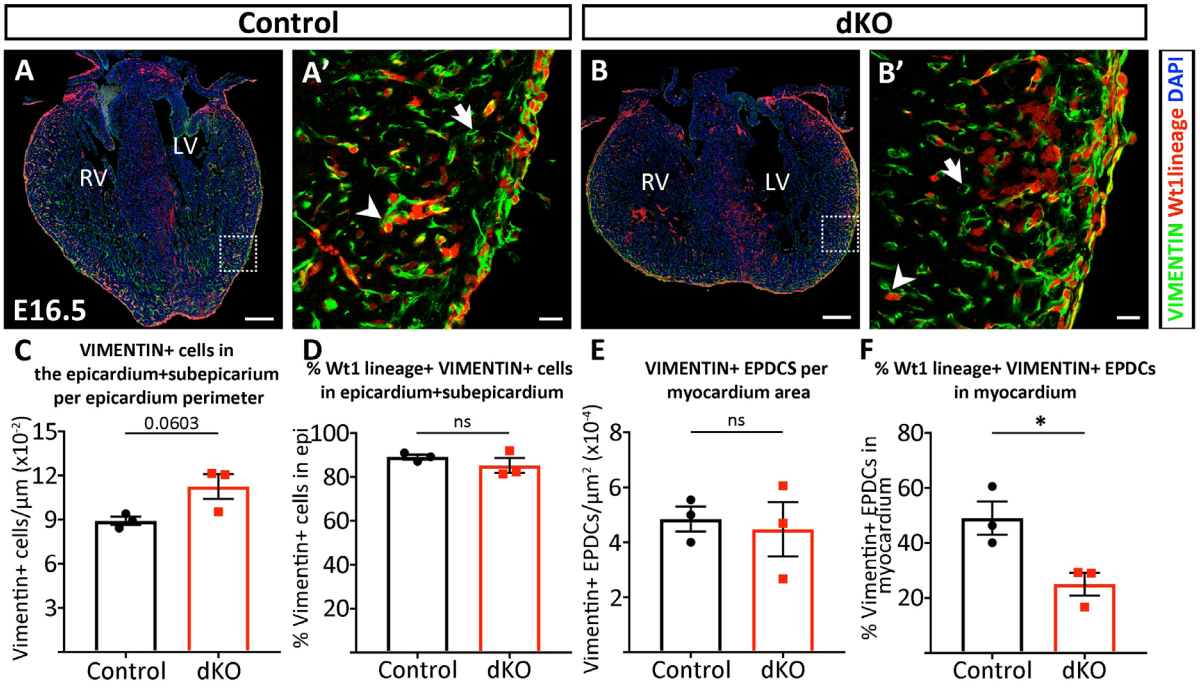

Figure 18. No major changes in epicardial contribution to total mesenchymal cells in Meis dKOs. (A-B') VIMENTIN immunofluorescence of E16.5 *Wt1^{Cre}; Rosa26^{tdtmt}* (Control, A-A') and *Wt1^{Cre}; Meis1$^{flox/flox}$; Meis2$^{flox/flox}$; Rosa26^{tdtmt}* (dKO, B-B') cardiac sections showing examples of mesenchymal cells (VIMENTIN+) that derive from *Wt1+ lineage* (arrowheads) and that derive from additional sources (arrows). A' and B' are higher magnifications of the boxed regions in A and B. (C) Quantification of the VIMENTIN+ cells in the epicardium and subepicardium per epicardium perimeter. (D) Proportion of VIMENTIN+ cells in the epicardium and subepicardium that derive from *Wt1+ lineage*. (E) Quantification of the total VIMENTIN+ cells in the free walls of the compact myocardium. (F) Proportion of VIMENTIN+ cells in the compact myocardium that derive from *Wt1+ lineage*. (n=3 hearts per genotype; 3 whole sections per heart were quantified). Unpaired t test. Ns: p value ≥ 0.05; * p value <0.05. Error bars represent SEM. LV: left ventricle; RV: right ventricle. Scale bar: Scale bar: 200 µm in A, B and 20 µm in A', B'.

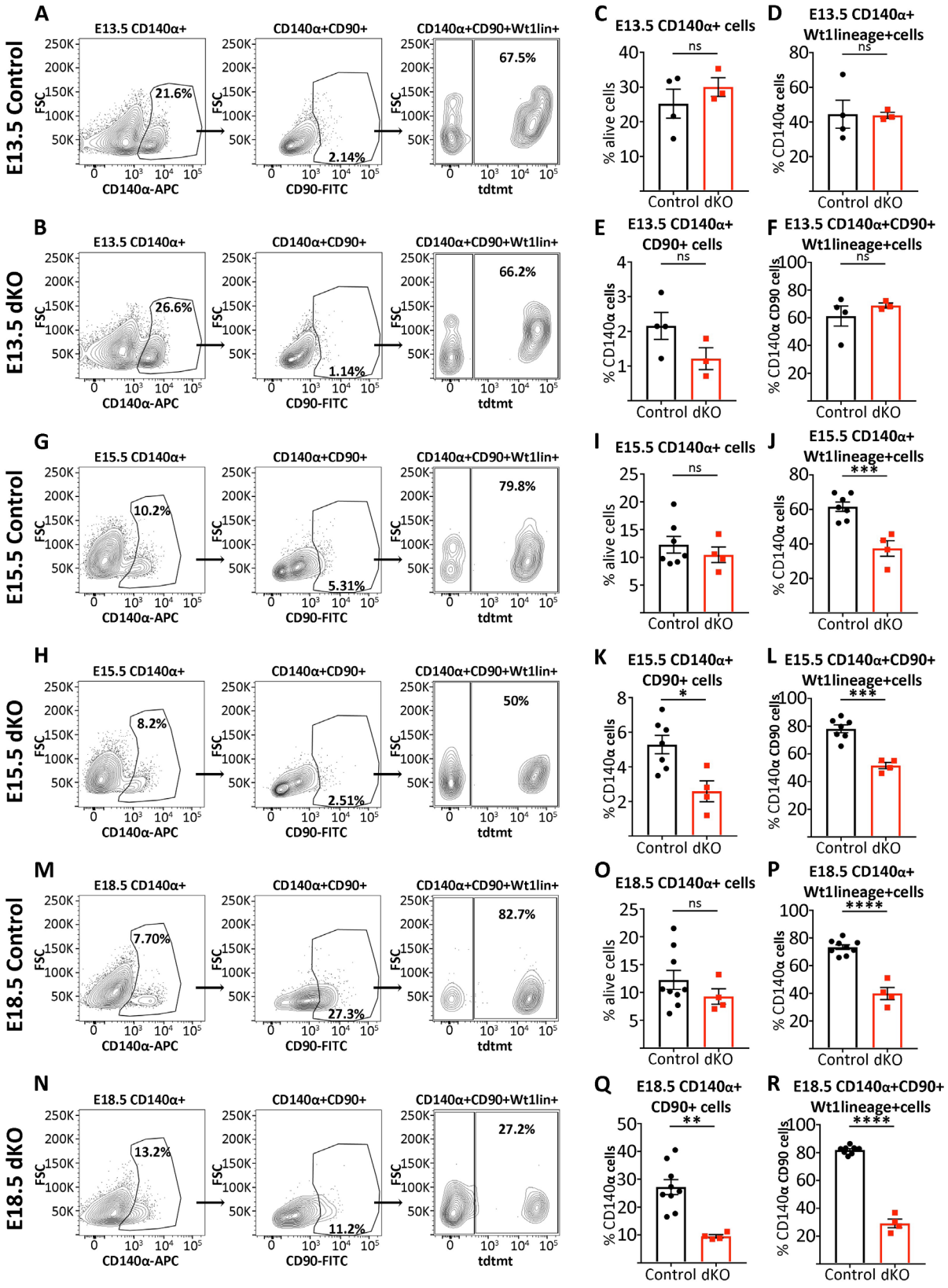
A
E13.5 Control
E13.5 CD140α+
CD140α+CD90+
CD140α+CD90+Wt1lin+
21.6%
2.14%
67.5%
CD140α-APC
CD90-FITC
tdtmt
B
E13.5 dKO
26.6%
1.14%
66.2%
C
E13.5 CD140α+ cells
% alive cells
ns
Control dKO
D
E13.5 CD140α+ Wt1lineage+cells
% CD140α cells
E
E13.5 CD140α+ CD90+ cells
% CD140α cells
F
E13.5 CD140α+CD90+ Wt1lineage+cells
% CD140α CD90 cells
G
E15.5 Control
E15.5 CD140α+
10.2%
5.31%
79.8%
I
E15.5 CD140α+ cells
J
E15.5 CD140α+ Wt1lineage+cells
***
H
E15.5 dKO
8.2%
2.51%
50%
K
E15.5 CD140α+ CD90+ cells
*
L
E15.5 CD140α+CD90+ Wt1lineage+cells
M
E18.5 Control
E18.5 CD140α+
7.70%
27.3%
82.7%
O
E18.5 CD140α+ cells
P
E18.5 CD140α+ Wt1lineage+cells
****
N
E18.5 dKO
13.2%
11.2%
27.2%
Q
E18.5 CD140α+ CD90+ cells
**
R
E18.5 CD140α+CD90+ Wt1lineage+cells

Figure 19. *Wt1Cre lineage+* cardiac fibroblasts are underrepresented in Meis dKOs. (A-B, G-H, M-N) Representative flow cytometry gating strategy used for E13.5 (A-B), E15.5 (G-H) and E18.5 (M-N) control (A, G, M) and dKO (B, H, N) disaggregated hearts stained against CD140α and CD90 (n≥3 hearts per genotype). (C, I, O) Quantification of CD140α+ cells at the different stages. (D, J, P) Quantification of proportion of CD140α+ cells that derive from *Wt1+ lineage* at the different stages. (E, K, Q) Quantification of proportion of CD140α+ cells that are CD140α+CD90+ at the different stages. (F, L, R) Quantification of proportion of CD140α+CD90+ cells that derive from *Wt1+ lineage* at the different stages. Unpaired t test. ns: p value ≥ 0.05; * p value <0.05; ** p value <0.01; *** p value < 0.001; **** p value < 0.0001. Error bars represent SEM.

We disaggregated E13.5, E15.5 and E18.5 hearts and performed flow cytometry analysis to determine the total number of CD140α+ cells and from this, the proportion of CD90+ CD140α+ double positive fibroblasts. At E13.5, *Meis* deletion produces no changes in the proportion of CD140α+ cells (Figure 19A-C) or CD90+ CD140α+ cells (Figure 19A-B, E). We did not find differences in the total proportion of cells expressing CD140α+ at E15.5 or E18.5 either (Figure 19G-I, M-O). However, at E15.5 and E18.5, we did observe a reduced proportion of CD90+ CD140α+ cells in the dKOs (Figure 19K, Q). With this strategy, we also aimed to determine the proportion of these cells that derive from the *Wt1+* cell lineage in controls and Meis dKOs. At E13.5, about 40% of the CD140α+ cells derive from the *Wt1+ lineage* in both, the controls and dKOs (Figure 19D). In controls, this proportion grows to 60% at E15.5 (Figure 19J) and to 70% at E18.5 (Figure 19P). In contrast, this proportion remains at about 40% at all stages in Meis dKOs. These differences were even more pronounced in CD90+ CD140α+ *Wt1Cre lineage+* fibroblasts. In the controls, about 60% of the double-positive fibroblasts derive from the *Wt1+ lineage* at E13.5 (Figure 19F) and 80% at E15.5 and E18.5 (Figure 19L, R). In contrast, in the dKOs, CD90+ CD140α+ *Wt1Cre lineage+* fibroblasts were 68% at E13.5 (Figure 19F), 50% at E15.5 (Figure 19L) and 30% at E18.5 (Figure 19R). These observations suggest: A) a deficiency in the contribution of the mutant epicardium to CD140α+ cell pool and an ability of other sources to compensate for this loss; B) This deficiency specially affects the CD90+ CD140α+ fibroblast population.

Therefore, these results suggest that *Meis* mutation reduces the ability of the epicardium to give rise to cardiac fibroblasts.

SMC distribution and abundance are severely altered in Meis dKOs

We performed whole mount IF against SM22α to study the overall distribution of SMCs in control and mutant E16.5 hearts and we found striking differences (Figure 20A-B'). In the controls, most of the SM22α+ cells were found around the coronary vessels and therefore can be identified as SMCs (Figure 20A-A'). In contrast, the majority of SM22α+ cells in dKOs do not associate with coronary vessels but appear widespread and accumulate in the subepicardium throughout the heart (Figure 20B and B'). This phenotype, however, seems to be transient and mostly compensated at later stages. At E18.5, although some SM22α+ cells are still located in the subepicardium in the mutants (arrowheads in Figure 20D-D'), most of them now surround the coronary arteries and veins as in the controls (Figure 20C-C').

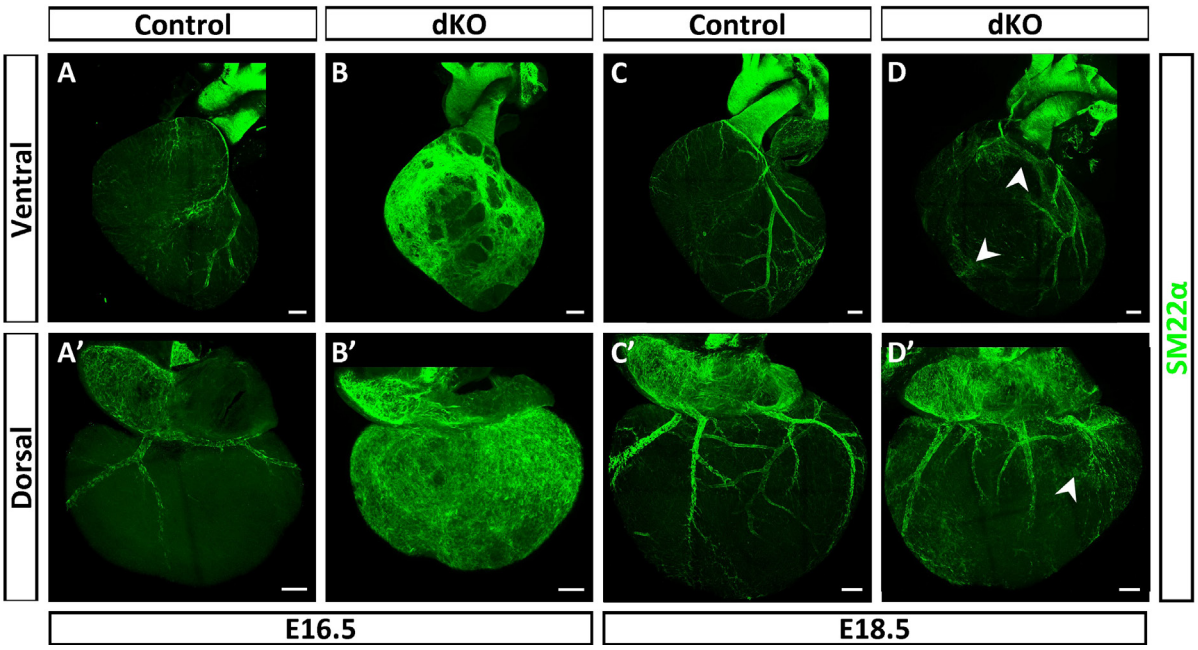

Figure 20. Epicardial *Meis* deletion causes a transient accumulation of SM22α+ cells in the subepicardium. Whole mount SM22α immunostaining in control E16.5 (A-A') and E18.5 (C-C') hearts reveal that SMCs are predominantly forming the coronary arteries and veins. However, in E16.5 Meis dKOs, SM22α+ cells are accumulated in the subepicardium both in the ventral (B) and dorsal (B') sides of the heart. At E18.5, although some SM22α+ cells remain in this area (arrowheads), most of them are surrounding the coronary vessels (D-D'). Scale bars: 200 μm

Nevertheless, some questions remained to be answered: are all the SM22α+ in the dKOs in the subepicardium? What is the nature of the subepicardial SM22α+ cells found in the mutants? Are SM22α+ overall more abundant in the mutants? Are the SMCs derived from the epicardium the only ones affected? What is the lineage of the SMCs recovered at later stages in the dKOs?

In order to study this in further detail, we performed immunostaining on *Wt1*^{Cre}*; Rosa26*^{tdtmt} (control) and *Wt1*^{Cre}*; Meis1*$^{flox/flox}$*; Meis2*$^{flox/flox}$*; Rosa26*^{tdtmt} (dKO) cardiac sections (Figure 21). CD31 was used as an endothelial marker and the location of the vessel was used to discriminate between coronary veins or lymphatics (in the subepicardial region) and coronary arteries (in the myocardium). We found that at E16.5, the SM22α+ cells that derive from *Wt1+ lineage* are increased in mutants when compared to controls (Figure 21I). In agreement with our observations in whole-mounts, we found that most of these cells are accumulated in the subepicardium of the mutants (Figure 21C-C'', L). The number of SM22α+ cells in contact with endothelial cells in the subepicardium –which then could be considered SMCs– is similar in both genotypes (Figure 21K). However, although in controls these ECs are mostly organised in big vessels, presumably veins, in the dKOs the endothelial plexus seems more immature (Figure 21C-C''). This, and the huge accumulation of SMCs in the same region, makes it difficult to determine whether in the dKOs the SMCs in contact with ECs in this area are surrounding veins or whether the contacts detected are random and due to cell crowding in the region. In addition, a subset of these epicardial-derived SMCs does migrate into the myocardium and reaches the coronary

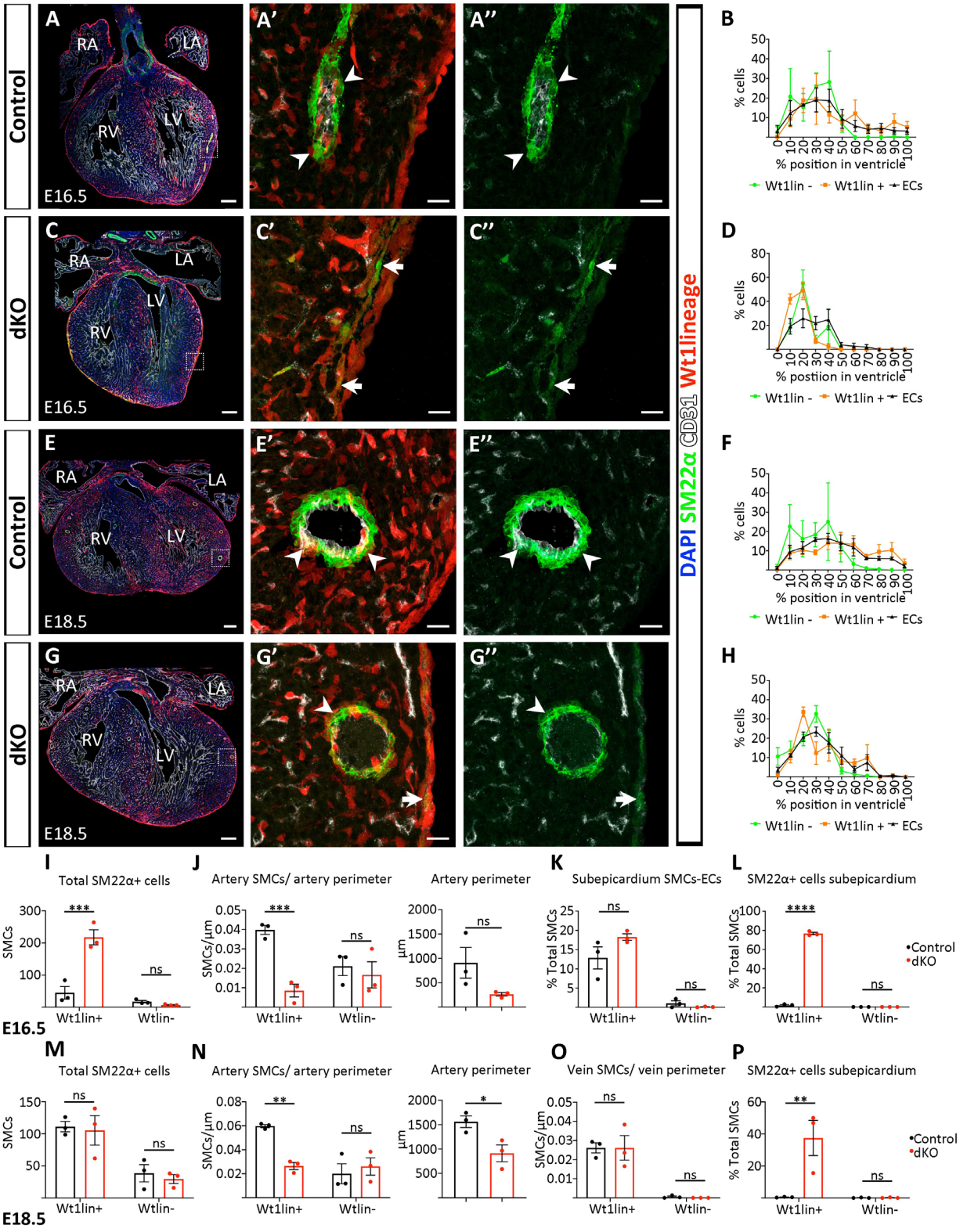
Control
dKO
Control
dKO
A
A'
A''
B
C
C'
C''
D
E
E'
E''
F
G
G'
G''
H
RA
LA
RV
LV
E16.5
E18.5
DAPI SM22α CD31 Wt1lineage
% cells
% position in ventricle
% postiion in ventricle
Wt1lin -
Wt1lin +
ECs
I
Total SM22α+ cells
J
Artery SMCs/ artery perimeter
Artery perimeter
K
Subepicardium SMCs-ECs
L
SM22α+ cells subepicardium
SMCs
SMCs/µm
µm
% Total SMCs
Wt1lin+
Wtlin-
•Control
•dKO
E16.5
M
Total SM22α+ cells
N
Artery SMCs/ artery perimeter
Artery perimeter
O
Vein SMCs/ vein perimeter
P
SM22α+ cells subepicardium
E18.5
ns

Figure 21. Alterations in the amount and location of SMCs in dKOs. (A-A'', C-C'', E-E'', G-G'') Immunostaining of ECs (CD31+) and SMCs (SM22α+) in *Wt1^{Cre}; Rosa26^{tdtmt}* (Control) and *Wt1^{Cre}; Meis1$^{flox/flox}$; Meis2$^{flox/flox}$; Rosa26^{tdtmt}* (dKO) E16.5 and E18.5 hearts. A'-A'', C'-C'', E'-E'', G'-G'' show higher magnifications of the boxed regions in A, C, E and G, respectively, pointing to SMCs around the coronary arteries (arrowheads) and in the subepicardium (arrows). (B, D, F, H) Frequency distribution of arterial ECs and *Wt1Cre lineage*+ (Wt1lin+), *Wt1Cre lineage*-negative (Wt1lin-) SMCs according to the basal-to-apical position of the arteries in the ventricles of E16.5 control (B), E16.5 dKO (D), E18.5 control (F) and E18.5 dKO (H) hearts. (I, M) Quantification of total SM22α+ cells per section at E16.5 (I) and E18.5 (M). (J, N) Quantification of SMCs per total artery perimeter per section showing lower artery *Wt1Cre lineage*+ SMCs coverage in dKOs at E16.5 (J) and E18.5 (N). The quantification of total artery perimeter is also shown. (K) Percentage of total SM22α+ cells that are in the subepicardial region in contact with endothelial cells. (L, P) Quantification of the proportion of total SM22α+ cells per section in the subepicardium at E16.5 (L) and E18.5 (P). (O) Quantification of SMCs per vein perimeter per section at E18.5. (n=3 hearts per genotype, per stage; at least 4 sections were quantified per heart). Two-way ANOVA, for artery perimeter comparisons. Unpaired t test. ns: p value ≥ 0.05; * p value <0.05; ** p value <0.01; *** p value < 0.001; **** p value < 0.0001. Error bars represent SEM. LA: left atrium; LV: left ventricle; RA: right atrium; RV: right ventricle. Scale bar: 200 µm in A, C, E, G and 20 µm in A'-A'', C'-C'', E'-E'' and G'-G''.

arteries. However, their coverage of the arteries is lower than in controls, with less SMCs per artery perimeter (Figure 21J). Interestingly, the proportions of *Wt1 lineage*-negative SMCs are similar in the dKOs and controls at E16.5 and E18.5 (Figure 21I-P). This indicates that the amelioration of the phenotype at late stages is not due to an increased contribution of other lineages, such as cNCCs or SHF, and that the mutation only affects epicardial-derived SMCs.

At E18.5 most of the values are compensated to a certain degree. The total number of SMCs and their colonization of veins in the dKOs do not differ from those in the controls (Figure 21M, O). Nevertheless, there is still some accumulation of SM22α+ cells in the subepicardium (Figure 21P) and a lower coverage of the arteries by SMCs (Figure 21N).

Moreover, we also found that at E18.5 the average total artery perimeter quantified in the dKOs was lower than in the controls (Figure 21N), which suggests that *Meis* mutation results in impaired/delayed arterial development. Furthermore, we observed that both, arteries and SMCs did not reach positions as distal in the ventricles of dKOs as in the ventricles of controls (Figure 21B, D, F, H). In controls, both at E16.5 and E18.5, arterial SMCs and ECs are found throughout the length of the ventricles and the distribution of *Wt1Cre lineage*+ SMCs in controls parallels that of arteries (Figure 21B, F). In contrast, in E16.5 dKOs, arteries appear very reduced further than 50 % of the distance between the base and the apex of the ventricles, while SMCs are very reduced beyond 30% and totally absent beyond 50% (Figure 21D). Although at E18.5 arteries have grown more distally in the mutants, they do not reach the apex (Figure 21H). These results indicate a delay in coronary artery development and a reduced coverage of coronary arteries by SMCs in the mutants.

Myofibroblasts accumulate in the subepicardium of Meis dKOs

We further investigated the identity of the *Wt1Cre lineage*+ SM22α+ cells accumulated in the subepicardium. SM22α expression is compatible with a pericyte/SMC identity or with a myofibroblast identity. To discriminate between these possibilities, we studied the fibroblast marker PERIOSTIN, which is also expressed in myofibroblasts (Davis and Molkentin, 2014). Therefore, we performed PERIOSTIN IF on *Wt1^{Cre}; Rosa26^{tdtmt}* (Figure 22A-A'''') and *Wt1^{Cre}; Meis1$^{flox/flox}$; Meis2$^{flox/flox}$; Rosa26^{tdtmt}* (Figure 22B-B'''') E15.5 sagittal cardiac sections. In the controls, most PERIOSTIN+ cells are found in the myocardium and few in the subepicardium (arrowhead in Figure 22A''-A'''). In contrast, most PERIOSTIN+ *Wt1Cre lineage*+ cells accumulate in the subepicardium in dKOs (Figure 22B-B' and arrowheads in Figure 22B''-B'''). Therefore, these results suggest that the SM22α+ *Wt1Cre lineage*+ cells accumulated in the subepicardium of Meis dKOs (Figure 20B-B') also express fibroblasts markers as PERIOSTIN. This agrees with a myofibroblast identity, which also fits their lack of association with vessels.

Coronary vein and artery development in Meis mutants

Our results indicate a primary deficiency of EPDC lineages and poorly developed arteries in the apical part of the ventricles (Figure 21D, H). This could have important implications, so we decided to further characterize the defects in the coronary blood vessels.

At E16.5 coronary arteries and veins are usually quite advanced in their development in control hearts, as shown by connexin-40 and endomucin (EMCN) whole-mount IF, respectively (Figure 23A, I)

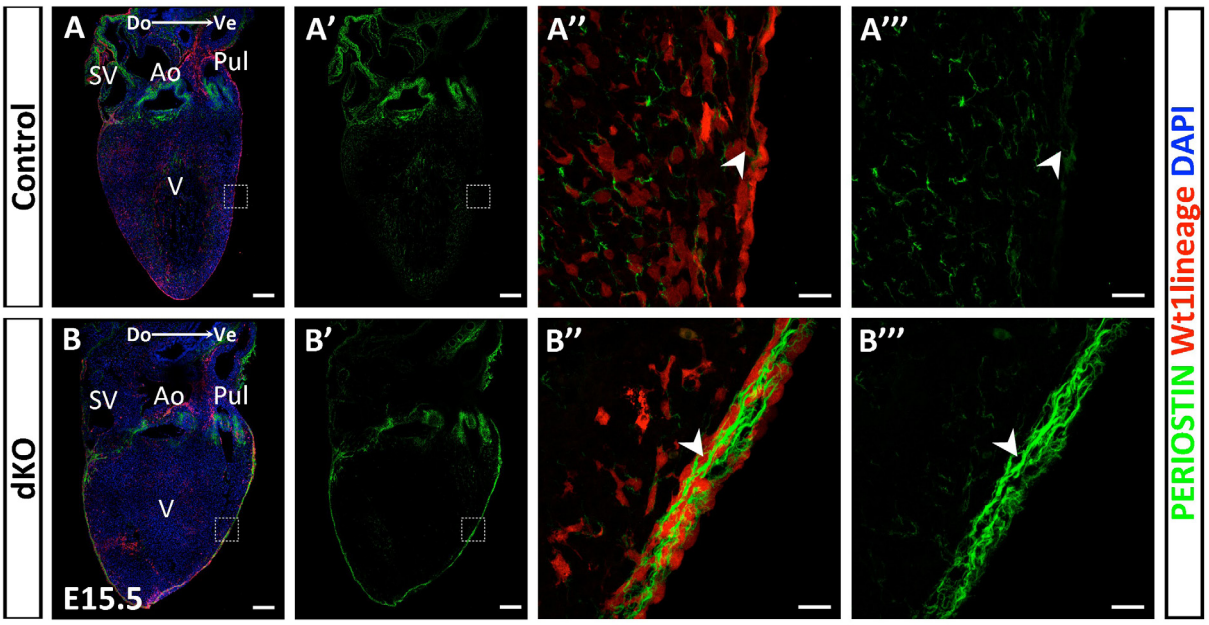

Figure 22. Myofibroblasts accumulate in the subepicardium of Meis dKOs. (A-B''') PERIOSTIN IF of *Wt1^{Cre}; Rosa26^{tdtmt}* (control, A-A''') and *Wt1Cre; Meis1$^{flox/flox}$; Meis2$^{flox/flox}$; Rosa26^{tdtmt}* (dKO, B-B''') E15.5 cardiac sagittal sections. (A', B') PERIOSTIN single channel of A and B. A''-A''' and B''-B''' are higher magnifications of the boxed regions in A-A' and B'B' respectively. Arrowheads point to examples of the PERIOSTIN+ *Wt1Cre lineage*+ cells found in the subepicardium of controls and dKOs. Ao: aorta; Do: dorsal; Pul: pulmonary artery; SV: sinus venosus; V: ventricle; Ve: ventral. Scale bar 200 μm in A-A', B-B' and 20 μm in A''-A''' and B''-B'''.

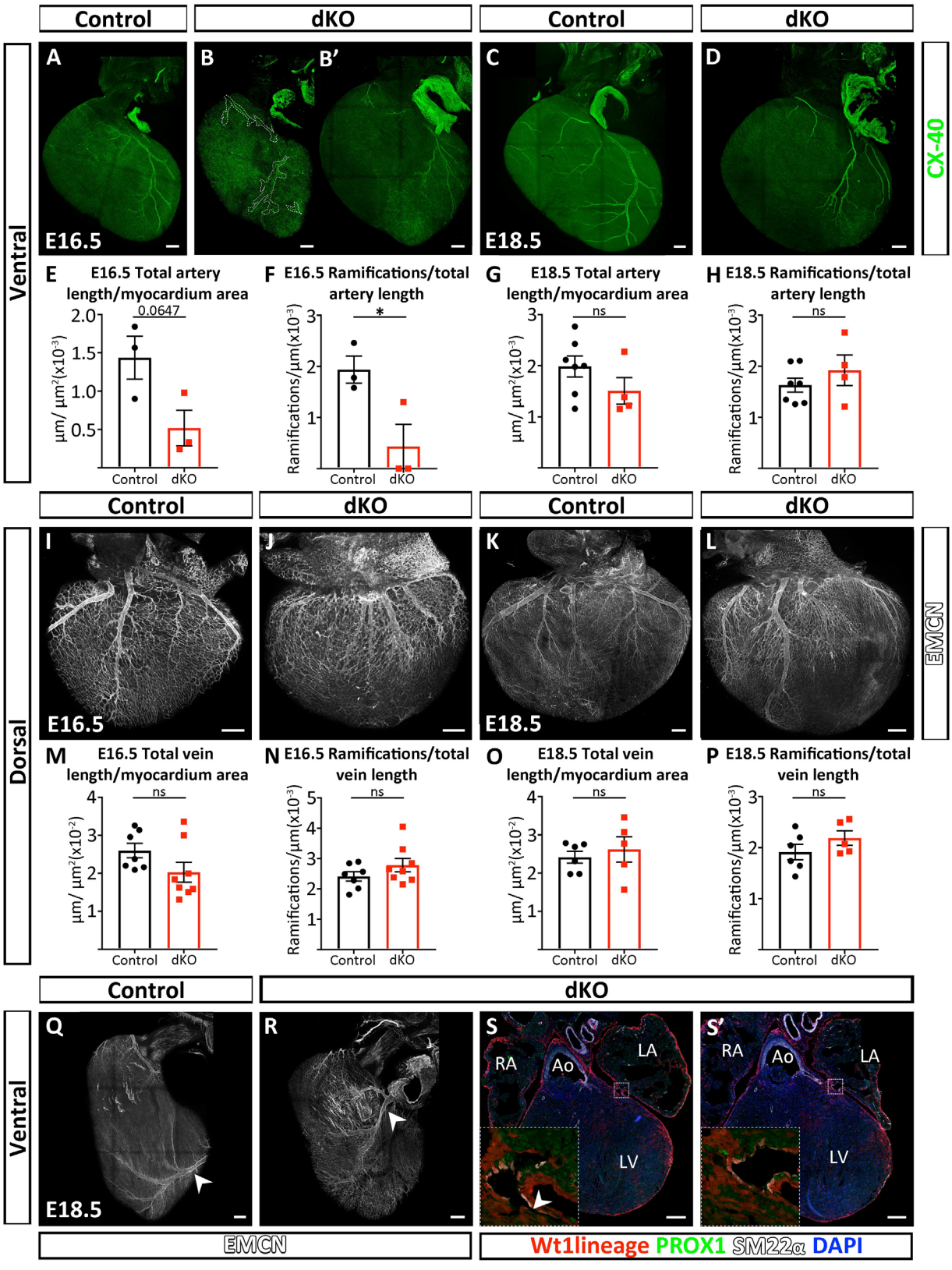
Control
dKO
Control
dKO
Ventral
A
B
B'
C
D
E16.5
E18.5
CX-40
E E16.5 Total artery length/myocardium area
0.0647
µm/ µm²(x10⁻³)
Control
dKO
F E16.5 Ramifications/total artery length
*
Ramifications/µm(x10⁻³)
G E18.5 Total artery length/myocardium area
ns
H E18.5 Ramifications/total artery length
Control
dKO
Control
dKO
Control
dKO
Dorsal
I
J
K
L
EMCN
M E16.5 Total vein length/myocardium area
µm/ µm²(x10⁻²)
N E16.5 Ramifications/total vein length
O E18.5 Total vein length/myocardium area
P E18.5 Ramifications/total vein length
Control
dKO
Ventral
Q
R
S
S'
RA
Ao
LA
LV
EMCN
Wt1lineage PROX1 SM22α DAPI

Figure 23. Coronary vasculature development is delayed in dKOs. (A-D) Connexin-40 (CX-40) whole mount immunofluorescence shows coronary arteries in E16.5 control (A), E16.5 dKO (B, B'), E18.5 control (C) and E18.5 dKO hearts (D). Dashed lines in B delineate the immature CX40+ arteries. (E, G) Quantification of total artery length resulting from the sum of the length of each individual artery branch of left coronary artery divided by myocardium area at E16.5 (E) and E18.5 (G). (F, H) Ramifications per total artery length at E16.5 (F) and E18.5 (H). (n ≥ 3 hearts per genotype). (I-L) Whole mount EMCN IF shows dorsal coronary veins of E16.5 control (I), E16.5 dKO (J), E18.5 control (K) and E18.5 dKO hearts (L). (M-P) Quantification of the dorsal coronary veins. (M, O) Quantification of the total vein length resulting from the sum of the length of each individual vein divided by myocardium area at E16.5 (M) and E18.5 (O). (N, P) Ramifications per total vein length at E16.5 (N) and E18.5 (P). (n ≥ 5 hearts per genotype). Unpaired t test. Ns: p value ≥ 0.05; * p value < 0.05 Error bars represent SEM. (Q-R) Whole mount EMCN IF shows ventral coronary veins of E18.5 control (Q) and dKO (R) hearts. Arrowheads evidence the different location. (S-S') *Wt1*^{Cre}*; Meis1*$^{flox/flox}$*; Meis2*$^{flox/flox}$*; Rosa26*^{tdtmt} consecutive cardiac sections stained with DAPI, PROX1 and SM22α to visualise the myocardium and SMCs respectively. The bigger boxed regions are higher magnifications of the smaller boxed regions. Arrowhead points to a presumed coronary vein connecting with the left atrium. Ao: aorta; LA: left atrium; LV: left ventricle; RA: right atrium. Scale bar: 200 µm

As we suspected from our previous findings, the dKOs presented defects and showed immature blood coronary vessels at E16.5 (Figure 23B, B', J). At this stage, 2 out of 3 dKOs showed immature and dilated Connexin-40+ arteries (Figure 23B). The other dKO had normal but less developed coronary arteries (Figure 23B'). Their total length (Figure 23E) and ramifications (Figure 23F) were reduced compared to those in controls (Figure 23E-F). EMCN+ veins also appear slightly less developed and mispatterned (Figure 23J), nevertheless, we did not find significant differences in the total vein length (Figure 23M) or ramifications (Figure 23N) between controls and dKOs. Similar to what happens with SMCs, at E18.5 the coronary vasculature phenotype is partially recovered. In the dKOs, coronary arteries have acquired mature vessel-like structures (Figure 23D), although their patterning of ramifications is still different and they do not reach positions as distal as the controls (Figure 23C). Dorsal views of mutant E18.5 hearts reveal that their veins also show an altered ramification patterning (Figure 23L). Nevertheless, both dKOs arteries and veins have similar number of ramifications (Figure 23H, P) and total artery and vein length to that of controls (Figure 23G, O).

In summary, these results indicate that epicardial *Meis* deletion causes a delay in coronary artery and vein development, but the defects are mostly compensated from E16.5 to E18.5. Nevertheless, in spite of the compensatory mechanism, some patterning differences persist in the dKOs. In all studied dKOs at E18.5 (n=5), we found a thick vein on the surface of the left ventricle (Figure 23R) while we did not find it in any of the four analysed controls (Figure 23Q). Its position suggested a possible ectopic connection with the left atrium (arrowhead Figure 23R). We corroborated the ectopic connection between this coronary vein (arrowhead in Figure 23S) and the left atrium by analysis of consecutive cardiac sections in one specimen (Figure 23S-S'). These differences persist in the surviving adult mutant hearts (Figure 24). Gelatin and Indian ink injections performed in the LV of control and mutant adult hearts, reveal differences in patterning (arrowhead in Figure 24B) and mild differences in vessel morphology between control (Figure 24C) and dKO (Figure 24D) dorsal veins.

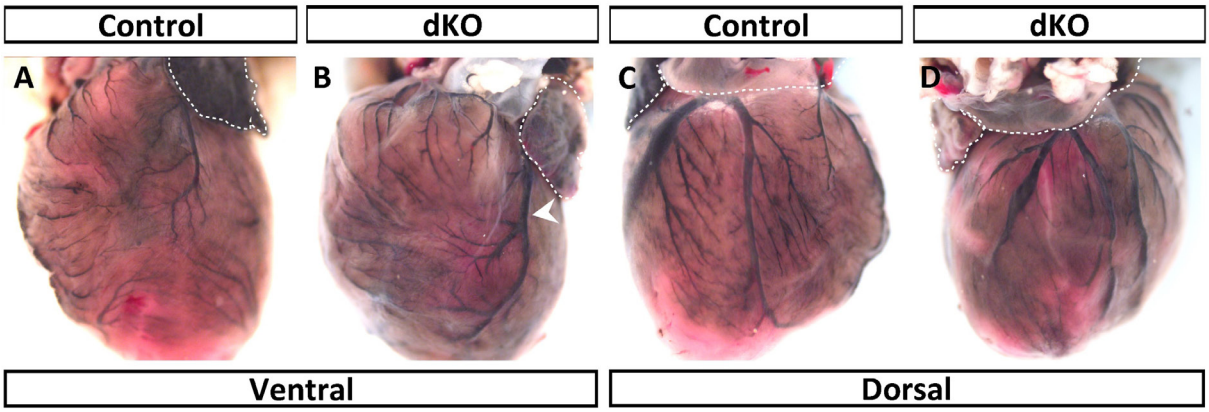

Figure 24. Adult dKOs hearts exhibit mild coronary patterning defects. Coronary vessels in the ventral (A-B) and dorsal (C-D) side of control (A, C) and dKO (B,D) adult hearts were visualised with the injection of Indian ink and gelatin. Alterations in coronary branching patterning and connections (arrowhead) persist in the surviving adult dKO mice.

These defects could be partially related to the activation of *Wt1*^{Cre} in the coronary endothelial cell lineage. These endothelial cells are unlikely to derive from the *Wt1+* epicardial lineage, since endothelial contribution of the epicardium derives from just a subset of Scx+, *Sema3d*+ and *Wt1 lineage*-negative epicardial cells (Katz et al., 2012). Therefore, most likely *Wt1Cre lineage*+ ECs derive from *in situ* activation of *Wt1* in a fraction of coronary endothelial cells (Rudat and Kispert, 2012). We have not detected *Meis* expression in coronary ECs (not shown), however, we cannot completely rule out an autonomous role of *Meis* TFs at some stage of the EC lineage development that may affect coronary development. Due to this, in our following study we distinguished between tdtmt+ and tdtmt-negative ECs.

In order to understand better the coronary defects, we enzymatically disaggregated E13.5, E15.5 and E18.5 hearts and performed flow cytometry analysis. We quantified CD31+ EMCN low/medium coronary endothelial cells and excluded endocardial cells based on their high levels of EMCN (Carmona et al., 2020; González-Hernández et al., 2020) (Figure 25). At E13.5, dKOs have less coronary ECs (Figure 25A-C), although the proportion of tdtmt+ ECs and tdtmt-negative ECs is similar to that in controls (Figure 25D). At E15.5, the total number of coronary ECs in mutants does not differ from that in controls (Figure 25E-G), but there is a higher contribution of tdtmt-negative ECs in dKOs (Figure 25H). However, this difference is compensated and, by E18.5, there are not differences regarding the total number or proportions between controls and dKOs (Figure 25I-L). These results show transient reduction in the contribution of *Wt1Cre*+ coronary endothelial cells in mutants, however, this reduction is compensated by *Wt1Cre*-negative cells.

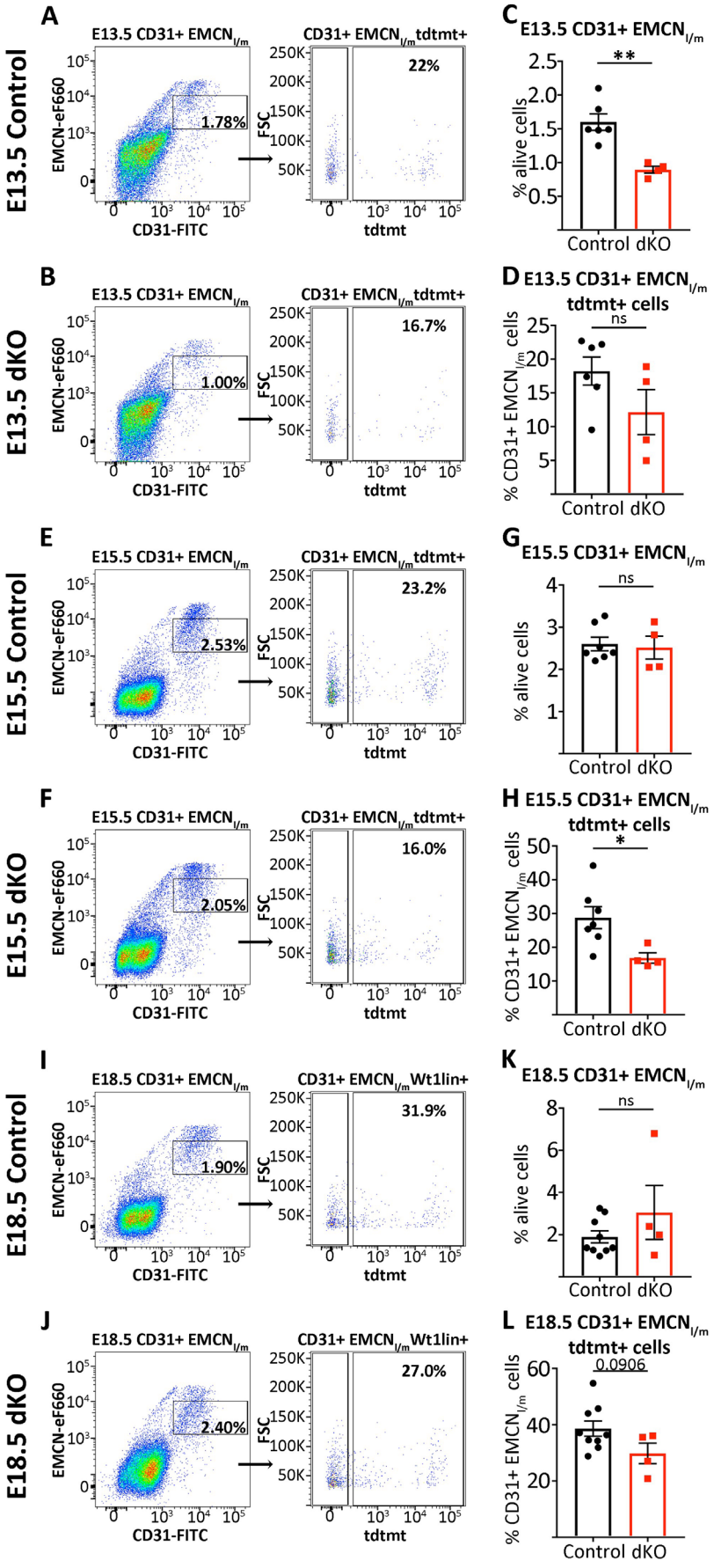

Figure 25. C o r o n a r y endothelial cells numbers are maintained in Meis dKOs. (A-L) *Wt1^{Cre}; Rosa26^{tdtmt}* (control) and *Wt1^{Cre}; Meis1$^{flox/flox}$; Meis2$^{flox/flox}$; Rosa26^{tdtmt}* (dKO) disaggregated hearts were stained against CD31-FITC and EMCN-eFluor660 for flow cytometry analysis of coronary ECs (CD31+ EMCN low/medium). (A-B, E-F, I-J) Gating strategy for E13.5 (A-B), E15.5 (E-F) or E18.5 (I-J) control and dKO hearts. Left panels show the selection of CD31+ EMCN low/medium cells. Right panels show the selection of CD31+ EMCN low/medium tdtmt+ cells. (C, G, K) Quantification of alive cells that are CD31+ EMCN low/medium coronary ECs at E13.5 (C), E15.5 (G) and E18.5 (K). (D, H, L) Proportion of CD31+ EMCN low/medium coronary ECs that are tdtmt+ at E13.5 (D), E15.5 (H) and E18.5 (L). (n ≥ 4 hearts per genotype per stage) Unpaired t test. ns: p value ≥ 0.05; * p value <0.05; ** p value <0.01. Error bars represent SEM.

Decreased cardiac innervation of Meis dKOs

Symphatetic cardiac nerves differentiate from the cardiac neural crest and enter the heart following the vagal tracts (Végh et al., 2016). Once at the base of the heart, nerves follow the path of coronary veins towards the apex in the subepicardium (Nam et al., 2013). It was described that SMCs that colonise first the veins, and later the coronary arteries, secrete attractant molecules that guide axon growth (Nam et al., 2013). Defective coronary development leads to abnormal sympathetic innervation (Nam et al., 2013).

As we found that Meis dKOs suffer alterations in coronary vessels and SMC development, we wondered whether Meis dKOs may also show defective cardiac innervation. In order to tackle this question, we performed whole mount immunostaining against Tyrosine Hydroxylase (TH) and EMCN of control (Figure 26A-B') and dKO (Figure 26C-D') E16.5 hearts. dKOs show decreased innervation of the ventral (Figure 26C-C', E) and dorsal sides of the ventricles (Figure 26D-D', F). Moreover, similar to the controls, nerves in the dKOs are found in close proximity to veins (Figure 26B, D).

Therefore, these results suggest that cardiac innervation is also impaired by epicardial *Meis* deletion as a secondary result of coronary defects.

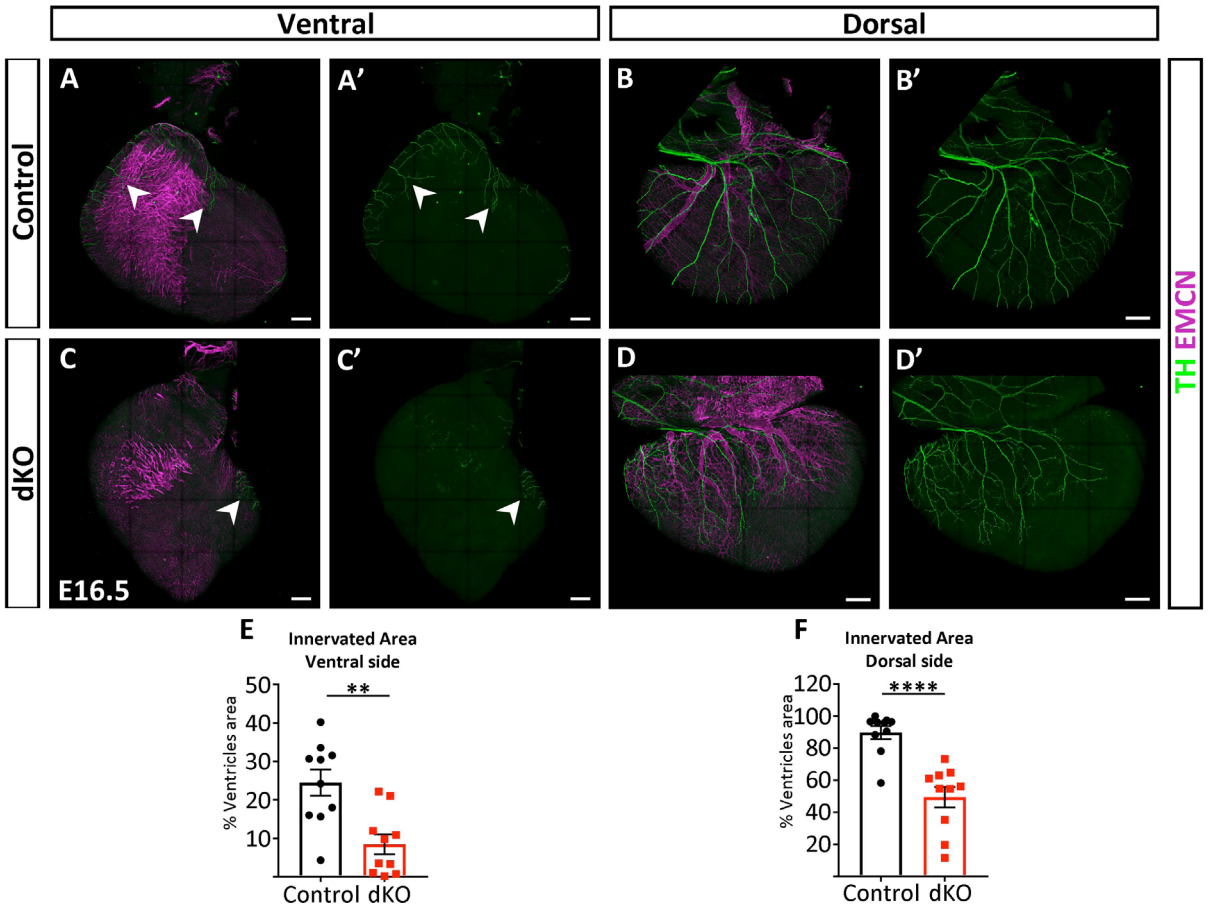

Figure 26. Decreased cardiac innervation upon *Meis* deletion. (A-D') Whole-mount EMCN and Tyrosine Hydroxylase (TH) IF to visualise cardiac veins and symphatetic nerves of control (A-B') and dKO (C-D') E16.5 hearts. (A, C, B, D) EMCN and TH staining overlay of ventral (A, C) and dorsal (B, D) sides acquisitions. (A', B', C', D') Single-TH+ channel to visualise cardiac nerves on the ventral (A', C') and dorsal (B', D') sides of the ventricles. Arrowheads point to growing cardiac nerves on the ventral side of the heart. (E, F) Percentage of the ventricles area innervated by TH+ cardiac nerves on the ventral (E) and dorsal sides of the ventricles (F) of control and mutant hearts. (n ≥ 9 hearts per genotype). Unpaired t test. ns: p value ≥ 0.05; ** p value <0.01; **** p value < 0.0001. Error bars represent SEM. Scale bar: 200 µm.

The phenotype of *Tbx18^{Cre}; Meis1$^{flox/flox}$; Meis2$^{flox/flox}$* embryos confirms the epicardial origin of the defects in *Meis* mutants recombined with *Wt1^{Cre}*.

While *Wt1^{Cre}* extensively recombines the developing epicardium and its derivatives, this line also recombines cardiac endothelium and some cardiomyocytes at lower frequency (Rudat and Kispert, 2012; Zhou and Pu, 2012; Zhou et al., 2008). To study whether the defects in *Wt1^{Cre}; Meis1$^{flox/flox}$; Meis2$^{flox/flox}$* hearts are due to the elimination of *Meis* from the epicardium, we used *Tbx18^{Cre}* as an additional epicardial driver to validate our results. With this purpose, we generated *Tbx18^{Cre}; Meis1$^{flox/flox}$; Meis2$^{flox/flox}$* (From now on referred to as Tbx18Cre; dKO) mice. Tbx18Cre; dKO mice show 85% lethality and the few mutants that survive beyond weaning need to be sacrificed due to kidney failure (Figure 27A).

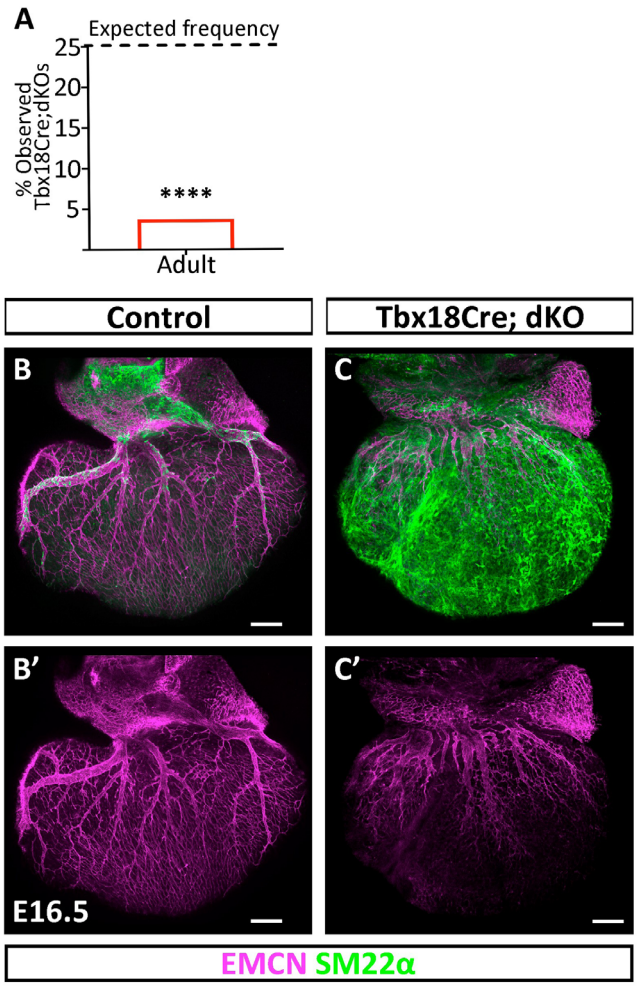

Figure 27. Tbx18^{Cre}; Meis1$^{flox/flox}$; Meis2$^{flox/flox}$ hearts recapitulate the same SMCs and coronary vein defects. (A) Observed and expected frequency of *Tbx18^{Cre}; Meis1$^{flox/flox}$; Meis2$^{flox/flox}$* (Tbx18Cre; dKO) at weaning. Chi-square statistical analysis reflects statistical significant differences. (B-C') Whole mount EMCN and SM22α immunofluorescence of E16.5 control (B-B') and Tbx18Cre; dKOs hearts (C-C'). Scale bars: 200 µm.

We studied whether this mouse model recapitulated the major alterations in Wt1Cre; dKOs regarding coronary vasculature development and EPDCs. We performed whole-mount IF against EMCN and SM22α to visualise coronary veins and SMCs/myofibroblasts, respectively (Figure 27B-C'). At E16.5, Tbx18Cre; dKOs presented underdeveloped coronary veins that showed less association to SMCs (Figure 27C-C') compared to controls (Figure 27B-B'). Furthermore, the mutant hearts also showed an extensive accumulation of SM22α+ cells in the subepicardium. Therefore, these results agree with our previous findings and reinforce our hypothesis that *Meis* expression in the epicardium/EPDCs is essential for coronary vasculature and EPDC development (Figure 20, Figure 21, Figure 23 and Figure 27).

RNAseq analysis to better understand the molecular mechanisms governing Meis dKOs phenotype

Our findings evidence that MEIS TFs are necessary in the epicardium but with these results, we could not determine the molecular mechanisms involved. On the one hand, the changes in SMCs and fibroblasts may suggest a function in EPDC specification and differentiation. On the other hand, the subepicardial accumulation of EPDCs may also be associated with paracrine signalling defects that prevent their migration and promote their differentiation into myofibroblasts. Another possibility is an autonomous role of *Meis* genes in fibroblasts or SMCs. Furthermore, we needed to determine whether the coronary defects are the cause or the consequence of the EPDC defects. To gain insight into the molecular mechanisms governing the phenotype, we performed an RNAseq analysis.

We decided to take advantage of a previous methodology developed in the group (Lioux et al., 2020), and we peeled off the epicardium/subepicardium of control and dKOs of E16.5 ventricles. With this approach, we focused on the epicardial alterations that may otherwise had been lost if we would have analysed the whole heart. Upon isolation of the tissue for the subsequent RNAseq analysis, we appreciated differences between the control and dKOs epicardium. The dKOs epicardium was more fragile and thicker than that of controls (not shown). Probably, this was due to the accumulation of cells in the subepicardium.

We compared dKO and control epicardia and obtained 3047 differentially expressed genes (DEGs), of which, 1359 were upregulated and 1688 were downregulated in the dKOs (adjusted p-value ≤ 0.05) (Figure 28C and Supp. Table 1). We performed Ingenuity Pathway Analysis and found that DEGs were related mainly to "Cardiovascular System Development and Function" and "Organismal Development" gene sets (Figure 28A). Interestingly, with this analysis we also found that DEGs grouped in categories associated with "Cellular movement" and "Cell morphology" (Figure 28B).

As we would have expected from the previously described alterations, some DEGs were linked to epicardial identity and function. *Wt1*, *Tbx18* and *Tcf21* epicardial markers were all downregulated in Meis dKOs (Figure 28D). In addition, we also found important changes in key genes for EMT, such as *Snai2*, F*gf2, Cdh1, Pdgfrα, Pdgfrβ* among others (Cao et al., 2020; Quijada et al., 2020). Moreover, the upregulation of some Notch receptors (*Notch1* and *Notch4*), ligands (*Jag2, Dll4*) and target genes

A

Name	p-value range
Cardiovascular System Development and Function	3.47E-07 - 1.51E-35
Organismal Development	2.67E-07 - 2.78E-30
Organ Morphology	3.47E-07 - 2.59E-29
Skeletal and Muscular System Development and Function	3.47E-07 - 6.86E-27

B

Name	p-value range
Cellular Movement	3.94E-07 - 2.73E-27
Cell Morphology	3.79E-07 - 3.94E-17
Molecular Transport	2.44E-07 - 2.25E-16
Lipid Metabolism	3.90E-07 - 4.06E-14
Small Molecule Biochemistry	3.90E-07 - 4.06E-14

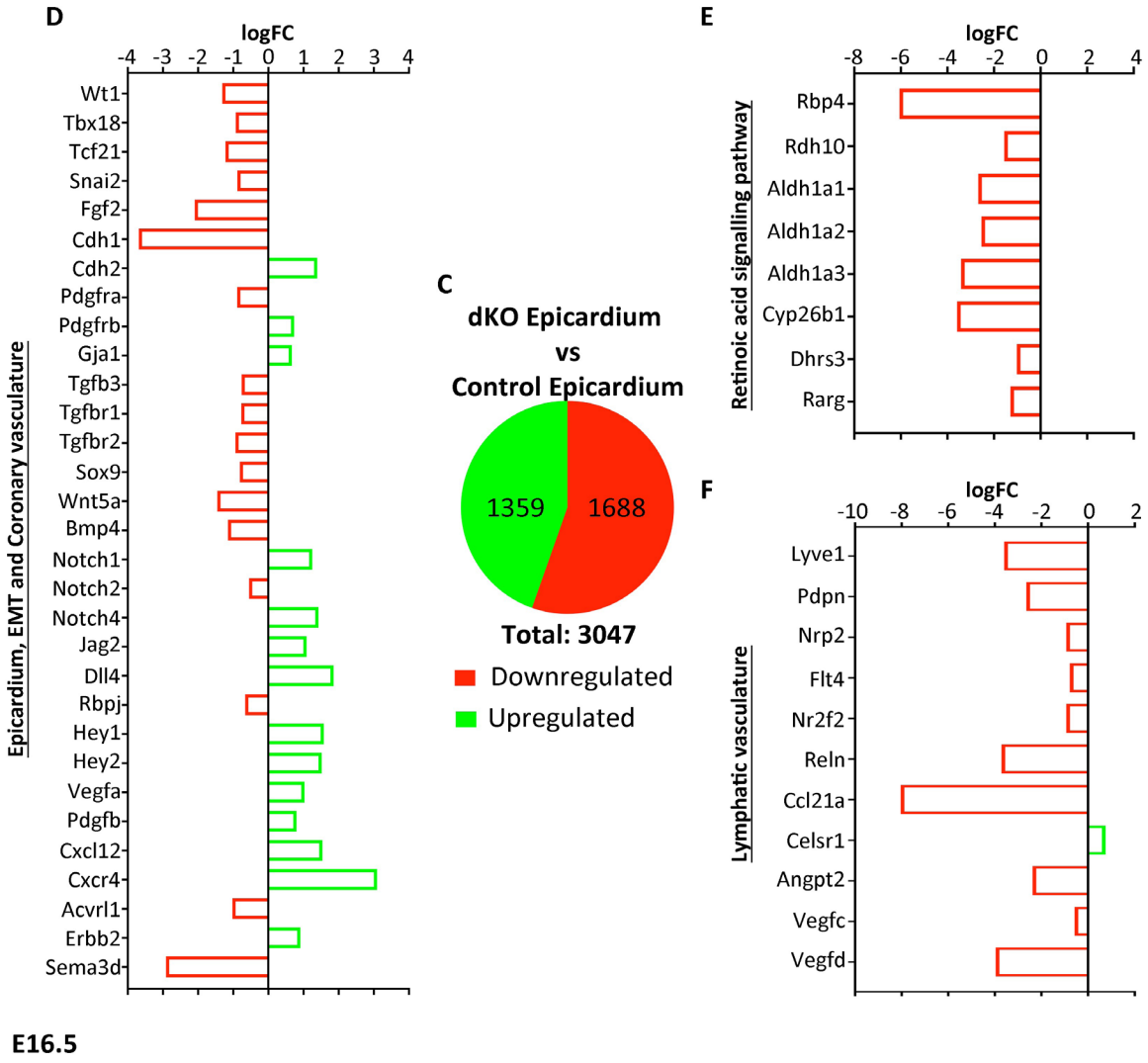

Figure 28. RNAseq analysis of dKO versus control E16.5 epicardium. (A, B) Ingenuity Pathway Analysis top categories affected by *Meis* deletion regarding Physiological System Development and Function (A) and Molecular and Cellular Function (B). (C) Total of Differentially expressed genes (DEGs) (adjusted p-value ≤ 0.05) in this RNAseq analysis. The proportion of downregulated genes in dKOs is depicted in red and the upregulated genes in green. (D) DEGs whose activity has been associated with the epicardium, EMT and coronary vasculature development in the literature. (E) DEGs associated with the Retinoic acid signalling pathway in the literature. (F) DEGs associated with the lymphatic vasculature in the literature.

(*Hey1, Hey2*) may suggest an increased activation of Notch pathway in Meis dKO epicardium (De La Pompa and Epstein, 2012). However, we would need to confirm these results, since RBPJ, essential TF for the activation of Notch pathway, was downregulated in *Meis* mutants (Figure 28D). If the Notch pathway was indeed activated, this would have important implications, because the Notch pathway is important for EMT and coronary vascular development (Grieskamp et al., 2011; Del Monte et al., 2011).

We also found a substantial inactivation of the Retinoic acid (RA) signalling pathway in dKOs (Figure 28E). This inactivation included all levels of the pathway. Genes downregulated included those coding for RA metabolism enzymes and RA targets. Expression of the genes encoding the three retinaldehyde dehydrogenases (Raldh1 (*Aldh1a1*), Raldh2 (*Aldh1a2*) and Raldh3 (*Aldh1a3*)), responsible for the final RA synthesis from retinaldehyde were downregulated in the mutants. From these, Raldh2 is responsible for the majority of RA synthesis during development (Nakajima, 2019). Gene encoding RA γ receptor *Rarg*, and the protein involved in transport of the RA precursor retinol (*Rbp4*), were downregulated. In agreement with these observations, the gene encoding the main RA degradation enzyme -CYP26B1-, also a direct RA target, is repressed in RNAseq.

Intriguingly, we also found many DEGs associated with lymphatic development and function (Figure 28F). *Lyve1, Pdpn, Nrp2*, Vegfr3 (*Flt4*) are expressed in LECs and all of them were downregulated in the dKOs. Moreover, *Celsr1* mild upregulation may suggest changes in LECs cell polarity and lumen formation, which are crucial aspects for lymphangiogenesis (Oliver et al., 2020). We also found decreased levels of molecules secreted by LECs, such as RELN and CCL21a, which could relate with reduced cardiac lymphatic function. Could all these changes mean that not only coronary arteries and veins, but also cardiac lymphatics may be impaired in Meis dKOs? Taking into account that little is known about the specific mechanisms that drive lymphatic development in the heart, we considered that this possibility was extremely interesting. We will address the possible relationship between the epicardium, Meis and cardiac lymphatics in the next chapter. However, we will first concentrate on the possible implications of the RA pathway in the epicardial EMT and EPDCs defects observed in Meis dKOs.

Decreased retinoic acid levels as a consequence of *Meis* deletion

The role of RA in different EMT-related processes is widely accepted. The relevance of this pathway in coronary vasculature development has also been described (Lin et al., 2010; Merki et al., 2005; Wang et al., 2018a). Further evidence also supports its role in avoiding premature SMC differentiation of EPDCs and inducing cytoskeletal epicardial cell rearrangement required for EMT and EPDC migration (Azambuja et al., 2010; Braitsch et al., 2012; Wang et al., 2018b). Therefore, the delayed coronary vasculature development and the accumulation of *Wt1Cre lineage+* cells in the subepicardium observed in Meis dKOs may be the consequence of decreased RA levels in the epicardium.

To explore this possibility, we first validated if dKOs had indeed lower expression of RA-synthesizing enzymes. Based on the assumption that Raldh2 activity correlates with RA accumulation and is the main RA-synthesizing enzyme in embryos (Moss et al., 1998), we performed whole mount IF

against RALDH2 (Figure 29A-D). E16.5 control hearts showed high RALDH2 expression in the epicardium (Figure 29A). In contrast, dKOs showed a strong reduction in RALDH2 detection, although some signal could still be observed (Figure 29C).

Recently, it was described that the mesothelium of the great vessels close to the base of the heart, has a characteristic negative region for RALDH2 and that this has important consequences for cardiac lymphatic specification and development (Lioux et al., 2020). This Raldh2-negative pattern can be observed in the controls (arrowhead in Figure 29B), establishing a sharp RALDH2 boundary of expression with the epicardial region. In contrast, this boundary cannot be clearly identified in the dKOs (Figure 29D). This suggests that the regulation of RALDH2 expression boundaries, as well as its epicardial expression are altered in *Meis* mutants.

We also performed RALDH2 immunostaining on cardiac sections of E16.5 *Wt1*^{Cre}*; Rosa26*^{tdtmt} and *Wt1*^{Cre}*; Meis1*$^{flox/flox}$*; Meis2*$^{flox/flox}$*; Rosa26*^{tdtmt} embryos (Figure 29E-F''). With this approach, we could determine more precisely the source of RA in the dKOs. As previously described (Pérez-Pomares et al., 2002b), epicardial cells (arrowheads) and some EPDCs (arrows) in controls showed high and lower levels of RALDH2, respectively (Figure 29E'-E''). *Meis* deficiency results in heterogeneous loss of RALDH2 expression. Certain regions showed almost no epicardial expression (Figure 29F, and arrowhead in F''), while others retained epicardial expression at lower levels than the controls (arrowhead in Figure 29F') The myofibroblasts-like cells accumulated in the subepicardium also showed mild RALDH2 levels (arrow in Figure 29F''). The observations in the dKOs on RALDH2 expression in myocardial EPDCs were similar to those in the controls, with some EPDCs positive for RALDH2 (arrow in Figure 29F'). Therefore, these results agree with the RNAseq data and confirm that the RA pathway is decreased in Meis dKOs. Thus, our next question to address was whether we could establish a relationship between *Meis* defects and RA. Would RA deficiency in the epicardial lineage result in EPDCs accumulation and delayed coronary development?

Epicardial-specific *Raldh2* mutants do not recapitulate Meis dKOs alterations

Previous work studying the role of RA in the epicardium was based on the use of full knockouts or exogenous treatments to block RA synthesis in the whole embryo and consequently, in the whole heart (Lin et al., 2010; Wang et al., 2018). Therefore, although the main source of RA in the heart is the epicardium, it would be difficult for us to extrapolate these results. Although Merki and colleagues (2005) did study epicardial specific RXRα conditional mutants, they did not analyse the effect on *in vivo* SMCs. Precise whole-mount acquisitions of the coronary vasculature in RA deficiency is also not available from previous studies to compare the patterning defects observed in Meis dKOs. We were therefore in need of an epicardial specific conditional mutant of the RA pathway. With that purpose, we generated *Wt1*^{Cre}*; Raldh2*$^{flox/flox}$ mutant mice in which *Raldh2* is deleted in the same lineage and cells than *Meis* in dKOs.

We extracted E16.5 hearts and performed whole-mount SM22α and EMCN IF to study the distribution of SMCs and the overall anatomy of the coronaries (Figure 30A-B'). SM22α+ cells were

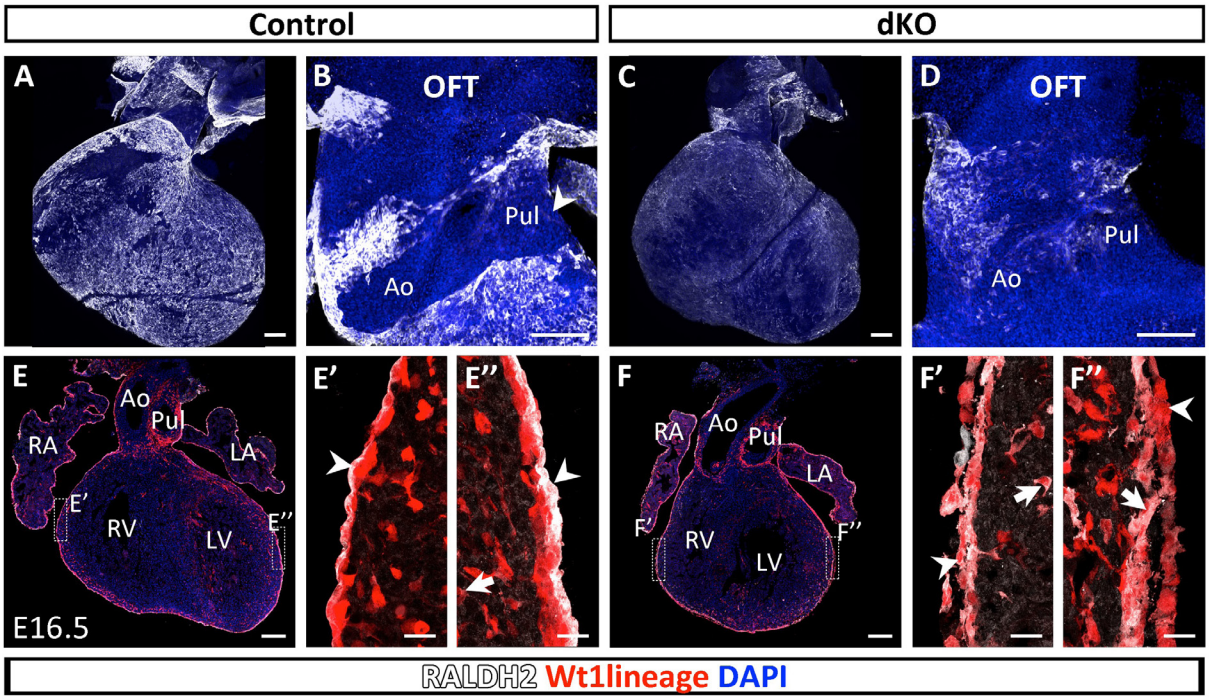

Figure 29. *Raldh2* is downregulated in Meis dKOs hearts. (A-D) RALDH2 and DAPI whole mount immunofluorescence of E16.5 control (A) and Meis dKO (C) hearts. (B, D) Maximum projection of the OFT region to compare the characteristic RALDH2-negative pattern (arrowheads) in the control (B) with the dKOs pattern (D). (E-F'') E16.5 *Wt1^{Cre}; Rosa26^{tdtmt}* (Control, E-E'') and Wt1^{Cre}; Meis1$^{flox/flox}$; Meis2$^{flox/flox}$; Rosa26^{tdtmt} (dKO, F-F'') cardiac sections stained with RALDH2 and DAPI. E'-E'' and F'-F'' are higher magnifications of the boxed regions in E and F respectively. Arrowheads point to epicardial cells and arrows to EPDCs. Ao: aorta; LA: left atrium; LV: left ventricle; Pul: Pulmonary artery; RA: right atrium; RV: right ventricle. Scale bar: 200 µm in A-D, E, F and 20 µm in E'-E'', F'-F''.

not accumulated in the subepicardium of *Wt1$^{Cre;}$ Raldh2$^{flox/flox}$* hearts (Figure 30B-B', D-D') and showed a similar distribution than SMCs in the controls (Figure 30A-A', C-C'). The coronary arteries, identified as EMCN-negative, SM22α+ vessels (dashed lines in Figure 30A, B), did not differ in their development between controls (Figure 30A-A') and *Wt1^{Cre}; Raldh2$^{flox/flox}$* hearts (Figure 30B-B'). The coronary veins on the dorsal side of the heart did not show substantial differences between controls and mutants either (Figure 30C, D). SMC coverage was also similar in both genotypes (Figure 30C-D').

These results suggest that *Raldh2* deletion in *Wt1lineage* has no severe consequences on coronary vasculature development or SM22α+ cells/SMCs distribution.

To further test the idea of the involvement of *Raldh2* downregulation in the defects observed in Meis dKO mutants, we studied a possible genetic interaction between *Meis1*, *Meis2* and *Raldh2*. We generated conditional triple heterozygous mutant embryos and analysed SMCs distribution and coronary vein anatomy by whole mount IF (Figure 30E-F'). We did not observe any differences in SM22α or EMCN staining between E16.5 *Wt1^{Cre}; Meis1$^{flox/wt}$; Meis2$^{flox/wt}$; Raldh2$^{flox/wt}$* (Figure 30F-F') and control (Figure 30E-E') hearts.

In conclusion, the observed *Raldh2* downregulation alone cannot explain the defects observed upon *Meis* deletion in the epicardium.

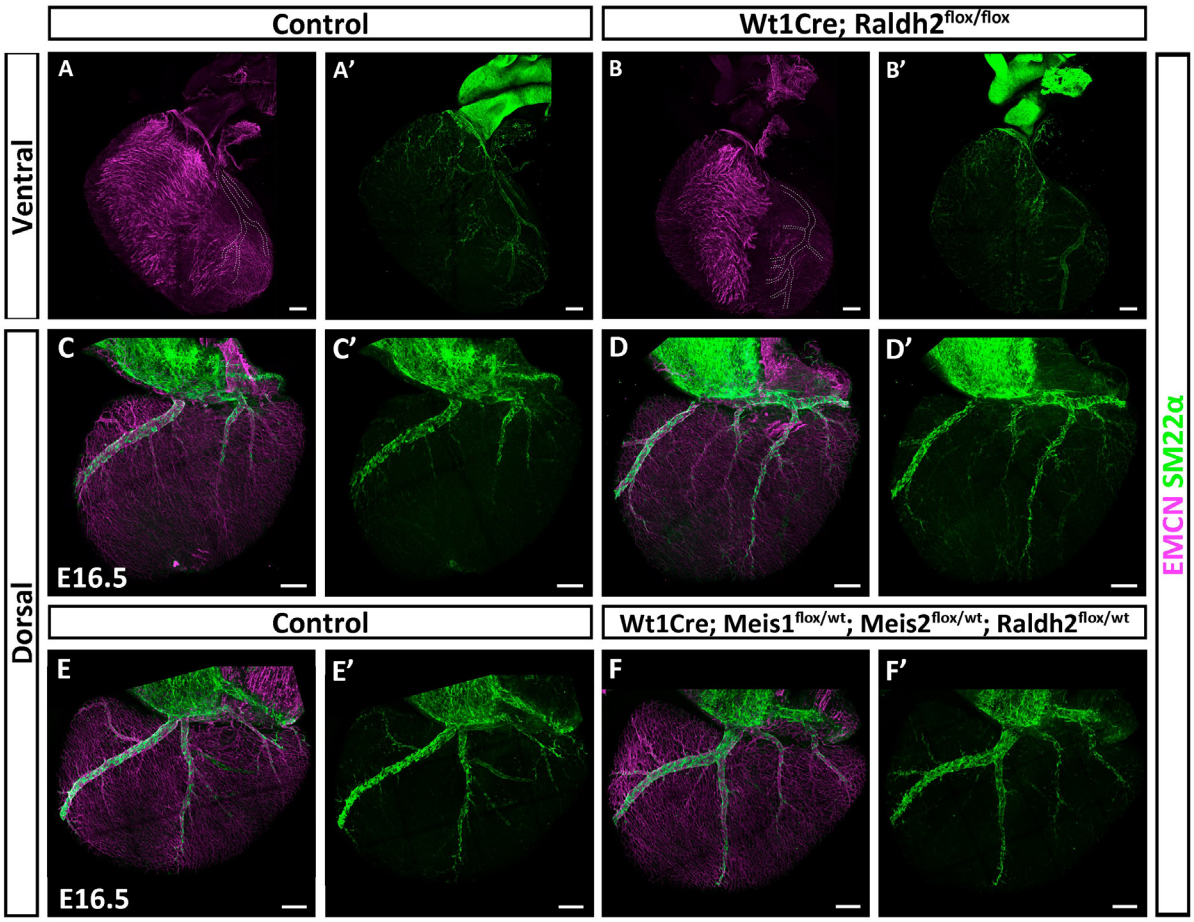

Figure 30. Neither *Raldh2* epicardial conditional mutants nor genetic interaction studies evidence relationship between *Meis* and RA. (A-F') Whole-mount IF against EMCN and SM22α to visualise coronary veins and SMCs on the ventral (A-B') and dorsal (C-F') side of E16.5 hearts. (A-B') Single-EMCN+ channel (B) and single-SM22α+ channel (B') of *Wt1^{Cre}; Raldh2$^{flox/flox}$* hearts can be compared with the respective control single-EMCN+ channel (A) and single-SM22α+ channel (A'). Dashed lines delineate EMCN-negative SM22α+ coronary arteries on single EMCN+ channel. (C-D') EMCN and SM22α staining overlay (D) and single-SM22α+ channel (D') of *Wt1^{Cre}; Raldh2$^{flox/flox}$* hearts can be compared with the respective control overlay (C) and single-SM22α+ channel (C'). (E-F') EMCN and SM22α overlay (F) and single-SM22α+ channel (F') of *Wt1^{Cre}; Meis1$^{flox/wt}$; Meis2$^{flox/wt}$; Raldh2$^{flox/wt}$* hearts can be compared with the respective control overlay (E) and single-SM22α+ channel (E'). Scale: 200 µm in A-F'.

Cardiac lymphatic development is severely impaired in epicardial-specific *Meis* mutants

We were really intrigued by the downregulation of many lymphatic-associated genes in Meis dKOs (Figure 28F). Could cardiac lymphatic development be impaired in these mutants?

We decided to perform whole mount IF for the lymphatic marker PROX1, to compare cardiac lymphatic development at different stages between control and dKO hearts. As previously described (Klotz et al., 2015), lymphatic vessels in controls start to colonise the dorsal side of the ventricles by E14.5 (arrowhead in Figure 31A'). At this stage, most of the ventral lymphatics are mainly found colonising the great vessels, in their way towards the ventricle. Few PROX1+ LECs, can be observed on the ventricle at E14.5 (arrowhead in Figure 31A), and their development is delayed compared to dorsal lymphatics. As development progresses, both ventral and dorsal side lymphatics continue their progression and development over the surface of the ventricular myocardium. This can be observed in E16.5 (Figure 31C, C') and E18.5 (Figure 31E, E') control immunostainings.

In agreement with our RNAseq analysis data, we found that cardiac lymphatic development is severely impaired upon *Meis* deletion in the epicardial lineage. Lymphangiogenesis does not seem to be generally compromised in these embryos, since lymphatic vessels do form in the periphery of the heart and reach the heart, as identified by the presence of PROX1+ LECs in both, the great arteries and SV (arrowheads in Figure 31B and B' respectively). We noted that, in the ventral side of the control hearts, lymphatics are found first mainly in the pulmonary artery and from there they extend into the ventricles (Figure 31A). In contrast, the lymphatic vessels in mutant hearts are found predominantly on the aorta at E14.5 (Figure 31B, G). While this increased colonisation of the aorta is maintained throughout development, differences in the lymphatics of the pulmonary artery are no longer observed at E16.5 or E18.5 (Figure 31D, F, K, O). We did not find major differences in the area covered by lymphatics in the SV region at any of the studied stages (Figure 31B', D', F', J, N, R).

Although in Meis dKOs cardiac lymphatics reach the base of the ventricles, they show a strong impairment in colonizing them. No lymphatic vessels can be observed at E14.5 (Figure 31B, H) or E16.5 on the ventral side of the ventricles (Figure 31D, L) and only few lymphatic vessels are found at E18.5, always in close proximity to the great arteries and never colonising apical regions of the ventricles (arrowheads in Figure 31F, P). The area of the ventral side of the ventricles covered by lymphatics is drastically reduced at all studied stages (Figure 31H, L, P). The colonisation of the dorsal side of the ventricles by lymphatics is also impaired in the dKOs. At E14.5, cardiomyocytes are the only PROX1+ cells in the dKO ventricles (Figure 31B', I) and at E16.5 and E18.5, only few PROX1+ LECs are seen on the surface of the dKOs ventricles (Figure 31D', F', M, Q). The proportion of the ventricles area covered by dorsal lymphatics is reduced at all stages (Figure 31I, M, Q). We found that in the dKOs, while dorsal lymphatic coverage is decreased by 85% at E16.5, and 63% at E18.5 when compared to the controls, ventral side lymphatics coverage is reduced by 93% at E16.5 and 77% at E18.5. These results show that epicardial *Meis* deletion impairs cardiac lymphangiogenesis throughout prenatal development, with a slightly higher affectation of ventral side lymphatics.

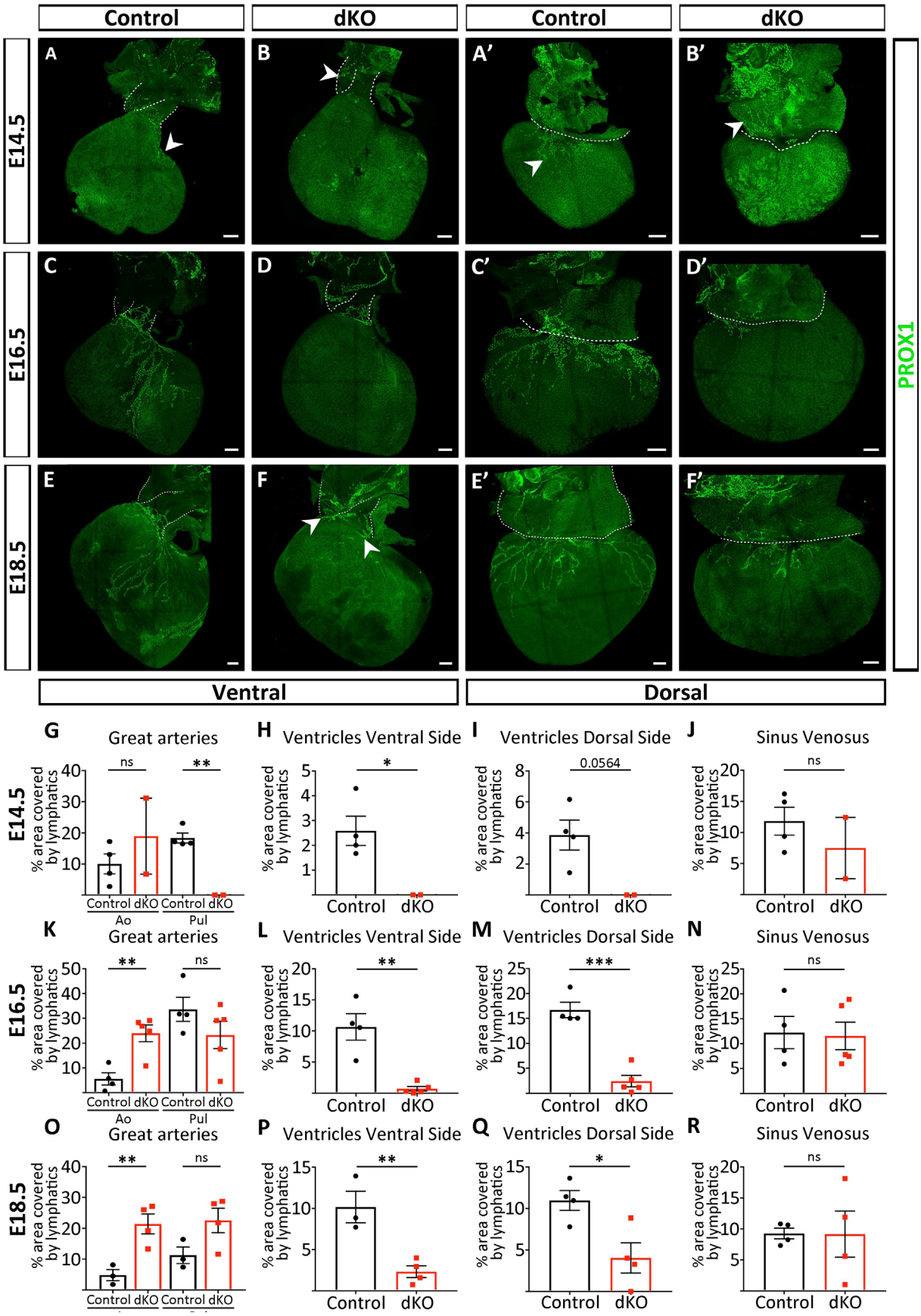
Control
dKO
Control
dKO
E14.5
E16.5
E18.5
PROX1
A
B
A'
B'
C
D
C'
D'
E
F
E'
F'
Ventral
Dorsal
G
Great arteries
H
Ventricles Ventral Side
I
Ventricles Dorsal Side
J
Sinus Venosus
K
L
M
N
O
P
Q
R
% area covered by lymphatics
ns
**
*
0.0564
***
Control
dKO
Ao
Pul

Figure 31. Cardiac lymphatics development is severely impaired in Meis dKOs. (A-F') Whole mount immunostaining against the lymphatic marker PROX1 of E14.5 (A-B'), E16.5 (C-D'), E18.5 hearts (E-F'). Cardiac lymphatic development on the ventral side of controls (A, C, E) can be compared to the dKOs (B, D, F). Dorsal cardiac lymphatics of the controls (A', C', E') can be compared to the dKOs (B', D', F'). Arrowheads highlight the location of growing lymphatic vessels that evidence differences between controls and dKO hearts. All scale bars 200 µm. (G-J) Quantification of the proportion of area of the different cardiac regions covered by lymphatic vessels in E14.5 controls and dKOs (n ≥ 2 hearts per genotype). (K-N) Quantification of the proportion of area of the different cardiac regions covered by lymphatic vessels in E16.5 controls and dKOs (n ≥ 4 hearts per genotype). (O-R) Quantification of the proportion of area of the different cardiac regions covered by lymphatic vessels in E18.5 controls and dKOs (n ≥ 3 hearts per genotype). Unpaired t test. ns: p value ≥ 0.05; * p value <0.05; ** p value <0.01; *** p value < 0.001. Error bars represent SEM.

A disorganised but functional lymphatic plexus is formed postnatally in Meis dKO hearts

We next wondered whether the cardiac lymphatic defects would persist postnatally in dKOs, or whether they would recover as it occurs with coronary blood vasculature development. For that purpose, we performed whole-mount IF against LYVE1 to visualise the cardiac lymphatic vasculature after the first week of life of control and mutant mice. Interestingly, at P7 some ventral and dorsal lymphatics are found colonising the ventricles of dKO hearts (Figure 32B, B'). Nevertheless, important differences between controls and mutants are still found in both the ventral (Figure 32A, B) and dorsal sides (Figure 32A', B'). Moreover, in the control situation, lymphatics continue their growth and remodelling for the first two weeks of life, as previously described (Klotz et al., 2015) (Figure 32C, C'). At P14, mutant lymphatics are still strongly underdeveloped in both the ventral and the dorsal sides of the heart (Figure 32D and D' respectively). In adults, a complete lymphatic plexus has developed in the mutant hearts, however it appears immature and disorganised compared to controls, as shown by whole mount LYVE1 immunohistochemistry (Figure 32F, E).

These results suggest that *Meis* deficiency prevents normal lymphatic development but that this is progressively compensated in adults. The morphological differences of the final lymphatic plexus, however, questioned their functionality. Therefore, we decided to assess the function of cardiac lymphatic vessels in adult control and mutant mice. We performed subepicardial Indian ink injections to evaluate their drainage capacity. With this aim, we put the mice under deep anaesthesia and performed several subepicardial injections on the beating hearts. As it can be observed in Figure 32G, in control hearts some lymphatics are filled with black ink as they drain it from the injected region close to the apex towards the base along the dorsal side of the heart. Similar injections in dKO hearts produced comparable results (Figure 32H). Although morphological differences are still observable with this methodology, at least some of the adult coronary lymphatics in mutants are capable of draining the injected ink.

We conclude that, in spite of their severe developmental impairment, cardiac lymphatics develop in adult Meis dKOs and are functional, although showing abnormal patterning.

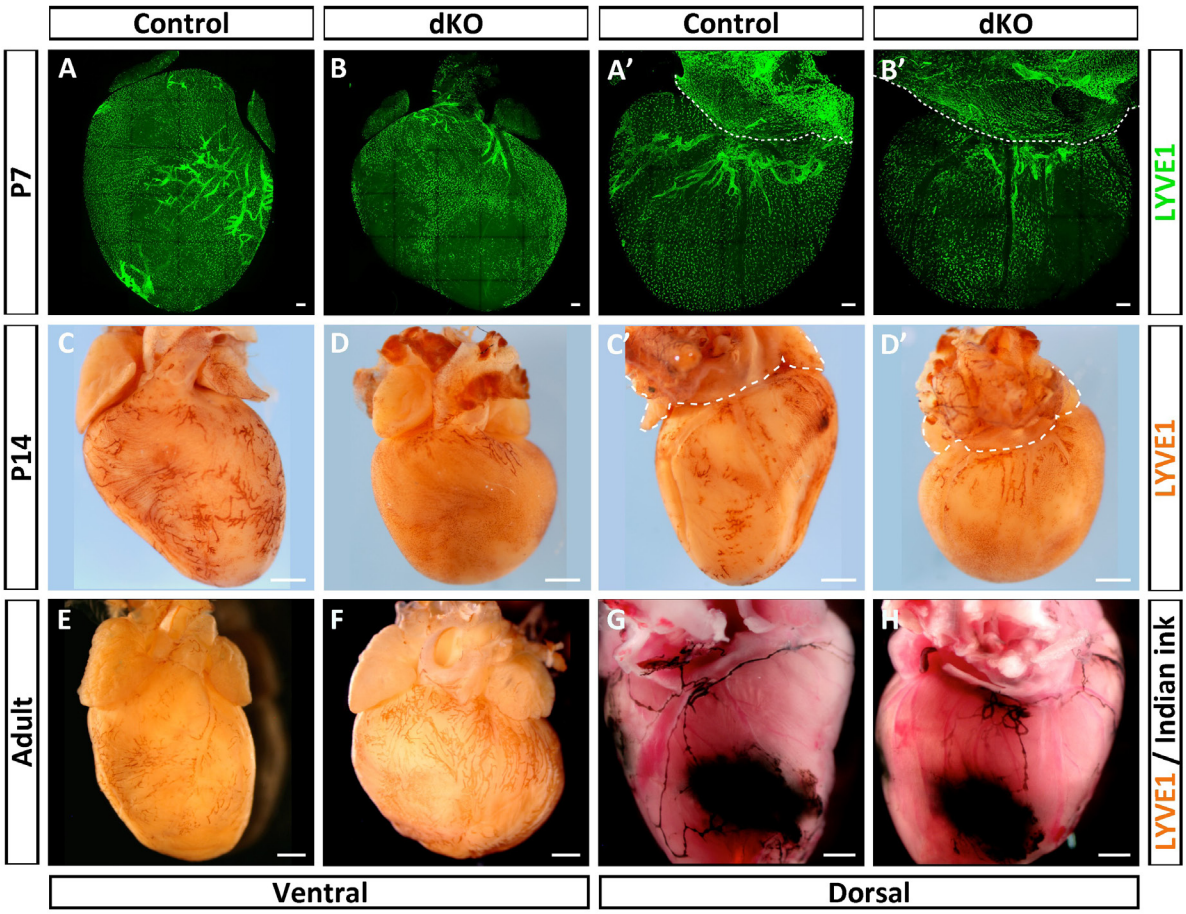

Figure 32. Postnatal cardiac lymphatics are partially recovered and functional in dKOs. (A-B') Whole mount LYVE1 immunofluorescence of P7 control (A, A') and dKO (B, B') hearts shows macrophages (LYVE1+ isolated cells) and cardiac lymphatic vasculature. Cardiac lymphatics can be observed in the ventral (A, B) and dorsal side of the heart (A', B'). (C-F) Whole mount immunohistochemistry against LYVE1 of P14 (C-D') and adult hearts (E-F). Cardiac lymphatic patterning is visualised in the ventral (C, D, E, F) and dorsal side (C', D') of control (C, C', E) and Meis dKOs (D, D', F). (G-H) Subepicardial Indian ink injections performed on controls (G) and dKOs (H) to assess cardiac lymphatic drainage capacity in basal conditions. Scale bar: 200 µm in A-B' and 1 mm in C-H.

Elimination of *Meis1/2* with *Tbx18^{Cre}* impairs cardiac lymphatic development

To test whether the observed phenotypes derived from recombination of *Meis* alleles in the epicardium and its derivatives, we took advantage of *Tbx18Cre* as an additional epicardial-recombination model. We performed whole mount PROX1 and LYVE1 immunostainings on E18.5 control and *Tbx18^{Cre}; Meis1$^{flox/flox}$; Meis2$^{flox/flox}$* hearts (Figure 33). Interestingly, cardiac lymphatic development is also severely impaired in this model. Only vestigial lymphatics are observed at the base of both, the ventral and dorsal sides of the mutant hearts (arrowhead in Figure 33B, B´), whereas controls show a well-developed lymphatic plexus at this stage (Figure 33A, A'). Thus, these mutants phenocopy *Wt1^{Cre}; Meis1$^{flox/flox}$; Meis2$^{flox/flox}$* cardiac lymphatic defects (Figure 31F-F'). The results in Wt1Cre; dKOs and Tbx18Cre; dKOs are in agreement with an epicardial-specific requirement of MEIS TFs for coronary lymphatic development.

Normal dermal lymphatics but patterning alterations in mesenteric lymphatics in Meis dKO mice

Lymphatic vessels form in the vicinity of the heart in *Wt1Cre*-recombined Meis dKO mutants (Figure 31) and, as we mentioned before, this could suggest that the alterations may be caused by a cardiac-specific defect and not a general problem in lymphangiogenesis. To study this aspect in more detail, we decided to evaluate lymphatic development in other organs.

We first assessed dermal lymphatic development at E16.5. We isolated the dorsal skin of control and *Wt1^{Cre}; Meis1$^{flox/flox}$; Meis2$^{flox/flox}$* embryos, and performed whole-mount PROX1 immunostaining on them. At this stage, the growing lymphatic vessels have formed an extensive network at both sides of the skin but have not met at the midline region yet (Figure 34A). We did not find any obvious alterations of the dermal lymphatic vasculature in dKOs compared to controls (Figure 34B). Lymphatics have colonised the dorsal skin, their calibre appears normal and the gap at the midline region is similar.

With these results, we confirmed that the problem in lymphangiogenesis is not extended to all organs in the embryo and that a general impairment of lymphangiogenesis can be discarded.

We also studied the mesenteric lymphatics of fetuses in advanced gestation. The mesenteric mesenchyme is a site of strong *Meis* expression and it is at least partially recombined by *Wt1^{Cre}* (Hisa et al., 2004; Machon et al., 2015; Wilm et al., 2005). We analysed the mesentery using PROX1 to label lymphatics, Smooth muscle actin (SMA) as SMC marker and CD31 as and endothelial marker of arteries, veins and lymphatics. We found that lymphatic vessels have formed and colonised the mesentery in both the controls and the dKOs (Figure 35A and B respectively). However, we found various patterning

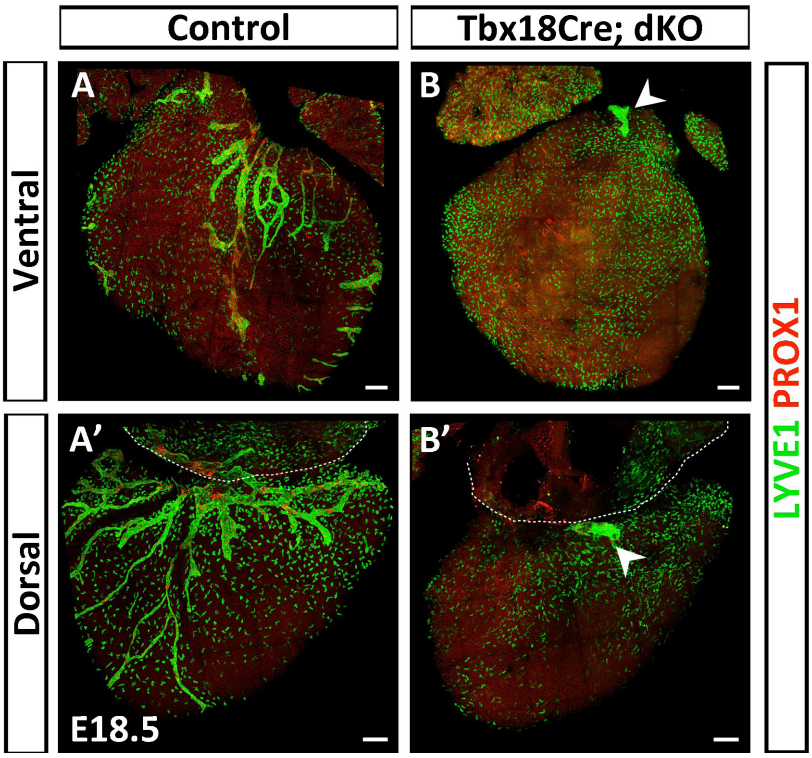

Figure 33. Tbx18^{Cre}; Meis1$^{flox/flox}$; Meis2$^{flox/flox}$ hearts recapitulate the cardiac lymphatic defects. (A-B') PROX1 and LYVE1 whole mount immunostaining performed on E18.5 hearts. Ventral (A) and dorsal lymphatics (A') in the control can be compared to *Tbx18^{Cre}; Meis1$^{flox/flox}$; Meis2$^{flox/flox}$* (Tbx18Cre; dKO) ventral (B) and dorsal (B') lymphatics. Arrowheads point to the only lymphatic vessels (PROX1+LYVE1+ cells) found on the ventricle of Tbx18Cre;dKO hearts. The other non-lymphatic cells stained by LYVE1 are macrophages. Scale bar: 200 µm.

alterations in the mesenteric lymphatics. In controls, lymphatic vessels align with mesenteric arteries and veins, which run parallel to each other and tightly associated (Figure 35A and A'). In contrast, in the dKOs arteries and veins have lost their strong association and show a mildly altered branching pattern, while lymphatics tend to lose alignment with them and follow more loosely their path (arrowhead in Figure 35B and Figure 35B'). Nevertheless, some lymphatic branches in Meis dKOs appear normal (asterisk in Figure 35B). Furthermore, lymphatic valves appear evenly spaced in the control lymphatics (arrows in Figure 35A), while they appear scarcely and irregularly spaced in mutant lymphatics (arrows in Figure 35B).

These results show that Meis function in the mesentery is required for lymphatic patterning, however, arrest of lymphangiogenesis due to loss of Meis function in the *Wt1Cre*-recombined lineage was observed only in the heart.

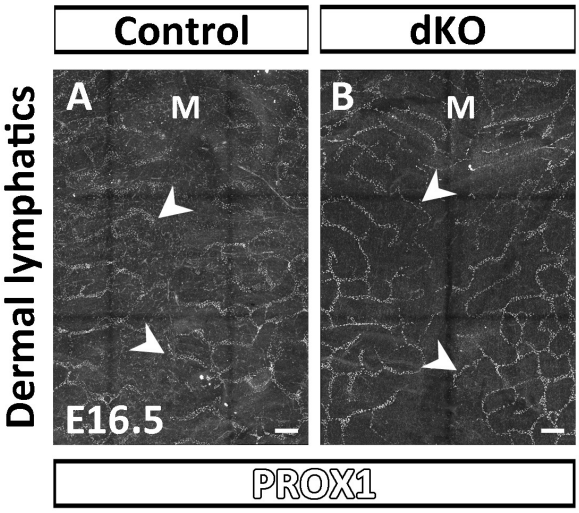

Figure 34. Meis dKOs present normal dermal lymphatics. (A-B) Whole-mount PROX1 immunostaining performed on the dorsal skin of E16.5 controls (A) and dKOs (B) to visualise dermal lymphatics. Arrowheads show examples of growing lymphatic vessels at both sides of the lymphatic plexus. M: midline. Scale bar: 200 µm.

LECs are tightly associated with *Wt1Cre lineage+* cells

Our results show that MEIS function in the epicardium and/or EPDCs is required for proper lymphatic development. This indicates that the epicardium and/or EPDCs are essential for coronary lymphatic development. Given that the epicardium does not contribute to the coronary LEC population (Klotz et al., 2015; Lioux et al., 2020; Wilting et al., 2007), crosstalk between the epicardium and/or EPDCs and LECs should be involved in this function. Therefore, we next studied the relationship between *Meis*, the epicardium, EPDCs and cardiac lymphatics.

We considered different possibilities: A) It could be that some lymphatic-associated EPDCs are required as a niche that serves as a scaffold for the growing cardiac lymphatics. B) The epicardium or EPDCs may produce paracrine signals that promote and/or guide cardiac lymphangiogenesis. C) A combination of both, direct cellular interactions and paracrine signalling from the epicardium/EPDCs, are needed for cardiac lymphatic development.

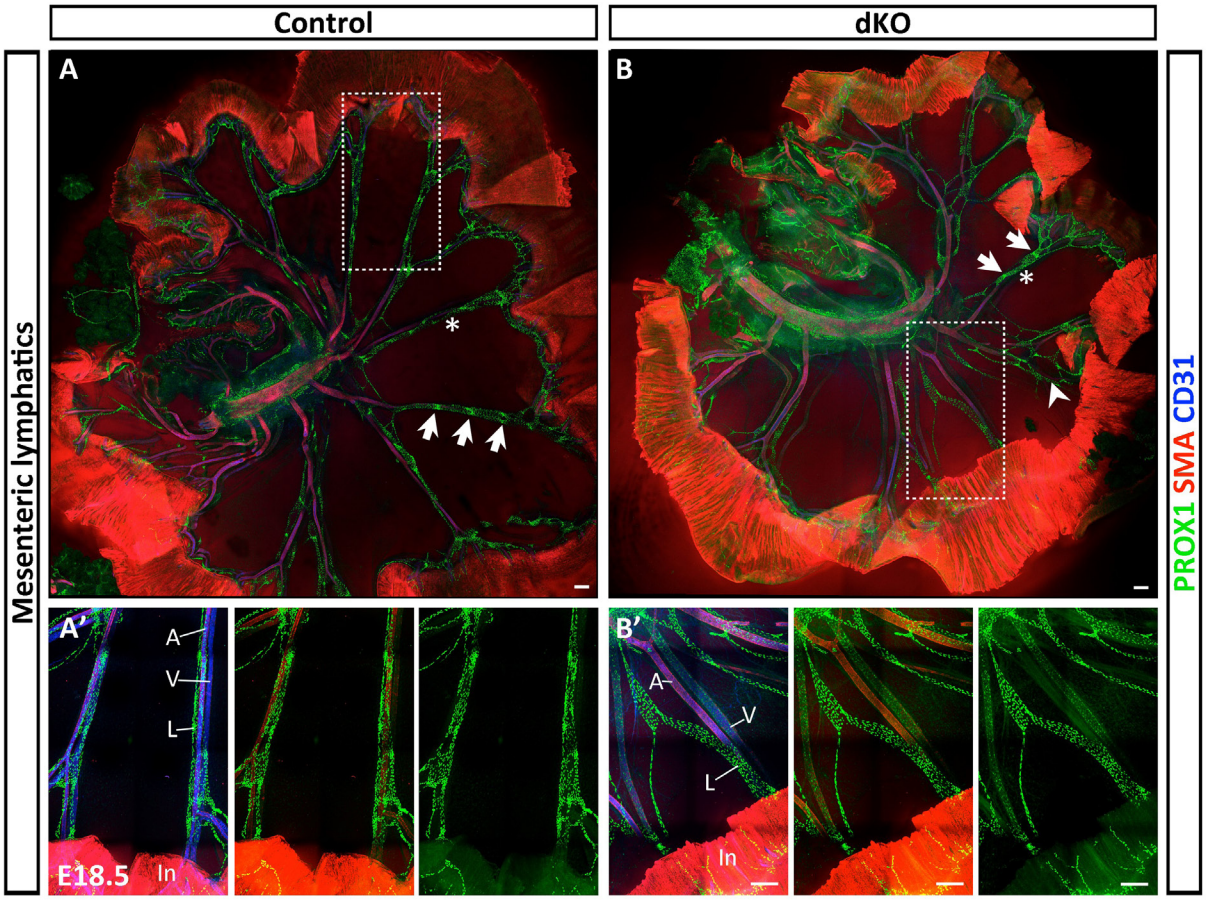

Figure 35. Branching and patterning alterations in Meis dKOs mesenteric lymphatics. (A-B') E18.5 whole mount immunostaining of control (A-A') and dKO (B-B') mesenteric lymphatics. PROX1, Smooth muscle actin (SMA) and CD31 were used as lymphatic, smooth muscle and endothelial markers respectively. Asterisks and arrowheads point to examples of regular and abnormal lymphatic arrangement respectively. Arrows point to evenly spaced lymphatic valves (condensed PROX1+ regions) in the controls and scarce and irregularly spaced valves in the dKOs. A' and B' are higher magnifications of the boxed regions in A and B. A: artery; In: intestine; L: lymphatic vessel; V: vein. Scale bar: 200 µm.

We first explored the idea of the contribution of direct cellular interactions. With that purpose, we studied the possible association between LECs and *Wt1Cre lineage+* cells at the stage when lymphatics start to colonise the ventricles: E14.5. We performed the co-staining for PROX1 and CD31 to visualise lymphatic vessels in *Wt1^{Cre}; Rosa26^{tdtmt}* cardiac sections. We found that LECs are placed in the subepicardium and are tightly surrounded by EPDCs derived from the *Wt1Cre+ lineage* (Figure 36). This association occurs both in the lymphatics found at the base of the great arteries (Figure 36A, A') and in those that start to colonise the subepicardial space of the ventricles (Figure 36A, A''). From this analysis, we confirmed that the *Wt1Cre+ lineage* does not contribute to the LEC population, despite their tight association with LECs, which are PROX1+ CD31+ *Wt1Cre-lineage*-negative (arrowheads in Figure 36A' and A'').

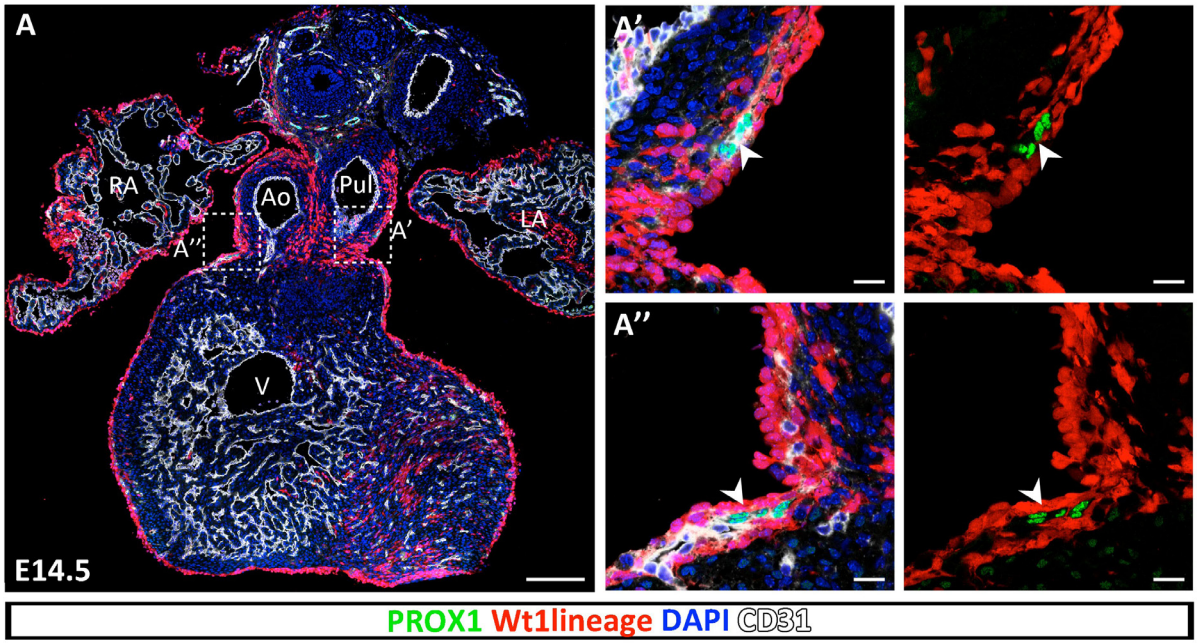

Figure 36. Epicardial non-autonomous effect on cardiac lymphatic development. (A-A'') E14.5 *Wt1^{Cre}; Rosa26^{tdtmt}* cardiac sections stained with DAPI, PROX1 and CD31 antibodies to label cardiac lymphatic vessels (CD31+ PROX1+) as well as *Wt1Cre lineage+* cells. A' and A'' are higher magnifications of the boxed regions in A. Arrowheads show LECs in the great vessels (A') and growing into the myocardium (A'') that are PROX1+CD31+ but negative for *Wt1lineage*. Ao: aorta; LA: left atrium; Pul: pulmonary artery; RA: right atrium; V: ventricle. Scale bar: 200 µm in A and 20 µm in A', A''.

These results show that LECs associate tightly with EPDCs and grow in the vicinity of the epicardium during cardiac lymphatic development. Thus, both direct cellular interactions and paracrine interactions could underlie the non-autonomous role of epicardium/EPDCs on cardiac lymphangiogenesis.

Characterization of EPDCs associated with LECs

We next studied the identity of the *Wt1Cre lineage+* cells associated with LECs. We immunostained sagittal cardiac sections of *Wt1^{Cre}; Rosa26^{tdtmt}* E15.5 hearts for PROX1 as well as for the epicardial marker WT1 (Figure 37A-A'''). As it can be observed in Figure 37A-A''', the epicardial cells express high levels of WT1 (arrow) but the *Wt1Cre lineage+* cells surrounding PROX1+ LECs, expressed low levels of WT1 (arrowhead), in agreement with an EPDC identity. Moreover, when we used the mesenchymal marker VIMENTIN, we found an important labelling of the lymphatic-associated *Wt1Cre lineage+* cells (Figure 37B-B'''). These data reinforce the idea that the cells in direct contact with the lymphatic endothelium are mesenchymal cells that derive from the epicardium. We called these cells lymphatic-associated EPDCs (from now on referred as LEPDCs).

But, what could be the identity of these LEPDCs and what could be their function during lymphangionesis? We studied whether they could be pericyte-like cells or SMCs already associating with the growing lymphatics vessels, as it occurs with capillaries, arteries and veins. Consequently, we

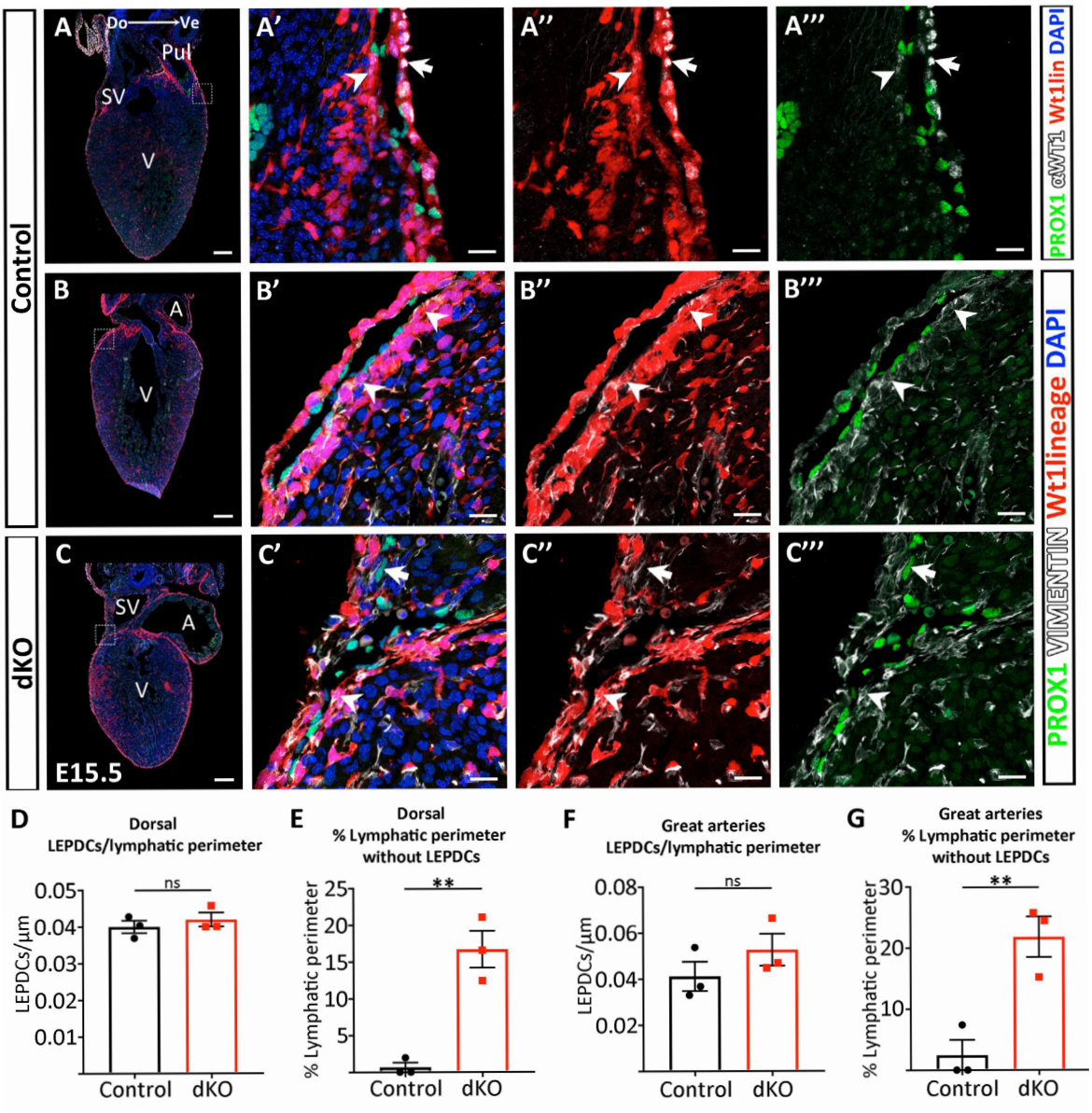

Figure 37. LECs associate differently with mesenchymal EPDCs in Meis dKOs during lymphatic development. (A-B''') E15.5 *Wt1^{Cre}; Rosa26^{tdtmt}* sagittal cardiac sections stained with PROX1, DAPI and WT1 (A-A''') or PROX1, DAPI and mesenchymal marker VIMENTIN (B-B'''). (A'-A''') Are different staining combinations of higher magnifications of the boxed region in A, showing the difference between epicardial cells (arrow) and EPDCs surrounding LECs (arrowhead). (B'-B''') are different staining combinations of higher magnifications of the boxed region in B, showing VIMENTIN+ EPDCs around the growing lymphatic vessels (arrowheads). (C-C''') E15.5 *Wt1^{Cre}; Meis1$^{flox/flox}$; Meis2$^{flox/flox}$; Rosa26^{tdtmt}* E15.5 cardiac sections stained with DAPI and PROX1 and VIMENTIN antibodies. (C'-C''') Are higher magnifications of the boxed region in C that show some LECs with (arrowhead) or without EPDCs (arrow). (D-G) Lymphatic-associated EPDCs (LEPDCs) quantifications. (D, F) LEPDCs per lymphatic perimeter. (E, G) Proportion of lymphatic perimeter lacking direct contact with LEPDCs. Quantifications were done on the dorsal subepicardium, close to the SV (D, E) and great arteries region (F, G). Each point represents a different heart. Each value was calculated by adding the quantified parameter on each section per heart. At least three different sections were quantified per heart for the dorsal region and at least two for the great arteries. Unpaired t test. Ns: p value ≥ 0.05; ** p value <0.01. Error bars represent SEM. A: atrium; Do: dorsal; Pul: pulmonary artery; SV: sinus venosus; V: ventricle; Ve: ventral. Scale bars 200 µm in A, B, C and 20 µm in A'-A''', B'-B''', C'-C'''.

stained E15.5 *Wt1^{Cre}; Rosa26^{tdtmt}* cardiac sections with the pericyte markers NG2 and CD140β (Figure 38A-A''') and the smooth muscle/pericyte marker SM22α (Figure 38B-B'''). We barely found any LEPDCs expressing NG2 or CD140β+ (arrowhead in Figure 38A'-A'''). Occasional cells expressing the pericyte markers were observed in the proximity of lymphatic vessels but not in direct contact with LECs. Most probably they are associated with the vein/capillary endothelium, very close underneath (arrow in Figure 38A-A'''). Similarly, we did not find evidence of SM22α+ LEPDCs. We can conclude that LEPDCs neither represent pericytes nor smooth muscle cells at this stage (Figure 38B-B''').

Having excluded these possibilities, an alternative may be that LEPDCs have a fibroblast-like identity. We immunostained control *Wt1^{Cre}; Rosa26^{tdtmt}* E15.5 cardiac sagittal sections with PERIOSTIN (Figure 38C-C'''). The great arteries and the dorsal side of the ventricle close to the SV were analysed. Remarkably, we found that around 54 % of LEPDCs in the controls (Figure 38C-C''', E) were indeed PERIOSTIN+. These data support the notion that, at least an important fraction of LEPDCs, are fibroblast-like cells.

The association between LEPDCs and cardiac lymphatics is maintained at least until birth

We next assessed the time frame of the association between LECs and LEPDCs, to determine if it might be transient during lymphangiognesis or it might be maintained throughout development. In order to answer this question, we performed VIMENTIN and PROX1 whole-mount IF of E18.5 *Wt1^{Cre}; Rosa26^{tdtmt}* hearts (Figure 39A-A''). We found that the association between *Wt1Cre lineage*+ mesenchymal cells and LECs persists at E18.5 (Figure 39A'-A''), although the ventral cardiac lymphatic vasculature shows slightly variable coverage of VIMENTIN+ LEPDCs. This can be appreciated in Figure 39A', where some LEPDCs are attached to the underlying lymphatic vessel at the surface of the heart (z1-2), as well as in deeper virtual slices (z3-4 and z5-6). In Figure 39A'', a proximal lymphatic branch with its associated LEPDCs is shown at different z-levels, starting at the surface of the heart (z1-2) through the whole thickness of the lymphatic vessel (z3-4 to z7-8).

We wondered whether at these later stages cardiac lymphatics may start to associate with smooth muscle cells or pericytes, as it happens with lymphatics in other organs (Tammela and Alitalo, 2010). We stained E18.5 *Wt1^{Cre}; Rosa26^{tdtmt}* cardiac sections with anti-SM22α and anti-PROX1 antibodies. With few exceptions, we did not find SM22α+ cells in direct contact with LECs (Figure 39B-B'''), unlike veins, which at this stage appear fully covered by SMCs (asterisks in Figure 39B'-B'''). The exceptional SM22α+ cells were mostly *Wt1Cre lineage*+ cells, likely indicating their epicardial origin. The occasional SM22α+ cells associated with cardiac lymphatics were also observed in whole-mount immunostainings, in which 4 out of 7 control hearts contained few and disperse SMCs attached to lymphatic vessels (Figure 39D-D'').

Thus, these results suggest that the association between cardiac lymphatic vessels and mesenchymal LEPDCs is maintained at least until birth. Moreover, the presence of few SMCs at this stage and only in some of the hearts, indicates an incipient recruitment around birth of pericytes/SMCs required for lymphatic maturation.

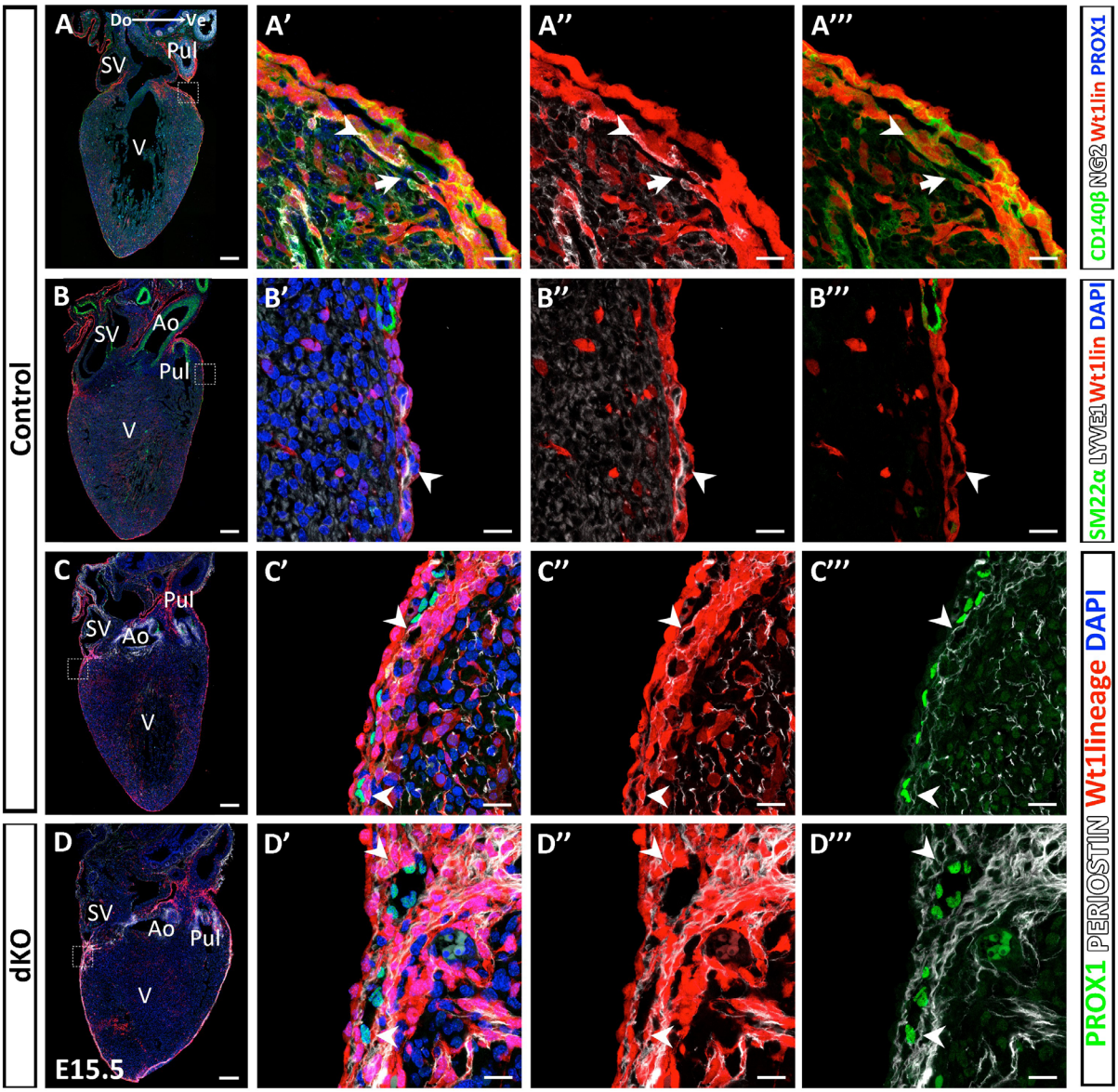
Control
dKO
A
A'
A''
A'''
B
B'
B''
B'''
C
C'
C''
C'''
D
D'
D''
D'''
Do
Ve
Pul
SV
V
Ao
E15.5
CD140β NG2 Wt1lin PROX1
SM22α LYVE1 Wt1lin DAPI
PROX1 PERIOSTIN Wt1lineage DAPI

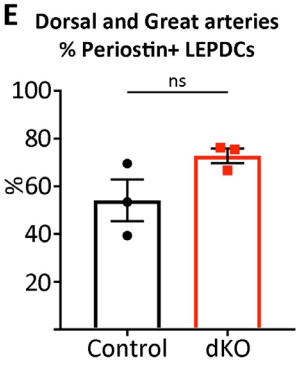
E
Dorsal and Great arteries
% Periostin+ LEPDCs
ns
100
80
%60
40
20
Control
dKO

Figure 38. High proportion of LEPDCs are fibroblast-like cells. (A-B''') E15.5 *Wt1^{Cre}; Rosa26^{tdtmt}* sagittal cardiac sections immunostained with the pericyte markers CD140β and NG2 and PROX1 (A-A''') or the smooth muscle cell marker SM22α, DAPI and LYVE1 (B-B'''). (A'-A''') Are higher magnifications of the boxed region in A, showing a *Wt1Cre lineage+* pericyte-like cell (arrowhead) with a capillary or vein underneath (arrow). (B'-B''') Are higher magnifications of the boxed region in B, and show predominant absence of SMCs around LYVE1+ lymphatic vessels (arrowhead). (C-D''') E15.5 control (C-C''') and dKOs (D-D''') immunofluorescence against PROX1 and the fibroblast marker PERIOSTIN. (C'-C''') and (D'-D''') are higher magnifications of the boxed regions in C and D respectively. Arrowheads point to *Wt1Cre lineage+* PERIOSTIN+ cells surrounding the growing lymphatic vessel. (E) Proportion of LEPDCs that are PERIOSTIN+ on the dorsal subepicardium of the ventricle, close to the sinus venosus and on the great arteries. Each point represents a different heart. Each value was calculated dividing the total number of PERIOSTIN+ LEPDCs quantified in all sections by the total number of LEPDCs quantified on those sections. At least three different sections were quantified per heart. Unpaired t test. Ns: p value ≥ 0.05. Error bars represent SEM. Ao: aorta; Do: dorsal; Pul: pulmonary artery; SV: sinus venosus; V: ventricle; Ve: ventral. Scale bars 200 µm in A, B, C, D and 20 µm in A'-A''', B'-B''', C'-C''', D'-D'''.

The association between LECs and LEPDCs is altered in Meis dKO mutants

We considered the possibility that the lymphatic defects observed in *Meis* mutants, were related to defects in the LEPDCs cell population. VIMENTIN IF on *Wt1^{Cre}; Meis1$^{flox/flox}$; Meis2$^{flox/flox}$; Rosa26^{tdtmt}* E15.5 sagittal cardiac sections, showed that a population of LEPDCs surrounds the vestigial lymphatic vessels of mutants (Figure 37C-C'''). However, LEPDCs appeared not as tightly associated with LECs as in the controls (arrow in Figure 37C'-C'''). Therefore, we quantified the association of *Wt1Cre lineage+* cells with the lymphatic vessels, as well as the percentage of the lymphatic endothelial perimeter devoid of LEPDCs. We performed these quantifications on the dorsal side of the ventricle, close to the SV region (Figure 37D-E) and around the base of the pulmonary artery and aorta (Figure 37F-G). We chose these regions because it is in these areas where the lymphatics reach their farthest positions in the dKO ventricles. We did not find differences between the controls and dKOs in the total number of *Wt1Cre lineage+* LEPDCs per lymphatic perimeter (Figure 37D, F), however, we observed an increased proportion of the lymphatic endothelium perimeter without LEPDCs in both the dorsal (Figure 37E) and ventral sides (Figure 37G).

A similar result was found at E18.5. LEPDCs were found around LECs (arrowhead in Figure 39C'-C''') but there was a looser association between them in the dKOs, and parts of the lymphatic endothelium were not covered by LEPDCs (arrow in Figure 39C'-C''').

We also confirmed the markers of LEPDCs in the dKOs at E15.5. The same regions than those shown in Figure 37 were analysed: the great arteries and the dorsal side of the ventricle close to the SV. We found that, like in the controls, most of LEPDCs in the dKOs are PERIOSTIN+ cells (Figure 38D-E) and, therefore, fibroblast-like cells.

These results suggest that, although LEPDCs are generated in similar numbers in controls and mutants, in Meis dKOs LEPDCs themselves or the LEC-LEPDC crosstalk is altered, resulting in a defective arrangement of *Wt1Cre lineage+* cells around the growing lymphatic vessels. These defects correlate with the defective coronary lymphatic development observed in the mutants.

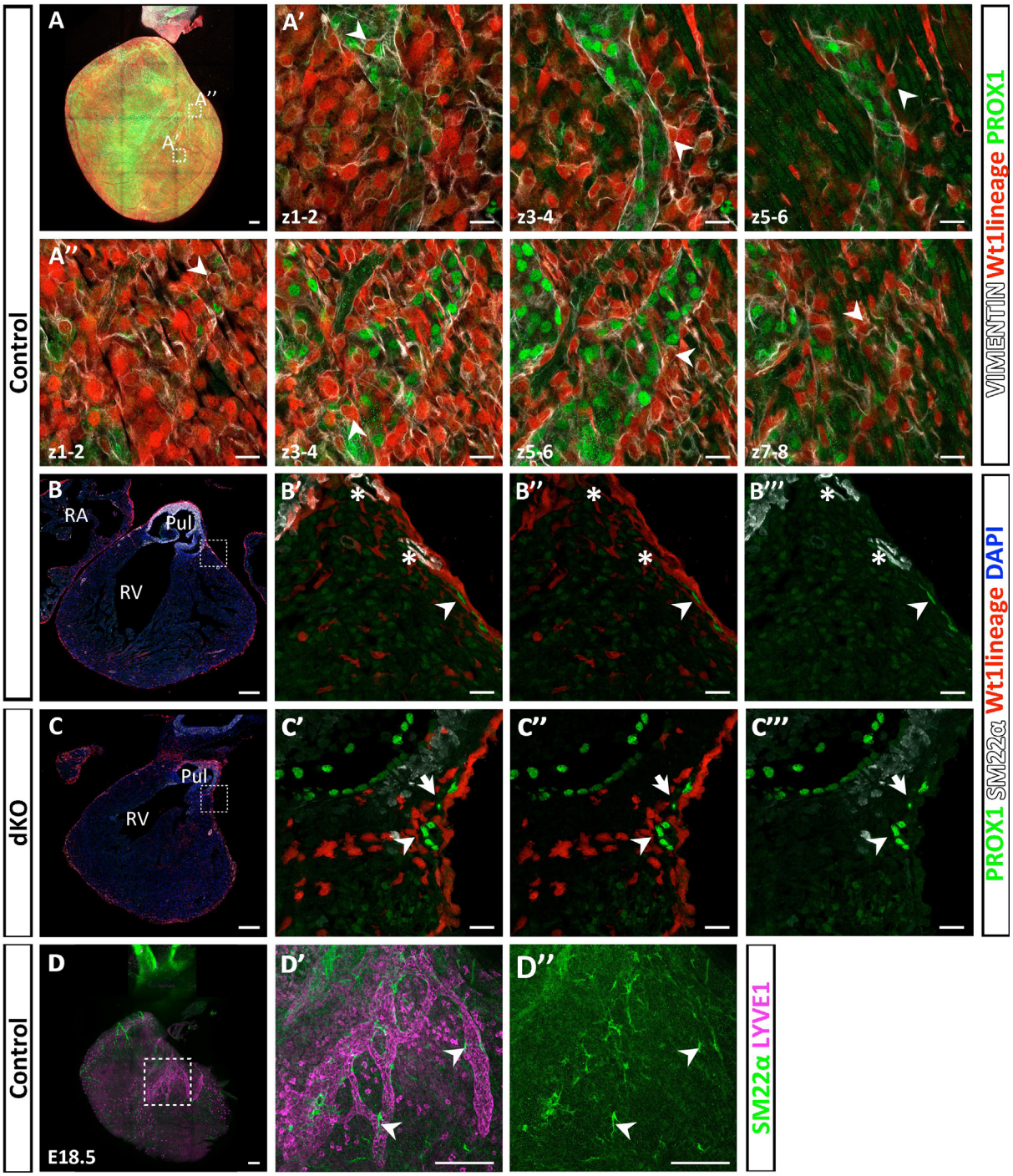

Figure 39. LECs-LEPDCs association is maintained at least until birth. (A-A'') Whole mount VIMENTIN and PROX1 IF of E18.5 *Wt1*^{Cre}*; Rosa26*^{tdtmt} heart. A' and A'' are higher magnifications of the boxed regions in A. z1-2, z3-4, z5-6, z7-8 are consecutive maximum projections of two virtual sections of z-stacks starting at the surface of the heart, towards the myocardium. Arrowheads point to examples of *Wt1Cre lineage*+ VIMENTIN+ LEPDCs. (B-C''') E18.5 *Wt1*^{Cre}*; Rosa26*^{tdtmt} control (B-B''') and *Wt1*^{Cre}*; Meis1*$^{flox/flox}$*; Meis2*$^{flox/flox}$*; Rosa26*^{tdtmt} (C-C''') cardiac sections with DAPI immunostained against SM22α and PROX1. (B'-B''') and (C'-C''') are higher magnifications of the boxed regions in B and C respectively and show different staining combinations. Arrowheads point to LEPDCs surrounding LECs, asterisks point to veins covered by SMCs and the arrow points to a region without tight LEPDC-LEC association. (D-D'') Whole mount SM22α and LYVE1 IF of control E18.5 heart. (D'-D'') are higher magnifications of the boxed region in D. Arrowheads point to SMCs on the lymphatic vessel. Pul: pulmonary artery; RA: right atrium; RV: right ventricle. Scale bars 200 µm in A, B, C, D and 20 µm in A'-A'',B'-B''', C'-C''', D-D''.

In search of lymphoangiocrine molecules that may be responsible for Meis phenotype

We previously proposed different hypotheses for the defects in cardiac lymphatics development observed in the dKOs: A) It could be that some LEPDCs are required as a niche that serves as a scaffold for the growing cardiac lymphatics. B) The epicardium or EPDCs may produce paracrine signals that promote and/or guide cardiac lymphangiogenesis. C) A combination of both, direct cellular interactions and paracrine signalling from the epicardium/LEPDCs, are needed for cardiac lymphatic development.

In any of the three possibilities, molecular alterations in the epicardium or LEPDCs should underlie the observed defects. We then decided to explore the RNAseq results in search of possible lymphoangiocrine molecules differentially expressed in Meis dKOs. Interestingly, we found downregulation of *Vegfc* and *Vegfd*, with log(Fold Change) of -0.58 and -3.97, respectively, (Figure 28F). Both are known paracrine molecules essential for lymphangiogenesis and lymphatic vessel maintenance.

VEGFC is essential for lymphatic development (Karkkainen et al., 2004). Moreover, VEGFC expression in the epicardium was previously reported and found functionally relevant for blood coronary patterning (Chen et al., 2014b), however, its possible involvement in cardiac lymphangiogenesis has not been addressed. On the other hand, *Vegfd* null mice do not present major lymphatic alterations, except for decreased lung lymphatic density and decreased calibre of dermal lymphatics (Baldwin et al., 2005; Paquet-Fifield et al., 2013). VEGFD does promote lymphatic development in zebrafish (Bower et al., 2017) and when it is overexpressed it is capable of inducing lymphangiogenesis, as it was reported for example by Chakraborty et al. (2019) and Haiko et al. (2008). Moreover, the role of VEGFD in mouse cardiac lymphangiogenesis has not been characterized.

This made VEGFC and VEGFD plausible candidates for our study. We first explored the possible involvement of VEGFC.

VEGFC is required in the *Wt1Cre+ lineage* for coronary lymphatic development

To functionally test the relevance of previously reported epicardial VEGFC (Chen et al., 2014b), we studied the effect of conditionally deleting *Vegfc* in the epicardium and its derivatives using $Wt1^{Cre}$. We generated $Wt1^{Cre}$; $Vegfc^{flox/flox}$ (from now on referred as Vegfc-KO) mice and studied their cardiac lymphatic development at E16.5, performing whole mount IF against LYVE1. We did not find differences in the lymphatics colonising the great arteries or the SV area between the control (Figure 40A, A') and Vegfc-KO hearts (Figure 40B, B'). The proportion of area covered by lymphatics in these regions did not differ significantly between genotypes (Figure 40E, I). In contrast, the lymphatics on either the ventral or the dorsal side of the ventricles are less developed in Vegfc-KOs than in controls (Figure 40B, B'). The percentage of the ventricles surface covered by lymphatics is decreased by around 50% on the ventral side (Figure 40F), and 68 % on the dorsal side (Figure 40J). Furthermore, we also found that the total length of all the lymphatics, resulting from the sum of the length of each individual branch, was

reduced on both sides of the mutants (Figure 40G, K). *Vegfc* deletion in *Wt1Cre+ lineage* also affects the branching pattern of cardiac lymphatics, producing a reduced number of bifurcations of both, the ventral (Figure 40H) and dorsal lymphatics (Figure 40L). Although lymphatic development is impaired in Vegfc-KOs, the coronary venous pattern appears normal, as revealed by EMCN staining (Figure 40C-D').

Thus, these data confirm the role of the epicardium/EPDCs in the development of the lymphatic vasculature of the heart. They also show that VEGFC is required in the epicardial lineage for cardiac lymphangiogenesis, a previously unknown function of VEGFC.

To further study the sensitivity of coronary lymphangiogenesis to epicardial VEGFC, we studied the effect of increasing VEGFC levels in the *Wt1Cre+ lineage*. We took advantage of a transgenic mouse line kindly provided by Dr. Guillermo Oliver's laboratory. In this line, a Cre-conditionally activatable *Vegfc* cDNA was knocked-in to the *Eef1a1* locus (Ubiquitous gene expression). Only upon Cre recombination, *Vegfc* cDNA is conditionally overexpressed (Pichol-Thievend et al., 2018). We crossed these mice with $Wt1^{Cre}$ animals and analysed the cardiac lymphatic development of control and $Wt1^{Cre}$; $Eef1a1^{VegfcGOF}$ (Vegfc-GOF) hearts at E16.5 with LYVE1 whole mount immunostaining (Figure 41). In agreement with the loss-of-function model, the increase of VEGFC expression in the *Wt1Cre+ lineage* provokes alterations in lymphangiogenesis. *Vegfc* overexpression resulted in hyperplastic lymphatics with disorganised vascular plexus in 2 out of 3 hearts, both at the ventral (Figure 41B) and dorsal sides (Figure 41B') of the ventricles. In these 2 mutants, the pulmonary artery, aorta and SV are almost completely covered by lymphatics too. However, due to the variability of the three VEGFC-GOF hearts, when we quantified the area of the different structures covered by lymphatics, we did not obtain statistically significant differences (Figure 41E-H). We also performed whole-mount EMCN IF on control and Vegfc-GOF hearts (Figure 41C-D') and we did not observe alterations of coronary vein development (Figure 41D, D').

Therefore, with the data from Vegfc-KOs and Vegfc-GOF models, we can conclude that tight regulation of *Vegfc* expression in the epicardial lineage is specifically required for proper cardiac lymphatic development.

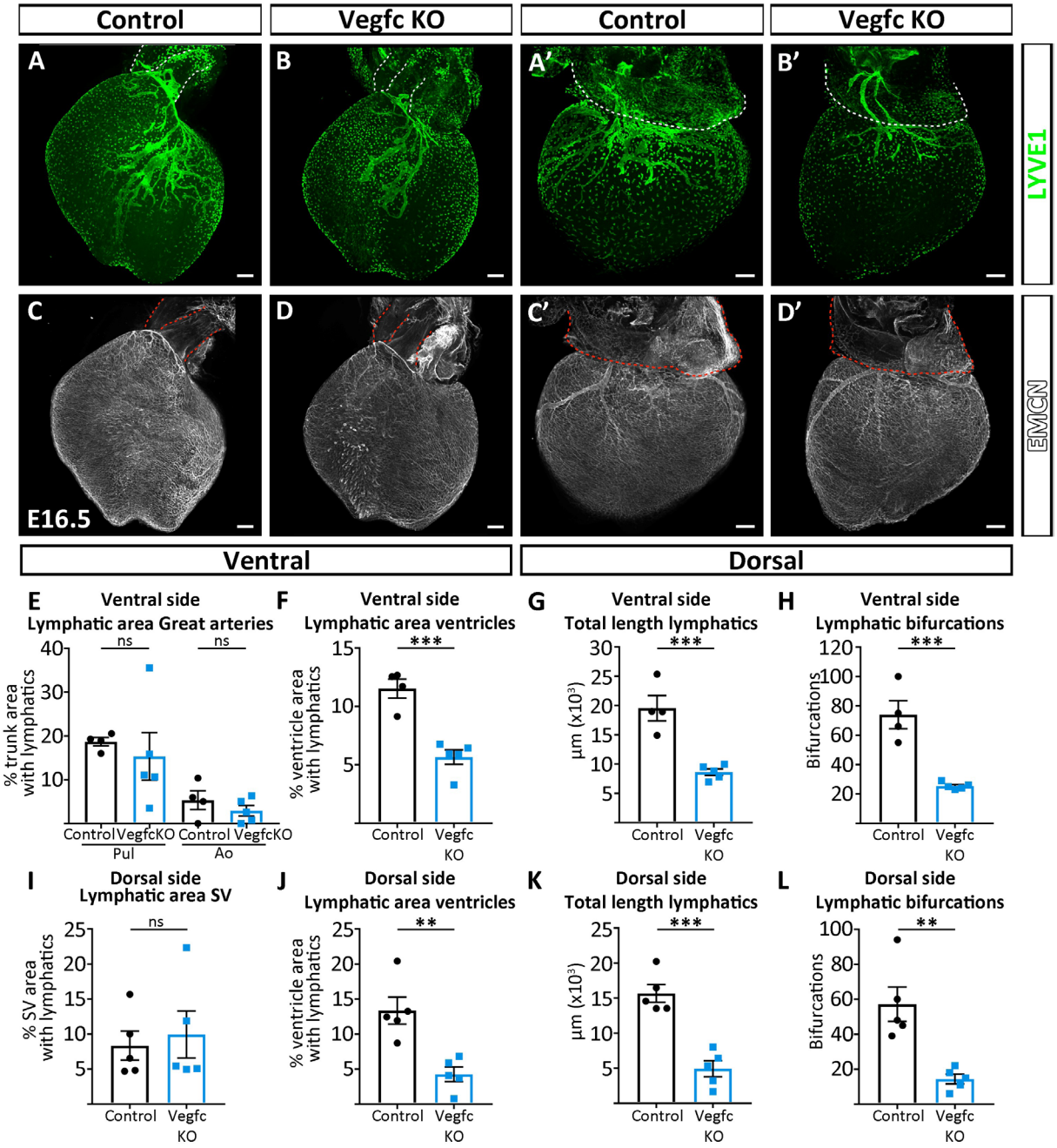

Figure 40. E16.5 *Wt1^{Cre}; Vegfc$^{flox/flox}$* hearts show normal coronary veins but impaired cardiac lymphatic development. (A-B') E16.5 whole mount LYVE1 immunostaining, showing lymphatic vasculature on the ventral (A-B) and dorsal (A'-B') sides of controls (A, A') and *Wt1^{Cre}; Vegfc$^{flox/flox}$* (Vegfc KO) hearts (B, B'). (C-D') Whole mount ENDOMUCIN immunofluorescence shows control (C, C') and Vegfc KO (D, D') coronary veins. Scale bars 200 µm. (E-L) Quantification of E16.5 control and Vegfc KO coronary lymphatics. (E, F, I, J) Pulmonary artery (Pul) and aorta (Ao) (E), ventral side of the ventricles (F), sinus venosus (SV) (I) and dorsal side of the ventricles (J) coverage by lymphatic vessels. (G, K) Total lymphatic length resulting from the sum of each individual lymphatic branch colonising the ventral (G) and dorsal side of the ventricle (K). (H, L) Total bifurcation points of ventral (H) and dorsal (L) cardiac lymphatics. (n ≥ 4 hearts per genotype). Unpaired t test. Ns: p value ≥ 0.05; ** p value <0.01; *** p value < 0.001. Error bars represent SEM.

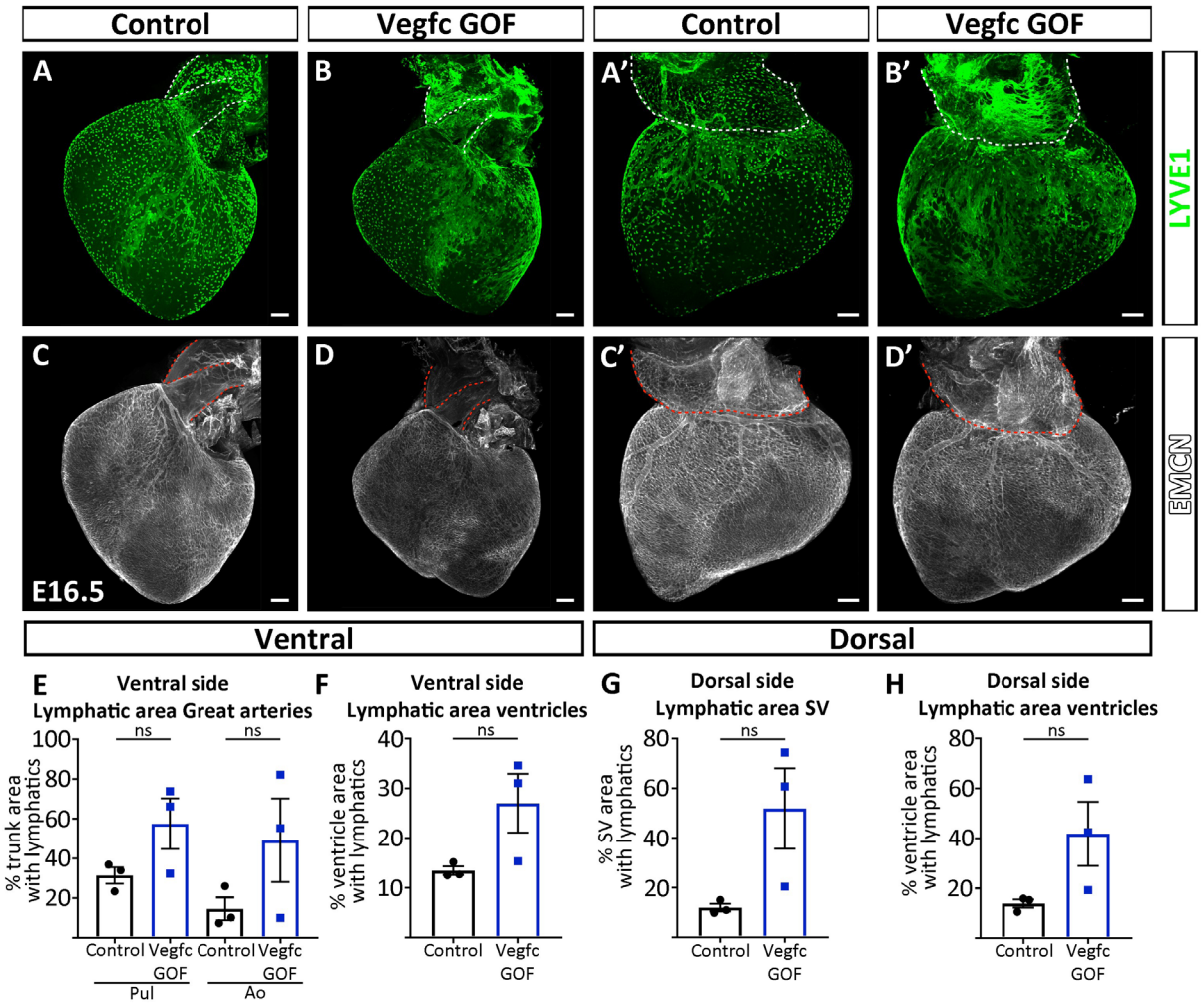

Figure 41. Epicardial *Vegfc* overexpression results in hyperplastic cardiac lymphatics but normal coronary veins. (A-B') E16.5 whole mount LYVE1 immunostaining, showing lymphatic vasculature on the ventral (A-B) and dorsal (A'-B') sides of controls (A, A') and *Wt1*^{Cre}*; Eef1a1*^{VegfcGOF} (Vegfc GOF) hearts (B, B'). (C-D') Whole mount EMCN immunofluorescence shows control (C, C') and Vegfc GOF (D, D') coronary veins. Scale bars 200 µm. (E-H) Quantification of E16.5 control and Vegfc GOF coronary lymphatics. Pulmonary artery (Pul) and aorta (Ao) (E), ventral side of the ventricles (F), sinus venosus (SV) (G) and dorsal side of the ventricles (H) coverage by lymphatic vessels. (n = 3 hearts per genotype). Unpaired t test. Ns: p value ≥ 0.05. Error bars represent SEM.

VEGFD is required for proper ventral coronary lymphatic development

Although the elimination of VEGFC affected coronary lymphatic development, the defects observed were milder than those observed in Meis dKOs, indicating that additional alterations should underlie the lymphatic defects in these mutants. Given that we found a strong downregulation of *Vegfd* in Meis dKO mutants, we next sought to determine whether VEGFD also contributes to coronary lymphatic development.

Whole mount VEGFD and PROX1 immunostainings performed on E16.5 *Wt1^{Cre}; Rosa26^{tdtmt}* hearts suggest that VEGFD is strongly expressed in epicardial cells (Figure 42A-A'). Additionally, we also found that some LEPDCs surrounding the growing lymphatic vessel express VEGFD (Figure 42B-B'). The epicardial expression of VEGFD is mildly stronger and more widespread in the ventral side of the ventricles than in the dorsal side (Figure 42D, D'). In the dKOs, we found decreased VEGFD epicardial expression (Figure 42C-C') when compared to controls (Figure 42A-A'). This is better appreciated on the whole view of the hearts (Figure 42D, D'; E, E'). Only few dispersed patches of cells express high levels of VEGFD on the ventral (Figure 42E) and dorsal epicardium (Figure 42E') of dKOs hearts. This is in clear contrast with the controls (Figure 42D-D').

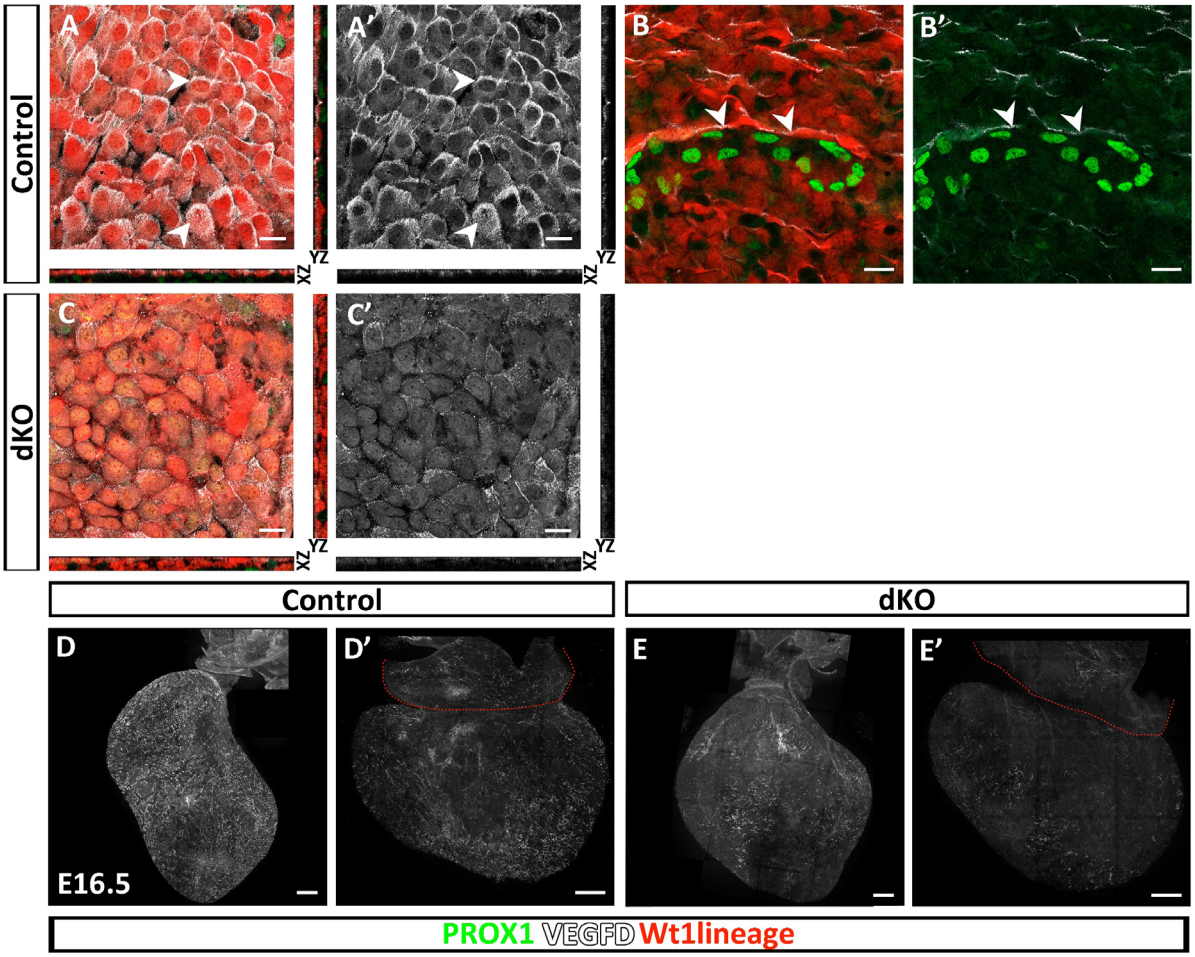

Figure 42. VEGFD may be downregulated in *Meis* mutants. (A-C') Whole mount PROX1 and VEGFD immunostaining of *Wt1^{Cre}; Rosa26^{tdtmt}* (A-B') and *Wt1^{Cre}; Meis1$^{flox/flox}$; Meis2$^{flox/flox;}$ Rosa26^{tdtmt}* E16.5 hearts (C-C'). (A-A', C-C') Maximum projection of three virtual slices of the ventral epicardial surface of whole mount hearts. Orthogonal YZ and XZ projections of the virtual z-stack (11 slices) are shown at the right and at the bottom of the image respectively. Arrowheads point to examples of epicardial cells secreting VEGFD. (B-B') Maximum projection of three virtual slices of ventral subepicardial region. Arrowheads point to examples of VEGFD+ LEPDCs. (D-D', E-E') Whole mount VEGFD immunostaining of control (D-D') and dKOs (E-E') E16.5 hearts. Scale bars 200 µm in D-E' and 20 µm in A-C'.

We next explored the possible involvement of VEGFD in cardiac lymphangiogenesis. Since VEGFD has not been as widely studied as VEGFC, there are not many tools available to address the question of interest. There are no mouse lines that would have allowed us an epicardial-specific *Vegfd* conditional deletion, so we opted for studying the role of VEGFD in cardiac lymphatic development in *Vegfd* null mice. For this, we generated a new *Vegfd* null mouse line using CRISPR-Cas9 technology. We designed sgRNAs that would target intron 2 and intron 4 of this gene. With this approach we deleted both exon 3 and 4, that codify a portion of VEGFD central receptor-binding domain, "VEGF homologous domain" (VHD), essential to perform its function (Achen et al., 1998; Baldwin et al., 2001a, b). Therefore, with this strategy we expected to generate a non-functional version of VEGFD.

We compared cardiac lymphatics of controls (Figure 43A, A') and *Vegfd* null (Vegfd KO) mice (Figure 43B, B') at E16.5. We immunostained in whole-mount for LYVE1 and PROX1 and quantified lymphatic coverage of the different cardiac regions (Figure 43C, D, G, H), total lymphatic length (Figure 43E, I) and total branching events (Figure 43F, J). We did not find differences in the lymphatics of the pulmonary artery, aorta, SV or dorsal side of the ventricles (Figure 43A-B', C, G-J). In contrast, *Vegfd* deletion does have an effect on ventral cardiac lymphatics growth. The coverage of the ventral side of the ventricles by lymphatics and the total length of all the ventral lymphatic branches are decreased in Vegfd KO hearts (Figure 43D, E). Moreover, although the difference is not statistically significant, ventral cardiac lymphatics tend to have fewer bifurcations in the mutants.

These results show a function of VEGFD in promoting ventral cardiac lymphangiogenesis. Taking into account that we observe a predominant VEGFD expression in the ventral epicardium and LEPDCs of the heart, the described defects are potentially due to the lack of VEGFD in these cells. Since both VEGFC and VEGFD are downregulated in *Meis* mutants, it is likely that the combined effects of the reduction of the two lymphangiogenic signals is responsible, at least partially, for the observed phenotypes in Meis dKOs.

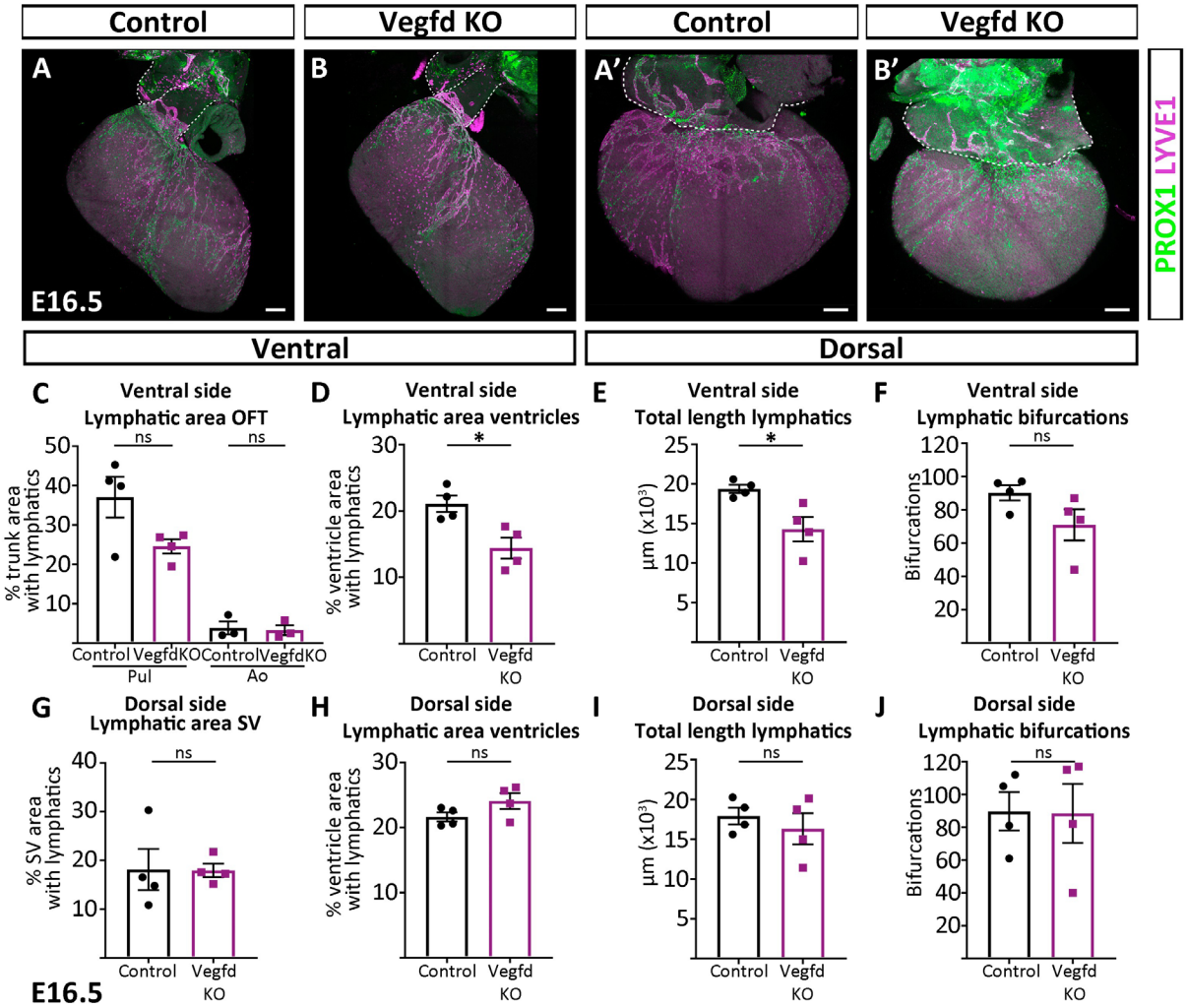

Figure 43. Ventral cardiac lymphatics are less developed in *Vegfd* null mice. (A-B') E16.5 whole mount LYVE1 and PROX1 immunostaining, showing lymphatic vasculature on the ventral (A-B) and dorsal (A'-B') sides of controls (A, A') and *Vegfd* null (Vegfd KO) hearts (B, B'). Scale bars 200 µm. (C-J) Quantification of E16.5 control and Vegfd KO coronary lymphatics. (C, D, G, H) Pulmonary artery and aorta (C), ventral side of the ventricle (D), sinus venosus (G) and dorsal side of the ventricle (H) coverage by lymphatic vessels. (E, I) Total lymphatic length resulting from the sum of each individual lymphatic branch colonising the ventral (E) and dorsal side of the ventricle (I). (F, J) Total bifurcation points of ventral (F) and dorsal (J) cardiac lymphatics. (n ≥ 3 hearts per genotype). Unpaired t test. Ns: p value ≥ 0.05; * p value <0.05. Error bars represent SEM.

DISCUSSION

"Always be willing to look at both sides of the argument. Understanding the other side is the best way to strengthen your own."
~ Jim Rohn

The work presented in this thesis has demonstrated that MEIS transcription factors play an important role in the epicardium during cardiac development. Epicardial-specific *Meis1* and *Meis2* deletion impairs the differentiation of EPDCs and delays blood coronary vessel maturation. Furthermore, this study has revealed an important function of the epicardium in the development of coronary lymphatics. Nevertheless, the implications of our discoveries, possible interpretations of controversial results and future perspectives will be addressed in the discussion of our results.

Cardiac Malformation in Meis dKOs

We found that MEIS transcription factors are expressed in the epicardium, AMC layer of the great arteries and in some EPDCs throughout development, which suggested that they may exert a role in the outermost layer of the heart and/or in its derivatives. This possibility had not been addressed in previous reports studying Meis function in the heart (Stankunas et al., 2008; González-Lázaro et al., 2014; Machon et al., 2015). Therefore, we generated *Meis1* and *Meis2* epicardial-specific conditional mutant mice using the $Wt1^{Cre}$ deleter allele. We did not obtain a complete deletion of these TFs as we observed 11% of *Wt1Cre lineage+* cells positive for Meis signal. This must be due to transient *Wt1* expression in those cells, enough to recombine the reporter but not the four *Meis* alleles. Another possibility would be that the antibody we have used might be recognising MEIS3, the other member of Meis family. However, we believe this is unlikely since *Meis3* expression is more than ten-fold lower than *Meis1* or *Meis2* in our transcriptomic analysis (not shown). Nevertheless, *Meis1* and *Meis2* deletion was sufficient to uncover an epicardial role of MEIS TFs. The mutation caused misalignment of the great vessels in 57% of E16.5 dKOs. Most of them suffered DORV but we also found one case of OA. Associated to the incorrect alignment, these defects were accompanied by VSD. We also found one embryo with VSD without alignment defect, indicating that this effect might not strictly depend on great arteries misalignment. The misalignment defects could explain the 50% lethality of *Meis* mutants, but what could explain the observed defects?

Single *Meis1* or *Meis2* full knockouts also present alterations of the septation of the OFT, resulting in alterations of the great vessels. Single *Meis1* and *Meis2* homozygous null embryos suffer from OA and PTA, respectively. Stankunas et al. (2008) and Machon et al. (2015) suggested an underlying defect in NCCs. Machon and colleagues (2015) demonstrated that indeed *Meis2* plays an autonomous role in NCCs and is required for proper semilunar valves development. However, *Meis2* neural crest-specific conditional mutants did not recapitulate the OFT septation defects of the full knockouts (PTA), producing DORV instead. These results suggest that *Meis1* and/or *Meis2* expression in other cells different from NCCs may be required for proper septation and alignment of the OFT. In agreement with this notion, elimination of *Meis1* and *2* alleles in the developing cardiomyocyte lineage produces a range of OFT alterations ranging from PTA to OA, depending on the number of alleles deleted (L. Carramolino and M. Torres, personal communication). Meis roles in OFT development are therefore multiple and involve different tissues. Here we describe a new tissue involved in OFT development: the epicardium/AMCs. In fact, we detected MEIS signal in AMCs and in some of their derivatives. The continuous sheet of

AMCs wrapping simultaneously the aorta and pulmonary artery observed in Meis dKOs, suggests that interactions between the AMC layer and OFT morphogenesis regulated by *Meis* are required for the proper alignment of the great vessels. To our knowledge, this is the first evidence of a function of the AMC layer in regulating OFT development. *Sema3C*, a myocardial signal that attracts cNCCs, is not affected in mutants, while *PlexinA2 in situ* hybridization suggested that cNCCs do reach the OFT in Meis dKOs (Brown et al., 2001; Feiner et al., 2001). Altogether, these results suggest that cNCCs colonize the OFT and reach the mutant hearts, but do they locate and condense properly? How could we explain the OFT defects then? These are questions that remain to be answered. We plan to perform further studies tracking the destination of those cNCCs into their final position in the OFT. Later alterations in the signalling coming from AMCs or AMC-derived cells may cause the incorrect positioning of cNCCs. We are not aware of any publications reporting $Wt1^{Cre}$ contribution to cNCCs, so we would not expect to have deleted MEIS TFs in this population in Meis dKOs. However, we would need to immunolabel cNCCs in dKOs and controls and see whether they are *Wt1lineage*-negative, in order to reject that an autonomous function of MEIS in cNCCs could cause the DORV and OA observed. Furthermore, epicardial alterations and defects in the development of the base of the heart, may also influence the alignment of the great vessels.

SHF contribution is also essential for OFT formation and alignment (Vincent and Buckingham, 2010). Different SHF progenitor pools contribute to two distinct domains, the superior and inferior OFT, which contribute to the future myocardium at the base of the aorta and pulmonary trunk, respectively (Bajolle et al., 2008). Therefore, other possibility is that SHF addition and aorta and pulmonary artery specification are impaired due to the absence of *Meis* genes in the AMC layer. It would be interesting to analyse *Sema3C* and *Hes1* expression or contribution at E10.5 to determine pulmonary artery and aorta specification respectively in Meis dKOs (Vincent & Buckingham, 2010).

Aside from DORV, OA and VSD defects, Meis dKOs embryonic hearts are normal. Moreover, we found that a proportion of dKO embryos suffered no misalignment defects and were born and survived without cardiac function alterations. Their cardiac function is preserved and the histological analysis revealed no malformations. The absence of defects in these animals could relate with a decreased recombination of *Meis* alleles or a reduced penetrance of the mutation. However, surviving dKOs did suffer from alterations in other organs with a strong contribution from *Wt1Cre*-recombined lineages, like the spleen and reproductive system, supporting an adequate *Meis* recombination and deletion. Nevertheless, these organs may be more sensitive to the absence of *Meis*. Meis dKOs sterility correlates with *Meis* expression in the reproductive system (Williams, Williams and Innis, 2005). MEIS expression in the spleen has not been reported but the defects suggest a role in its development or maintenance. In addition, *Meis1* function in hematopoiesis (Azcoitia et al., 2005) and the observed spleen defects, made us wonder about the hematopietic populations of Meis dKOs. However, no major alterations were found.

Epicardium, EMT and associated defects

Meis genes are not required for the initial formation of the epicardium, as this layer of cells is present in Meis dKOs. However, ZO-1 discontinuous expression suggests alterations in its epithelial structure. We found some epicardial and EMT-associated genes, like *Wt1, Tbx18, Tcf21, Snai2, Fgf2* and *Cdh1*, downregulated in the epicardial/subepicarial layer of Meis dKOs. However, EMT does not seem to be impaired in dKOs, as we observed EPDCs in the subepicardium and myocardium of dKOs, which differs from observations in EMT-deficient mutants (Moore et al., 1999; Smit, C.L, et al., 2011; von Gise et al., 2011). However, there may be a misregulation of this process as, for example, downregulation of E-cadherin (*Cdh1*) and upregulation of N-cadherin (*Cdh2*) would be indicative of active EMT status, and downregulation of *Snai2*, of reduced EMT (Lamouille, Xu and Derynck, 2014).

Another epicardial function is the paracrine communication between the epicardium and the myocardium, which is essential for proper myocardial growth. For example, alterations in RA epicardial signalling results in myocardial thinning as a consequence of defective epicardial-myocardial signalling (Merki et al., 2005; Lin et al., 2010; Wang et al., 2018b). It was proposed that RA promotes myocardial growth through FGF2 (Merki et al., 2005). We have found that both RA and *Fgf2* are downregulated in the epicardial/subepicardial layers of Meis dKOs, however, these hearts show no myocardial thinning. Nonetheless, additional sources of FGF2 or additional mitogens may compensate for the epicardial deficiency.

Interestingly, Meis dKOs suffer alterations in the distribution and specification of EPDCs. Meis deletion results in the accumulation of *Wt1Cre lineage+* cells in the epicardium/subepicardium and a decrease in the proportion of mesenchymal cells that colonise the myocardium. However, this deficiency seems to be compensated by the increased contribution of other non-epicardial lineages, as the total number of mesenchymal cells does not change. If we do not consider the cells accumulated in the subepicardium, EPDC migration capacity does not seem to be impaired in Meis dKOs, as they migrate as far from the epicardium as control EPDCs. Furthermore, characterization of the subpopulations of EPDCs revealed important information. At E13.5, we did not find differences in the number of CD140α+ cells (including epicardial cells and fibroblasts) or in the CD90+ CD140α+ fibroblast subpopulation. We did not observe changes in the proportion of these cells that derive from the epicardium either. At later stages, although the number of CD140α+ does not change, the CD90+ CD140α+ fibroblast subpopulation is severely reduced in Meis dKOs. More importantly, the proportion of these cells that derive from *Wt1lineage* is underrepresented. We suspect that the early-stage fibroblasts fail in their proliferation or expansion, or that they are differentiated into a different cell type as they exit the epicardium. Interestingly, *Tcf21* and *Pdgfrα* are important genes for fibroblast specification and both are downregulated in the transcriptomic analysis. Therefore, we hypothesise that the deficiency in these crucial factors may be responsible for the decreased numbers of epicardial-derived fibroblasts in Meis dKOs (Smith, C.L. et al., 2011; Acharya et al., 2012; Braitsch et al., 2012).

When we analysed the SMC population at E16.5 and E18.5, we observed a decreased coverage of arteries by *Wt1Cre lineage+* SMCs in Meis dKOs, suggesting an impaired SMC population specification

or proliferation. However, at E18.5 vein coverage by SMCs is unaffected. We speculate that this could be due to topological reasons, for being closer to the epicardium than arteries. In addition, we found that the accumulated subepicardial cells were SM22α+, potentially suggesting their SMC identity. Indeed, *Pdgfrβ* upregulation suggests increased SMC-lineage specification (Mellgren et al., 2008). *Tbx18* downregulation may also be indicative of premature SMC differentiation, as previously described (Greulich et al., 2012). These results may suggest that, in normal conditions, MEIS TFs also inhibit the premature expression of SMC markers, as TBX18 and TCF21 do (Braitsch et al., 2012; Greulich et al., 2012). Epicardial Notch over-activation also causes premature SMC differentiation (Grieskamp et al., 2011). In Meis dKOs, *Rbpj* downregulation contrasts with the overexpression of other components of the Notch pathway, so we cannot reach any conclusion regarding this pathway until we validate its activation or inactivation in *Meis* mutants. Indeed, similar to the findings in Meis dKOs, Notch inactivation causes decreased SMC differentiation and defective coating of the arteries (Del Monte et al., 2011; Grieskamp et al., 2011). Nevertheless, we found that the subepicardial *Wt1Cre lineage*+ cells were also positive for the fibroblast marker PERIOSTIN, suggesting that these cells could be myofibroblasts. Myofibroblasts are usually produced under stress and this is stimulated through Smad2/3 activation by TGFß signalling (Davis and Molkentin, 2014; Khalil et al., 2017). However, developmental myofibroblast transdifferentiation may be regulated by different mechanisms than pathological-driven transdifferentiation. From our RNAseq analysis, an activation of TGFß pathway cannot be inferred, as we did not find changes in *Smad* genes and *Tgfbr1* and *Tgfbr2* are downregulated instead of upregulated. However, a detailed analysis at the protein level should be performed in order to draw any conclusions.

Despite having decreased fibroblasts and SMCs, *Meis* mutants survive, likely due to the compensation by alternative cell lineages, as predicted from the already increased proportion of *Wt1Cre lineage*-negative fibroblasts observed at E15.5 and E18.5. However, this does not seem to be the case for SMCs, for which the compensation may start after birth. In fact, Smith et al. 2011 reported an expansion of non-epicardial populations in epicardial-SMC-depleted mice that allowed their survival, and that decreased fibroblasts were compatible with life.

In summary, we have shown that *Meis* deletion causes a reduced specification of fibroblasts and of SMCs that populate and colonise the coronary arteries. In contrast, a population of myofibroblasts that express both, SMC and fibroblasts markers, are produced and transiently accumulated in the subepicardium.

Blood coronary vasculature development upon epicardial *Meis* deletion

We have shown that epicardial *Meis* deletion causes a delay in the blood coronary vasculature development. Both, arteries and veins, appear immature in E16.5 dKOs but are mostly recovered by E18.5. As a result, adult hearts' blood coronary vessels present patterning alterations but are mostly normal. An important question is whether the SMCs defects are causative or consequence of the

alterations in coronary vessels. Similar recovery of coronary vessel development to the observed in Meis dKOs was reported in epicardial-specific *Pdgfrβ* mutants that affect SMCs specification (Mellgren et al., 2008). Moreover, a recent study in zebrafish reinforces the hypothesis that SMC recruitment is essential for coronary vessel development and that it can influence angiogenesis mechanisms (Ando et al., 2021). Therefore, we postulate that Meis dKOs coronary vessel defects are mostly due to the reduced SMC coverage, which impairs their proper maturation.

Nevertheless, we cannot discard the possibility that also epicardial signalling is affecting angiogenesis and maturation of coronary vessels, which may account for the patterning alterations. For example, epicardial cells and SMCs secrete CXCL12 that is sensed by CXCR4+ ECs, thereby promoting coronary artery maturation (Cavallero et al., 2015). Interestingly, *Cxcr4* and *Cxcl12* are both upregulated in Meis dKOs, according to the RNAseq analysis. We hypothesise that Meis dKOs may activate this pathway at E16.5 as a compensatory mechanism for the delay in angiogenesis and maturation defects, or that a tight regulation is required and both, inactivation or overactivation of the pathway, impair the normal artery remodelling.

Vegfc downregulation in dKOs may also underlie the coronary vein defects (Chen et al., 2014b). Therefore, we studied the effect of *Vegfc* epicardial-specific deletion or overexpression with $Wt1^{Cre}$, for comparison with Meis dKOs. Unexpectedly, we did not find coronary vein defects in Vegfc-KOs or Vegfc-GOF, which was intriguing. Although Chen et al. (2014b) proposed that the epicardium was the main source of VEGFC required for proper coronary development, they used full *Vegfc* knockouts for their studies, suggesting that additional sources of VEGFC are responsible for the phenotype they observed. It is possible that in $Wt1^{Cre}$; $Vegfc^{flox/flox}$ hearts, the loss of epicardial *Vegfc* is compensated with additional sources of VEGFC. Furthermore, Chen and colleagues (2014b) characterized the effects until E14.5 and we performed our study at E16.5. It may be possible that by that stage, there is a recovery of the phenotype similar to the improvement we have observed in Meis dKOs from E16.5 to E18.5.

Interestingly, we suspect that Meis dKOs also present patterning alterations that result in ectopic connections between coronary veins and the left atrium. From whole mount observations at E18.5, we infer their vein identity; from sections, we have confirmed the existence of an abnormal coronary vascular connection to the left atrium and its location at the surface of the heart. *Sema3d* downregulation in Meis dKOs transcriptome may correlate with this defect (Aghajanian et al., 2016). In a context of *Sema3d*-deficiency, venous ECs expressing SEMA3D receptors Erbb2 and Nrp1 (upregulated and without changes, respectively, in RNAseq analysis), would not be repelled by SEMA3D and, allowing them to form anomalous connections with the LA (Aghajanian et al., 2016). Abnormal vein connections to the LA have also been reported in humans (Pizarro et al., 2009), with implications for cardiovascular interventions. Importantly, anomalous pulmonary venous connections with the right atrium were also reported in *Sema3d* mutant mice (Degenhardt et al., 2013). Therefore, we should investigate in the future whether *Meis* mutants also present this alteration, as it could have important implications. An aminoacid substitution in SEMA3D in humans leads to "*Total anomalous pulmonary venous connection"* disorder which is potentially lethal (Degenhardt et al., 2013). Moreover, epicardial

connections between pulmonary veins and LA can also cause atrial fibrillation in humans (Pérez-Castellano et al., 2011). Therefore, understanding the possible involvement of MEIS TFs establishing boundaries for anomalous venous connections would be crucial.

We believe that the delay in coronary vessel maturation in Meis dKOs results from defective SMC recruitment. Nonetheless, the flow cytometry analysis of E13.5 coronary ECs, suggests an initial reduction of ECs that is later compensated. Therefore, we plan to perform a more detailed study of the initial stages of coronary vessel development, to evaluate possible angiogenic defects in Meis dKOs. In addition, we and others have observed MEIS expression in mesenchymal cells close to ECs but not in ECs themselves (Hisa et al., 2004; Azcoitia et al., 2005; Machon et al., 2015), suggesting that indeed a non-autonomous role could underlie the coronary defects. However, the causes of the mild changes in the proportion of *Wt1Cre lineage+* ECs should be further studied in order to make any final conclusion about the cell-autonomous involvement of Meis in the coronary endothelium.

We have also observed alterations of the innervation pattern of the heart. We postulate that the defects in coronary vein patterning account for the cardiac innervation defects , given that nerves grow following the main veins in the heart (Nam et al., 2013; Végh et al., 2016).

Is Retinoic acid responsible for the defects in EPDCs and coronary vasculature?

If blood coronary vessels defects may be the consequence of the SMCs defects, what molecular mechanisms might be driving the SMCs defects?

Extensive evidence suggests the relationship between RA and MEIS. *Meis* genes are both targets of RA (Mercader et al., 2000) and regulate RA availability by regulating genes encoding RA-metabolism, like Raldh2 and *Cyp26b1* (Roselló-Díez et al., 2014; Berenguer et al., 2020; Delgado et al., 2020). Considering that the RA pathway appears to be inactivated in the epicardium of Meis dKOs, and the known functions of this pathway in the heart, we hypothesised that a connection may be established.

With that purpose, we analysed $Wt1^{Cre}$; $Raldh2^{flox/flox}$ hearts, however, contrary to expectations, we have not observed major alterations. Some processes, like lymphatic maturation, might be more sensitive to the reduction of RA, given that lymphatic vasculature maturation is impaired in $Wt1^{Cre}$; $Raldh2^{flox/flox}$ mutant hearts (Lioux et al., 2020). Something we should consider is that although Raldh2 is the most relevant enzyme responsible for RA synthesis in the embryo, there are two other retinaldehyde dehydrogenases. In the absence of Raldh2, they may be upregulated and supply the heart with some levels of RA. Indeed, in the epicardium all RA-synthesizing enzymes, *Aldh1a1, Aldh1a2* and *Aldh1a3*, are expressed and in Meis dKOs all three of them are downregulated. This could explain why $Wt1^{Cre}$; $Raldh2^{flox/flox}$ mutant hearts do not recapitulate the phenotype of *Meis* mutants or that of other RA-pathway mutants (Merki et al., 2005; Lin et al., 2010; Wang et al., 2018a, b). Further experiments should focus on confirming the effective inactivation of RA pathway in $Wt1^{Cre}$; $Raldh2^{flox/flox}$. The expression of the other retinaldheyde dehydrogenases as well as the expression of downstream effectors of the

pathway should be analysed. If we found an inefficient inactivation, oral supplementation of pregnant females with BSM493, a RA antagonist, could avoid this possible compensation. In addition, oral supplementation with all-trans retinoic acid of pregnant females carrying *Wt1*^{Cre}*; Meis1*$^{flox/flox}$*; Meis2*$^{flox/flox}$ embryos, would be an interesting future experiment. If coronary vessels and EPDCs alterations were rescued, this would argue in favour of our hypothesis.

In an attempt to identify a genetic interaction between *Meis* and *Raldh2* loss of function, we studied *Wt1*^{Cre}*; Meis1*$^{flox/wt}$*; Meis2*$^{flox/wt}$*; Raldh2*$^{flox/wt}$ embryos, however this genetic combination did not produce any phenotypic alteration, which may be due to insufficient reduction in the function of the three loci assayed. In fact, *Wt1*^{Cre}*; Meis1*$^{flox/flox}$*; Meis2*$^{flox/wt}$ embryos show no defects (not shown). Therefore, it seems that just one *Meis* functional allele is sufficient to compensate for the loss of the others. Therefore, with these results we cannot exclude a possible genetic interaction between *Meis* genes and *Raldh2* in this context. Further experiments should be done in the future exploring other allelic combinations.

Azambuja and colleagues (2010) used quail proepicardial explants and embryos to study the role of RA on SMC differentiation. They observed that increased RA levels were associated with inhibition of differentiation and decreased RA levels, with premature SMC differentiation. Xiao et al. (2018) reported that the Hippo pathway also regulates fibroblast differentiation by directly regulating RA, while Braitsch and colleagues (2012) also showed that RA induces *Tcf21* expression to inhibit premature SMCs differentiation. They also showed that *Tcf21* null mice had an accumulation of SM22α+ cells in the subepicardium (Braitsch et al., 2012). However, in their Collagen1a1 immunostainings, an accumulation of positive signal in the subepicardium can be observed and here, we showed that this cell population also expresses the fibroblast marker PERIOSTIN. This could argue in favour of the hypothesis that the EPDCs that accumulate in the subepicardium are myofibroblasts, instead of SMCs. A caveat to this scheme is that Acharya et al. (2012) reported no accumulation of cells in the subepicardium of *Tcf21* null mice. However, the discrepancy between both *Tcf21* null mice studies may be due to the stage. While Braitsch et al. (2012) mostly characterised EPDC subpopulations at E17.5, Acharya et al. (2012) did their characterization at E18.5. At this stage, we have shown that most SM22α+ do not appear accumulated in the subepicardium, so this may explain the discrepancy. Moreover, this hypothesis is supported by the appearance of a new single-cell-RNAseq cell cluster expressing both fibroblast and pericyte markers in the analysis of *Lats1/2* mutants, which reduce RA levels in the epicardium (Xiao et al., 2018). In support of this idea, in the RNAseq analysis of *Meis* mutants, both the RA pathway and *Tcf21* are downregulated. A study of *Tbx18* mutants also reported premature SMC differentiation, however, in this study fibroblast populations were not characterized and therefore, the myofibroblast identity of the accumulated cells, cannot be discarded either (Greulich et al., 2012).

Thus, we propose a model in which *Meis* deficiency provokes low epicardial RA levels, which prevents *Tcf21* expression. As a consequence, a subpopulation of fibroblasts precursors differentiate into myofibroblasts. Given that the myofibroblast accumulate subepicardially, we think that soon after they undergo EMT and before they have the chance to migrate into de myocardium, EPDCs differentiate into myofibroblasts. It is plausible that altered epicardial signals in the mutants contribute to this

phenomenon. The alterations of EPDC populations also include decreased numbers of fibroblasts and SMCs populating the myocardium (Figure 44). Myofibroblasts differentiation could also be activated as a compensatory mechanism once the heart senses a stress due to the mutations. Nevertheless, the aforementioned experiments should be performed in order to validate our hypothesis as well as further characterization of myofibroblast-like cells.

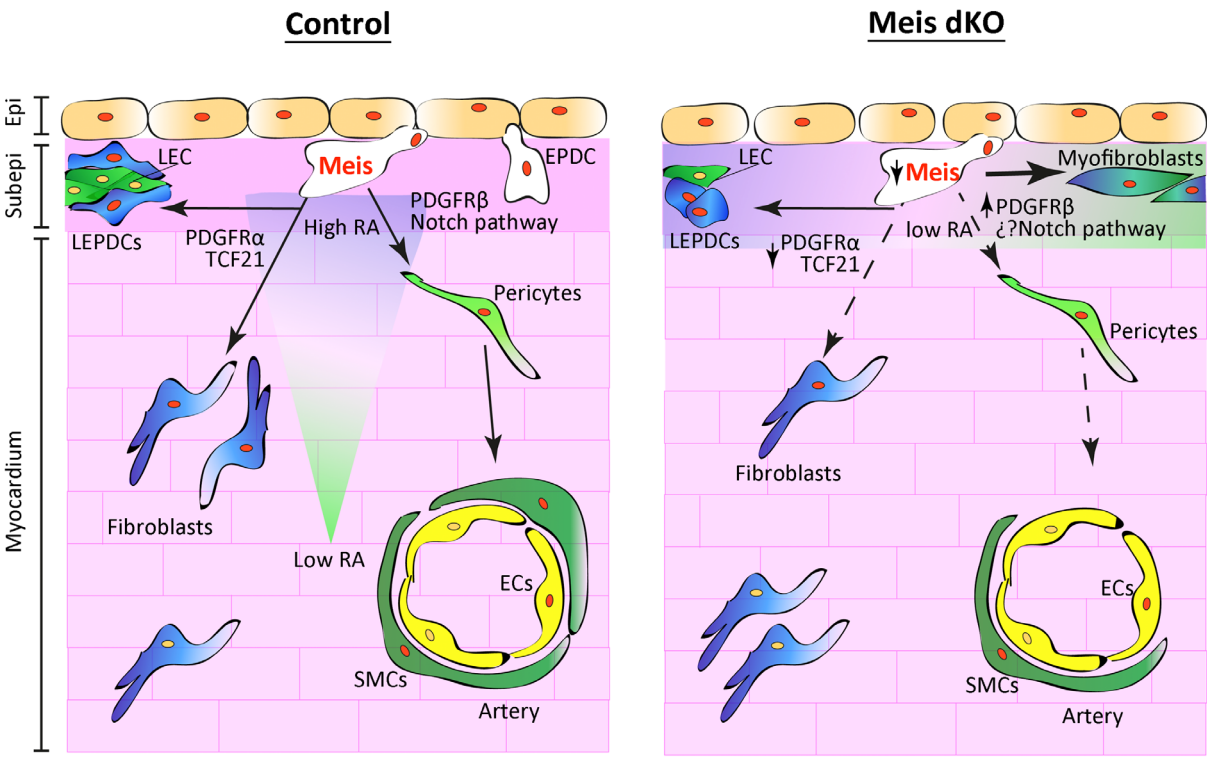

Figure 44. Proposed model for the role of MEIS transcription factors in EPDCs specification. We hypothesise that *Meis* deficiency results in decreased epicardial and subepicardial retinoic acid levels (RA) which prevents *Tcf21* expression. As a consequence, epicardial-derived cells (EPDCs) express prematurely smooth muscle (SMCs) genes and myofibroblasts accumulate in the subepicardium. The alterations of EPDC populations also include decreased numbers of fibroblasts and SMCs populating the myocardium, as well as, defective crosstalk between lymphatic-associated EPDCs (LEPDCs) and lymphatic endothelial cells (LECs). Red nuclei represent EPDCs, and yellow nuclei cells that do not derive from the epicardium. Endothelial cells (ECs) are depicted in yellow and cardiomyocytes in pink. Epi: epicardium; Subepi: subepicardium.

Lymphatics and LEPDCs: a new non-autonomous role of the epicardium/EPDCs in lymphatic development

We have shown that *Meis* deletion causes a severe impairment of cardiac lymphatic development, with a drastic reduction of the lymphatics colonising the ventral and dorsal sides of the ventricles. While no changes were found at E16.5 or E18.5 in the mutant SV or pulmonary artery lymphatics, the aorta showed a higher lymphatic coverage than in controls. This suggests that lymphatic vessels retain their angiogenic potential but colonize alternative paths, as a response to the defects caused by *Meis* deletion in *Wt1Cre lineage+* cells. Interestingly, lymphatics develop postnatally in the dKOs and Indian ink injections suggest that they are functional. Other lymphatic-deficient models have reported a postnatal recovery (Klotz et al., 2015). We hypothesise that alternative sources of cells or growing mechanisms may compensate for the lack of coronary lymphatics at birth. These results also suggest that no essential roles are played by coronary lymphatics during gestation or the early postnatal growth.

Here we have shown that, while cardiac lymphatics do not derive from the epicardium (Wilting et al., 2007; Klotz et al., 2015; Lioux et al., 2020; present study), they associate tightly with LEPDCs in the subepicardial region. We detected this association as early as E14.5 and at least until birth. We have provided evidence to postulate that these LEPDCs are required for cardiac lymphangiogenesis. LEPDCs are present in the dKOs in similar numbers than in the controls, however, their distribution ensheathing the lymphatic endothelium is altered. In the mutants, we found a higher proportion of the lymphatic perimeter devoid of LEPDCs in contact with LECs. We propose that the crosstalk between LECs and LEPDCs may be impaired in *Meis* mutants, so that the physical association is not properly established and LECs do not receive the cues that, in normal conditions, would promote and/or guide their growth.

We found that LEPDCs are negative for epicardial markers but mostly positive for VIMENTIN, which suggested a mesenchymal identity. We discarded their pericyte-like or SMC identity, as they were negative for markers of these populations. Interestingly, we found that a high proportion of LEPDCs were positive for the fibroblast marker PERIOSTIN, suggesting that LEPDCs represent a subtype of fibroblasts. Actually, previous *in vitro* co-culture studies showed that, when grown together with fibroblasts, LECs organised into stable lymphatic capillary networks. In this setting, fibroblasts provided extracellular matrix and molecules as VEGFC and HGF that promoted lymphangiogenesis (Gibot et al., 2016). Furthermore, Wang and colleagues (2020) proposed that, in zebrafish, a subpopulation of fibroblasts guide lymphatic growth through providing mature VEGFC. They showed that these fibroblasts express *Vegfc* in a salt-and-pepper-like fashion as well as the proteases responsible for VEGFC processing and maturation (Wang et al., 2020). In addition, it is plausible that this subpopulation of fibroblasts is conserved among species. Wang and colleagues (2020) found an equivalent unannotated subpopulation in a published single-cell-RNAseq dataset from mouse limb muscle.

These results support the idea that, in the mouse heart, LECs also associate with fibroblasts that promote their growth. In agreement with this, we found that some LEPDCs express VEGFD, and therefore, LEPDCs may be exerting a similar function to that reported by Wang et al. (2020) in secreting and/or processing VEGFC/D. While we found a reduction in *Vegfc/d* expression in mutants, we did not

find changes in *Ccbe1, Adamts3,* plasmin, prostate-specific antigen, Cathepsin D or thrombin, previously associated with VEGFC and VEGFD processing (Künnapuu and Bokharaie, 2021), indicating that probably *Meis* deficiency specifically affects the expression of Vegfc/d but not that of their processing enzymes. Future experiments studying cardiac lymphatic development in fibroblast-deficient mice, like *Tcf21* mutants, could help us to corroborate the requirement of fibroblast-LEC association for their development.

We also plan to determine whether it is a cardiac-specific function of MEIS TFs, or whether it is extended to other organs. The patterning alterations observed in mesenteric lymphatics suggest some relevance of Meis function in the *Wt1Cre lineage+* cells, however, lymphatic agenesis was only observed in the heart and further characterization needs to be performed to understand the lymphatic alterations in the mesentery.

In contrast to the novelty of fibroblast-lymphatic association, the relationship between lymphatics and SMCs is well established. As part of their maturation process, lymphatics recruit SMCs that allow their contraction (Brakenhielm and Alitalo, 2019). Usually, precollector and collector lymphatics are covered by a thick layer of SMCs, but cardiac lymphatics are characterized by sparse SMCs coverage (Brakenhielm and Alitalo, 2019). We explored the colonization of the lymphatic surface by SMCs and only found few and disperse SMCs coating the lymphatic vasculature in some E18.5 hearts. This observation suggests that in the mouse, lymphatic maturation and SMC recruitment starts late in development. Thus, these results suggest a specific role for lymphatic vasculature ensheathing by fibroblast-like LEPDCs during cardiac lymphangiogenesis. This function would be different from that of pericytes/SMCs, which appear at later stages. We cannot discard that the mature lymphatic pericyte/SMC population may derive through transdifferentiation from LEPDCs, given that most SM22α+ cells observed at E18.5 associated to lymphatic vessels were also positive for the *Wt1Cre+* cell lineage.

The role of epicardial/LEPDC-produced VEGFC in cardiac lymphangiogenesis

The RNAseq analysis showed *Vegfc* downregulation in the epicardium/subepicardium of Meis dKOs. We then decided to explore the paracrine signalling that may be involved in LEPDC-LEC crosstalk. As previously mentioned, extensive reports have shown VEGFC involvement in lymphangiogenesis. Therefore, a reduction of VEGFC in the epicardium and/or LEPDCs may be responsible for the defects observed in lymphangiogenesis. Furthermore, *Vegfc* expression in the epicardium had already been reported in previous studies which supported a possible function in cardiac lymphangiogenesis (Chen et al., 2014b).

Our analysis of Vegfc-KO and Vegfc-GOF hearts confirmed a role of epicardial- and/or EPDC-produced VEGFC in regulating lymphangiogenesis. Furthermore, we have shown that tight regulation of VEGFC levels in the epicardial lineage are required for adequate cardiac lymphatic development. Epicardial-specific *Vegfc* deletion affected lymphatic growth and maturation, as extent and

ramifications of the lymphatic vasculature were decreased in the mutants. The results from Vegfc-GOF also reinforce this idea, as increased VEGFC levels resulted in increased growth and hyperplastic and dilated lymphatics. Nevertheless, only two out three hearts developed this phenotype, maybe due to an incomplete penetrance of the overexpression. We plan to increase the number of Vegfc-GOF hearts to further validate these results.

Therefore, *Vegfc* downregulation may be responsible, at least partially, for the observed defects in epicardial *Meis*-deficient hearts. In previous studies, strong *Vegfc* expression in the epicardium was reported as early as E10.5 and until E13.5 (Chen et al., 2014b). Nevertheless, it was not mentioned whether they observed sustained expression at later stages or not. Therefore, a more detailed expression analysis of *Vegfc* at different stages and with different techniques will be required to dissect its regulation by *Meis* in the *Wt1Cre lineage* and how it can affect lymphangiogenesis. In addition, we plan to analyse coronary and lymphatic vasculature of $Wt1^{Cre}$; $Meis1^{flox/flox}$; $Meis2^{flox/flox}$; $Eef1a1^{VegfcGOF}$ embryos and study whether epicardial *Vegfc* overexpression in *Meis*-deficient *Wt1Cre lineage*+ cells is capable of rescuing coronary lymphatic development.

We have explored the function of VEGFC in the epicardium and EPDCs and its involvement promoting cardiac lymphangiogenesis. However, other factors regulated by *Meis* in the epicardium/EPDCs must be involved in lymphangiogenesis, since lymphatics are not as affected in Vegfc-KOs as in *Meis* mutants.

The role of VEGFD in cardiac lymphangiogenesis

We analysed VEGFD expression in the heart and found that it is highly expressed in the epicardium, in some LEPDCs. As for *Vegfc*, *Vegfd* transcription is reduced in the epicardium/subepicardium of *Meis* mutants. Therefore, its expression pattern could suggest a cooperative role with VEGFC in promoting cardiac lymphatic development. We confirmed *Vegfd* downregulation in Meis dKOs by immunofluorescence and we found that only some heterogeneous patches of epicardial cells still expressed VEGFD. Therefore, we next sought to understand the possible function of VEGFD in cardiac lymphatic development. Our results analysing Vegfd-KOs revealed a selective role of VEGFD in ventral lymphatics development. While dorsal lymphatics appear normal, ventral lymphatics are less developed in Vegfd-KO. We wondered about this differential effect. It is possible that VEGFD is slightly more expressed on the ventral side of the epicardium than on the dorsal side but we do not know what specific regulation may be controlling it. SHF lymphatics contribute only to ventral lymphatics and are essential for their development (Maruyama et al., 2019; Lioux et al., 2020) so a possibility is that SHF-derived LECs are more sensitive to VEGFD loss than the rest of cardiac LECs.

With these results, we can confirm that VEGFD is a lymphoangiocrine molecule required for cardiac lymphatic development. It is possible that in the epicardium and/or LEPDCs, VEGFC and VEGFD cooperate in promoting lymphatic development, as it has been described in other organs (Haiko et al., 2008; Astin et al., 2014; Nurmi et al., 2015; Bower et al., 2017).

Therefore, it is possible that the combined downregulation of *Vegfc* and *Vegfd* in the epicardial lineage significantly contributes to the lymphatic defects observed in Meis dKOs.

Other possible epicardial paracrine molecules involved in cardiac lymphangiogenesis

Nevertheless, it is possible that other molecules may contribute to the lymphatic defects in Meis dKOs. Previous reports have shown that RA is required for lymphatic differentiation and maturation in other organs (Marino et al., 2011; Bowles et al., 2014; Burger et al., 2014) and in the heart (Lioux et al., 2020). Therefore, we cannot rule out the possibility that RA inactivation in the epicardium of *Meis* mutants, may account also for the lymphatic defects. In addition, the loss of RALDH2 boundaries at the base of the great arteries in the dKOs could have important implications. Lioux and colleagues (2020) proposed that SHF-derived LECs are specified in a low RA acid environment at the base of the pulmonary artery, thereafter contributing to ventral lymphatics. If this specification is affected by *Meis* deletion and *Raldh2* misregulation, it could explain the stronger affection of ventral side lymphatics. These lymphatics are specified at E14.5, a stage where no lymphatics were observed on the pulmonary artery of Meis dKOs .

Another potentially involved signalling molecule is FGF2, which expression is reduced in *Meis* mutants. This cytokine was shown to promote lymphangiogenesis and to induce VEGFC and VEGFD expression in vascular endothelial and perivascular cells (Kubo et al., 2002; Chang et al., 2004). Its downregulation in Meis dKOs may suggest an involvement too in the role of the epicardium in lymphangiogenesis.

Recently, it was demonstrated that macrophages promote the growth and remodelling of the cardiac lymphatic vasculature through the secretion of hyaluronan (Cahill et al., 2021). However, macrophages are present on the surface of *Meis*-deficient hearts (as can be seen in (Figure 33)), so we do not think that this cell population is involved in the lymphatic defects of *Meis* mutants. Therefore, macrophage function promoting lymphatic vessel growth and patterning (Cahill et al., 2021), must be independent of the role of the epicardium and LEPDCs in promoting lymphangiogenesis.

In summary, although in the last few years the knowledge regarding the function and origin of cardiac lymphatics has increased and their relevance in the cardiovascular system has been demonstrated, many questions remain to be answered. For example, from Klotz and colleagues (2015), we learnt that cardiac lymphatics derive mostly but not completely from veins. From Maruyama et al. (2019) and Lioux et al. (2020), we learnt that the SHF also contributes to ventral lymphatics. However, why SHF cells only contribute to ventral lymphatics and not to the dorsal portion, or whether functionally or at the molecular level they are different, it is not known. In a similar direction, before this study, the specific mechanisms and tissues involved in cardiac lymphangiogenesis were largely unknown. Here, we have shown that the epicardium and/or fibroblast-like LEPDCs play an important role in cardiac lymphatic development and that they exert their function, at least in part, through the secretion of

paracrine molecules as VEGFC and VEGFD. This process is regulated by MEIS transcription factors by a yet unknown mechanism. (Figure 45).

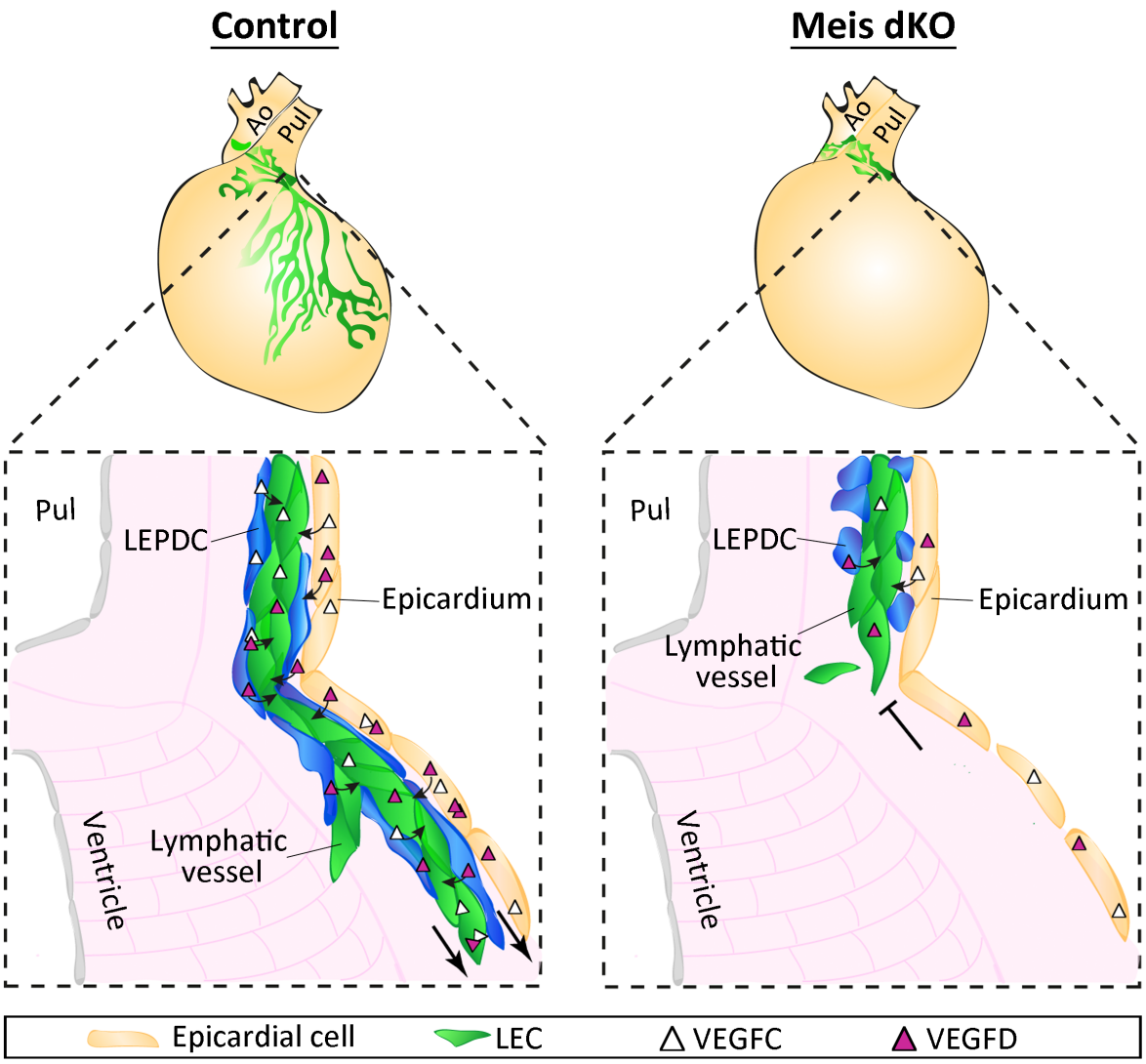

Figure 45. Proposed model for the role of LEPDCs and MEIS transcription factors in cardiac lymphangiogenesis. Schematic representation of cardiac lymphangiogenesis where fibroblasts-like lymphatic-associated epicardial-derived cells (LEPDCs) associate in the subepicardium with lymphatic endothelial cells (LEC) as the lymphatic vessel grows into the heart. The epicardium and/or LEPDCs secrete paracrine molecules as VEGFC and VEGFD to promote lymphatic growth and maturation (left panel). However, LEPDC-LEC association is disrupted in Meis dKOs which impairs lymphatic growth (right panel). Ao: aorta; Pul: pulmonary artery.

CONCLUSIONS

"You may not always end up where you thought you were going, But you will always end up where you were meant to be."
~ Jessica Taylor

1) MEIS1 and MEIS2 transcription factors are expressed in the epicardium and in a subset of EPDCs throughout cardiac development in the mouse.

2) *Meis1* and *Meis2* epicardial-specific conditional deletion is 50 % lethal due to misalignment of the great arteries. The surviving adult mice present no cardiac malformation.

3) Epicardial epithelial-to-mesenchymal transition of the epicardium is preserved in *Meis1* and *Meis2* epicardial-specific conditional mutant mice; however, the specification of EPDCs subsets is impaired.

4) Deletion of *Meis1* and *Meis2* in the epicardial lineage causes a delay in the development and maturation of coronary arteries and veins, which associates with impaired cardiac innervation.

5) The Retinoic acid pathway is strongly downregulated in *Meis1* and *Meis2* mutant epicardium, which may influence the delayed coronary vasculature development and EPDCs specification defects.

6) MEIS transcription factors regulate a non-autonomous function of the epicardium/EPDCs required for cardiac lymphangiogenesis.

7) Cardiac lymphatics associate with fibroblast-like LEPDCs as they grow into the heart. A looser LECs-LEPDCs association in *Meis* mutants may underlie the coronary lymphatic vasculature defects.

8) MEIS elimination reduces the epicardial/subepicardial expression of the lymphoangiocrine signals *Vegfc* and *Vegfd*.

9) Epicardial VEGFC expression is required for promotion of coronary lymphangiogenesis and sufficient to stimulate its overgrowth.

10) VEGFD is required for coronary lymphangiogenesis in the ventral side of the heart.

CONCLUSIONES

1) Los factores de transcripción MEIS1 y MEIS2 se expresan en el epicardio y en un subconjunto de células derivadas del epicardio (EPDCs) a lo largo del desarrollo del corazón del ratón.

2) La deleción específica de *Meis1* y *Meis2* en el epicardio provoca una letalidad del 50% debido al incorrecto alineamiento de la aorta y arteria pulmonar. Los ratones adultos que sobreviven, no presentan malformaciones cardíacas.

3) La transición epitelio-mesenquimal del epicardio no se ve muy alterada en los mutantes epicardio-específicos de *Meis1* y *Meis2*. Sin embargo, la especificación de subpoblaciones de EPDCs se encuentra alterada.

4) La deleción de *Meis1* y *Meis2* en el linaje del epicardio provoca un retraso en el desarrollo y maduración de las arterias y venas coronarias, lo que se asocia con defectos en la inervación cardíaca.

5) La ruta del ácido retinoico se encuentra muy reducida en los mutantes de *Meis1* y *Meis2* en el epicardio, lo cual podría influir en el retraso del desarrollo de la vasculatura coronaria y en los defectos en la especificación de EPDCs.

6) Los factores de transcripción MEIS regulan una función no autónoma del epicardio/EPDCs necesaria para la linfangiogénesis cardíaca.

7) Los linfáticos cardíacos, conforme crecen en el corazón, se asocian con LEPDCs similares a fibroblastos. Una asociación menos estrecha entre LECs y LEPDCs podría ser la causa subyacente de los defectos de la vasculatura linfática de los mutantes de *Meis*.

8) La eliminación de MEIS reduce la expresión de las señales paracrinas *Vegfc* y *Vegfd* en el epicardio/subepicardio.

9) La expresión de VEGFC en el epicardio es necesaria para promover la linfangiogénesis cardíaca y suficiente para promover su crecimiento excesivo.

10) VEGFD es necesario para la linfangiogénesis coronoria de la parte ventral del corazón.

BIBLIOGRAPHY

Acharya, A., Baek, S.T., Huang, G., Eskiocak, B., Goetsch, S., Sung, C.Y., Banfi, S., Sauer, M.F., Olsen, G.S., Duffield, J.S., et al. (2012). The bHLH transcription factor Tcf21 is required for lineagespecific EMT of cardiac fibroblast progenitors. Dev. 139, 2139–2149.

Achen, M.G., Jeltsch, M., Kukk, E., Mäkinen, T., Vitali, A., Wilks, A.F., Alitalo, K., and Stacker, S.A. (1998). Vascular endothelial growth factor D (VEGF-D) is a ligand for the tyrosine kinases VEGF receptor 2 (Flk1) and VEGF receptor 3 (Flt4). Proc. Natl. Acad. Sci. U. S. A. 95, 548–553.

Aghajanian, H., Cho, Y.K., Manderfield, L.J., Herling, M.R., Gupta, M., Ho, V.C., Li, L., Degenhardt, K., Aharonov, A., Tzahor, E., et al. (2016). Coronary vasculature patterning requires a novel endothelial ErbB2 holoreceptor. Nat. Commun. 7, 1–9.

Aitken, S., Bates, T., Bharathavikru, R., Charlton, J., Chau, Y.-Y., Cleal, L., Dudnakova, T., Englert, C., Fazal-Salom, J., Hadoke, P., et al. (2016). The Wilms' Tumor (WT1) Methods and Protocols.

Ali, S.R., Ranjbarvaziri, S., Talkhabi, M., Zhao, P., Subat, A., Hojjat, A., Kamran, P., Müller, A.M.S., Volz, K.S., Tang, Z., et al. (2014). Developmental heterogeneity of cardiac fibroblasts does not predict pathological proliferation and activation. Circ. Res. 115, 625–635.

Alitalo, K., and Carmeliet, P. (2011). Molecular mechanisms of lymphangiogenesis in health and disease. Cancer Cell 1, 219–227.

Ando, K., Shih, Y., Ebarasi, L., Grosse, A., and Portman, D. (2021). Conserved and context-dependent roles for Pdgfrb signaling during zebrafish vascular mural cell development. bioRxiv 2021.03.29.437552; doi: https://doi.org/10.1101/2021.03.29.437552

Andrés-Delgado, L., Ernst, A., Galardi-Castilla, M., Bazaga, D., Peralta, M., Münch, J., González-Rosa, J.M., Marques, I., Tessadori, F., de la Pompa, J.L., et al. (2019). Actin dynamics and the Bmp pathway drive apical extrusion of proepicardial cells. Development 146, 1-15

Arima, Y., Miyagawa-Tomita, S., Maeda, K., Asai, R., Seya, D., Minoux, M., Rijli, F.M., Nishiyama, K., Kim, K.S., Uchijima, Y., et al. (2012). Preotic neural crest cells contribute to coronary artery smooth muscle involving endothelin signalling. Nat. Commun. 3, 1267

Armstrong, E.J., and Bischoff, J. (2004). Heart valve development: Endothelial cell signaling and differentiation. Circ. Res. 95, 459–470.

Armulik, A., Genové, G., and Betsholtz, C. (2011). Pericytes: Developmental, Physiological, and Pathological Perspectives, Problems, and Promises. Dev. Cell 21, 193–215.

Astin, J.W., Haggerty, M.J.L., Okuda, K.S., Le Guen, L., Misa, J.P., Tromp, A., Hogan, B.M., Crosier, K.E., and Crosier, P.S. (2014). Vegfd can compensate for loss of Vegfc in zebrafish facial lymphatic sprouting. Dev. 141, 2680–2690.

Azambuja, A.P., Portillo-Sánchez, V., Rodrigues, M. V., Omae, S. V., Schechtman, D., Strauss, B.E., Costanzi-Strauss, E., Krieger, J.E., Perez-Pomares, J.M., and Xavier-Neto, J. (2010). Retinoic acid and VEGF delay smooth muscle relative to endothelial differentiation to coordinate inner and outer coronary vessel wall morphogenesis. Circ. Res. 107, 204–216.

Azcoitia, V., Aracil, M., Martínez-A, C., and Torres, M. (2005). The homeodomain protein Meis1 is essential for definitive hematopoiesis and vascular patterning in the mouse embryo. Dev. Biol. 280, 307–320.

Bajolle, F., Zaffran, S., Meilhac, S.M., Dandonneau, M., Chang, T., Kelly, R.G., and Buckingham, M.E. (2008). Myocardium at the base of the aorta and pulmonary trunk is prefigured in the outflow tract of the heart and in subdomains of the second heart field. Dev. Biol. 313, 25–34.

Baldwin, M.E., Catimel, B., Nice, E.C., Roufail, S., Hall, N.E., Stenvers, K.L., Karkkainen, M.J., Alitalo, K., Stacker, S.A., and Achen, M.G. (2001a). The Specificity of Receptor Binding by Vascular Endothelial Growth Factor-D Is Different in Mouse and Man. J. Biol. Chem. 276, 19166–19171.

Baldwin, M.E., Roufail, S., Halford, M.M., Alitalo, K., Stacker, S.A., and Achen, M.G. (2001b). Multiple Forms of Mouse Vascular Endothelial Growth Factor-D Are Generated by RNA Splicing and Proteolysis. J. Biol. Chem. 276, 44307–44314.

Baldwin, M.E., Halford, M.M., Roufail, S., Williams, R.A., Hibbs, M.L., Grail, D., Kubo, H., Stacker, S.A., and Achen, M.G. (2005). Vascular Endothelial Growth Factor D Is Dispensable for Development of the Lymphatic System. Mol. Cell. Biol. 25, 2441–2449.

Balmer, G.M., Bollini, S., Dubé, K.N., Martinez-Barbera, J.P., Williams, O., and Riley, P.R. (2014). Dynamic haematopoietic cell contribution to the developing and adult epicardium. Nat. Commun. 5, 4054.

Berenguer, M., Meyer, K.F., Yin, J., and Duester, G. (2020). Discovery of genes required for body axis and limb formation by global identification of retinoic acid-regulated epigenetic marks. PLoS Biol. 18, 1–29.

Bergwerff, M., Verberne, M.E., DeRuiter, M.C., Poelmann, R.E., and Gittenberger-de Groot, A.C. (1998). Neural crest cell contribution to the developing circulatory system implications for vascular morphology? Circ. Res. 82, 221–231.

Bondue, A., Lapouge, G., Paulissen, C., Semeraro, C., Iacovino, M., Kyba, M., and Blanpain, C. (2008). Mesp1 acts as a master regulator of multipotent cardiovascular progenitor specification. Cell Stem Cell 3, 69–84.

Bower, N.I., Vogrin, A.J., Le Guen, L., Chen, H., Stacker, S.A., Achen, M.G., and Hogan, B.M. (2017b). Vegfd modulates both angiogenesis and lymphangiogenesis during zebrafish embryonic development. Dev. 144, 507–518.

Bowles, J., Secker, G., Nguyen, C., Kazenwadel, J., Truong, V., Frampton, E., Curtis, C., Skoczylas, R., Davidson, T.L., Miura, N., et al. (2014). Control of retinoid levels by CYP26B1 is important for lymphatic vascular development in the mouse embryo. Dev. Biol. 386, 25–33.

Brade, T., Kumar, S., Cunningham, T.J., Chatzi, C., Zhao, X., Cavallero, S., Li, P., Sucov, H.M., Ruiz-Lozano, P., and Duester, G. (2011). Retinoic acid stimulates myocardial expansion by induction of hepatic erythropoietin which activates epicardial Igf2. Development 138, 139–148.

Braitsch, C.M., Combs, M.D., Quaggin, S.E., and Yutzey, K.E. (2012). Pod1/Tcf21 is regulated by retinoic acid signaling and inhibits differentiation of epicardium-derived cells into smooth muscle in the developing heart. Dev. Biol. 368, 345–357.

Braitsch, C.M., Kanisicak, O., van Berlo, J.H., Molkentin, J.D., and Yutzey, K.E. (2013). Differential expression of embryonic epicardial progenitor markers and localization of cardiac fibrosis in adult ischemic injury and hypertensive heart disease. J. Mol. Cell. Cardiol. 65, 108–119.

Brakenhielm, E., and Alitalo, K. (2019). Cardiac lymphatics in health and disease. Nat. Rev. Cardiol. 16, 56–68.

Le Bras, B., Barallobre, M.J., Homman-Ludiye, J., Ny, A., Wyns, S., Tammela, T., Haiko, P., Karkkainen, M.J., Yuan, L., Muriel, M.P., et al. (2006). VEGF-C is a trophic factor for neural progenitors in the vertebrate embryonic brain. Nat. Neurosci. 9, 340–348.

Brown, C.B., Feiner, L., Lu, M.M., Li, J., Ma, X., Webber, A.L., Jia, L., Raper, J.A., and Epstein, J.A. (2001). PlexinA2 and semaphorin signaling during cardiac neural crest development. Development 128, 3071–3080.

Bu, L., Jiang, X., Martin-Puig, S., Caron, L., Zhu, S., Shao, Y., Roberts, D.J., Huang, P.L., Domian, I.J., and Chien, K.R. (2009). Human ISL1 heart progenitors generate diverse multipotent cardiovascular cell lineages. Nature 460, 113–117.

Buckingham, M., Meilhac, S., and Zaffran, S. (2005). Building the mammalian heart from two sources of myocardial cells. Nat. Rev. Genet. 6, 826–835.

Burger, N.B., Stuurman, K.E., Kok, E., Konijn, T., Schooneman, D., Niederreither, K., Coles, M., Agace, W.W., Christoffels, V.M., Mebius, R.E., et al. (2014). Involvement of neurons and retinoic acid in lymphatic development: New insights in increased nuchal translucency. Prenat. Diagn. 34, 1312–1319.

Butler, A.M., Yin, X., Evans, D.S., Nalls, M.A., Smith, E.N., Tanaka, T., Li, G., Buxbaum, S.G., Whitsel, E.A., Alonso, A., et al. (2012). Novel loci associated with PR interval in a genome-wide association study of 10 African American cohorts. Circ. Cardiovasc. Genet. 5, 639–646.

Cahill, T.J., Sun, X., Ravaud, C., Villa del Campo, C., Klaourakis, K., Lupu, I.-E., Lord, A.M., Browne, C., Jacobsen, S.E.W., Greaves, D.R., et al. (2021). Tissue-resident macrophages regulate lymphatic vessel growth and patterning in the developing heart. Development 148, dev194563.

Cai, C., Martin, J.C., Sun, Y., Cui, L., Wang, L., Yang, L., Bu, L., Liang, X., Zhang, X., Stallcup, W.B., et al. (2008). A myocardial lineage derives from Tbx18 epicardial cells. Nature 454, 104–108.

Cai, C.L., Liang, X., Shi, Y., Chu, P.H., Pfaff, S.L., Chen, J., and Evans, S. (2003). Isl1 identifies a cardiac progenitor population that proliferates prior to differentiation and contributes a majority of cells to the heart. Dev. Cell 5, 877–889.

Cao, J., and Poss, K.D. (2018). The epicardium as a hub for heart regeneration. Nat. Rev. Cardiol. 15, 631–647.

Cao, Y., Duca, S., and Cao, J. (2020). Epicardium in heart development. Cold Spring Harb. Perspect. Biol. 12, 1–18.

Carmona, R., Barrena, S., López Gambero, A.J., Rojas, A., and Muñoz-Chápuli, R. (2020). Epicardial cell lineages and the origin of the coronary endothelium. FASEB J. 34, 5223–5239.

Carramolino, L., Fuentes, J., García-Andrés, C., Azcoitia, V., Riethmacher, D., Torres, M. (2010). Platelets play an essential role in separating the blood and lymphatic vasculatures during embryonic angiogenesis. Circ. Res. 106, 1197-1201.

Cavallero, S., Shen, H., Yi, C., Lien, C.L., Kumar, S.R., and Sucov, H.M. (2015). CXCL12 Signaling is Essential for Maturation of the Ventricular Coronary Endothelial Plexus and Establishment of Functional Coronary Circulation. Dev. Cell 33, 469–477.

Cecconi, F., Proetzel, G., Alvarez-Bolado, G., Jay, D., and Gruss, P. (1997). Expression of Meis2, a knotted-related murine homeobox gene, indicates a role in the differentiation of the forebrain and the somitic mesoderm. Dev. Dyn. 210, 184–190.

Chakraborty, A., Barajas, S., Lammoglia, G.M., Reyna, A.J., Morley, T.S., Johnson, J.A., Scherer, P.E., and Rutkowski, J.M. (2019). Vascular Endothelial Growth Factor–D (VEGF-D) Overexpression and Lymphatic Expansion in Murine Adipose Tissue Improves Metabolism in Obesity. Am. J. Pathol. 189, 924–939.

Chang, C.P., Jacobs, Y., Nakamura, T., Jenkins, N.A., Copeland, N.G., and Cleary, M.L. (1997). Meis proteins are major in vivo DNA binding partners for wild-type but not chimeric Pbx proteins. Mol. Cell. Biol. 17, 5679–5687.

Chang, L.K., Garcia-Cardeña, G., Farnebo, F., Fannon, M., Chen, E.J., Butterfield, C., Moses, M.A., Mulligan, R.C., Folkman, J., and Kaipainen, A. (2004). Dose-dependent response of FGF-2 for lymphangiogenesis. Proc. Natl. Acad. Sci. U. S. A. 101, 11658–11663.

Chau, Y.Y., Bandiera, R., Serrels, A., Martínez-Estrada, O.M., Qing, W., Lee, M., Slight, J., Thornburn, A., Berry, R., Mchaffie, S., et al. (2014). Visceral and subcutaneous fat have different origins and evidence supports a mesothelial source. Nat. Cell Biol. 16, 367–375.

Chen, H.I., Poduri, A., Numi, H., Kivela, R., Saharinen, P., Mckay, A.S., Raftrey, B., Churko, J., Tian, X., Zhou, B., et al. (2014a). VEGF-C and aortic cardiomyocytes guide coronary artery stem development . J. Clin. Invest. 124, 1–10.

Chen, H.I., Sharma, B., Akerberg, B.N., Numi, H.J., Kivelä, R., Saharinen, P., Aghajanian, H., McKay, A.S., Bogard, P.E., Chang, A.H., et al. (2014b). The sinus venosus contributes to coronary vasculature through VEGFC-stimulated angiogenesis. Dev. 141, 4500–4512.

Chen, J., Kubalak, S.W., and Chien, K.R. (1998). Ventricular muscle-restricted targeting of the RXRα gene reveals a non-cell-autonomous requirement in cardiac chamber morphogenesis. Development 125, 1943–1949.

Chen, L., Fulcoli, F.G., Tang, S., and Baldini, A. (2009). Tbx1 regulates proliferation and differentiation of multipotent heart progenitors. Circ. Res. 105, 842–851.

Chen, Q., Zhang, H., Liu, Y., Adams, S., Eilken, H., Stehling, M., Corada, M., Dejana, E., Zhou, B., and Adams, R.H. (2016). Endothelial cells are progenitors of cardiac pericytes and vascular smooth muscle cells. Nat. Commun. 7, 1–13.

Chen, T.H.P., Chang, T.C., Kang, J.O., Choudhary, B., Makita, T., Tran, C.M., Burch, J.B.E., Eid, H., and Sucov, H.M. (2002). Epicardial induction of fetal cardiomyocyte proliferation via a retinoic acid-inducible trophic factor. Dev. Biol. 250, 198–207.

Christoffels, V.M., Grieskamp, T., Norden, J., Mommersteeg, M.T.M., Rudat, C., and Kispert, A. (2009). Tbx18 and the fate of epicardial progenitors. Nature 458, 2008–2010.

Combs, M.D., Braitsch, C.M., Lange, A.W., James, J.F., and Yutzey, K.E. (2011). NFATC1 promotes epicardium-derived cell invasion into myocardium. Development 138, 1747–1757.

Compton, L.A., Potash, D.A., Mundell, N.A., and Barnett, J. V. (2006). Transforming growth factor-β induces loss of epithelial character and smooth muscle cell differentiation in epicardial cells. Dev. Dyn. 235, 82–93.

Concordet, J.P., and Haeussler, M. (2018). CRISPOR: Intuitive guide selection for CRISPR/Cas9 genome editing experiments and screens. Nucleic Acids Res. 46, W242–W245.

Craig, E.A., Austin, A., Vaillancourt, R.R., Barnett, J. V., and Camenisch, T.D. (2010). TGFβ2-Mediated Production of Hyaluronan is Important for the Induction of Epicardial Cell Differentiation and Invasion. Exp. Cell Res. 316, 3397–3405.

Crowley, M.A., Conlin, L.K., Zackai, E.H., Deardorff, M.A., Thiel, B.D., and Spinner, N.B. (2010). Further evidence for the possible role of MEIS2 in the development of cleft palate and cardiac septum. Am. J. Med. Genet. Part A 152, 1326–1327.

Davis, J., and Molkentin, J.D. (2014). Myofibroblasts: Trust your heart and let fate decide. J. Mol. Cell. Cardiol. 70, 9–18.

Degenhardt, K., Singh, M.K., Aghajanian, H., Massera, D., Wang, Q., Li, J., Li, L., Choi, C., Yzaguirre, A.D., Francey, L.J., et al. (2013). Semaphorin 3d signaling defects are associated with anomalous pulmonary venous connections. Nat. Med. 19, 760–765.

Delgado, I., López-Delgado, A.C., Alberto, R.D., Giovinazzo, G., Cadenas, V., Fernández-De-Manuel, L., Sánchez-Cabo, F., Anderson, M.J., Lewandoski, M., and Torres, M. (2020). Proximo-distal positional information encoded by an Fgf-regulated gradient of homeodomain transcription factors in the vertebrate limb. Sci. Adv. 6, 1–10.

Dettman, R.W., Denetclaw, W., Ordahl, C.P., and Bristow, J. (1998). Common epicardial origin of coronary vascular smooth muscle, perivascular fibroblasts, and intermyocardial fibroblasts in the avian heart. Dev. Biol. 193, 169–181.

Dumont, D.J., Jussila, L., Taipale, J., Lymboussaki, A., Mustonen, T., Pajusola, K., Breitman, M., and Alitalo, K. (1998). Cardiovascular failure in mouse embryos deficient in VEGF receptor-3. Science (80-.). 282, 946–949.

Dyer, L., Wu, Y., Moser, M., and Patterson, C. (2014). BMPER-induced BMP signaling promotes coronary artery remodeling. Dev. Biol. 386, 385–394.

Elkouby, Y.M., Elias, S., Casey, E.S., Blythe, S.A., Tsabar, N., Klein, P.S., Root, H., Liu, K.J., and Frank, D. (2010). Mesodermal Wnt signaling organizes the neural plate via Meis3. Development 137, 1531–1541.

Fahed, A.C., Gelb, B.D., Seidman, J.G., and Seidman, C.E. (2013). Genetics of congenital heart disease: The glass half empty. Circ. Res. 112, 707–720.

Farbehi, N., Patrick, R., Dorison, A., Xaymardan, M., Janbandhu, V., Wystub-Lis, K., Ho, J.W.K., Nordon, R.E., and Harvey, R.P. (2019). Single-cell expression profiling reveals dynamic flux of cardiac stromal, vascular and immune cells in health and injury. Elife 8, 1–39.

Feiner, L., Webber, A.L., Brown, C.B., Lu, M.M., Jia, L., Feinstein, P., Mombaerts, P., Epstein, J.A., and Raper, J.A. (2001). Targeted disruption of semaphorin 3C leads to persistent truncus arteriosus and aortic arch interruption. Development 128, 3061–3070.

Flaht, A., Jankowska-Steifer, E., Radomska, D.M., Madej, M., Gula, G., Kujawa, M., and Ratajska, A. (2012). Cellular phenotypes and spatio-temporal patterns of lymphatic vessel development in embryonic mouse hearts. Dev. Dyn. 241, 1473–1486.

Flaht-Zabost, A., Gula, G., Ciszek, B., Czarnowska, E., Jankowska-Steifer, E., Madej, M., Niderla-Bielińska, J., Radomska-Leśniewska, D., and Ratajska, A. (2014). Cardiac Mouse Lymphatics: Developmental and Anatomical Update. Anat. Rec. 297, 1115–1130.

François, M., Caprini, A., Hosking, B., Orsenigo, F., Wilhelm, D., Browne, C., Paavonen, K., Karnezis, T., Shayan, R., Downes, M., et al. (2008). Sox18 induces development of the lymphatic vasculature in mice. Nature 456, 643–647.

Fredriksson, L., Li, H., and Eriksson, U. (2004). The PDGF family: Four gene products form five dimeric isoforms. Cytokine Growth Factor Rev. 15, 197–204.

Gancz, D., Raftrey, B.C., Perlmoter, G., Marín-Juez, R., Semo, J., Matsuoka, R.L., Karra, R., Raviv, H., Moshe, N., Addadi, Y., et al. (2019). Distinct origins and molecular mechanisms contribute to lymphatic formation during cardiac growth and regeneration. Elife 8, 1–30.

Gibot, L., Galbraith, T., Kloos, B., Das, S., Lacroix, D.A., Auger, F.A., and Skobe, M. (2016). Cell-based approach for 3D reconstruction of lymphatic capillaries in vitro reveals distinct functions of HGF and VEGF-C in lymphangiogenesis. Biomaterials 78, 129–139.

Giliberti, A., Currò, A., Papa, F.T., Frullanti, E., Ariani, F., Coriolani, G., Grosso, S., Renieri, A., and Mari, F. (2020). MEIS2 gene is responsible for intellectual disability, cardiac defects and a distinct facial phenotype. Eur. J. Med. Genet. 63, 103627.

von Gise, A., Zhou, B., Honor, L.B., Ma, Q., Petryk, A., and Pu, W.T. (2011). WT1 regulates epicardial epithelial to mesenchymal transition through β-catenin and retinoic acid signaling pathways. Dev. Biol. 356, 421–431.

Gittenberger-de-Groot, A.C., vrancken peeters, M.-P.F.M., Bergwerff, M., Mentink, M.M.T., and Poelmann, R.E. (2000). Epicardial Outgrowth Inhibition Leads to Compensatory Mesothelial Outflow Tract Collar and Abnormal Cardiac Septation and Coronary Formation. Circ. Res. 87, 969–971.

Gittenberger-de Groot, A.C., Vrancken Peeters, M.P.F.M., Mentink, M.M.T., Gourdie, R.G., and Poelmann, R.E. (1998). Epicardium-derived cells contribute a novel population to the myocardial wall and the atrioventricular cushions. Circ. Res. 82, 1043–1052.

González-Hernández, S., Gómez, M.J., Sánchez-Cabo, F., Méndez-Ferrer, S., Muñoz-Cánoves, P., and Isern, J. (2020). Sox17 Controls Emergence and Remodeling of Nestin-Expressing Coronary Vessels. Circ. Res. 252–270.

González-Lázaro, M., Roselló-Díez, A., Delgado, I., Carramolino, L., Sanguino, M.A., Giovinazzo, G., and Torres, M. (2014). Two new targeted alleles for the comprehensive analysis of Meis1 functions in the mouse. Genesis 52, 967–975.

Gonzalez-Rosa, J.M., Martin, V., Peralta, M., Torres, M., and Mercader, N. (2011). Extensive scar formation and regression during heart regeneration after cryoinjury in zebrafish. Development 138, 1663–1674.

González-Rosa, J.M., Peralta, M., and Mercader, N. (2012). Pan-epicardial lineage tracing reveals that epicardium derived cells give rise to myofibroblasts and perivascular cells during zebrafish heart regeneration. Dev. Biol. 370, 173–186.

Gordon, K., Schulte, D., Brice, G., Simpson, M.A., Roukens, M.G., Van Impel, A., Connell, F., Kalidas, K., Jeffery, S., Mortimer, P.S., et al. (2013). Mutation in vascular endothelial growth factor-c, a ligand for vascular endothelial growth factor receptor-3, is associated with autosomal dominant milroy-like primary lymphedema. Circ. Res. 112, 956–960.

Greulich, F., Farin, H.F., Schuster-Gossler, K., and Kispert, A. (2012). Tbx18 function in epicardial development. Cardiovasc. Res. 96, 476–483.

Grieskamp, T., Rudat, C., Lüdtke, T.H.W., Norden, J., and Kispert, A. (2011). Notch signaling regulates smooth muscle differentiation of epicardium-derived cells. Circ. Res. 108, 813–823.

Guadix, J.A., Carmona, R., Muñoz-Chápuli, R., and Pérez-Pomares, J.M. (2006). In vivo and in vitro analysis of the vasculogenic potential of avian proepicardial and epicardial cells. Dev. Dyn. 235, 1014–1026.

Hägerling, R., Pollmann, C., Andreas, M., Schmidt, C., Nurmi, H., Adams, R.H., Alitalo, K., Andresen, V., Schulte-Merker, S., and Kiefer, F. (2013). A novel multistep mechanism for initial lymphangiogenesis in mouse embryos based on ultramicroscopy. EMBO J. 32, 629–644.

Haiko, P., Makinen, T., Keskitalo, S., Taipale, J., Karkkainen, M.J., Baldwin, M.E., Stacker, S.A., Achen, M.G., and Alitalo, K. (2008). Deletion of Vascular Endothelial Growth Factor C (VEGF-C) and VEGF-D Is Not Equivalent to VEGF Receptor 3 Deletion in Mouse Embryos. Mol. Cell. Biol. 28, 4843–4850.

Hari, L., Miescher, I., Shakhova, O., Suter, U., Chin, L., Taketo, M., Richardson, W.D., Kessaris, N., and Sommer, L. (2012). Temporal control of neural crest lineage generation by wnt/β-catenin signaling. Dev. 139, 2107–2117.

Harrison, M.R., Feng, X., Mo, G., Aguayo, A., Villafuerte, J., Yoshida, T., Pearson, C.A., Schulte-Merker, S., and Ching-Ling, L. (2019). Late developing cardiac lymphatic vasculature supports adult zebrafish heart function and regeneration. Elife 8, 1–21.

Hellström, M., Kalén, M., Lindahl, P., Abramsson, A., and Betsholtz, C. (1999). Role of PDGF-B and PDGFR-β in recruitment of vascular smooth muscle cells and pericytes during embryonic blood vessel formation in the mouse. Development 126, 3047–3055.

Henri, O., Pouehe, C., Houssari, M., Galas, L., Nicol, L., Edwards-Lévy, F., Henry, J.P., Dumesnil, A., Boukhalfa, I., Banquet, S., et al. (2016). Selective Stimulation of Cardiac Lymphangiogenesis Reduces Myocardial Edema and Fibrosis Leading to Improved Cardiac Function Following Myocardial Infarction. Circulation 133, 1484–1497.

High, F., and Epstein, J.A. (2007). Signalling pathways regulating cardiac neural crest migration and differentiation. Novartis Found. Symp. 283, 152–161.

Hisa, T., Spence, S.E., Rachel, R.A., Fujita, M., Nakamura, T., Ward, J.M., Devor-Henneman, D.E., Saiki, Y., Kutsuna, H., Tessarollo, L., et al. (2004). Hematopoietic, angiogenic and eye defects in Meis1 mutant animals. EMBO J. 23, 450–459.

Hoffman, J.I.E., and Kaplan, S. (2002). The incidence of congenital heart disease. J. Am. Coll. Cardiol. 39, 1890–1900.

Hortells, L., Johansen, A.K.Z., and Yutzey, K.E. (2019). Cardiac fibroblasts and the extracellular matrix in regenerative and nonregenerative hearts. J. Cardiovasc. Dev. Dis. 6, 1–17.

Hotta, Y., Sasaki, S., Konishi, M., Kinoshita, H., Kuwahara, K., Nakao, K., and Itoh, N. (2008). Fgf16 is required for cardiomyocyte proliferation in the mouse embryonic heart. Dev. Dyn. 237, 2947–2954.

Huang, G.N., Thatcher, J.E., McAnally, J., Kong, Y., Qi, X., Tan, W., DiMaio, J.M., Amatruda, J.F., Gerard, R.D., Hill, J.A., et al. (2012). C/EBP Transcription Factors Mediate Epicardial Activation During Heart Development and Injury. Science (80-.). 338, 1599–1603.

Huang, Y., Harrison, M.R., Osorio, A., Kim, J., Baugh, A., Duan, C., Sucov, H.M., and Lien, C.L. (2013). Igf Signaling is Required for Cardiomyocyte Proliferation during Zebrafish Heart Development and Regeneration. PLoS One 8.

Huntington, G.S., and McClure, C.F.W. (1910). The anatomy and development of the jugular lymph sacs in the domestic cat (Felis domestica). Am. J. Anat. 10, 177–312.

Irrthum, A., Karkkainen, M.J., Devriendt, K., Alitalo, K., and Vikkula, M. (2000). Congenital hereditary lymphedema caused by a mutation that inactivates VEGFR3 tyrosine kinase. Am. J. Hum. Genet. 67, 295–301.

Ivanovitch, K., Temiño, S., and Torres, M. (2017). Live imaging of heart tube development in mouse reveals alternating phases of cardiac differentiation and morphogenesis. Elife 6, 1–30.

Ivey, M.J., and Tallquist, M.D. (2016). Defining the Cardiac Fibroblast: A New Hope. Circ. J. 80, 2269–2276.

Ivins, S., Chappell, J., Vernay, B., Suntharalingham, J., Martineau, A., Mohun, T.J., and Scambler, P.J. (2015). The CXCL12/CXCR4 Axis Plays a Critical Role in Coronary Artery Development. Dev. Cell 33, 455–468.

Jacobs, Y., Schnabel, C.A., and Cleary, M.L. (1999). Trimeric Association of Hox and TALE Homeodomain Proteins Mediates Hoxb2 Hindbrain Enhancer Activity. Mol. Cell. Biol. 19, 5134–5142.

Johansson, S., Berland, S., Gradek, G.A., Bongers, E., de Leeuw, N., Pfundt, R., Fannemel, M., Rødningen, O., Brendehaug, A., Haukanes, B.I., et al. (2014). Haploinsufficiency of MEIS2 is associated with orofacial clefting and learning disability. Am. J. Med. Genet. Part A 164, 1622–1626.

Kang, J., Gu, Y., Li, P., Johnson, B.L., Sucov, H.M., and Thomas, P.S. (2008). PDGF-A as an epicardial mitogen during heart development. Dev. Dyn. 237, 692–701.

Karkkainen, M.J., Saaristo, A., Jussila, L., Karila, K.A., Lawrence, E.C., Pajusola, K., Bueler, H., Eichmann, A., Kauppinen, R., Kettunen, M.I., et al. (2001). A model for gene therapy of human hereditary lymphedema. Proc. Natl. Acad. Sci. U. S. A. 98, 12677–12682.

Karkkainen, M.J., Haiko, P., Sainio, K., Partanen, J., Taipale, J., Petrova, T. V., Jeltsch, M., Jackson, D.G., Talikka, M., Rauvala, H., et al. (2004). Vascular endothelial growth factor C is required for sprouting of the first lymphatic vessels from embryonic veins. Nat. Immunol. 5, 74–80.

Karra, R., Foglia, M.J., Choi, W.Y., Belliveau, C., DeBenedittis, P., and Poss, K.D. (2018). Vegfaa instructs cardiac muscle hyperplasia in adult zebrafish. Proc. Natl. Acad. Sci. U. S. A. 115, 8805–8810.

Karunamuni, G., Yang, K., Doughman, Y.Q., Wikenheiser, J., Bader, D., Barnett, J., Austin, A., Parsons-Wingerter, P., and Watanabe, M. (2010). Expression of lymphatic markers during avian and mouse cardiogenesis. Anat. Rec. 293, 259–270.

Kattman, S.J., Huber, T.L., and Keller, G.M.M. (2006). Multipotent Flk-1+ Cardiovascular Progenitor Cells Give Rise to the Cardiomyocyte, Endothelial, and Vascular Smooth Muscle Lineages. Dev. Cell 11, 723–732.

Katz, T.C., Singh, M.K., Degenhardt, K., Rivera-Feliciano, J., Johnson, R.L., Epstein, J.A., and Tabin, C.J. (2012). Distinct Compartments of the Proepicardial Organ Give Rise to Coronary Vascular Endothelial Cells. Dev. Cell 22, 639–650.

Kelly, R.G. (2012). The Second Heart Field (Elsevier Inc.).

Kelly, R.G., Brown, N.A., and Buckingham, M.E. (2001). The Arterial Pole of the Mouse Heart Forms from Fgf10-Expressing Cells in Pharyngeal Mesoderm. Dev. Cell 1, 435–440.

Khalil, H., Kanisicak, O., Prasad, V., Correll, R.N., Fu, X., Schips, T., Vagnozzi, R.J., Liu, R., Huynh, T., Lee, S.J., et al. (2017). Fibroblast-specific TGF-β-Smad2/3 signaling underlies cardiac fibrosis. J. Clin. Invest. 127, 3770–3783.

Kikuchi, K., Holdway, J.E., Werdich, A. a, Anderson, R.M., Egnaczyk, G.F., Evans, T., Macrae, C. a, Didier, Y.R., and Poss, K.D. (2011). Primary contribution to zebrafish heart regeneration by gata4+ cardiomyocytes. 464, 601–605.

Kim, J., Wu, Q., Zhang, Y., Wiens, K.M., Huang, Y., Rubin, N., Shimada, H., Handin, R.I., Chao, M.Y., Tuan, T.L., et al. (2010). PDGF signaling is required for epicardial function and blood vessel formation in regenerating zebrafish hearts. Proc. Natl. Acad. Sci. U. S. A. 107, 17206–17210.

Kirby, M.L., and Hutson, M.R. (2010). Factors controlling cardiac neural crest cell migration. Cell Adhes. Migr. 4, 609–621.

Kirby, M.L., Gale, T.F., and Stewart, D.E. (1983). Neural crest cells contribute to normal aorticopulmonary septation. Science (80-.). 220, 1059–1061.

Klotz, L., Norman, S., Vieira2, J., Masters, M., Rohling, M., Dube, K., Bollini, S., Matsuzaki, F., Carr, C., and Riley, P.R. (2015). Cardiac lymphatics are heterogeneous in origin and respond to injury. Nature 522, 62–97.

Komiyama, M., Ito, K., and Shimada, Y. (1987). Origin and development of the epicardium in the mouse embryo. Anat. Embryol. (Berl). 176, 183–189.

Kristiansen, E. (1998). Splenic pigment deposition in C57BL mice - An age-related phenomenon ? Scand. J. Lab. Anim. Sci. 25, 62–67.

Kubo, H., Cao, R., Bräkenhielm, E., Mäkinen, T., Cao, Y., and Alitalo, K. (2002). Blockade of vascular endothelial growth factor receptor-3 signaling inhibits fibroblast growth factor-2-induced lymphangiogenesis in mouse cornea. Proc. Natl. Acad. Sci. U. S. A. 99, 8868–8873.

Kukk, E., Lymboussakl, A., Taira, S., Kaipainen, A., Jeltsch, M., Joukov, V., and Alitalo, K. (1996). VEGF-C receptor binding and pattern of expression with VEGFR-3 suggests a role in lymphatic vascular development. Development 122, 3829–3837.

Künnapuu, J., and Bokharaie, H. (2021). Proteolytic Cleavages in the VEGF Family : Generating Diversity among Angiogenic VEGFs , Essential for the Activation of Lymphangiogenic VEGFs. Biology 10, 167.

Kwee, L., Baldwin, H.S., Shen, H.M., Stewart, C.L., Buck, C., Buck, C.A., and Labow, M.A. (1995). Defective development of the embryonic and extraembryonic circulatory systems in vascular cell adhesion molecule (VCAM-1) deficient mice. Development 121, 489–503.

De La Pompa, J.L., and Epstein, J. (2012). Coordinating tissue interactions: Notch signaling in cardiac development and disease. Dev. Cell 22, 244–254.

Lamouille, S., Xu, J., and Derynck, R. (2014). Molecular mechanisms of epithelial-mesenchymal transition. Nat. Rev. Mol. Cell Biol. 15, 178–196.

Lavine, K.J., Yu, K., White, A.C., Zhang, X., Smith, C., Partanen, J., and Ornitz, D.M. (2005). Endocardial and epicardial derived FGF signals regulate myocardial proliferation and differentiation in vivo. Dev. Cell 8, 85–95.

Lavine, K.J., White, A.C., Park, C., Smith, C.S., Choi, K., Long, F., Hui, C.C., and Ornitz, D.M. (2006). Fibroblast growth factor signals regulate a wave of Hedgehog activation that is essential for coronary vascular development. Genes Dev. 20, 1651–1666.

Lee, K.M., Danuser, R., Stein, J. V, Graham, D., Nibbs, R.J., and Graham, G.J. (2014). The chemokine receptors ACKR 2 and CCR 2 reciprocally regulate lymphatic vessel density. EMBO J. 33, 2564–2580.

Lepilina, A., Coon, A.N., Kikuchi, K., Holdway, J.E., Roberts, R.W., Burns, C.G., and Poss, K.D. (2006). A Dynamic Epicardial Injury Response Supports Progenitor Cell Activity during Zebrafish Heart Regeneration. Cell 127, 607–619.

Li, J., Miao, L., Zhao, C., Mohiuddin, W., Qureshi, S., Shieh, D., Guo, H., Lu, Y., Hu, S., Huang, A., et al. (2017). CDC42 is required for epicardial and pro-epicardial development by mediating FGF receptor trafficking to the plasma membrane. 1635–1647.

Li, P., Cavallero, S., Gu, Y., Chen, T.H.P., Hughes, J., Hassan, A.B., Brüning, J.C., Pashmforoush, M., and Sucov, H.M. (2011). IGF signaling directs ventricular cardiomyocyte proliferation during embryonic heart development. Development 138, 1795–1805.

Lim, A.H., Suli, A., Yaniv, K., Weinstein, B., Li, D.Y., and Chien, C. Bin (2011). Motoneurons are essential for vascular pathfinding. Development 138, 4813.

Lim, H.Y., Thiam, C.H., Yeo, K.P., Bisoendial, R., Hii, C.S., McGrath, K.C.Y., Tan, K.W., Heather, A., Alexander, J.S.J., and Angeli, V. (2013). Lymphatic vessels are essential for the removal of cholesterol from peripheral tissues by SR-BI-Mediated transport of HDL. Cell Metab. 17, 671–684.

Lin, C.-J., Lin, C.-Y., Chen, C.-H., Zhou, B., and Chang, C.-P. (2012). Partitioning the heart: mechanisms of cardiac septation and valve development. Development 139, 3277–3299.

Lin, S.-C., Dolle, P., Ryckebusch, L., Noseda, M., Zaffran, S., Schneider, M.D., and Niederreither, K. (2010). Endogenous retinoic acid regulates cardiac progenitor differentiation. Proc. Natl. Acad. Sci. 107, 9234–9239.

Lioux, G., Liu, X., Temiño, S., Oxendine, M., Ayala, E., Ortega, S., Kelly, R.G., Oliver, G., and Torres, M. (2020). A Second Heart Field-Derived Vasculogenic Niche Contributes to Cardiac Lymphatics. Dev. Cell 52, 350–363.e6.

Liu, X., and Oliver, G. (2019). New insights about the lymphatic vasculature in cardiovascular diseases [version 1; peer review: 2 approved]. F1000Research 8, 1–6.

Liu, Q., Huang, X., Oh, J.H., Lin, R.Z., Duan, S., Yu, Y., Yang, R., Qiu, J., Melero-Martin, J.M., Pu, W.T., et al. (2014). Epicardium-to-fat transition in injured heart. Cell Res. 24, 1367–1369.

Liu, X., De la Cruz, E., Gu, X., Balint, L., Oxendine-Burns, M., Terrones, T., Ma, W., Kuo, H.H., Lantz, C., Bansal, T., et al. (2020). Lymphoangiocrine signals promote cardiac growth and repair. Nature 588, 705–711.

López-Delgado, A.C., Delgado, I., Cadenas, V., Sánchez-Cabo, F., and Torres, M. (2021). Axial skeleton anterior-posterior patterning is regulated through feedback regulation between Meis transcription factors and retinoic acid. Development 148.

Louw, J.J., Corveleyn, A., Jia, Y., Hens, G., Gewillig, M., and Devriendt, K. (2015). MEIS2 involvement in cardiac development, cleft palate, and intellectual disability. Am. J. Med. Genet. Part A 167, 1142–1146.

Luo, W., Garcia-Gonzalez, I., Fernández-Chacón, M., Casquero-Garcia, V., Sanchez-Muñoz, M.S., Mühleder, S., Garcia-Ortega, L., Andrade, J., Potente, M., and Benedito, R. (2021). Arterialization requires the timely suppression of cell growth. Nature 589, 437–441.

Lupu, I.E., Redpath, A.N., and Smart, N. (2020). Spatiotemporal Analysis Reveals Overlap of Key Proepicardial Markers in the Developing Murine Heart. Stem Cell Reports 14, 770–787.

Luttun, A., and Carmeliet, P. (2003). De novo vasculogenesis in the heart. Cardiovasc. Res. 58, 378–389.

Macgrogan, D., Münch, J., and De La Pompa, J.L. (2018). Notch and interacting signalling pathways in cardiac development, disease, and regeneration. Nat. Rev. Cardiol. 15, 685–704.

Machon, O., Masek, J., Machonova, O., Krauss, S., and Kozmik, Z. (2015). Meis2 is essential for cranial and cardiac neural crest development. BMC Dev. Biol. 15, 1–16.

Madisen, L., Zwingman, T.A., Sunkin, S.M., Oh, S.W., Zariwala, H.A., Gu, H., Ng, L.L., Palmiter, R.D., Hawrylycz, M.J., Jones, A.R., et al. (2010). A robust and high-throughput Cre reporting and characterization system for the whole mouse brain. Nat. Neurosci. 13, 133–140.

Mäkinen, T., Jussila, L., Veikkola, T., Karpanen, T., Kettunen, M.I., Pulkkanen, K.J., Kauppinen, R., Jackson, D.G., Kubo, H., Nishikawa, S.I., et al. (2001). Inhibition of lymphangiogenesis with resulting lymphedema in transgenic mice expressing soluble VEGF receptor-3. Nat. Med. 7, 199–205.

Manasek, F.J. (1968). Embryonic development of the heart. I. A light and electron microscopic study of myocardial development in the early chick embryo. J. Morphol. 125, 329–365.

Manasek, F.J. (1969). Embryonic development of the heart. II. Formation of the epicardium. J. Embryol. Exp. Morphol. 22, 333–348.

Mann, R.S., and Affolter, M. (1998). Hox proteins meet more partners. Curr. Opin. Genet. Dev. 8, 423–429.

Männer, J. (1993). Experimental study on the formation of the epicardium in chick embryos. Anat. Embryol. (Berl). 187, 281–289.

Männer, J. (1999). Does the subepicardial mesenchyme contribute myocardioblasts to the myocardium of the chick embryo heart? A quail-chick chimera study tracing the fate of the epicardial primordium. Anat. Rec. 255, 212–226.

Männer, J. (2009). The anatomy of cardiac looping: A step towards the understanding of the morphogenesis of several forms of congenital cardiac malformations. Clin. Anat. 22, 21–35.

Marino, D., Dabouras, V., Brändli, A.W., and Detmar, M. (2011). A role for all-trans-retinoic acid in the early steps of lymphatic vasculature development. J. Vasc. Res. 48, 236–251.

Martinez-Corral, I., Ulvmar, M.H., Stanczuk, L., Tatin, F., Kizhatil, K., John, S.W.M., Alitalo, K., Ortega, S., and Makinen, T. (2015). Nonvenous origin of dermal lymphatic vasculature. Circ. Res. 116, 1649–1654.

Maruyama, K., Miyagawa-tomita, S., Mizukami, K., and Matsuzaki, F. (2019). Isl1 -expressing non-venous cell lineage contributes to cardiac lymphatic vessel development. Dev. Biol. 452, 134–143.

Mellgren, A.M., Smith, C.L., Olsen, G.S., Eskiocak, B., Zhou, B., Kazi, M.N., Ruiz, F.R., Pu, W.T., and Tallquist, M.D. (2008). Platelet-derived growth factor receptor β signaling is required for efficient epicardial cell migration and development of two distinct coronary vascular smooth muscle cell populations. Circ. Res. 103, 1393–1401.

Mercader, N., Leonardo, E., Azpiazu, N., Serrano, A., Morata, G., Martínez-A, C., and Torres, M. (1999). Conserved regulation of proximodistal limb axis development by Meis1/Hth. Nature 402, 425–429.

Mercader, N., Leonardo, E., Piedra, M.E., Martínez-A, C., Ros, M.A., and Torres, M. (2000). Opposing RA and FGF signals control proximodistal vertebrate limb development through regulation of Meis genes. Development 127, 3961–3970.

Merki, E., Zamora, M., Raya, A., Kawakami, Y., Wang, J., Zhang, X., Burch, J., Kubalak, S.W., Kaliman, P., Belmonte, J.C.I., et al. (2005). Epicardial retinoid X receptor is required for myocardial growth and coronary artery formation. Proc. Natl. Acad. Sci. 102, 18455–18460.

Mikawa, T., and Fischman, D.A. (1992). Retroviral analysis of cardiac morphogenesis: discontinuous formation of coronary vessels. Proc. Natl. Acad. Sci. 89, 9504–9508.

Mikawa, T., and Gourdie, R.G. (1996). Pericardial mesoderm generates a population of coronary smooth muscle cells migrating into the heart along with ingrowth of the epicardial organ. Dev. Biol. 174, 221–232.

Milasan, A., Dallaire, F., Mayer, G., and Martel, C. (2016). Effects of LDL Receptor Modulation on Lymphatic Function. Sci. Rep. 6, 1–13.

Milasan, A., Smaani, A., and Martel, C. (2019). Early rescue of lymphatic function limits atherosclerosis progression in Ldlr −/− mice. Atherosclerosis 283, 106–119.

Mizutani, M., Wu, J.C., and Nusse, R. (2016). Fibrosis of the neonatal mouse heart after cryoinjury is accompanied by Wnt signaling activation and epicardial-to-mesenchymal transition. J. Am. Heart Assoc. 5, 1–15.

Molin, D.G.M., Bartram, U., Van der Heiden, K., Van Iperen, L., Speer, C.P., Hierck, B.P., Poelmann, R.E., and Gittenberger-de-Groot, A.C. (2003). Expression patterns of Tgfβ1-3 associate with myocardialisation of the outflow tract and the development of the epicardium and the fibrous heart skeleton. Dev. Dyn. 227, 431–444.

Del Monte, G., Casanova, J.C., Guadix, J.A., MacGrogan, D., Burch, J.B.E., Pérez-Pomares, J.M., and De La Pompa, J.L. (2011). Differential notch signaling in the epicardium is required for cardiac inflow development and coronary vessel morphogenesis. Circ. Res. 108, 824–836.

Moore, A.W., McInnes, L., Kreidberg, J., Hastie, N.D., and Schedl, A. (1999). YAC complementation shows a requirement for Wt1 in the development of epicardium, adrenal gland and throughout nephrogenesis. Development 126, 1845–1857.

Moore-Morris, T., Guimarães-Camboa, N., Banerjee, I., Zambon, A.C., Kisseleva, T., Velayoudon, A., Stallcup, W.B., Gu, Y., Dalton, N.D., Cedenilla, M., et al. (2014). Resident fibroblast lineages mediate pressure overload-induced cardiac fibrosis. J. Clin. Invest. 124, 2921–2934.

Moretti, A., Caron, L., Nakano, A., Lam, J.T., Bernshausen, A., Chen, Y., Qyang, Y., Bu, L., Sasaki, M., Martin-Puig, S., et al. (2006). Multipotent Embryonic Isl1+ Progenitor Cells Lead to Cardiac, Smooth Muscle, and Endothelial Cell Diversification. Cell 127, 1151–1165.

Moskow, J.J., Bullrich, F., Huebner, K., Daar, I.O., and Buchberg, A.M. (1995). Meis1, a PBX1-related homeobox gene involved in myeloid leukemia in BXH-2 mice. Mol. Cell. Biol. 15, 5434–5443.

Moss, J., Xavierneto J, Shapiro Md, Nayeem Sm, McCaffery P, Drager Uc, and Rosenthal N (1998). Dynamic Patterns Of Retinoic Acid Synthesis and Response In the Developing Mammalian Heart. Dev Biol 199, 55–71.

Nakajima, Y. (2019). Retinoic acid signaling in heart development. Genesis 57, 1–17.

Nam, J., Onitsuka, I., Hatch, J., Uchida, Y., Ray, S., Huang, S., Li, W., Zang, H., Ruiz-Lozano, P., and Mukouyama, Y.S. (2013). Coronary veins determine the pattern of sympathetic innervation in the developing heart. Dev. 140, 1475–1485.

Nicenboim, J., Malkinson, G., Lupo, T., Asaf, L., Sela, Y., Mayseless, O., Gibbs-Bar, L., Senderovich, N., Hashimshony, T., Shin, M., et al. (2015). Lymphatic vessels arise from specialized angioblasts within a venous niche. Nature 522, 56–61.

Nurmi, H., Saharinen, P., Zarkada, G., Zheng, W., Robciuc, M.R., and Alitalo, K. (2015). VEGF -C is required for intestinal lymphatic vessel maintenance and lipid absorption. EMBO Mol. Med. 7, 1418–1425.

Oliver, G., Kipnis, J., Randolph, G.J., and Harvey, N.L. (2020). The Lymphatic Vasculature in the 21st Century: Novel Functional Roles in Homeostasis and Disease. Cell 182, 270–296.

Oulad-Abdelghani, M., Chazaud, C., Bouillet, P., Sapin, V., Chambon, P., and Dollé, P. (1997). Meis2, a novel mouse Pbx-related homeobox gene induced by retinoic acid during differentiation of P19 embryonal carcinoma cells. Dev. Dyn. 210, 173–183.

Paquet-fifield, S., Levy, S.M., Sato, T., Shayan, R., Karnezis, T., Davydova, N., Nowell, C.J., Roufail, S., Ma, G.Z., Zhang, Y., et al. (2013). Vascular Endothelial Growth Factor-d Modulates Caliber and Function of Initial Lymphatics in the Dermis. J. Invest. Dermatol. 133, 2074–2084.

Peralta, M., Steed, E., Harlepp, S., González-Rosa, J.M., Monduc, F., Ariza-Cosano, A., Cortés, A., Rayón, T., Gómez-Skarmeta, J.L., Zapata, A., et al. (2013). Heartbeat-driven pericardiac fluid forces contribute to epicardium morphogenesis. Curr. Biol. 23, 1726–1735.

Pérez-Castellano, N., Villacastín, J., Salinas, J., Vega, M., Moreno, J., Doblado, M., Ruiz, E., and MacAya, C. (2011). Epicardial connections between the pulmonary veins and left atrium: Relevance for atrial fibrillation ablation. J. Cardiovasc. Electrophysiol. 22, 149–159.

Perez-Pomares, J.M., Carmona, R., González-Iriarte, M., Atencia, G., Wessels, A., and Muñoz-Chapuli, R. (2002a). Origin of coronary endothelial cells from epicardial mesothelium in avian embryos. Int. J. Dev. Biol. 46, 1005–1013.

Pérez-Pomares, J.M., Phelps, A., Sedmerova, M., Carmona, R., González-Iriarte, M., Muoz-Chápuli, R., and Wessels, A. (2002b). Experimental studies on the spatiotemporal expression of WT1 and RALDH2 in the embryonic avian heart: A model for the regulation of myocardial and valvuloseptal development by epicardially derived cells (EPDCs). Dev. Biol. 247, 307–326.

Pérez-Pomares, J.M., Phelps, A., Sedmerova, M., and Wessels, A. (2003). Epicardial-like cells on the distal arterial end of the cardiac outflow tract do not derive from the proepicardium but are derivatives of the cephalic pericardium. Dev. Dyn. 227, 56–68.

Pfeufer, A., Noord, C. Van, Marciante, K.D., Arking, D.E., Larson, M.G., Smith, A.V., Tarasov, K. V, Müller, M., Sotoodehnia, N., Sinner, M.F., et al. (2010). Genome-wide association study of PR interval. Nat. Genet. 42.

Pichol-Thievend, C., Betterman, K.L., Liu, X., Ma, W., Skoczylas, R., Lesieur, E., Bos, F.L., Schulte, D., Schulte-Merker, S., Hogan, B.M., et al. (2018). A blood capillary plexus-derived population of progenitor cells contributes to genesis of the dermal lymphatic vasculature during embryonic development. Dev. 145.

Pinto, A.R., Ilinykh, A., Ivey, M.J., Kuwabara, J.T., Michelle, L., Antoni, D., Debuque, R., Chandran, A., Wang, L., and Arora, K. (2016). Revisiting Cardiac Cellular Composition Alexander. Circ. Res. 118, 400–409.

Pizarro, G., Castillo, J.G., Gaztanaga, J., and Garcia, M.J. (2009). Total coronary vein-left atrial drainage. Circulation 120, 914–917.

Plein, A., Fantin, A., Denti, L., Pollard, J.W., and Ruhrberg, C. (2018). Erythro-myeloid progenitors contribute endothelial cells to blood vessels. Nature 562, 223–228.

Porras, D., and Brown, C.B. (2008). Temporal-spatial ablation of neural crest in the mouse results in cardiovascular defects. Dev. Dyn. 237, 153–162.

Porrello, E.R., Mahmoud, A.I., Simpson, E., Hill, J. a, James, A., Olson, E.N., and Sadek, H. (2011). Transient Regeneration Potential of the Neonatal Mouse Heart. Science. 331, 1078–1080.

Poss, K.D., Wilson, L.G., and Keating, M.T. (2002). Heart regeneration in zebrafish. Science. 298, 2188–2190.

Potente, M., and Carmeliet, P. (2017). The Link between Angiogenesis and Endothelial Metabolism. Annu. Rev. Physiol. 79, 43–66.

Quijada, P., Trembley, M.A., and Small, E.M. (2020). The Role of the Epicardium during Heart Development and Repair. Circ. Res. 377–394.

Ramjee, V., Li, D., Manderfield, L.J., Liu, F., Engleka, K.A., Aghajanian, H., Rodell, C.B., Lu, W., Ho, V., Wang, T., et al. (2017). Epicardial YAP/TAZ orchestrate an immunosuppressive response following myocardial infarction. J. Clin. Invest. 127, 899–911.

Rana, M.S., Christoffels, V.M., and Moorman, A.F.M. (2013). A molecular and genetic outline of cardiac morphogenesis. Acta Physiol. 207, 588–615.

Red-horse, K., Ueno, H., Weissman, I.L., and Krasnow, M.A. (2010). Coronary arteries form by developmental reprogramming of venous cells. Nature 464, 549–554.

Rinda Soong, T., Pathak, A.P., Asano, H., Fox-Talbot, K., and Baldwin, W.M. (2010). Lymphatic injury and regeneration in cardiac allografts. Transplantation 89, 500–508.

Risebro, C.A., Vieira, J.M., Klotz, L., and Riley, P.R. (2015). Characterisation of the human embryonic and foetal epicardium during heart development. Dev. 142, 3630–3636.

Rodgers, L.S., Lalani, S., Runyan, R.B., and Camenisch, T.D. (2008). Differential growth and multicellular villi direct proepicardial translocation to the developing mouse heart. Dev. Dyn. 237, 145–152.

Roselló-Díez, A., Arques, C.G., Delgado, I., Giovinazzo, G., and Torres, M. (2014). Diffusible signals and epigenetic timing cooperate in late proximo-distal limb patterning. Dev. 141, 1534–1543.

Rudat, C., and Kispert, A. (2012). Wt1 and epicardial fate mapping. Circ. Res. 111, 165–169.

Sabin, F.R. (1902). On the origin of the lymphatic system from the veins and the development of the lymph hearts and thoracic duct in the pig. Am. J. Anat. 1, 367–389.

Saga, Y., Kitajima, S., and Miyagawa-Tomita, S. (2000). Mesp1 expression is the earliest sign of cardiovascular development. Trends Cardiovasc. Med. 10, 345–352.

Schoppmann, S.F., Birner, P., Stöckl, J., Kalt, R., Ullrich, R., Caucig, C., Nagy, K., Alitalo, K., and Kerjaschki, D. (2002). Tumor-associated macrophages express lymphatic endothelial growth factors and are related to peritumoral lymphangiogenesis. Am. J. Pathol. 161, 947–956.

Schulte, I., Schlueter, J., Abu-Issa, R., Brand, T., and Männer, J. (2007). Morphological and molecular left-right asymmetries in the development of the proepicardium: A comparative analysis on mouse and chick embryos. Dev. Dyn. 236, 684–695.

Sengbusch, J.K., He, W., Pinco, K.A., and Yang, J.T. (2002). Dual functions of α4β1 integrin in epicardial development: Initial migration and long-term attachment. J. Cell Biol. 157, 873–882.

Sharma, B., Chang, A., and Red-Horse, K. (2017). Coronary Artery Development: Progenitor Cells and Differentiation Pathways. Annu. Rev. Physiol. 79, 1–19.

Shin, Y.J., Choi, J.S., Lee, J.Y., Choi, J.Y., Cha, J.H., Chun, M.H., and Lee, M.Y. (2008). Differential regulation of vascular endothelial growth factor-C and its receptor in the rat hippocampus following transient forebrain ischemia. Acta Neuropathol. 116, 517–527.

Simões, F.C., and Riley, P.R. (2018). The ontogeny, activation and function of the epicardium during heart development and regeneration. Development 145, dev155994.

Singh, A., Ramesh, S., Cibi, D.M., Yun, L.S., Li, J., Li, L., Manderfield, L.J., Olson, E.N., Epstein, J.A., and Singh, M.K. (2016). Hippo Signaling Mediators Yap and Taz Are Required in the Epicardium for Coronary Vasculature Development. Cell Rep. 15, 1384–1393.

Smart, N., Risebro, C.A., Melville, A.A.D., Moses, K., Schwartz, R.J., Chien, K.R., and Riley, P.R. (2007). Thymosin β4 induces adult epicardial progenitor mobilization and neovascularization. Nature 445, 177–182.

Smart, N., Dubé, K.N., and Riley, P.R. (2009). Coronary vessel development and insight towards neovascular therapy. Int. J. Exp. Pathol. 90, 262–283.

Smith, C.L., Baek, S.T., Sung, C.Y., and Tallquist, M.D. (2011). Epicardial-derived cell epithelial-to-mesenchymal transition and fate specification require PDGF receptor signaling. Circ. Res. 108.

Smith, J.G., Magnani, J.W., Palmer, C., Meng, Y.A., Soliman, E.Z., Musani, S.K., Kerr, K.F., Schnabel, R.B., Lubitz, S.A., Sotoodehnia, N., et al. (2011). Genome-wide association studies of the PR interval in African Americans. PLoS Genet. 7.

Soonpaa, M.H., Kim, K.K., Pajak, L., Franklin, M., and Field, L.J. (1996). Cardiomyocyte DNA synthesis and binucleation during murine development. Am. J. Physiol. - Hear. Circ. Physiol. 271.

Spieler, D., Kaffe, M., Knauf, F., Bessa, J., Tena, J.J., Giesert, F., Schormair, B., Tilch, E., Lee, H., Horsch, M., et al. (2014). Restless Legs Syndrome-Associated intronic common variant in Meis1 alters enhancer function in the developing telencephalon. Genome Res. 24, 592–603.

Sridurongrit, S., Larsson, J., Schwartz, R., Ruiz-Lozano, P., and Kaartinen, V. (2008). Signaling via the Tgf-β type I receptor Alk5 in heart development. Dev. Biol. 322, 208–218.

Srinivasan, R.S., Dillard, M.E., Lagutin, O. V., Lin, F.J., Tsai, S., Tsai, M.J., Samokhvalov, I.M., and Oliver, G. (2007). Lineage tracing demonstrates the venous origin of the mammalian lymphatic vasculature. Genes Dev. 21, 2422–2432.

Srinivasan, R.S., Geng, X., Yang, Y., Wang, Y., Mukatira, S., Studer, M., Porto, M.P.R., Lagutin, O., and Oliver, G. (2010). The nuclear hormone receptor Coup-TFII is required for the initiation and early maintenance of Prox1 expression in lymphatic endothelial cells. Genes Dev. 24, 696–707.

Stanczuk, L., Martinez-Corral, I., Ulvmar, M.H., Zhang, Y., Laviña, B., Fruttiger, M., Adams, R.H., Saur, D., Betsholtz, C., Ortega, S., et al. (2015). CKit lineage hemogenic endothelium-derived cells contribute to mesenteric lymphatic vessels. Cell Rep. 10, 1708–1721.

Stankunas, K., Shang, C., Twu, K.Y., Kao, S.C., Jenkins, N.A., Copeland, N.G., Sanyal, M., Selleri, L., Cleary, M.L., and Chang, C.P. (2008). Pbx/Meis deficiencies demonstrate multigenetic origins of congenital heart disease. Circ. Res. 103, 702–709.

Stenmark, K.R., Yeager, M.E., El Kasmi, K.C., Nozik-Grayck, E., Gerasimovskaya, E. V, Li, M., Riddle, S.R., and Frid, M.G. (2013). The adventitia: Essential regulator of vascular wall structure and function. Annu. Rev. Physiol. 75, 23–47.

Stone, O.A., and Stainier, D.Y.R. (2019). Paraxial Mesoderm Is the Major Source of Lymphatic Endothelium. Dev. Cell 50, 247–255.e3.

Swift, G.H., Liu, Y., Rose, S.D., Bischof, L.J., Steelman, S., Buchberg, A.M., Wright, C.V.E., and MacDonald, R.J. (1998). An Endocrine-Exocrine Switch in the Activity of the Pancreatic Homeodomain Protein PDX1 through Formation of a Trimeric Complex with PBX1b and MRG1 (MEIS2). Mol. Cell. Biol. 18, 5109–5120.

Tammela, T., and Alitalo, K. (2010). Lymphangiogenesis: Molecular Mechanisms and Future Promise. Cell 140, 460–476.

Tian, X., Hu, T., He, L., Zhang, H., Huang, X., Poelmann, R.E., Liu, W., Yang, Z., Yan, Y., Pu, W.T., et al. (2013). Peritruncal coronary endothelial cells contribute to proximal coronary artery stems and their aortic orifices in the mouse heart. PLoS One 8, 1–9.

Timmerman, L.A., Grego-Bessa, J., Raya, A., Bertrán, E., Pérez-Pomares, J.M., Díez, J., Aranda, S., Palomo, S., McCormick, F., Izpisúa-Belmonte, J.C., et al. (2004). Notch promotes epithelial-mesenchymal transition during cardiac development and oncogenic transformation. Genes Dev. 18, 99–115.

Tomanek, R.J., Ratajska, A., Kitten, G.T., Yue, X., and Sandra, A. (1999). Vascular endothelial growth factor expression coincides with coronary vasculogenesis and angiogenesis. Dev. Dyn. 215, 54–61.

Trembley, M.A., Velasquez, L.S., de Mesy Bentley, K.L., and Small, E.M. (2015). Myocardin-related transcription factors control the motility of epicardium-derived cells and the maturation of coronary vessels. Dev. 142, 21–30.

Unnisa, Z., Clark, J.P., Roychoudhury, J., Thomas, E., Tessarollo, L., Copeland, N.G., Jenkins, N.A., Grimes, H.L., and Kumar, A.R. (2012). Meis1 preserves hematopoietic stem cells in mice by limiting oxidative stress. Blood 120, 4973–4981.

Uribe, R.A., and Bronner, M.E. (2015). Meis3 is required for neural crest invasion of the gut during zebrafish enteric nervous system development. Mol. Biol. Cell 26, 3728–3740.

Vaahtomeri, K., Karaman, S., Mäkinen, T., and Alitalo, K. (2017). Lymphangiogenesis guidance by paracrine and pericellular factors. Genes Dev. 31, 1615–1634.

Vega-Hernández, M., Kovacs, A., de Langhe, S., and Ornitz, D.M. (2011). FGF10/FGFR2b signaling is essential for cardiac fibroblast development and growth of the myocardium. Development 138, 3331–3340.

Végh, A., Duim, S., Smits, A., Poelmann, R., ten Harkel, A., DeRuiter, M., Goumans, M., and Jongbloed, M. (2016). Part and Parcel of the Cardiac Autonomic Nerve System: Unravelling Its Cellular Building Blocks during Development. J. Cardiovasc. Dev. Dis. 3, 28.

Vermot, J., Niederreither, K., Garnier, J.M., Chambon, P., and Dollé, P. (2003). Decreased embryonic retinoic acid synthesis results in a DiGeorge syndrome phenotype in newborn mice. Proc. Natl. Acad. Sci. U. S. A. 100, 1763–1768.

Vieira, J.M., Norman, S., Del Campo, C.V., Cahill, T.J., Barnette, D.N., Gunadasa-Rohling, M., Johnson, L.A., Greaves, D.R., Carr, C.A., Jackson, D.G., et al. (2018). The cardiac lymphatic system stimulates resolution of inflammation following myocardial infarction. J. Clin. Invest. 128, 3402–3412.

Villa del Campo, C., Lioux, G., Carmona, R., Sierra, R., Muñoz-Chápuli, R., Clavería, C., and Torres, M. (2016). Myc overexpression enhances of epicardial contribution to the developing heart and promotes extensive expansion of the cardiomyocyte population. Sci. Rep. 6, 35366.

Vincent, S.D., and Buckingham, M.E. (2010). How to make a heart. The origin and regulation of cardiac progenitor cells. In Current Topics in Developmental Biology, pp. 1–41.

Vivien, C.J., Pichol-Thievend, C., Sim, C.B., Smith, J.B., Bower, N.I., Hogan, B.M., Hudson, J.E., Francois, M., and Porrello, E.R. (2019). Vegfc/d-dependent regulation of the lymphatic vasculature during cardiac regeneration is influenced by injury context. Npj Regen. Med. 4, 18.

Volz, K.S., Jacobs, A.H., Chen, H.I., Poduri, A., Mckay, A.S., Riordan, D.P., Kofler, N., Kitajewski, J., Weissman, I., and Red-horse, K. (2015). Pericytes are progenitors for coronary artery smooth muscle. Elife 4, 1–22.

Waldo, K., Miyagawa-Tomita, S., Kumiski, D., and Kirby, M.L. (1998). Cardiac neural crest cells provide new insight into septation of the cardiac outflow tract: Aortic sac to ventricular septal closure. Dev. Biol. 196, 129–144.

Waldo, K.L., Hutson, M.R., Stadt, H.A., Zdanowicz, M., Zdanowicz, J., and Kirby, M.L. (2005). Cardiac neural crest is necessary for normal addition of the myocardium to the arterial pole from the secondary heart field. Dev. Biol. 281, 66–77.

Wang, G., Muhl, L., Padberg, Y., Dupont, L., Peterson-Maduro, J., Stehling, M., le Noble, F., Colige, A., Betsholtz, C., Schulte-Merker, S., et al. (2020). Specific fibroblast subpopulations and neuronal structures provide local sources of Vegfc-processing components during zebrafish lymphangiogenesis. Nat. Commun. 11, 1–21.

Wang, S., Huang, W., Castillo, H.A., Kane, M.A., Xavier-Neto, J., Trainor, P.A., and Moise, A.R. (2018a). Alterations in retinoic acid signaling affect the development of the mouse coronary vasculature. Dev. Dyn. 247, 976–991.

Wang, S., Yu, J., Jones, J.W., Pierzchalski, K., Kane, M.A., Trainor, P.A., Xavier-Neto, J., and Moise, A.R. (2018b). Retinoic acid signaling promotes the cytoskeletal rearrangement of embryonic epicardial cells. FASEB J. 32, 3765–3781.

Ward, M.C., and Cunningham, A.M. (2015). Developmental expression of vascular endothelial growth factor receptor 3 and vascular endothelial growth factor C in forebrain. Neuroscience 303, 544–557.

Ward, N.L., Van Slyke, P., Sturk, C., Cruz, M., and Dumont, D.J. (2004a). Angiopoietin 1 Expression Levels in the Myocardium Direct Coronary Vessel Development. Dev. Dyn. 229, 500–509.

Ward, N.L., Slyke, P. Van, and Dumont, D.J. (2004b). Functional inhibition of secreted angiopoietin: A novel role for angiopoietin 1 in coronary vessel patterning. Biochem. Biophys. Res. Commun. 323, 937–946.

Wei, Y., and Mikawa, T. (2000). Fate diversity of primitive streak cells during heart field formation in ovo. Dev. Dyn. 219, 505–513.

Wesselhoeft, H., Fawcett, J.S., and Johnson, A.L. (1968). Anomalous origin of the left coronary artery from the pulmonary artery. Circulation 38, 403–425.

Wessels, A., Hoffb, van den M., Adamo, R., Phelps, A., Lockharts, M., Sauls, K., Briggs, L.E., Norrisa, R.A., Wijk, B. van, Perez-Pomares, J.M., et al. (2012). Epicardially-derived Fibroblasts Preferentially Contribute to the Parietal Leaflets of the Atrioventricular Valves in the Murine Heart. Dev Biol 100, 130–134.

Wigle, J.T., and Oliver, G. (1999). Prox1 function is required for the development of the murine lymphatic system. Cell 98, 769–778.

Williams, T.M., Williams, M.E., and Innis, J.W. (2005). Range of HOX/TALE superclass associations and protein domain requirements for HOXA13:MEIS interaction. Dev. Biol. 277, 457–471.

Wilm, B., Ipenberg, A., Hastie, N.D., Burch, J.B.E., and Bader, D.M. (2005). The serosal mesothelium is a major source of smooth muscle cells of the gut vasculature. Development 132, 5317–5328.

Wilting, J., Buttler, K., Schulte, I., Papoutsi, M., Schweigerer, L., and Männer, J. (2007). The proepicardium delivers hemangioblasts but not lymphangioblasts to the developing heart. Dev. Biol. 305, 451–459.

Winkelmann, J., Schormair, B., Lichtner, P., Ripke, S., Xiong, L., Jalilzadeh, S., Fulda, S., Pütz, B., Eckstein, G., Hauk, S., et al. (2007). Genome-wide association study of restless legs syndrome identifies common variants in three genomic regions. Nat. Genet. 39, 1000–1006.

Witte, M.H., Dumont, A.E., Clauss, R.H., Rader, B., Levine, N., and Breed, E.S. (1969). Lymph circulation in congestive heart failure: effect of external thoracic duct drainage. Circulation 39, 723–733.

Wu, B., Zhang, Z., Lui, W., Chen, X., Wang, Y., Chamberlain, A.A., Moreno-rodriguez, R.A., Markwald, R.R., Rourke, B.P.O., Sharp, D.J., et al. (2012). Endocardial Cells Form the Coronary Arteries by Angiogenesis through Myocardial-Endocardial VEGF Signaling. Cell 151, 1083–1096.

Wu, H., Lee, S.H., Gao, J., Liu, X., and Iruela-Arispe, M.L. (1999). Inactivation of erythropoietin leads to defects in cardiac morphogenesis. Development 126, 3597–3605.

Wu, M., Smith, C.L., Hall, J.A., Lee, I., Luby-Phelps, K., and Tallquist, M.D. (2010). Epicardial Spindle Orientation Controls Cell Entry into the Myocardium. Dev. Cell 19, 114–125.

Wu, S.M., Fujiwara, Y., Cibulsky, S.M., Clapham, D.E., Lien, C. ling, Schultheiss, T.M., and Orkin, S.H. (2006). Developmental Origin of a Bipotential Myocardial and Smooth Muscle Cell Precursor in the Mammalian Heart. Cell 127, 1137–1150.

Wurdak, H., Ittner, L.M., Lang, K.S., Leveen, P., Suter, U., Fischer, J.A., Karlsson, S., Born, W., and Sommer, L. (2005). Inactivation of TGFβ signaling in neural crest stem cells leads to multiple defects reminiscent of DiGeorge syndrome. Genes Dev. 19, 530–535.

Xiao, Y., Hill, M.C., Zhang, M., Martin, T.J., Morikawa, Y., Wang, S., Moise, A.R., Wythe, J.D., and Martin, J.F. (2018). Hippo Signaling Plays an Essential Role in Cell State Transitions during Cardiac Fibroblast Development. Dev. Cell 45, 153–169.e6.

Yamaguchi, Y., Cavallero, S., Patterson, M., Shen, H., Xu, J., Kumar, S.R., and Sucov, H.M. (2015). Adipogenesis and epicardial adipose tissue: A novel fate of the epicardium induced by mesenchymal transformation and PPARγ activation. Proc. Natl. Acad. Sci. U. S. A. 112, 2070–2075.

Yang, J.T., Rayburn, H., and Hynes, R.O. (1995). Cell adhesion events mediated by α4 integrins are essential in placental and cardiac development. Development 121, 549–560.

Yaniv, K., Isogai, S., Castranova, D., Dye, L., Hitomi, J., and Weinstein, B.M. (2006). Live imaging of lymphatic development in the zebrafish. Nat. Med. 12, 711–716.

Zaffran, S., Kelly, R.G., Meilhac, S.M., Buckingham, M.E., and Brown, N.A. (2004). Right ventricular myocardium derives from the anterior heart field. Circ. Res. 95, 261–268.

Zhang, H., Pu, W., Li, G., Huang, X., He, L., Tian, X., Liu, Q., Zhang, L., Wu, S.M., Sucov, H.M., et al. (2016). Endocardium Minimally Contributes to Coronary Endothelium in the Embryonic Ventricular Free Walls. Circ. Res. 118, 1880–1893.

Zhou, B., and Pu, W.T. (2012). Genetic Cre-loxP assessment of epicardial cell fate using Wt1-Driven cre alleles. Circ. Res. 111, 276–280.

Zhou, B., Ma, Q., Rajagopal, S., Wu, S.M., Domian, I., Rivera-Feliciano, J., Jiang, D., Von Gise, A., Ikeda, S., Chien, K.R., et al. (2008). Epicardial progenitors contribute to the cardiomyocyte lineage in the developing heart. Nature 454, 109–113.

Zhou, B., Honor, L.B., He, H., Qing, M., Oh, J.H., Butterfield, C., Lin, R.Z., Melero-Martin, J.M., Dolmatova, E., Duffy, H.S., et al. (2011). Adult mouse epicardium modulates myocardial injury by secreting paracrine factors. J. Clin. Invest. 121, 1894–1904.

ANNEXES

- Paper:

Liu, X., **De la Cruz, E**., Gu, X., Balint, L., Oxendine-Burns, M., Terrones, T., Ma, W., Kuo, H.H., Lantz, C., Bansal, T., et al. (2020). Lymphoangiocrine signals promote cardiac growth and repair. Nature 588, 705–711.

Digital content:

- Supplementary Table 1: DEGs obtained from RNA_seq dKO vs control E16.5 epicardium.

- Video 1: 3D recontruction of *Wt1Cre lineage+* cells of E18.5 control outflow tract.

- Video 2: 3D reconstruction of *Wt1Cre lineage+* cells of E18.5 Meis dKO outflow tract.

Article

Lymphoangiocrine signals promote cardiac growth and repair

https://doi.org/10.1038/s41586-020-2998-x

Received: 13 June 2019

Accepted: 7 October 2020

Published online: 9 December 2020

Check for updates

Xiaolei Liu[1], Ester De la Cruz[2], Xiaowu Gu[3], Laszlo Balint[4,5], Michael Oxendine-Burns[1], Tamara Terrones[6], Wanshu Ma[1], Hui-Hsuan Kuo[7], Connor Lantz[8], Trisha Bansal[1], Edward Thorp[8], Paul Burridge[7], Zoltán Jakus[4,5], Joachim Herz[6,9,10], Ondine Cleaver[3], Miguel Torres[2] & Guillermo Oliver[1]✉

Recent studies have suggested that lymphatics help to restore heart function after cardiac injury[1–6]. Here we report that lymphatics promote cardiac growth, repair and cardioprotection in mice. We show that a lymphoangiocrine signal produced by lymphatic endothelial cells (LECs) controls the proliferation and survival of cardiomyocytes during heart development, improves neonatal cardiac regeneration and is cardioprotective after myocardial infarction. Embryos that lack LECs develop smaller hearts as a consequence of reduced cardiomyocyte proliferation and increased cardiomyocyte apoptosis. Culturing primary mouse cardiomyocytes in LEC-conditioned medium increases cardiomyocyte proliferation and survival, which indicates that LECs produce lymphoangiocrine signals that control cardiomyocyte homeostasis. Characterization of the LEC secretome identified the extracellular protein reelin (RELN) as a key component of this process. Moreover, we report that LEC-specific *Reln*-null mouse embryos develop smaller hearts, that RELN is required for efficient heart repair and function after neonatal myocardial infarction, and that cardiac delivery of RELN using collagen patches improves heart function in adult mice after myocardial infarction by a cardioprotective effect. These results highlight a lymphoangiocrine role of LECs during cardiac development and injury response, and identify RELN as an important mediator of this function.

The molecular and functional characterization of the lymphatic vasculature has greatly improved[1]. Recent data suggest that natural or therapeutic formation of new lymphatics (lymphangiogenesis) correlates with improved systolic function after experimental myocardial infarction; it delays atherosclerotic plaque formation, facilitates the healing process after myocardial infarction, and can be a natural response to fluid accumulation into the myocardium during cardiac oedema[2–4]. These findings indicate that stimulation of lymphangiogenesis in the infarcted heart could improve cardiac function and prevent adverse cardiac remodelling[3]. Studies in mouse and zebrafish have suggested that newly formed lymphatics provided a route for the clearance of immune cells in the injured heart, and therefore promote cardiac repair[5,6]. However, whether lymphatics have additional functional roles during heart development and cardiac repair is not known.

Lymphatics regulate heart growth

As previously reported[2], at around embryonic day (E) 14.5 cardiac lymphatics become evident, particularly over the dorsal side of the heart (Fig. 1a). As development progresses, lymphatics expand over the dorsal and ventral surfaces, and into the myocardium during embryonic and postnatal stages (Fig. 1a). To evaluate a possible developmental role of cardiac-associated lymphatics, we took advantage of *Prox1* floxed mice[7]. *Prox1* is a master regulator required to promote and maintain LEC fate identity[8,9] and germline deletion of *Prox1* in mice results in complete lack of LECs and embryonic lethality at around E14.5[8]. To conditionally delete *Prox1* from LECs, we crossed *Cad5(PAC)-creER^{T2}* mice[10] with *Prox1* floxed mice and injected pregnant females with tamoxifen (TAM) at E13.5 and E14.5. Analysis of E17.5 *Cad5(PAC)-creER^{T2};Prox1$^{f/f}$*-null embryos (*Prox1$^{\Delta LEC/\Delta LEC}$*) revealed the development of oedema (Fig. 1b, arrow)—a phenotype associated with defective lymphatics and death soon after birth. Notably, these mutant embryos have significantly smaller hearts than control littermates (approximately one-third smaller) (Fig. 1c, j). Most, if not all, cardiac lymphatics were missing (Fig. 1d, g, Extended Data Fig. 1a) and the blood vasculature was not affected in *Prox1$^{\Delta LEC/\Delta LEC}$* embryos (Fig. 1e, f, h, i).

Decreased CM mass causes heart size reduction

Haematoxylin and eosin (H&E) staining confirmed that the overall size of the ventricles in *Prox1$^{\Delta LEC/\Delta LEC}$* embryos is smaller; however, cardiac

[1]Center for Vascular and Developmental Biology, Feinberg Cardiovascular and Renal Research Institute, Feinberg School of Medicine, Northwestern University, Chicago, IL, USA. [2]Cardiovascular Development Program, Centro Nacional de Investigaciones Cardiovasculares, CNIC, Madrid, Spain. [3]Department of Molecular Biology, University of Texas Southwestern Medical Center, Dallas, TX, USA. [4]Department of Physiology, Semmelweis University School of Medicine, Budapest, Hungary. [5]MTA-SE "Lendulet" Lymphatic Physiology Research Group of the Hungarian Academy of Sciences and the Semmelweis University, Department of Physiology, Semmelweis University School of Medicine, Budapest, Hungary. [6]Department of Molecular Genetics, University of Texas Southwestern Medical Center, Dallas, TX, USA. [7]Department of Pharmacology, Feinberg School of Medicine, Northwestern University, Chicago, IL, USA. [8]Department of Pathology, Feinberg School of Medicine, Northwestern University, Chicago, IL, USA. [9]Department of Neuroscience, University of Texas Southwestern Medical Center, Dallas, TX, USA. [10]Department of Neurology & Neurotherapeutics, University of Texas Southwestern Medical Center, Dallas, TX, USA. ✉e-mail: guillermo.oliver@northwestern.edu

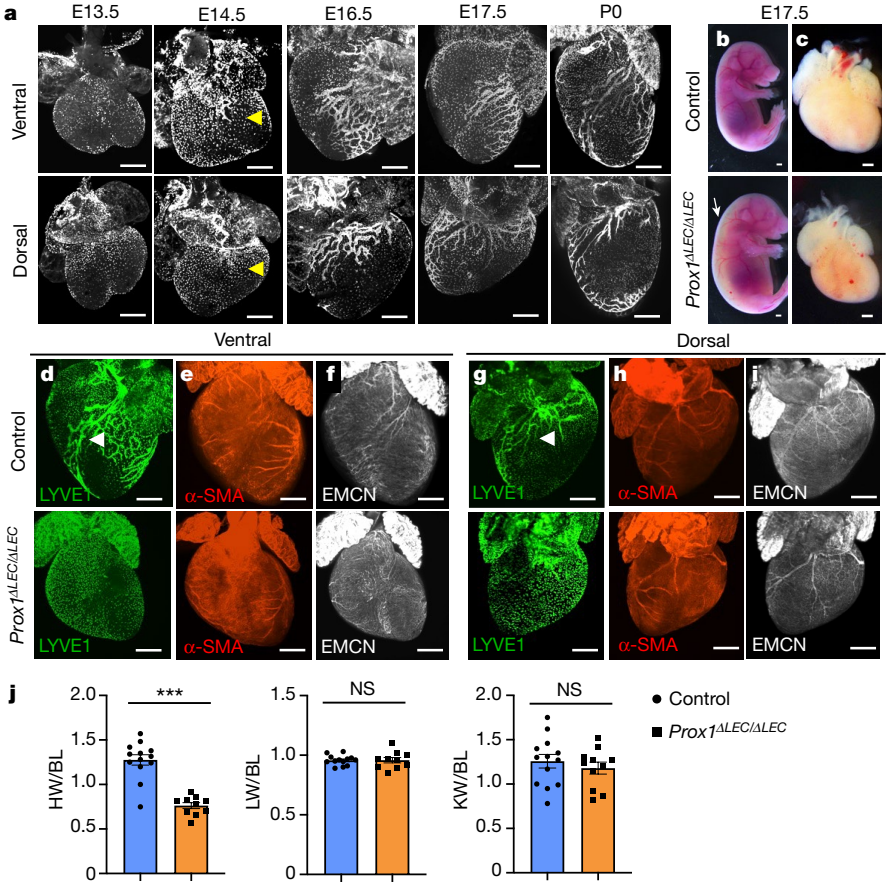

Fig. 1 | Lymphatics are required for embryonic heart growth. a, Wild-type mouse cardiac lymphatic vasculature development as depicted by anti-LYVE1 whole-mount immunostaining. Yellow arrowheads indicate cardiac lymphatics at E14.5. **b**, **c**, Bright-field images of E17.5 control and *Prox1*$^{\Delta LEC/\Delta LEC}$ embryos and hearts. White arrow indicates oedema in *Prox1*$^{\Delta LEC/\Delta LEC}$ embryos. **d**–**i**, Whole-mount immunostaining shows that E17.5 *Prox1*$^{\Delta LEC/\Delta LEC}$ hearts lack LYVE1^{+} cardiac lymphatics and have normal major coronary arteries and veins, as indicated by α-SMA and endomucin (EMCN) staining. Arrowheads indicate developing lymphatics in control hearts. **j**, Quantification of organ weight relative to body length (BL) shows reduced heart size (HW, heart weight) and normal liver and kidney sizes (LW, liver weight; KW, kidney weight) in E17.5 *Prox1*$^{\Delta LEC/\Delta LEC}$ embryos ($n = 13$ controls and $n = 10$ *Prox1*$^{\Delta LEC/\Delta LEC}$ embryos; 3 different litters). Data are mean ± s.e.m. ***$P = 3.19062 \times 10^{-6}$ by unpaired two-tailed Student's *t*-test. NS, not significant. Control embryos are *cre*$^{-}$ and *cre*$^{+}$;*Prox1*$^{+/+}$ littermates treated with TAM. $n = 3$ embryos per genotype (**a**, **d**–**i**). Scale bars, 500 µm (**a**, **c**–**i**), 2 mm (**b**).

valves appear normal (Fig. 2a, arrows). Immunostaining of heart sections against α-actinin and F-actin show that, overall, cardiac muscle structure and arrangement are not disrupted in *Prox1*$^{\Delta LEC/\Delta LEC}$ hearts (Extended Data Fig. 1b). Flow cytometry analysis (FACS) indicated that the percentage of cardiomyocytes (CMs) is significantly reduced (approximately one-third reduction) (Extended Data Fig. 1c), a result suggesting that a decrease in CM mass underlies the reduction in heart size. Hoechst 33342 labelling showed no differences in CM ploidy in *Prox1*$^{\Delta LEC/\Delta LEC}$ hearts (Extended Data Fig. 1d). However, an increased percentage of multinucleated CMs was observed in these E17.5 mutant hearts after CM dissociation and overnight plating (Extended Data Fig. 1e, f), but no overall differences in CM size were detected (Extended Data Fig. 1e, g). Similarly, α-laminin staining showed that the overall CM size was not affected in the mutant hearts (Fig. 2b). Next, we evaluated possible alterations in CM proliferation and survival. Indeed, CM proliferation is greatly reduced in E17.5 *Prox1*$^{\Delta LEC/\Delta LEC}$ embryos, as indicated by EdU labelling (Fig. 2c, g, Extended Data Fig. 2a–e) and phospho-histone H3 (pH3), Ki67 and aurora kinase B (auroraB) immunostainings (Fig. 2d–g). This reduction in proliferation is seen in different regions of the E17.5 mutant heart (Extended Data Fig. 2f). In addition, CM apoptosis was significantly increased in *Prox1*$^{\Delta LEC/\Delta LEC}$ hearts (Fig. 2h). These alterations in CM proliferation and apoptosis were not seen in other cardiac cell types (blood endothelial cells, fibroblasts or macrophages) or other organs (nephron progenitors and hepatocytes) in these mutant embryos (Extended Data Fig. 2g).

To support these findings, we performed similar analysis using another mouse model without lymphatics. Accordingly, we used *Vegfr3*$^{kd/kd}$, a naturally occurring mouse strain with a point mutation in the kinase domain of VEGFR3 that affects *Vegfr3* (also known as *Flt4*) signalling and, therefore, lymphatic development[11]. As seen in Extended Data Fig. 3a, b, E17.5 *Vegfr3*$^{kd/kd}$ embryos lacking cardiac-associated lymphatics also have smaller hearts. Similar to *Prox1*$^{\Delta LEC/\Delta LEC}$ embryos (Fig. 1j), no significant size differences were seen in E17.5 *Vegfr3*$^{kd/kd}$ livers or kidneys (Extended Data Fig. 3a). Also, similar to *Prox1*$^{\Delta LEC/\Delta LEC}$ embryos, CM proliferation was significantly reduced in E17.5 *Vegfr3*$^{kd/kd}$ hearts (Extended Data Fig. 3c–g), CM apoptosis was significantly increased (Extended Data Fig. 3h), and proliferation in other cardiac cell types or in nephron progenitors and hepatocytes was not affected (Extended Data Fig. 3i). Because E17.5 *Prox1*$^{\Delta LEC/\Delta LEC}$ embryos develop oedema, their reduced heart size could be secondary to haemodynamic defects as a consequence of their lack of lymphatics and therefore, of lymphatic flow. However, E17.5 *Cad5(PAC)-creER*^{T2};*Prox1*$^{f/+}$ embryos (*Prox1*$^{\Delta LEC/+}$) also exhibited severe oedema and their cardiac lymphatics showed reduced branching, but their heart size and CM proliferation were normal (Extended Data Fig. 4a–e). Similarly, E14.5 *Prox1*$^{\Delta LEC/\Delta LEC}$ null embryos (a stage at which cardiac lymphatics will just start to grow into the heart) (Fig. 1a; TAM injection at E10.5 and E11.5) also lacked LECs and exhibited severe oedema, but their heart size and CM proliferation were normal (Extended Data Fig. 4f–h).

To investigate the molecular basis of these lymphatics-dependent defects, we performed RNA sequencing (RNA-seq) analysis of the ventricular portions of E17.5 control and *Prox1*$^{\Delta LEC/\Delta LEC}$ hearts. Gene set expression analysis revealed that genes and pathways related to cell cycle were greatly reduced; instead, the expression of genes and pathways involved in apoptosis was enriched (Extended Data Fig. 5a). These results were validated by quantitative PCR (qPCR), which showed that the expression of pro-apoptotic genes was significantly upregulated, but cell-cycle-related genes were significantly downregulated (Extended Data Fig. 5b).

LEC medium promotes CM proliferation

Signalling between blood endothelial cells and CMs is important during cardiac growth and repair[12,13]. To evaluate whether LECs produce

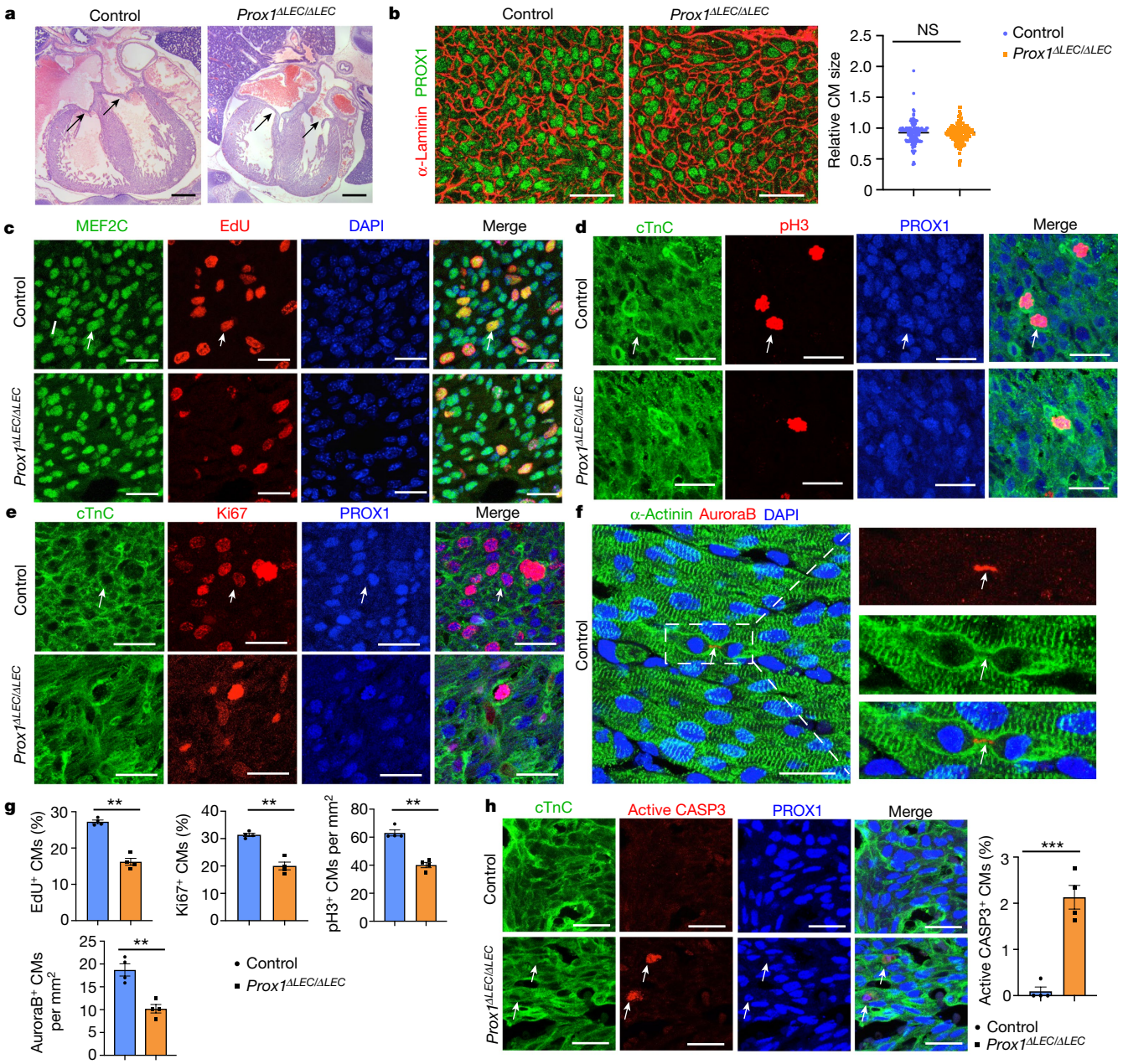

Fig. 2 | Lymphatics are required for CM proliferation and survival. a, H&E staining shows no obvious defects in cardiac valves (arrows) or ventricular wall compaction in E17.5 *Prox1*$^{\Delta LEC/\Delta LEC}$ hearts (TAM injected at E13.5 and E14.5). $n = 4$ embryos per genotype. **b**, α-Laminin staining shows no differences in PROX1$^+$ CM size between E17.5 controls and *Prox1*$^{\Delta LEC/\Delta LEC}$ hearts. Right, quantification of PROX1$^+$ CM size (α-laminin$^+$ area). Average cell size was measured from 5 fields per ventricle, 8–10 PROX1$^+$ CMs per field, 3 embryos per genotype; $n = 152$ (control) and 155 (*Prox1*$^{\Delta LEC/\Delta LEC}$). **c**–**f**, Immunostaining with proliferation markers (EdU, pH3, Ki67 and auroraB) together with CM markers (cardiac troponin C (cTnC), PROX1, α-actinin and/or MEF2C). In all images, arrows indicate the double-positive CMs selected for counting. $n = 4$ embryos per genotype from 3 separate litters. **g**, Quantification of the immunostaining in **c**–**f** shows reduced number of EdU$^+$, Ki67$^+$, auroraB$^+$ and pH3$^+$ CMs in E17.5 *Prox1*$^{\Delta LEC/\Delta LEC}$ hearts. $n = 4$ embryos per genotype from 3 separate litters. $^{**}P = 0.003$ (EdU, Ki67 and auroraB), $^{**}P = 0.002$ (pH3). **h**, Active caspase-3 (CASP3) immunostaining shows increased CM apoptosis in PROX1$^+$ CMs in E17.5 *Prox1*$^{\Delta LEC/\Delta LEC}$ hearts. Arrows indicate apoptotic CMs. $n = 4$ embryos per genotype from 3 separate litters. $^{***}P = 0.0003$, unpaired two-tailed Student's *t*-test. Control embryos are TAM-treated *cre*$^-$ and *cre*$^+$;*Prox1*$^{+/+}$ littermates. Data are mean ± s.e.m. Scale bars, 1 mm (**a**), 25 μm (**b**, **c**–**f**, **h**). Lower magnification images of **c**–**e** and **h** are included in Supplementary Fig. 1.

lymphoangiocrine signals that promote CM proliferation and survival, we first cultured CMs derived from human induced pluripotent stem (iPS) cells with LEC-conditioned medium obtained from culturing commercially available human dermal LECs. We then examined *AKT* (also known as *AKT1*) and *ERK* (*MAPK1*) signalling, as phosphorylated AKT and ERK (p-AKT and p-ERK, respectively) are frequently used as readouts of proliferative signalling. Compared with DMEM-control medium, LEC-conditioned medium significantly increased p-AKT and p-ERK signalling in the cultured human iPS cell-derived CMs (Fig. 3a). Similar results were seen using primary mouse CMs isolated from wild-type E14.5–E17.5 hearts (Fig. 3b). Furthermore, treatment of mouse primary CMs with LEC-conditioned medium significantly increased cell proliferation, as indicated by Ki67 staining (Extended Data Fig. 5c), and protected CM from apoptosis when cultured under $CoCl_2$-induced hypoxic

conditions (Extended Data Fig. 5d). Together, these results indicate that LEC-conditioned medium promotes CM proliferation and survival in vitro, and that lymphoangiocrine factor(s) present in that conditioned medium have an important role during heart development in vivo.

RELN is required for heart growth

To identify such secreted factor(s), we performed mass spectrometry of the LEC-conditioned medium and identified 317 unique proteins. From that list, we initially focused on all secreted proteins by comparing changes in their expression levels in the RNA-seq dataset described above. Among those candidates, *Reln* was greatly reduced in *Prox1*$^{\Delta LEC/\Delta LEC}$ hearts ($\log_2$-transformed fold change of −0.6098 compared to control). qPCR analysis confirmed about an 80% reduction in *Reln* expression in *Prox1*$^{\Delta LEC/\Delta LEC}$ hearts (Extended Data Fig. 6a). We then validated by qPCR the gene expression levels of *Reln*, as well as of several other enriched proteins identified in the LECs secretome (Extended Data Fig. 6b). Quantification of RELN secretion in three separate LEC preparations by ELISA revealed similar concentrations of this protein in their supernatants (average $A_{450\,nm}$ was 0.453 ± 0.065 (mean ± s.d.)) (Extended Data Fig. 6c). RELN is an extracellular matrix protein widely known for its roles during neuronal development and migration, and *Reln* mutant mice are ataxic[14,15]. RELN is also expressed in LECs and regulates the maturation of collecting lymphatic vessels[16]. In agreement with those results[16], in the heart RELN is mainly expressed in LECs (Extended Data Fig. 6d), although some cardiac blood vessels also express low levels of RELN (Extended Data Fig. 6e). Accordingly, the observed qPCR reduction in *Reln* expression in *Prox1*$^{\Delta LEC/\Delta LEC}$ hearts is a consequence of their lack of lymphatics. RELN was almost undetected in E17.5 *Prox1*$^{\Delta LEC/\Delta LEC}$ hearts (Extended Data Fig. 6f).

Notably, the heart size of E17.5 *Reln*$^{-/-}$ embryos[17] was also significantly reduced, but cardiac lymphatics appeared normal (Extended Data Fig. 6g–i). To further demonstrate that the smaller heart phenotype was a consequence of *Reln* loss in LECs, we deleted RELN from LECs (*Reln*$^{\Delta LEC/\Delta LEC}$) by crossing *Reln* floxed mice[18] with *Prox1-creER*^{T2} mice[19] (TAM injections at E13.5 and E14.5). Immunostaining confirmed efficient deletion of RELN in cardiac lymphatics at E17.5 (Extended Data Fig. 7a). Notably, E17.5 *Reln*$^{\Delta LEC/\Delta LEC}$ embryos also developed smaller hearts (although no significant differences were seen in the size of other organs such as kidneys and livers) (Fig. 3c). In addition, CM proliferation was also reduced in *Reln*$^{\Delta LEC/\Delta LEC}$ embryos as indicated by EdU, pH3, Ki67 and auroraB labelling (Fig. 3d–h), and CM apoptosis was increased as indicated by active caspase-3 staining (Fig. 3i). No changes in proliferation and apoptosis were detected in other cardiac cell types or in kidney and liver (Extended Data Fig. 7b). These results agree with those seen in *Reln*$^{-/-}$ embryos, indicating that LEC-derived RELN has a crucial role during heart development and growth by regulating CM proliferation and apoptosis. To validate this finding, we collected LEC-conditioned medium from LECs treated with *Reln* short interfering RNA (siRNA) and control siRNA. Analysis by qPCR showed that *Reln* expression is efficiently silenced in LECs treated with *Reln* siRNA (Extended Data Fig. 8a). Western analysis showed that the identified increase in p-AKT and p-ERK signalling induced by the LEC-conditioned medium was greatly reduced when using the *Reln*-deficient LEC-conditioned medium (Extended Data Fig. 8b).

RELN signalling requires integrin-β1

Previous studies about the role of RELN during neuronal development, neuronal migration and in tumour cells identified VLDLR[20,21], ApoER2[20,21] and integrin-β1[22,23] as RELN receptors. After binding to those receptors, RELN stimulates intracellular signalling transduction through the phosphorylation of the intracellular protein DAB1 and the activation of the PI3K–AKT–GSK3β[24] and mTOR[25] signalling cascades. Integrin-β1 (encoded by *Itgb1*) has been shown to have important roles in heart development, as its deletion in embryonic CMs results in smaller hearts with reduced CM proliferation[26]. Therefore, we investigated whether LEC-derived RELN regulates CM proliferation and survival by regulating *Itgb1* signalling. Western analysis confirmed that CMs treated with LEC-conditioned medium increased the activity of integrin-β1 and RELN downstream signals such as FAK, DAB1, AKT and ERK; by contrast, LEC-conditioned medium from *Reln*-deficient LECs was unable to induce *Itgb1* signalling activity (Extended Data Fig. 8b). More importantly, blocking *Itgb1* signalling in CMs by adding integrin-β1 blocking antibodies to the LEC-conditioned medium partially abolished the pro-survival effects of the intact LEC-conditioned medium (Extended Data Fig. 8b). Furthermore, LEC-conditioned medium from *Reln*-deficient LECs or medium containing integrin-β1-blocking antibodies also failed to promote CM proliferation or protect against CM apoptosis (Extended Data Fig. 8c, d). These data further support our proposal that LEC-secreted RELN regulates CM proliferation and survival mainly by activating the *Itgb1* signalling pathway. Furthermore, we also observed an increase in *Reln* or *Itgb1* signalling activity in mouse primary CMs after RELN stimulation (addition of supernatant from *Reln*-transfected 293T cells), and this signalling was greatly inhibited by the addition of integrin-β1-blocking antibodies (Extended Data Fig. 8e). Moreover, E17.5 *Itgb1*$^{fl/+}$,*Myh6-cre* ;*Reln*$^{+/-}$ (*β1*$^{\Delta CM/+}$;*Reln*$^{+/-}$) double heterozygous embryos generated by crossing *Itgb1*$^{fl/+}$,*Myh6-cre* (*β1*$^{\Delta CM/+}$) with *Reln*$^{+/-}$ mice, also developed smaller hearts without significant size differences in livers or kidneys (Extended Data Fig. 8f). *Reln*$^{+/-}$ and *β1*$^{\Delta CM/+}$ littermates exhibited no differences in heart size compared to wild-type mice (Extended Data Fig. 8f), and embryo size and cardiac lymphatics appear normal in all three genotypes resulting from those crosses (Extended Data Fig. 8g). Consistently, CM proliferation was also significantly reduced and apoptosis was increased in E17.5 *β1*$^{\Delta CM/+}$;*Reln*$^{+/-}$ embryos (Extended Data Fig. 9a, b). No changes in proliferation and apoptosis were detected in other cardiac cell types or in kidney and liver (Extended Data Fig. 9c). Together, these data support our proposal that LEC-secreted RELN regulates CM proliferation and survival through the *Itgb1* signalling pathway.

Neonatal heart repair requires RELN

At E17.5, RELN is highly expressed in cardiac lymphatics nearby the epicardium, as well as in the base of the myocardium; however, its expression levels get steadily reduced from postnatal day (P) 2 to P14, such that at P14 it is barely detected (Extended Data Fig. 10a). This reduction in the levels of RELN is accompanied by a similar change in the levels of *Reln* mRNA (Extended Data Fig. 10b), suggesting that *Reln* expression levels are temporally regulated in cardiac lymphatics.

Because this reduction in RELN expression coincides with the loss of cardiac regenerative potential in mice[27], we first examined the role of *Reln* in wild-type mouse neonatal cardiac regeneration. We performed neonatal myocardial infarction at P2 and the analysis of P7 pups showed LYVE1-expressing lymphatics in both the infarcted and the nearby non-infarcted cardiac tissue. RELN expression was re-activated in the infarcted hearts, with higher levels in the infarcted area and lower levels in the non-infarcted tissue (Extended Data Fig. 10c). A similar analysis in P7 *Reln*-null pups showed that similar to wild-type controls, LYVE1-expressing lymphatics were present in the infarcted and non-infarcted tissues, although in both cases RELN expression was not detected (Extended Data Fig. 10c). Compared with wild-type controls, although cardiac function was not affected in *Reln*$^{-/-}$ hearts at P7, it was reduced at P14 and P21, as determined by echocardiography (Fig. 4a). In line with this reduced cardiac function, Masson's trichrome staining showed increased fibrosis in P21 *Reln*$^{-/-}$ hearts (Fig. 4b). Immunostaining revealed that neither lymphatic density nor LEC proliferation was affected in P21 *Reln*$^{-/-}$ hearts after injury (Extended Data Fig. 10d, e). Similar to the results observed in E17.5 *Reln*-null embryos, CM proliferation was reduced and CM apoptosis was increased in the infarcted area of P7 *Reln*$^{-/-}$ hearts (Fig. 4c, d, Extended Data Fig. 11a–e). Notably, no alterations in cardiac function or increased fibrosis were

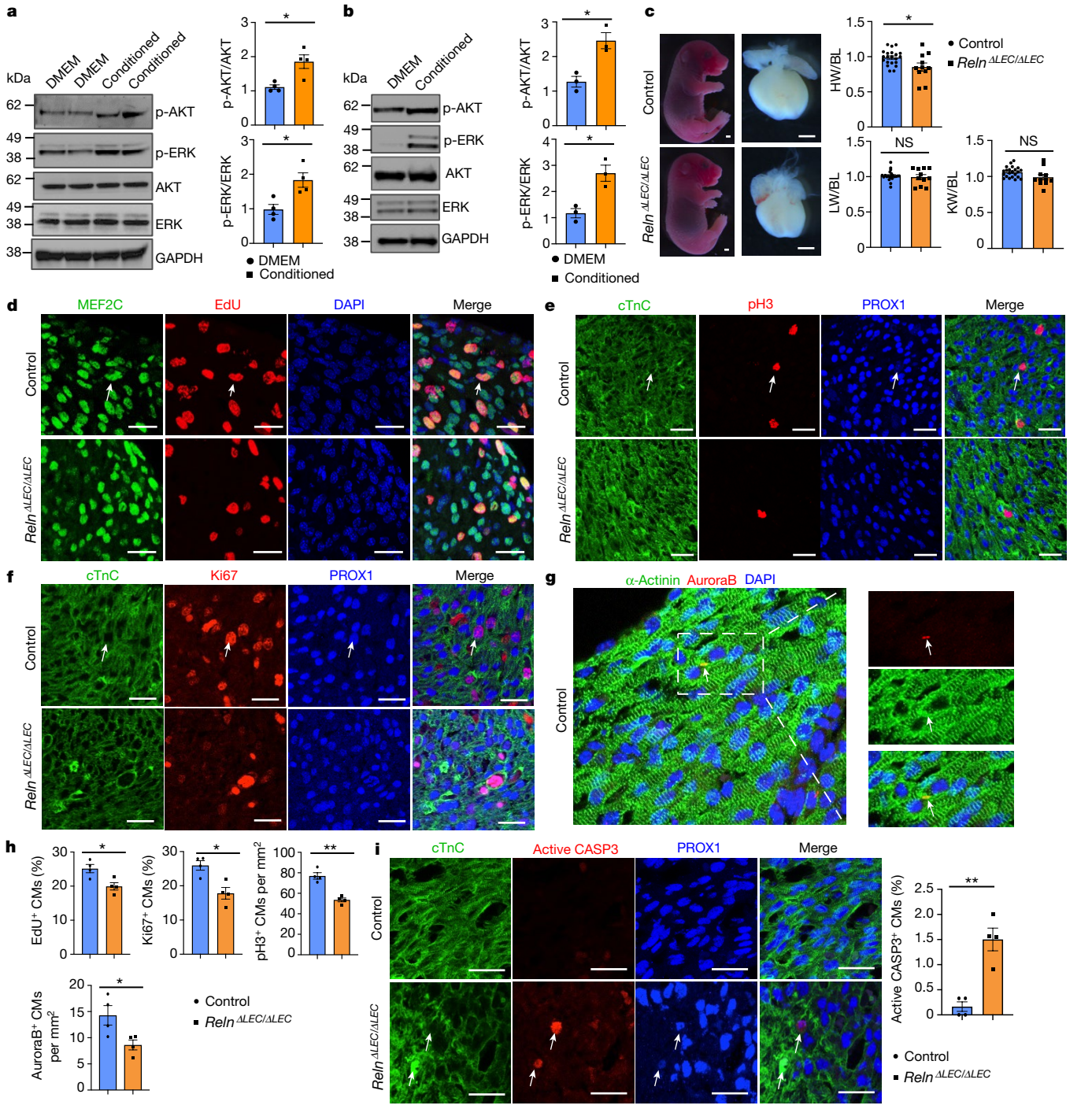

Fig. 3 | LEC-secreted RELN promotes CM proliferation and survival. **a**, **b**, Quantitative western blot results show increased p-AKT and p-ERK in human iPS-cell-derived CMs (**a**) and mouse primary CMs (**b**) treated with LEC-conditioned medium. *P = 0.012 (p-AKT, **a**), *P = 0.015 (p-ERK, **a**), *P = 0.013 (p-AKT and p-ERK, **b**). n = 4 (**a**) and n = 3 (**b**). **c**, Bright-field images of E17.5 *Reln*$^{\Delta LEC/\Delta LEC}$ and control embryos and hearts (TAM injected at E13.5 and E14.5). Quantification of organ weight (heart, liver and kidney) relative to body length indicates that hearts are smaller in *Reln*$^{\Delta LEC/\Delta LEC}$ embryos. n = 22 (controls) and n = 11 (*Reln*$^{\Delta LEC/\Delta LEC}$) from 5 litters. *P = 0.016. Controls are TAM-treated *cre*$^{-}$ embryos and *cre*$^{+}$;*Reln*$^{+/+}$ littermates. **d**–**g**, Double immunostaining using markers of proliferation (EdU, pH3, Ki67 and auroraB) and CM (cTnC, PROX1, α-actinin and/or MEF2C) shows reduced CM proliferation in E17.5 *Reln*$^{\Delta LEC/\Delta LEC}$ hearts. Arrows indicate proliferating CMs. **h**, Quantification of the immunostaining in **d**–**g** shows reduced number of EdU^{+}, Ki67^{+}, auroraB^{+} and pH3^{+} CMs in E17.5 *Reln*$^{\Delta LEC/\Delta LEC}$ hearts. n = 4 embryos per genotype from three separate litters. *P = 0.02 (EdU), *P = 0.01 (Ki67), **P = 0.001 (pH3) and *P = 0.035 (auroraB). **i**, Active caspase-3 (CASP3) immunostaining shows increased CM apoptosis (arrows) in E17.5 *Reln*$^{\Delta LEC/\Delta LEC}$ hearts. Right, quantification of the percentage of active CASP3^{+} CMs in E17.5 control and *Reln*$^{\Delta LEC/\Delta LEC}$ hearts. n = 4 embryos per genotype from three separate litters. **P = 0.002, unpaired two-tailed Student's t-test. Control embryos are TAM-treated *cre*$^{-}$ embryos and *cre*$^{+}$;*Reln*$^{+/+}$ littermates. Data are mean ± s.e.m. Scale bars, 1 mm (**c**), 25 µm (**d**–**g**, **i**). Lower magnification images for **d**–**f** and **i** are included in Supplementary Fig. 2. For western blot source data, see Supplementary Figs. 6, 7.

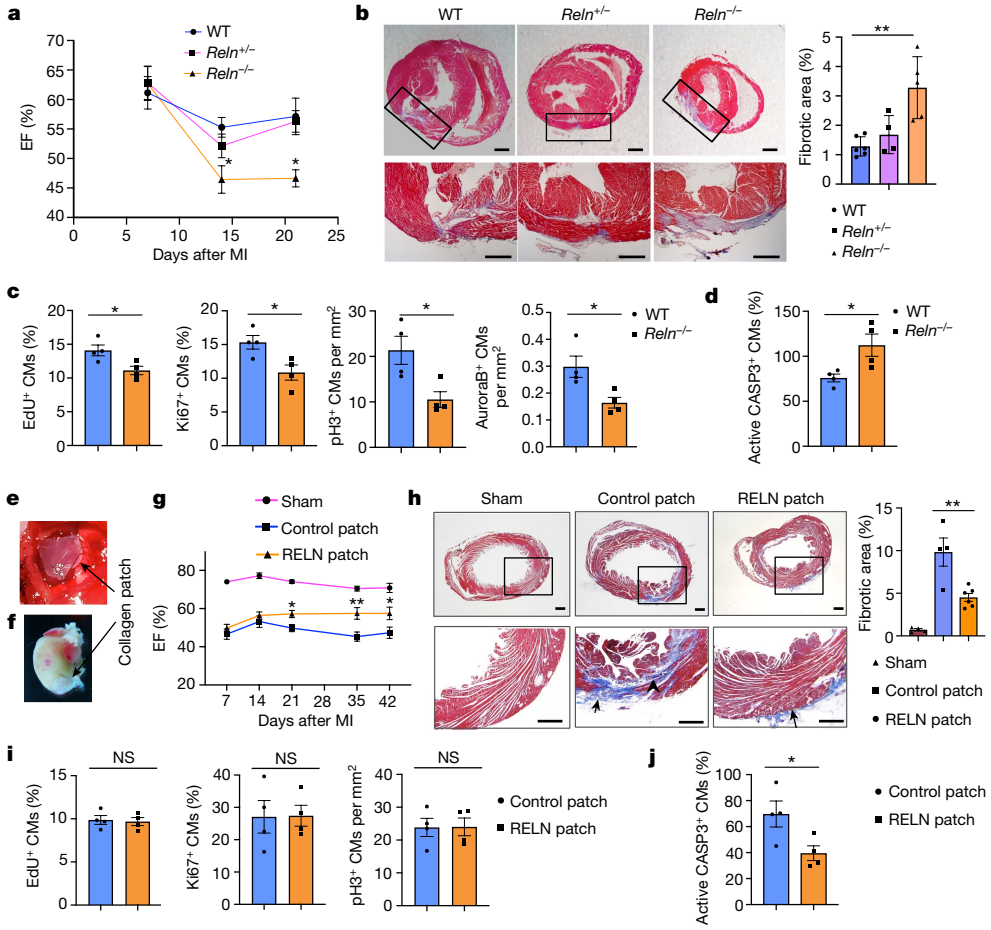

Fig. 4 | RELN improves neonatal and adult cardiac function after myocardial infarction. a, Echocardiography reveals relatively normal cardiac function at P7 and reduced at P14 and P21 in *Reln*$^{-/-}$ mice after myocardial infarction at P2. EF, ejection fraction. P7: $n = 9$ (WT), $n = 9$ (*Reln*$^{+/-}$), $n = 10$ (*Reln*$^{-/-}$); P14: $n = 10$ (WT), $n = 8$ (*Reln*$^{+/-}$), $n = 7$ (*Reln*$^{-/-}$); P21: $n = 9$ (WT), $n = 13$ (*Reln*$^{+/-}$), $n = 8$ (*Reln*$^{-/-}$). $^{*}P = 0.04$ (P14) and $^{*}P = 0.012$ (P21) by two-way analysis of variance (ANOVA) followed by Bonferroni test. **b**, Masson's trichrome staining shows increased fibrosis in P21 *Reln*$^{-/-}$ hearts (myocardial infarction at P2). Right, quantification of the percentage of fibrotic area. $n = 6$ (WT), $n = 4$ (*Reln*$^{+/-}$), $n = 5$ (*Reln*$^{-/-}$). $^{**}P = 0.002$, one-way ANOVA followed by Tukey's test. **c**, CM proliferation is decreased in the border of the infarcted area of P7 *Reln*$^{-/-}$ hearts ($n = 4$ mice per genotype). $^{*}P = 0.026$ (EdU), $^{*}P = 0.025$ (Ki67), $^{*}P = 0.022$ (pH3), $^{*}P = 0.023$ (auroraB), unpaired two-tailed Student's *t*-test. **d**, CM apoptosis increases significantly in the infarcted area of P7 *Reln*$^{-/-}$ hearts ($n = 4$ mice per genotype). $^{*}P = 0.032$, unpaired two-tailed Student's *t*-test. **e**, Sutured collagen patch onto the adult mouse heart after myocardial infarction. **f**, Residual collagen patch remains up to 42 days after myocardial infarction. **g**, Echocardiography reveals significantly improved cardiac function (percentage of ejection fraction) in adult mice with RELN patches starting at around 21 days after myocardial infarction and up to 42 days after myocardial infarction. $n = 6$ (sham), $n = 6$ (control patch) and $n = 7$ (RELN patch). $^{*}P = 0.04$ (P21), $^{**}P = 0.001$ (P35), $^{*}P = 0.01$ (P42), two-way ANOVA followed by Bonferroni test. **h**, Masson's trichrome staining shows reduced cardiac fibrotic area in RELN patch-treated mice 42 days after myocardial infarction. Arrowhead shows fibrotic area; arrows indicate residual collagen patch. Right, quantification of the percentage of fibrotic area. $n = 4$ (sham), $n = 4$ (control patch), $n = 6$ (RELN patch). $^{**}P = 0.003$ by one-way ANOVA followed by Tukey's test. **i**, No differences in CM proliferation between mouse hearts treated with control patch or RELN patch were observed in the infarcted areas 7 days after myocardial infarction ($n = 4$ hearts per group). *P* values determined by unpaired two-tailed Student's *t*-test. **j**, CM apoptosis is reduced in the infarcted area of RELN patch-treated hearts ($n = 4$ mice per group). $^{*}P = 0.039$, unpaired two-tailed Student's *t*-test. Data are mean ± s.e.m. Scale bars, 500 µm (**b**, **h**). Representative images of **c**, **d**, **i** and **j** are in Extended Data Fig. 11. Functional parameters for the neonatal and adult myocardial infarction echocardiography are in Source Data.

seen in *Reln*$^{+/-}$ mice (Fig. 4a, b). Immunostaining revealed that neither lymphatic density nor LEC proliferation was affected in *Reln*$^{-/-}$ hearts after injury (Extended Data Fig. 10d, e). These results demonstrate that re-expression of RELN in cardiac-associated lymphatics of the injured neonatal heart improves cardiac regeneration and function after myocardial infarction.

RELN improves adult myocardial infarction recovery

We next assessed whether delivery of RELN directly into the heart could improve cardiac repair in adult wild-type mice after myocardial infarction. We took advantage of well-established bioengineered collagen patches[28,29] as a scaffold to deliver recombinant RELN protein into the heart. RELN-containing patches and control patches were surgically sutured onto approximately two-month-old injured hearts immediately after acute myocardial infarction (Fig. 4e, f). Cardiac function was evaluated weekly (1–6 weeks after myocardial infarction), and 21 days after myocardial infarction, the ejection fraction was significantly improved in mice with RELN patches (Fig. 4g). Consistent with this improved heart function, 42 days after myocardial infarction the size of the fibrotic scar in the infarcted area was notably reduced in RELN-patched mice (Fig. 4h). To evaluate whether this improved cardiac function and reduced fibrotic tissue was a consequence of increased CM proliferation and/or reduced CM cell death, we performed immunostaining 7 days after myocardial infarction—a stage at which increased CM proliferation is normally detected after injury. No differences in CM proliferation were observed

in the infarcted area between mice with control or RELN patches, as indicated by EdU labelling and Ki67 or pH3 immunostaining (Fig. 4i, Extended Data Fig. 11f). Notably, CM apoptosis was greatly reduced in the infarcted area of RELN-patched mice (Fig. 4j, Extended Data Fig. 11g). These data indicate that after adult cardiac injury, RELN protects CMs from apoptosis, which correlates with a reduced scar and improved heart function.

Discussion

Using mouse embryos that lack LECs or LEC-produced RELN, we demonstrate that their hearts are smaller as a consequence of increased CM apoptosis and reduced CM proliferation. We showed that the percentage of CMs is significantly reduced in E17.5 $Prox1^{\Delta LEC/\Delta LEC}$ and $Reln^{\Delta LEC/\Delta LEC}$ hearts, suggesting that communication between LECs and CMs is required for CM survival during cardiac development. We also found that LEC-conditioned medium increases CM survival and prevents CM apoptosis as a consequence of hypoxia; a result suggesting potent LEC lymphoangiocrine cardioprotective effects. We identified RELN as a factor performing such functional role, probably via the *Itgb1* signalling pathway, both in vivo and in vitro. Finally, we provide additional insight into the proposed beneficial roles of lymphatics on cardiac repair by showing that it is at least partially mediated by RELN activity. We demonstrate the relevance of RELN in endogenous cardiac regenerative ability by showing that after myocardial infarction at P2, RELN expression in LECs is particularly reactivated in the myocardial infarction area of wild-type mice, and that $Reln^{-/-}$ mice do not fully regenerate. We found that RELN is required for CM proliferative activity at P7, although proliferation was not completely abolished in $Reln^{-/-}$ pups, indicating that other factors contribute to CM proliferation. Cardiomyocytes apoptosis was also increased in $Reln^{-/-}$ mice during an extended period after myocardial infarction (up to P21), which suggests that in addition to the reduced proliferation, loss of CM protection underlies the inability of $Reln^{-/-}$ postnatal hearts to fully regenerate.

We also demonstrate that exogenously applied RELN is useful for cardiac repair after myocardial infarction in adult mice. During cardiac growth and in neonatal cardiac regeneration, RELN promotes both CM proliferation and survival; however, the beneficial activity of RELN on cardiac function in adult mice seems to be mostly as a result of reduced CM cell death and a smaller scarred myocardial area, which are both features indicative of a cardioprotective effect.

Our results suggest that RELN regulation of integrin-mediated signalling is specifically crucial for CM proliferation and survival, but it is likely that alternative signals or receptors mask similar effects on other cardiac cell types such as fibroblasts and blood endothelial cells. Furthermore, it is also likely that RELN and/or other lymphoangiocrines have similar homeostatic roles in other organs.

In summary, our study highlights the importance of LECs and RELN during heart growth and repair, and provides some ideas about possible paths to improve cardiac regeneration and cardioprotection in mammals. Our results suggest that the use of RELN could be a valuable therapeutic approach to improve cardiac function in humans.

Online content

Any methods, additional references, Nature Research reporting summaries, source data, extended data, supplementary information, acknowledgements, peer review information; details of author contributions and competing interests; and statements of data and code availability are available at https://doi.org/10.1038/s41586-020-2998-x.

1. Oliver, G., Kipnis, J., Randolph, G. J. & Harvey, N. L. The lymphatic vasculature in the 21st century: novel functional roles in homeostasis and disease. *Cell* **182**, 270–296 (2020).
2. Klotz, L. et al. Cardiac lymphatics are heterogeneous in origin and respond to injury. *Nature* **522**, 62–67 (2015).
3. Vuorio, T., Tirronen, A. & Ylä-Herttuala, S. Cardiac lymphatics - a new avenue for therapeutics? *Trends Endocrinol. Metab.* **28**, 285–296 (2017).
4. Henri, O. et al. Selective stimulation of cardiac lymphangiogenesis reduces myocardial edema and fibrosis leading to improved cardiac function following myocardial infarction. *Circulation* **133**, 1484–1497 (2016).
5. Vieira, J. M. et al. The cardiac lymphatic system stimulates resolution of inflammation following myocardial infarction. *J. Clin. Invest.* **128**, 3402–3412 (2018).
6. Harrison, M. R. et al. Late developing cardiac lymphatic vasculature supports adult zebrafish heart function and regeneration. *eLife* **8**, e42762 (2019).
7. Harvey, N. L. et al. Lymphatic vascular defects promoted by *Prox1* haploinsufficiency cause adult-onset obesity. *Nat. Genet.* **37**, 1072–1081 (2005).
8. Wigle, J. T. & Oliver, G. Prox1 function is required for the development of the murine lymphatic system. *Cell* **98**, 769–778 (1999).
9. Johnson, N. C. et al. Lymphatic endothelial cell identity is reversible and its maintenance requires Prox1 activity. *Genes Dev.* **22**, 3282–3291 (2008).
10. Sörensen, I., Adams, R. H. & Gossler, A. DLL1-mediated Notch activation regulates endothelial identity in mouse fetal arteries. *Blood* **113**, 5680–5688 (2009).
11. Zhang, L. et al. VEGFR-3 ligand-binding and kinase activity are required for lymphangiogenesis but not for angiogenesis. *Cell Res.* **20**, 1319–1331 (2010).
12. Hsieh, P. C. H., Davis, M. E., Lisowski, L. K. & Lee, R. T. Endothelial–cardiomyocyte interactions in cardiac development and repair. *Annu. Rev. Physiol.* **68**, 68–51 (2006).
13. Brutsaert, D. L. & Cotran, R. S. Cardiac endothelial-myocardial signaling: its role in cardiac growth, contractile performance, and rhythmicity. *Physiol. Rev.* **83**, 59–115 (2003).
14. Jossin, Y. Neuronal migration and the role of reelin during early development of the cerebral cortex. *Mol. Neurobiol.* **30**, 225–251 (2004).
15. D'Arcangelo, G. Reelin in the years: controlling neuronal migration and maturation in the mammalian brain. *Adv. Neurosci. (Hindawi)* **2014**, 1–19 (2014).
16. Lutter, S., Xie, S., Tatin, F. & Makinen, T. Smooth muscle-endothelial cell communication activates Reelin signaling and regulates lymphatic vessel formation. *J. Cell Biol.* **197**, 837–849 (2012).
17. D'Arcangelo, G. et al. A protein related to extracellular matrix proteins deleted in the mouse mutant reeler. *Nature* **374**, 719–723 (1995).
18. Lane-Donovan, C. et al. Reelin protects against amyloid β toxicity in vivo. *Sci. Signal.* **8**, ra67–ra67 (2015).
19. Srinivasan, R. S. et al. Lineage tracing demonstrates the venous origin of the mammalian lymphatic vasculature. *Genes Dev.* **21**, 2422–2432 (2007).
20. Trommsdorff, M. et al. Reeler/Disabled-like disruption of neuronal migration in knockout mice lacking the VLDL receptor and ApoE receptor 2. *Cell* **97**, 689–701 (1999).
21. Hiesberger, T. et al. Direct binding of Reelin to VLDL receptor and ApoE receptor 2 induces tyrosine phosphorylation of disabled-1 and modulates tau phosphorylation. *Neuron* **24**, 481–489 (1999).
22. Lin, L. et al. Reelin promotes the adhesion and drug resistance of multiple myeloma cells via integrin β1 signaling and STAT3. *Oncotarget* **7**, 9844–9858 (2016).
23. Dulabon, L. et al. Reelin binds α3β1 integrin and inhibits neuronal migration. *Neuron* **27**, 33–44 (2000).
24. Beffert, U. et al. Reelin-mediated signaling locally regulates protein kinase B/Akt and glycogen synthase kinase 3β. *J. Biol. Chem.* **277**, 49958–49964 (2002).
25. Jossin, Y. & Goffinet, A. M. Reelin signals through phosphatidylinositol 3-kinase and Akt to control cortical development and through mTor to regulate dendritic growth. *Mol. Cell. Biol.* **27**, 7113–7124 (2007).
26. Ieda, M. et al. Cardiac fibroblasts regulate myocardial proliferation through β1 integrin signaling. *Dev. Cell* **16**, 233–244 (2009).
27. Porrello, E. R. et al. Transient regenerative potential of the neonatal mouse heart. *Science* **331**, 1078–1080 (2011).
28. Wei, K. et al. Epicardial FSTL1 reconstitution regenerates the adult mammalian heart. *Nature* **525**, 479–485 (2015).
29. Serpooshan, V. et al. The effect of bioengineered acellular collagen patch on cardiac remodeling and ventricular function post myocardial infarction. *Biomaterials* **34**, 9048–9055 (2013).

Methods

Mouse models

LEC-specific *Prox1*-deficient mice were generated by crossing *Prox1*$^{f/f}$ mice[7] with *Cad5(PAC)-creER*^{T2} mice[10]. These mice are maintained in a mixed C57B6 and NMRI background. LEC-specific *Reln*-deficient mice were generated by crossing *Reln*$^{f/f}$ mice[18] with *Prox1-creER*^{T2} mice[19]. These mice are in a mixed 129, FVB and C57B6 background. *Reln*$^{+/-}$ mice were provided by B. Brunne and are originally from the Jackson Laboratory and are maintained in a mixed BALB/C and C57B6 background. For induction of *cre*-mediated recombination in *Prox1*$^{\Delta LEC/\Delta LEC}$ and *Reln*$^{\Delta LEC/\Delta LEC}$ embryos, two consecutive intraperitoneal TAM injections of 5 mg per 40 g were administered to pregnant dams. *Itgb1*$^{f/f}$ mice and *Myh6-cre* mice were obtained from the Jackson laboratory and are in a mixed C57B6 and NMRI background. These strains were bred to generate *Myh6-cre;Itgb1*$^{f/+}$ mice that were crossed with *Reln*$^{+/-}$ mice to obtain *Myh6-cre;Itgb1*$^{f/+}$*;Reln*$^{+/-}$ (*β1*$^{\Delta CM/+}$*;Reln*$^{+/-}$) embryos. Heterozygous mice carrying the kinase-dead *Flt4*^{Chy} allele (*Vegfr3*^{kd}) (MRC Harwell) were previously described[30] and are maintained in the NMRI background. Mice of both sexes from 12 weeks to 6 months old were used for breeding and experiments. Mice were not randomized into experimental groups, but were age- and sex-matched and littermates were used whenever possible. All the myocardial infarction surgeries and the echocardiography analyses were performed blinded. Experiments with embryos were not blinded as the mutant embryos showed very obvious phenotypes (such as oedema). All other experiments were not blinded as they required grouping by genotypes (flow cytometry) or were treated with different reagents (siRNA knockdown).

All animal husbandry was performed in accordance with protocols approved by Northwestern University and UT Southwestern Medical Center Institutional Animal Care and Use Committee, as well as Animal Experimentation Review Board of the Semmelweis University. Animal facilities are equipped with a 14 h:10 h or 12 h:12 h light cycle. Temperatures are maintained between 18 and 23 °C with 40–60% humidity.

Mouse embryonic CM isolation

CMs were isolated from E14.5–17.5 mouse embryos using the Pierce Primary Cardiomyocyte Isolation Kit (Thermo Fisher). In brief, ventricles were isolated from embryonic hearts and minced and washed with cold HBSS and further digested according to the manufacture instructions. To examine the relative CM cell size, dissociated cells were cultured in DMEM containing 10% FBS overnight and then cells were fixed in 4% paraformaldehyde (PFA) for immunostaining. For any other experiments, primary cells were cultured in DMEM containing 10% FBS and cardiomyocyte growth supplements for 3–4 days before experiments.

Human iPS cell-derived CMs

Cardiac differentiation was performed using the CDM3 (chemically defined medium, three components) system as described with slight modifications[31,32]. Human iPS cells are split at 1:15 ratios and grown in B8 medium for 4 days reaching approximately 80% confluence. On day 0, B8 medium is changed to CDM3[31], consisting of RPMI 1640 (Corning, 10-040-CM), 500 μg ml^{-1} fatty acid-free bovine serum albumin (GenDEPOT), and 200 μg ml^{-1} L-ascorbic acid 2-phosphate (Wako), supplemented with 6 μM of CHIR99021 (LC Labs, C-6556). After 24 h (day 1), medium was changed to CDM3. On day 2, medium was changed to CDM3 supplemented with 2 μM of Wnt-C59 (Biorbyt, orb181132). Medium was then changed every other day for CDM3 starting on day 4. Contracting cells are noted from day 7. On day 16 of differentiation, CMs were dissociated using DPBS for 20 min at 37 °C followed by 1:200 Liberase TH (Roche) diluted in DPBS for 20 min at 37 °C, centrifuged at 300*g* for 5 min, and filtered through a 100-μm cell strainer (Falcon). The purity of the differentiated cells was determined by expression of CM cell marker TNNT2 using flow cytometry. Only cell lines that show over 85% were TNNT2^{+} were used for experiments.

LEC-conditioned medium

Human dermal LECs were purchased from Lonza and cultured with endothelial basal medium (EBM) complemented with supplement mix (Lonza). Authentication of the human dermal LECs was performed by immunostaining with a PROX1 antibody. Cells were negative for mycoplasma contamination. Passages 4 or 5 were cultured in 10-cm dishes until confluent, washed with cold PBS three times and then 8 ml of serum-free DMEM (without phenol red) with penicillin/streptomycin was added. Cells were then cultured overnight before collecting the conditioned medium that was filtered through a 0.22-μm pore membrane (Millipore). Control conditioned medium (DMEM) was prepared in the same way but without LECs.

siRNA knockdown

Human LECs were transfected as previously described[33]. In brief, P4 human LECs were transfected with scrambled or *Reln* siRNA (Santa Cruz) with Lipofectamine 2000 (Invitrogen), according to the manufacture's instruction. After 48 h, cells were washed and replaced with DMEM and further cultured overnight to collect the conditioned medium. LECs were collected and qPCR was performed to check transfection efficiency.

LEC-conditioned medium treatment

To examine the effects of the LEC-conditioned media, mouse primary CM or human iPS cell-derived CMs were cultured in 12-well plates (about 80% confluence), and cells were treated with DMEM, conditioned medium, conditioned medium from scrambled siRNA-treated LECs (siCtrl-conditioned), conditioned medium from siReln-treated LECs (siReln-conditioned) or conditioned medium with integrin-β1 blocking antibodies (10 μg ml^{-1}, BD Biosciences) o/n. Cells were either fixed in 4% PFA for immunofluorescent staining, or lysed in RIPA buffer for western blot analysis.

RELN-conditioned medium and treatment

HEK-293T cells (ATCC) were cultured in DMEM with 10% fetal bovine serum and transfected with the *Reln* cDNA construct pCrl, provided by G. D'Arcangelo, using Lipofectamine 2000 (Invitrogen). Control cells were mock-transfected in the same way without adding the vector. Twenty-four hours after transfection, the medium was changed to serum-free DMEM, and RELN-conditioned medium and mock conditioned medium (control) was collected two days after the medium change. The conditioned medium was filtered through a 0.22-μm pore membrane. To examine the effects of the RELN-conditioned medium, mouse primary CMs were starved overnight with DMEM and stimulated for 30 min with RELN-conditioned medium (supernatant from transfected cells) or control medium (supernatant from mock-transfected cells). To examine the RELN/integrin-β1 pathway, primary CMs were treated in the presence or absence of integrin-β1-blocking antibodies (10 μg ml^{-1}, BD Biosciences) for 3 h before RELN-conditioned medium treatment. The HEK-293T cell line was not authenticated but tested negative for mycoplasma contamination.

Western blot analysis

To examine signalling changes in primary CMs or iPS cell-derived CMs, cells were lysed in RIPA buffer and subject to western blot analysis. The following primary antibodies were used: p-AKT (rabbit, Cell Signaling, 4060, 1:500), p-ERK (rabbit, Cell Signaling, 4370, 1:1,000), total AKT (rabbit, Cell Signaling, 4691, 1:500), total ERK (rabbit, Cell Signaling, 4695, 1:500), p-DAB1 (rabbit, Cell Signaling, 3327S, 1:100), p-FAK (rabbit, Cell Signaling, 3284, 1:200), integrin-β1 (mouse, BD, 610467, 1:100), GAPDH (rabbit, Santa Cruz, sc32233, 1:5,000). Blots were imaged using a ChemiDock imaging system (Bio-Rad) and bands were acquired using Quantity One 1-D software. Quantification of western blot was analysed using ImageJ 1.51. Included images are representative blots.

All raw data used for the quantifications are included in the Supplementary Information.

Mass spectrometry analysis of LEC-conditioned medium

LEC-conditioned medium (50 ml) was collected from five 10-cm dishes of cultured LECs and filtered through a 0.22-µm pore membrane as mentioned above. LEC-conditioned medium was further concentrated into 500 µl using the Protein-Concentrate Kit (Millipore) according to the manufacturer's instruction. Protein concentration was then measured by the BCA protein assay (Thermo Fisher). Experiments were repeated three times and three biological samples were submitted to Northwestern Proteomics Core for untargeted quantitative proteomics analyses by Label-free Quantitative Proteomics. In brief, samples were analysed using an UltiMate 3000 RSLCnano system (ThemoFisher Scientific) that is coupled with electrospray ionization (ESI) to a linear ion trap (LTQ) Orbitrap mass spectrometer (iLTQ-Orbitrap, ThermoFisher). The resulting raw mass spectra from all three replicates were analysed by the MaxQuant search engine (version 1.6.0.16) using UniprotKB human database with the allowance of up to two missed cleavages and precursor mass tolerance of 20 ppm. The secretome was acquired using software Scaffold 4 and annotated using Gene Ontology (GO), which assigns putative cellular compartmentalization, biological process and molecular functions.

ELISA

To validate the presence of RELN in the LEC-conditioned medium, three different batches of commercial LECs were cultured and their conditioned medium was collected as described. Sandwich ELISA was performed to examine the relative levels of RELN in the three different batches of LEC-conditioned medium. In brief, conditioned medium was pre-coated to Nunc MaxiSorp Flat-Bottom 96-well plates (Invitrogen) o/n and blocked with 5% milk in TBS-T. Plates were then incubated with RELN primary antibody (R&D, AF3820, 1:100) and followed by incubation with HRP-conjugated donkey anti-goat antibody (Jackson ImmunoResearch, 705-035-003, 1:1,000). Subsequently, plates were washed and the substrate solution (3,3,5,5-tetramethylbenzidine liquid substrate system for ELISA, Abcam) was added. The reaction was stopped by adding 2 N H_2SO_4, and plates were measured at 450 nm using the Opsys Mr microplate reader (Dynex Technologies). Relative RELN levels in different batches of conditioned medium were quantified by absorbance at 450 nm ($A_{450\,nm}$).

FACS analyses and sorting

For analysis of percentages of CMs in the heart, whole E17.5 ventricles were dissociated from control and *Prox1*$^{\Delta LEC/\Delta LEC}$ hearts using the Pierce Primary Cardiomyocyte Isolation Kit (Thermo Fisher). Cells were fixed and permeabilized using a permeabilization kit for intracellular staining (eBioscience) following manufacturer's instruction. Cells were then incubated with Cy3-conjugated mouse anti-cTnC antibody (Abcam, ab45931, 1:100) and Hoechst 33342 (Invitrogen, 1:1,000) at room temperature for 1 h. Cells were washed and percentage of cTnC$^+$ CMs was determined after 20,000 total cell counts by flow cytometry. Percentage of polyploidy CMs was determined by Hoechst 33342 intensity. Flow data were collected using the flow software BD FACS Diva 8.0.3 and analysed by FlowJo v.10.

For analysis of the purity of differentiated human iPS cell-derived CMs, dissociated CMs were fixed with 4% PFA and permeabilized using 0.5% saponin. Cells were then incubated with 647-conjugated mouse anti-cardiac TNNT2 antibody (BD Biosciences, clone 13-11, 1:200) for 1 h. Cells were washed and the percentage of TNNT2$^+$ CMs was determined after 10,000 total cell counts by flow cytometry.

Neonate myocardial infarction

Neonatal myocardial infarction was performed in P2 pups. In brief, P2 pups were anaesthetized under isoflurane anaesthesia (1–2%). Once pups did not respond to toe pinch, they were moved to a cold platform to undergo hypothermia anaesthesia. Each neonate undergoes acute myocardial infarction by ligation of the left anterior descending coronary artery. Thoracic wall incisions were sutured and the wound closed using skin adhesive. Pups were warmed on a warm pad. After confirmation of spontaneous movement pups received a dose of subcutaneous buprenorphine (0.05 mg kg^{-1}). Once neonate recovered from hypothermia, they were moved back to its fostering mother's cage.

Compressed collagen patches

Compressed acellular collagen patches were prepared as previously described. In brief, control collagen patches were prepared by adding 1.1 ml DMEM to 0.9 ml of sterile rat tail type I collagen solution in acetic acid (3.84 mg ml^{-1}, Millipore) and neutralized with 0.1 M NaOH (50 µl). RELN collagen patches were prepared by adding 20 µg of recombinant human RELN protein (R&D) into the collagen mix. Then, 0.9 ml of the collagen solution was added into one well of 24-well plates and placed into a tissue culture incubator for 30 min at 37 °C for polymerization. Polymerized collagen gel was then compressed by application of a static compressive stress of approximately 1,400 Pa for 5 min as described[28]. Each collagen patch was then trimmed to three even pieces for application in vivo.

Myocardial infarction and insertion of collagen patches in adult mice

Nine-to-eleven-week-old NMRI female mice were anaesthetized using an isoflurane inhalational chamber, endotracheally intubated using a 22-gauge angiocatheter and connected to a small animal volume-control ventilator (NEMI Scientific). All mice underwent acute myocardial infarction by ligation of the left anterior descending coronary artery and ligation was considered successful when the left ventricle wall turned pale. Immediately after ligation, prepared collagen patches (with and without RELN) were sutured (at two points) onto the surface of the ischaemic myocardium (Fig. 4e). The patch size used was approximately one-third of the 15.6 mm-diameter collagen gel. Mice were kept on a heating pad until they recovered. After confirmation of spontaneous movement, mice received a dose of subcutaneous buprenorphine (0.05 mg kg^{-1}) and then every 8–12 h for 48 h post-surgery.

Echocardiography

Two-dimensional echocardiograms were measured on a 55 MHz probe using Vevo 3100 micro-ultrasound imaging system (VisualSonics), short axis views of the left ventricles were taken at the level of papillary muscles and used to calculate end-diastolic and -systolic dimensions using Vevo LAB 3.2.6 software (VisualSonics). All echocardiography measurements were performed in a blinded manner.

Histology, immunohistochemistry and immunofluorescent staining

For H&E staining, samples were embedded in paraffin and sectioned longitudinally at 6 µm thickness and staining was performed according to standard protocols.

For whole mount heart staining, isolated hearts were fixed in 4% PFA overnight and blocked. Antibodies were used as followed: LYVE1 (goat, R&D, AF2125, 1:200), EMCN (rat, Invitrogen, 14-5851-82, 1:500), RELN (Goat, R&D, AF3820, 1:50), PROX1 (Goat, R&D, AF2727, 1:100) and Cy3-conjugated α-SMA (mouse, Sigma, C6198, 1:300). Cy3-conjugated donkey anti-goat (Jackson ImmunoResearch, 705-165-147, 1:300) and Cy5-conjugated donkey anti-rat (Jackson ImmunoResearch, 712-175-150, 1:300) were used for immunofluorescent staining.

For cryosections, embryos or isolated hearts were fixed in 4% PFA overnight and dehydrated in 30% sucrose. Samples were embedded in OCT compound and frontal sectioned at 10-µm thickness to show four chambers. Primary antibodies were used as follows: α-actinin

(Mouse, Sigma, A7811, 1:500), cTnC (mouse, Abcam, ab8295, 1:1,000), Ki67 (rabbit, Invitrogen, SP6, MA5-14520, 1:200), active CASP3^{+} (rabbit, BD Pharmingen, C92- 605, 559565, 1:200), LYVE1 (goat, R&D, AF2125, 1:200), RELN (goat, R&D, AF3820, 1:50), LYVE1 (rabbit, AngioBio, 11-034, 1:500), PROX1 (rabbit, AngioBio, 11002, 1:500), PROX1 (goat, R&D, AF2727, 1:100) and MEF2C (rabbit, LSBio, LSC356188, 1:1,000). Secondary antibodies were used as follows: Alexa 488-conjugated donkey anti-rabbit (Invitrogen, A21206, 1:300); Alexa 488-conjugated donkey anti-goat (Invitrogen, A11055, 1:300); Cy3-conjugated donkey anti-rabbit (Jackson ImmunoResearch, 711-165-152, 1:300); Alexa 488-conjugated donkey anti-mouse (Invitrogen, A21202, 1:300); Cy3-conjugated donkey anti-goat (Jackson ImmunoResearch, 705-165-147, 1:300) and Cy5-conjugated donkey anti-goat (Jackson ImmunoResearch, 705-495-147, 1:300).

For cell staining, cells were fixed in 4% PFA for 30 min on ice, blocked and incubated with primary antibody against α-actinin (Mouse, Sigma, A7811, 1:500), cTnC (Mouse, Abcam, ab8295, 1:1,000), Ki67 (Rabbit, Invitrogen, SP6, MA5-14520, 1:200), PROX1 (goat, R&D, AF2727, 1:100) and active CASP3^{+} (rabbit, BD Pharmingen, C92- 605, 559565, 1:200). Secondary antibodies were used as follows: Alexa 488-conjugated donkey anti-mouse (Invitrogen, A21202, 1:300) and Cy3-conjugated donkey anti-rabbit (Jackson ImmunoResearch, 711-165-152, 1:300). At least three heart samples per genotype were used for whole-mount staining and three sections per heart per staining for immunohistochemistry and immunofluorescent staining, respectively. Cell staining was repeated at least three times.

For Masson's Trichrome staining, mouse hearts were obtained and fixed in 4% PFA and embedded. Paraffin sections were cut from apex to base into serial sections at 0.8-μm thickness. Masson's trichrome staining was performed according to standard procedures (Sigma) and used for detection of fibrosis. Scar size was quantified using NIH ImageJ 1.51 software and the percentage of the fibrosis area was calculated relative to left ventricle area.

EdU administration

To examine the EdU incorporation in *Prox1*$^{\Delta LEC/\Delta LEC}$, *Vegfr3*$^{kd/kd}$, *β1*$^{\Delta CM/+}$;*Reln*$^{+/-}$ or *Prox1*$^{\Delta LEC/\Delta LEC}$ strains, 5-ethynyl-2′-deoxyuridine (EdU, 3 mg per mouse) was administrated into pregnant females by intraperitoneal injections. Two hours after injections, mice were euthanized and hearts, livers and kidneys were collected and cryosectioned as described above. To examine EdU incorporation in control or RELN patches sutured mice after myocardial infarction, EdU (3 mg per mouse) was injected intraperitoneally for 3 days starting 4 days after myocardial infarction. Hearts were collected at day 7 and subjected to EdU immunohistochemistry using Click-iT EdU Alexa Fluor 488 Imaging Kit (Life Technologies) according to the manufacturer's instruction.

qRT–PCR

Total RNAs was extracted using RNeasy Mini Kit (Qiagen). cDNA was generated (Clontech Laboratories) and 20 ng used for qRT–PCR using Power SYBR Green PCR Master Mix (Life Technologies) on a StepOnePlus Real-Time PCR system (Applied Biosystems). At least three individual samples per group were performed for each run of qPCR. Primer sequences used in this study are listed below.

For mouse qPCR: *Bcl2l11*: GAGATACGGATTGCACAGGA, ATTTGAGGG TGGTCTTCAGC; *P21* GAAAGAAGCGGAAGATCCTCC, GGGCCTCAGGG ATTGTTTGG; *Pdcd4* GAAATTGGATTTCCGCATCT, TAACCGCTTCACTT CCATT; *Stat1*: AGGGGCCATCACATTCACAT, AGATACTTCAGGGGA TTCTC; *Trp53inp1*: TCCTCAGCAGAGCACACTTC, TCCATTGGACAGGA CTCAAA; *Cdc6*: AGGGTGACTTTGAGCCAAGA, ATGAAGATTCTGGGGG CTCT; *E2f1*: TGCAGAAACGGCGCATCTAT, CCGCTTACCAATCCCCACC; *Pcna*: TTGCACGTATATGCCGAGACC, GGTGAACAGGCTCA TTCA TCTCT; *Mcm5*: GGAGGCTATTGTGCGCATTG, CTGGTCCTCCTGGGTAGTGA; *Ccne2*: TCTGTGCATTCTAGCCATCG, ACAAAAGGCACCATCCAGTC; *Reln*: GGACTAAGAATGCTTATTTCC, GGAAGTAGAATTCATCCATCAG; *Rlp32*: GCCTCTGGTGAAGCCCAAG, TTGTTGCTCCCATAACCGATGT.

For human qPCR: *RELN*: CAATCTGAATGGCGAAACC, CTTTCGCTAT AAATCGGAGAGAGA; *GAPDH*: TGACCACAGTCCATGCCATC, GACGG ACACATTGGGGGTAG; *MMRN1*: TTGGATTGGAGGTGCTGTC, GCCTGGTTGGTGTGTATCA; *THBS1*: CACCAACCGCATTCCAGAG, TCAGGGATGCCAGAAGGAG; *HSPG2*: CTCCATCGTCATCTCCGTCT, GTCTGCCCTTCTGCCACTC; *FN1*: CCATCGCAAACCGCTGCCAT; AACACTTCTCAGCTATGGGCT T; *FSTL1*: CGATGGACACTGCAAAG AGA, CCAGCCATCTGGAATGATCT; *LAMA4*: GCGGCCGAGAAATGCA, AGTCGCAGGGCACACATTC; *SERPINE1*: ACAAGTTCAACTATACTG AGTTCACCACGCCC, TGAAACTGTCTGAACATGTCGGTCATTCCC.

All sequences are included forward and reversed and are annotated from 5′ to 3′.

RNA-seq

Total RNA was extracted using the RNeasy Mini Kit (Qiagen) according to the manufacturer's instructions. Extracted total RNAs were quantitated by NanoDrop and RNA integrity number value measured with an Agilent Bioanalyzer. In all RNA-seq samples, quality control was performed using the 2100 Bioanalyzer (Agilent). RNA library was prepared using the TruSeq mRNA-Seq Library Prep and sequenced using the HiSEQ Next-generation Sequencing System at the NUSeq Core.

Imaging acquisition and quantification

Confocal images in Fig. 1a, d–i, Extended Data Figs. 1a, 3b, 4b, 6i and 8g were acquired using a Nikon W1 Dual CAM Spinning Disk confocal microscope. All other confocal images were acquired using Zeiss LSM510 laser-scanning confocal microscope. All confocal images represent maximum projection images of *z*-stacks. For quantifications of CM proliferation and apoptosis, images were taken from three myocardium regions of frontal heart sections: myocardium nearby left ventricle, myocardium nearby right ventricle and septum. At least nine images were taken from each heart (at least three images per region) and at least three hearts from each genotype were quantified. Bright-field images were taken using a Leica stereomicroscope. Embryo body length was measured from head to tail (crown–rump) using Image J 1.51 with all the images under the same magnification. CM cell size, as well as fibrosis area were also measured by Image J 1.51 software with all the images under the same magnification.

Statistical analysis

No statistical analysis was used to predetermine sample size. Statistical analysis was performed using GraphPad Prism 7 and Microsoft Excel 2016. Differences between two groups were determined by two-tailed unpaired *t*-test, and differences between multiple groups were calculated using one-way ANOVA or two-way ANOVA. $^{*}P < 0.05$ $^{**}P < 0.01$ and $^{***}P < 0.001$ were considered statistically significant.

Reporting summary

Further information on research design is available in the Nature Research Reporting Summary linked to this paper.

Data availability

All data from the manuscript are available from the corresponding author on request. RNA-seq raw data have been deposited to the Gene Expression Omnibus (GEO) repository with accession number GSE158504. Source data are provided with this paper.

30. Karkkainen, M. J. et al. A model for gene therapy of human hereditary lymphedema. *Proc. Natl Acad. Sci. USA* **98**, 12677–12682 (2001).
31. Burridge, P. W. et al. Chemically defined generation of human cardiomyocytes. *Nat. Methods* **11**, 855–860 (2014).
32. Burridge, P. W., Holmström, A. & Wu, J. C. Chemically defined culture and cardiomyocyte differentiation of human pluripotent stem cells. *Curr. Prot. Human Genet.* **87**, 21.3.1–21.3.15 (2015).

33. Liu, X. et al. Rasip1 controls lymphatic vessel lumen maintenance by regulating endothelial cell junctions. *Development* **145**, dev165092 (2018).

Acknowledgements This work was supported by NIH grant (RO1HL073402-16) to G.O., AHA grant (18CDA34110356) to X.L., 5T32HL134633 to W.M., FPU grant from the Spanish Ministry of Education, Culture and Sports and EMBO Short-Term Fellowship to E.D.C., Leducq TNE-17CVD and RD16/0011/0019 (ISCIII) from the Spanish Ministry of Science, Innovation, and Universities to M.T., NIH T32 GM008061 to C.L., HL63762, and NS093382 to J.H. We thank G. M. Rune and B. Brunne for the *Reln*$^{+/-}$ strain. RNA-seq work was supported by the Northwestern University NUSeq Core Facility. We thank the Robert H. Lurie Cancer Center Flow Cytometry facility supported by NCI CCSG P30 CA060553 for their invaluable assistance. Flow Cytometry Cell Sorting was performed on a BD FACSAria SORP system and BD FACSymphony S6 SORP system, purchased through the support of NIH 1S10OD011996-01 and 1S10OD026814-01. Imaging work was performed at the Northwestern University Center for Advanced Microscopy supported by NCI CCSG P30 CA060553 awarded to the Robert H Lurie Comprehensive Cancer Center. Spinning disk confocal microscopy was performed on an Andor XDI Revolution microscope, purchased through the support of NCRR 1S10 RR031680-01. Proteomics services were performed by the Northwestern Proteomics Core Facility supported by NCI CCSG P30 CA060553 awarded to the Robert H Lurie Comprehensive Cancer Center, instrumentation award (S10OD025194) from NIH Office of Director, and the National Resource for Translational and Developmental Proteomics supported by P41 GM108569. We thank the George M. O'Brien Kidney Research Core Center (NU GoKidney, supported by a P30 DK114857 award from NIDDK) for the use of the Echocardiography machine. The myocardial infarction surgeries were performed by the comprehensive Transplant Center Microsurgery Core, partially supported by NIH NIAID P01AI112522. We thank J. Jin and P. Liu for help with the ELISA reagents and data analysis, R. Ma for help with DNA polyploidy analysis, A. Shi for the MEF2C antibodies, M. Dellinger for the *Prox1-creER*^{T2} mice and H. Ardehali for the *Myh6-cre* mice. We specially thank B. Sosa-Pineda for advice and suggestions and P. Ruiz-Lozano for sharing her expertise in the preparation of the collagen patches.

Author contributions X.L. and G.O. designed the experiments and analysed the data. X.L. performed most of the experiments and data analysis. E.D.C. performed the neonate myocardial infarction and acquired data. T.T. and J.H. provided the *Reln* conditional mouse strain and generated some of the conditional crosses. X.G. helped with the generation, isolation and data analysis of *Reln* conditional embryos. C.L. and E.T. provided valuable advice with the neonate myocardial infarction and Echo data protocols. Z.J. and L.B. generated the *Vegfr3*$^{kd/kd}$ embryos and analysed that data. M.O.-B. and W.M. helped with the generation of mouse lines, histology and discussions. H.K. and P.B. generated the iPS cell-derived CMs. T.B. helped with the primary cell culture experiments and qPCR analysis. O.C. helped to obtain and generate some of the mutant strains. M.T. provided valuable experimental advice and critical reading of the manuscript. X.L. and G.O. wrote the manuscript.

Competing interests J.H. is a shareholder of Reelin Therapeutics and a co-inventor on a pending US patent application filed by his institution (UT Southwestern; application number 15/763,047 and publication number 20180273637, title "Methods and Compositions for Treatment of Atherosclerosis"; Inventors: J.H., Y. Ding, X. Xian, L. Huang, C. Mineo, P. Shaul and L. Calvier). This patent application covers no aspects of the current manuscript. Findings regarding the potential applications and methods for using RELN to treat cardiac diseases are the subject of provisional patent application (US63/091,558) owned by Northwestern University and list X.L. and G.O. as inventors. All other authors declare no competing interests.

Additional information

Supplementary information is available for this paper at https://doi.org/10.1038/s41586-020-2998-x.

Correspondence and requests for materials should be addressed to G.O.

Peer review information *Nature* thanks Kristy Red-Horse and the other, anonymous, reviewer(s) for their contribution to the peer review of this work.

Agradecimientos

No podría terminar esta tesis sin daros las gracias a todos los que habéis hecho posible que yo llegue hasta aquí.

En primer lugar, me gustaría agradecerte, Miguel, la oportunidad que me diste hace ya casi 6 años. Gracias por confiar en mí y por dejar que haya podido aprender tantísimo en todos estos años. Gracias por la libertad que nos das para ir más allá, por tu pasión por la Ciencia y por tener siempre tu puerta abierta para nosotros.

Y por supuesto, muchas gracias a todos vosotros, los LAB_MT. No sé qué hubiera sido de mí sin vosotros todos estos años. Los que estabais cuando empecé y los que estáis ahora. Me considero muy afortunada de haber trabajado codo con codo con gente tan especial, de quien he podido aprender muchísimo, tanto en lo personal como en lo profesional. Gracias por la ayuda con los experimentos, por escuchar mis penas, por las risas, por los momentos de locura transitoria, por todo eso que hace que todo merezca la pena, aunque no te salga nada. Súper Vane: puedo decir que esta tesis es tan tuya como mía. Mil gracias. No hay "dibujos" que puedan agradecerte todo lo que has hecho por mí, en especial en estos últimos meses. Aunque no tuvieras tiempo, nunca me has dicho que no (o al menos en serio jaja) y he sentido que siempre podía contar contigo y no sólo en lo profesional, sino por todo. Susana y Rocío, muchas gracias. Las 3 hacéis que el laboratorio salga adelante y que no caigamos en el caos. Siempre con una sonrisa me habéis ayudado hasta con mis prisas y peticiones de última hora. Gracias por el cariño que me habéis dado. Lin, José, Isaac, Noelia, Sandra, Ghislaine, Miquel, Morena, Cova: ¡compañeros de viaje! Todos hemos coincidido y compartido las penas y alegrías de hacer el doctorado en el grupo. Noelia, Sandra, Ghislaine, gracias por enseñarme tanto! No sé qué hubiera sido de mí sin vosotras cuando llegué al labo! Ay Sandra! Cuánto echo de menos nuestros viajes en el tren! Y muchas gracias en especial por tu ayuda estos últimos meses! Lin, mi compi en este camino! Nosotras podemos! Yo de mayor quiero ser como tú, con esa fuerza y esa actitud ante la vida. José, Isaac, gracias por esas risas. José, gracias en especial por el apoyo este último año. Isaac, tranquilo, no te tiraré por las escaleras. Miquel, Morena, Cova: Muchas gracias por vuestra ayuda, por vuestras sonrisas. Llegaréis allá donde os lo propongáis. Pero también gracias a todos por esos bailes, esas cenas, ese parapente, esa escalada, esas cervezas improvisadas, esas comidas con concierto incluido… gracias por los momentos compartidos fuera de las cuatro paredes del laboratorio. ¡Cuánto los echo

de menos! ¿Y qué haría yo sin mis postdocs favoritos? Irene: ¡Equipo Meis al poder! Me encantan tu optimismo y sonrisa constante. Mil gracias por tu ayuda con las in situs y mil cosas más. Cris: Sin ti esta tesis no tendría figuras ni estaría escrita! Con eso lo digo todo! Gracias por enseñarme tanto y con tanta paciencia! ¡Gracias a las dos por mantener la calma que a veces me ha hecho tanta falta! Lorena, ¡qué crack! Gracias por escuchar mis penas, por esos western blot, por estar siempre dispuesta a darme una idea y animarme. Óscar, gracias por tu entusiasmo por la Ciencia, por tus ideas y por estar siempre dispuesto a echarme una mano. Consuelo, muchas gracias por tu amabilidad. Jorge, Inés, Teresa, muchas gracias y buena suerte!

Muchas gracias Guillermo por haberme dado la oportunidad de hacer la estancia en tu laboratorio. Y muchas gracias por haberme acogido en Chicago de la manera en qué lo hiciste. Xiaolei, Michael, Wanshu, Nozomu: I can't be anything but grateful. You all made me feel at home. I had such an amazing experience thanks to you! Now I know that you should cross everything in order to be lucky in this life.

Bea, Iván y Tere. Porque es como si fuerais LAB_MT y lo mismo que se aplica a ellos, se aplica a vosotros. Muchas gracias Silvia por todo el apoyo estos años y por todo lo que siempre me has ayudado con los distintos favores que te hemos pedido. Y por supuesto, muchas gracias a la 3N!! A los JLP, RB, IF y NM! A cada uno de vosotros muchas gracias por esas charlas por los pasillos, por esos ratos por las lupas, por las risas, por los anticuerpos, por los reactivos...

Gracias a todas las unidades del CNIC con las que he tenido la suerte de trabajar ya que facilitáis todo muchísimo. Histología (Antonio, Pedro, Roisin, Claudio, muchas gracias!), Imagen Avanzada (gracias María, Ana y Lorena por toooodas esas ecos), Genómica, Bioinformática, Transgénesis, Tecnología de células pluripotentes. A todos muchas gracias! Microscopía: Vero, Elvira, Olga, Alfonsa, gracias por pelear por mis cuantificaciones y ayudarme siempre que lo he necesitado.

José, no sé qué hubiera sido de mi tesis sin tu ayuda en el animalario. Siempre has resuelto con rapidez y eficacia todas mis peticiones precipitadas y caóticas. ¡Muchas gracias! Pero también muchas gracias Merche, Laura, Guille, Vir y Rubén por toda vuestra ayuda en estos años.

¡Gracias al resto de personas del CNIC que hacéis que todo funcione y nosotros podamos hacer lo que hacemos! Muchas gracias Cristina por la ayuda con todas las memorias de la FPU!

A vosotros, papá, mámá, Yoli, Carlos. No hay palabras para agradeceros todo lo que habéis hecho por mí. Por ser mi apoyo constante. Es obvio que soy la persona que soy gracias a vosotros. Me habéis enseñado a trabajar duro, a no rendirme pero sobre todo, a que juntos podemos con todo. En especial, gracias por estos últimos meses porque no he sido ni han sido fáciles.

Sara, Víctor, Pablo, Manu, Julio, Raquel, Cris, Ramón. Son tantos años juntos y tantas vivencias… porque sois la mejor válvula de escape. Porque sé que siempre puedo contar con vosotros. Muchas gracias. A mis chicas de la uni! Gracias por esos viajes, por esas quedadas, por esos ratos de locura. Porque aunque pase el tiempo, con vosotras es como si nos hubiéramos visto ayer. Elena, Irene: ha sido duro, pero ánimo, ¡que ya no nos queda nada! David, por esos desayunos y porque sabes más de mi tesis que muchas personas, porque siempre sabes cómo animarme y porque tus planes locos alguna vez saldrán a la luz. Muchas gracias. José, sin ti estos últimos meses habría perdido la poca cordura que me queda. Gracias por tu paciencia y por conseguir animarme siempre. Por estar ahí, por todo y.

En resumen:

¡Muchas gracias a todos!